uOttawa

L'Université canadienne
Canada's university

FACULTÉ DES ÉTUDES SUPÉRIEURES ET POSTOCTORALES

uOttawa

L'Université canadienne
Canada's university

FACULTY OF GRADUATE AND POSDOCTORAL STUDIES

Joel Laurin
AUTEUR DE LA THÈSE / AUTHOR OF THESIS

M.Sc. (Earth Sciences)
GRADE / DEGREE

Department of Earth Sciences
FACULTÉ, ÉCOLE, DÉPARTEMENT / FACULTY, SCHOOL, DEPARTMENT

Geology, Gold Mineralization and Alteration of the Horne West Property Rouyn-Noranda
TITRE DE LA THÈSE / TITLE OF THESIS

Mark Hannington
DIRECTEUR (DIRECTRICE) DE LA THÈSE / THESIS SUPERVISOR

CO-DIRECTEUR (CO-DIRECTRICE) DE LA THÈSE / THESIS CO-SUPERVISOR

Richard Cox

Tony Fowler

Gary W. Slater
Le Doyen de la Faculté des études supérieures et postdoctorales / Dean of the Faculty of Graduate and Postdoctoral Studies

Geology, Gold Mineralization and Alteration of the Horne West Property Rouyn-Noranda

By

Joel Laurin

A thesis submitted to the department of graduate studies
of the University of Ottawa in partial fulfillment of the
requirements for the degree of
Master of Science in Earth Sciences

University of Ottawa

Ottawa, Canada

Your file Votre référence
ISBN: 978-0-494-65540-5
Our file Notre référence
ISBN: 978-0-494-65540-5

Table of Contents

Chapter 4. Alteration and Gold Mineralization

Chapter 5. Summary and Conclusions

Appendices

References

Abstract

The Horne deposit in the Noranda Mining Camp, northwestern Quebec, is one of the largest volcanic-hosted massive sulfide deposits in the world. Nearly all historical production came from massive sulfide orebodies; however, the occurrence of widespread disseminated gold mineralization has been well established. A new exploration program by Xstrata Copper Canada and Alexis Minerals Corporation was initiated in late 2006 to evaluate the mineral potential of the Horne West occurrence, located ~1km to the west of the Horne deposit. Gold grades in historical exploration drill core from Horne West included 4.56 g/t Au over 14.63 m, 4.27g/t Au over 9.32 m, 5.49 g/t Au over 20.63 m and 3.37 g/t Au over 15.58 m. In addition, significant zinc mineralization was encountered in some of the drill holes. Integration of historical assay data with the results of new drill-core logging indicates two distinct zones of gold mineralization, at the stratigraphic base and in the upper part of the Horne West succession. Surface and subsurface mapping suggests that the mineralization may have formed in a localized basin adjacent to a synvolcanic structure. Sulfide mineralization in the gold zone close to the stratigraphic base of the succession is characterized by sulfide veining and sulfide impregnations in aphyric coherent rhyolite and associated volcaniclastic rocks. The mineralized rhyolite facies association is overlain by a mass-flow derived, fining-upward succession of normally-graded wispy clast-rich breccia and sandstone that contains conspicuous pyrite-rich sulfide clasts at the base of coarse-grained beds. A second zone of gold mineralization is located within the upper portion of the stratigraphic succession within lithic clast-dominated sandstone and breccia, coherent xenolith-bearing rhyolite, and a distinct quartz-phyric rhyolite- and sulfide clast-bearing lithic breccia. The mineralized zone steps up stratigraphically with depth below surface and is typically overlain by, or contained within, a sulfide-clast-bearing volcaniclastic rock interval. Gold

mineralization occurs mainly in discordant sulfide stingers and disseminations. Although field observations indicate that elevated precious metal contents occur in coarse-grained volcaniclastic rocks containing abundant sulfide clasts, the sulfide clasts themselves do not contribute significantly to gold grade. These sulfide clast-bearing mass-flow derived volcaniclastic deposits define a broad paleo-seafloor position within the volcanic succession where massive sulfide mineralization occurred down dip or along strike. The gold-rich disseminated and stinger sulfide mineralization and alteration at Horne West occurred in spatial and temporal association with the seafloor massive sulfides that were the source of the sulfide clasts. Distribution of gold is controlled in part by the shallowly emplaced synvolcanic coherent rhyolite intrusions that may have intruded along, or acted as barriers to, an area of hydrothermal upflow and mineralization. Late mafic intrusions, which occur more prominently in the mineralized zones and possibly along synvolcanic structures, have remobilized gold locally.

Acknowledgements

Thanks to the friends and colleagues at the department at the University of Ottawa for your support and encouragement. There really are too many of you to name! Hello and thanks to all the friends I have made over the past few summers in Noranda: Russel, Abhidheya Wright, Lindsay Moore, Diana Kuiper and others. Thanks to the many partners who collaborated with me on this project. Thanks to Louis Martin, Pierre Riopel, and the whole gang at Xstrata Copper Canada Exploration for the interest they showed in me and for the opportunity that I had to learn and grow in knowledge with you. Thanks to Denys Vermette and others at Alexis Minerals who made this project possible and fun. Thanks to Benoit Dubé, Patrick Mercier-Langevin and others with the GSC who have always been encouraging and patient. Thanks to the ever enthusiastic and interested Jean Goutier and Harold Gibson. Thanks to my brothers, sisters and parents for being there for me. Special thanks to Thomas Monecke and Mark Hannington for showing so much patience and for being so positive. I hope the results of this study help.

This project was funded by a joint venture of Xstrata Copper Canada Ltd, Alexis Minerals Corporation, and the University of Ottawa as well as the TGI-3 Program of the Geological Survey of Canada. Support was also provided by the Society of Economic Geologists.

Foreword

This study omits detailed information concerning the grade and tonnage of this gold occurrence to protect the interest of the exploration companies involved. Discussion focuses on the distribution of gold and alteration relative to the volcanic lithofacies, the origins and significance of the sulfide and gold mineralization, as well as the paleoenvironmental reconstruction of the volcanic succession.

1. Introduction

The Horne Deposit in the Noranda Mining Camp, northwestern Quebec, is one of the largest volcanic-hosted massive sulfide deposits in the world. Nearly all historic production came from massive sulfide orebodies, however the occurrence of widespread disseminated gold mineralization has been well established. Gold grades in historic exploration drill core related to Horne West property, located ~1 km from the Horne deposit included 4.56 g/t Au over 14.63 m, 4.27g/t Au over 9.32 m, 5.49 g/t Au over 20.63 m and 3.37 g/t Au over 15.58 m. In addition, significant zinc mineralization was encountered in some of the historic drill holes. A new drilling exploration program by Xstrata Copper Canada and Alexis Minerals Corporation was initiated in late 2006 to evaluate the mineral potential of Horne West, providing a unique opportunity to map the gold and sulfide mineralization, rock alteration, and stratigraphic relationships in the vicinity of the giant Cu-Zn Horne deposit.

The major objectives of this study were to establish the relationship between gold and sulfide mineralization and the volcanic stratigraphy of the Horne Block, and to document the origin and character of distal sulfide clast-bearing units within the Horne stratigraphy. The stratigraphic context and facies characteristics of the sulfide clasts-bearing units were used to assess whether new massive sulfide mineralization might be present along strike or at depth below the Horne West outcrops. New geochemical information and information concerning the depositional environment, distribution of sulfide-bearing clasts, alteration, and gold mineralization in this study have provided new insight into the mineral potential of the area and will help to focus future exploration efforts. The origin and timing of the gold mineralization, the structural and stratigraphic relationships of the Horne Block to the rest of the mining camp, and the unusually large size and high gold grade of the Horne deposit compared to the other massive

sulfide deposits of the district have been important questions. The information provided in this study contributes to the answers to some of these questions. Previous studies focusing on the stratigraphy of the Horne Block that include details about the Horne West property are limited. They include works by Price (1934-1949) focusing principally on the Horne Mine, and more recent reports by Kerr and Mason (1990) and Kerr and Gibson (1993). Current mapping and sampling of the surface rocks by Dr. Thomas Monecke and Dr. Harold Gibson have been reported in Monecke et al. (2008). The present study focuses principally on data collected from drill core, new and old, most of which originates from the Remnor mining project that ceased in the early 1980s. This work was carried out with other researchers in the area as well as the exploration companies.

2. Regional Setting

2.1 Geological setting

The study area is located within the Archean Blake River Group (BRG) in the Abitibi subprovince (Figure 1) of the Superior Province. The BRG volcanic succession has a stratigraphic thickness of 13 km that originally covered an area of 200 by 80 km (Baragar, 1968; Goodwin, 1982). The Destor-Porcupine and Cadillac-Larder Lake faults delimit the BRG to the north and south, respectively. The BGR is interpreted to have formed in a primitive rifted arc setting (rifting occurred in oceanic lithosphere in proximity to an oceanic arc) and has been compared in size and tectonic origin to the Monowai caldera located within the Kermadec and Tonga-Fiji suprasubduction tectonic zone (Gibson and Galley, 2007). The volcanic rocks belonging to the BRG have been divided into six formations that were deposited by relatively continuous submarine volcanism between 2704 and 2696 Ma in an environment that was dominantly below storm wave base (Kerr and Gibson, 1993; Gibson and Kerr, 2000; Gibson and Galley, 2007). The six formations lack bounding unconformities and may represent a single regional volcanic complex or several overlapping volcanic edifices typified by discrete episodes of volcanism (Gibson and Kerr, 2000; Gibson and Galley, 2007).

The structural style of the six formations of the BRG is variable. The Hebecourt, Rouyn-Pelletier and Reneault-Dufresnoy formations underwent structural shortening, which was accommodated by steep faults and steep isoclinal folds. The deformation produced steeply dipping beds that strike parallel to the bounding faults of the formations (Gibson and Galley, 2007). There is an abrupt change to shallowly dipping (~30 degrees) strata within the central Noranda and Duprat Montbray formations across the bounding faults (Gibson and Galley, 2007).

The central portion of the BRG is occupied by the Noranda Volcanic Complex (NVC) (Gibson and Galley, 2007). The NVC comprises a 7-9 km thick, bimodal volcanic succession that represents at least one volcanic edifice (Figure 2). The complex can be divided into five volcanic cycles that were deposited within <3 m.y. (Gibson and Galley, 2007). Each volcanic cycle typically consists of an andesitic to basaltic, flow-dominated basal unit and a bimodal upper unit that is composed of andesite-basalt and rhyolite flow deposits with subordinate volcaniclastic rocks (de Rosen Spence, 1976; Kerr and Gibson, 1993; Gibson and Galley, 2007).

The central portion of the NVC includes an area of synvolcanic subsidence, referred to as the Noranda Cauldron (Figure 3). This area has a surface extent of 15 by 20 km and is bounded by the Hunter Creek fault in the north and the Horne Creek fault in the south. The western margin of the area of subsidence is occupied by the Flavrian Pluton, whereas the D'Alembert shear is the eastern boundary (deRosen Spence, 1976; Dimroth et al., 1982; Gibson et al., 2000). The Noranda Cauldron is centered on the northeast-trending Old Waite Paleo-Fissure, which is represented by a 1 km-wide sheeted intrusive complex that contains basaltic, rhyolitic, and composite dikes and sills (Gibson, 1990; Gibson and Watkinson, 1990; Gibson and Galley, 2007). The Flavrian Powell Intrusive Complex (FPIC), which consists of the Flavrian Pluton and its faulted equivalent, the Powell Pluton, was intruded into the Old Waite Paleo-Fissure (Kerr and Gibson, 1993; Gibson and Galley, 2007). The FPIC has been described as a multiphase intrusion that contains numerous shallowly dipping sill-like felsic intrusions, with rocks dating from 2701 to 2697 Ma (Mortensen, 1987). It is considered to be a late intrusive equivalent of the shallow magma chamber that fed volcanism within the NVC (Kerr and Gibson, 1993). Evacuation of the magma from magma chamber(s) related to the FPIC is inferred to have been the cause of subsidence within the NVC (Kerr and Gibson, 1993; Gibson and Galley, 2007).

Stratigraphic reconstruction of the NVC by Gibson and Galley (2007) indicated that a minimum subsidence of 0.5 km and 1.2 km occurred along the northern and southern margins of the Noranda Cauldron, respectively. An additional subsidence of 1-2 km took place within the Delbridge Cauldron that is located at the south margin of the Noranda Cauldron (Gibson, 1990; Gibson and Kerr, 2000). Recently, the occurrence of several larger subsidence structures has been proposed for the Blake River Group, including the New Senator Caldera and the Misema Caldera, the latter possibly encompassing the entire BRG (Pearson, 2005).

Metamorphism in the Noranda district ranges from subgreenschist facies to the greenschist-amphibolite facies transition and is attributed largely to burial and local contact metamorphism (Goodwin, 1982; Powell et al., 1995). Low-grade metamorphism of the NVC occurred between 2677 and 2643 Ma (Powell et al., 1995). Field observations suggest that the study area was only affected by subgreenschist facies metamorphic conditions (Powell et al., 1995) although higher grades are represented in the Horne Block closer to the Cadillac Larder-Lake Fault.

2.2 Volcanogenic massive sulfide deposits

The NVC hosts 30 significant base metal occurrences (Figures 1 and 2), including at least 20 deposits that have been mined in the past (Gibson and Galley, 2007). Most deposits are located in the Noranda Cauldron and individually are less than 5 Mt in size. These deposits are hosted by mafic or felsic flow deposits (Gibson, et al. 1993; Gibson and Galley, 2007). The flow-hosted VMS deposits typically consist of concordant lenses of massive sulfides that are cone or mound shaped and underlain by vertically extensive, discordant stockworks of stringer mineralization and vertically extensive well-defined alteration pipes. These alteration pipes

consist of a core of Fe-rich chlorite that grades outwards through Mg-rich chlorite into sericite at the margins. Intense silicification occurs in the immediate footwall of the massive sulfides. The flow-hosted massive sulfide deposits formed at, or close to, the former seafloor as evidenced by the occurrence of fine-grained silicified volcaniclastic rocks observed on a horizon lateral to the deposits and referred to as exhalites (Gibson and Galley, 2007). These fine-grained volcaniclastic rocks record a hiatus in volcanism within the NVC and were probably formed by suspension-sedimentation of ash particles derived from explosive volcanism taking place outside the NVC.

Two of the largest and most gold-rich deposits in the NVC are the Horne (54 Mt grading 6.10 g/t Au) and Quemont (16.65 Mt grading 5.50 g/t Au) deposits, which occur close to the southern margin of the Noranda Cauldron and are hosted in predominantly felsic volcaniclastic successions within the Rouyn-Pelletier and Noranda formations, respectively (Gibson and Galley, 2007). Together they constitute more than 50 % of the total tonnage of massive sulfides within the main Camp. Volcaniclastic-hosted deposits in the NVC tend to form sheet-like sulfide lenses that are underlain by diffuse and vertically restricted or semiconformable zones of sulfide veins and disseminations. Sericite dominates the footwall alteration zones, but Fe-rich chlorite occurs locally in narrow zones that crosscut sericite-quartz alteration. The orebodies of the volcaniclastic-hosted deposits were largely emplaced by sub-seafloor replacement processes (Gibson and Galley, 2007).

More than 90% of the past producing VMS deposits occur within the subsidence structure of the NVC. Gibson and Galley (2007) suggested that one factor contributing to the high concentration of deposits in this area was that hydrothermal activity occurred coevally with subsidence. The locations of most deposits within the NVC are controlled by synvolcanic faults,

some of which may have accommodated the subsidence. These faults were later replaced or intruded by swarms of dikes and sills of varying composition (Gibson and Galley, 2007).

In addition to volcanogenic massive sulfide deposits, the Noranda District also contains 19 small orogenic gold deposits, including the Chadbourne deposit, and intrusion-related base metal deposits including the Don-Rouyn Cu-Mo porphyry deposit (Gibson and Galley, 2007).

2.3 The Horne Mine and the Horne Block

The Horne deposit is hosted by the Rouyn-Pelletier formation. It is located within the east-west trending Horne Block that is situated outside the Noranda Cauldron and bounded to the north by the Horne Creek Fault and to the south by the Andesite Fault (Gibson et al., 2000). Structural complications within the mine area are caused by a NE-trending set of curviplanar splays off the Andesite fault that slice the volcanic succession into a number of smaller blocks.

Volcanic strata within the Horne Block face to the north, have a subvertical dip and strike east-southeast in the vicinity of the main orebodies. According to Gibson et al. (2000), the up to 900 m-thick volcanic succession forming the Horne Block is dominated by felsic volcaniclastic rocks, with less abundant rhyolitic lobe-hyaloclastite lava flows and related autoclastic breccias, as well as minor dacitic lava flows and cryptodomes (Gibson et al., 2000). The volcaniclastic rocks of the Horne Block include monomictic to polymictic volcaniclastic mass flow deposits that were formed by syn-eruptive redsedimentation of volcanic debris and reworking of previously existing volcaniclastic deposits (cf. McPhie et al. 1993).

Kerr and Gibson (1993) divided the Horne succession into three conformable members from footwall to hanging wall referred to as West 3913, Main Mine, and Remnor, respectively

(Figure 4). The lowermost West 3913 member contains three known zones of Au-rich sulfide mineralization including the New Zone and West Zone.

Within the Main Mine member two principal horizons of sulfide mineralization are present (Figure 4). Most of the historic production of the Horne deposit came from the Upper H and Lower H orebodies, which occur between the surface and a depth of 950 m in the lower part of the Main Mine member (Gibson et al., 2000). These orebodies are bowl-shaped in mine plan, but elongate down-dip. Both massive sulfide lenses are locally underlain by stringer and disseminated sulfide stockwork zones that are contained within a broad discordant alteration pipe that extends at least 450 m stratigraphically below the orebodies. The massive sulfide lenses are stratabound and occur at the same stratigraphic horizon suggesting that they were coeval (Gibson et al., 2000). They are interpreted to have formed from two separate hydrothermal vent sites within a synvolcanic graben-like structure (Gibson et al., 2000). The massive sulfides are primarily composed of pyrite and pyrrhotite with lesser amounts of chalcopyrite, magnetite, and sphalerite, as well as traces of native gold and Au-Ag tellurides (Price, 1934; Gibson et al., 2000).

In addition to the Upper H and Lower H orebodies, significant sulfide mineralization is located within the presently subeconomic No. 5 Zone, also belonging to the Main Mine member but stratigraphically above the Upper and Lower H orebodies (Figure 4) (Gibson et al., 2000). The No. 5 Zone is a tabular and stratiform zone of gold-bearing disseminated pyrite containing less abundant stringers and irregularly shaped bodies of massive sphalerite hosted by intensely sericitized and silicified felsic volcanic rocks (Sinclair, 1971; Gibson et al., 2000). The No. 5 Zone is oriented at approximately 284/90 and extends to a depth of at least 2650 m (Sinclair, 1971; Gibson et al., 2000). Massive sulfide fragments that range up to 60 cm in diameter form

part of rhyolitic breccias overlying the No. 5 Zone. These sulfide fragments have been interpreted to originate from massive sulfide of the No. 5 Zone (Sinclair, 1971).

The Main Mine member is overlain by the Remnor member (Figure 4), which contains a series of rhyolite flows. Volcanic rocks of this member host the G orebody that has also been mined (Gibson et al., 2000).

Hydrothermal alteration and sulfide mineralization are widespread and pervasive, affecting almost all volcanic rocks within the Horne Block, including Horne West. Alteration is dominated by quartz-sericite with chloritization locally associated with the most intense sulfide mineralization (Gibson et al., 2000).

The Horne Block has been intruded by at least four types of intrusive rocks, namely porphyritic cryptodomes of intermediate composition, a swarm of mafic to intermediate dikes and sills (referred to in this report as mafic dikes and sills), narrow post-metamorphic syenite dikes of late Archean age, and two thick Proterozoic dikes (Gibson et al., 2000). Gold and sulfide mineralization occur along some of these intrusive bodies which has provoked an ongoing discussion concerning the timing of gold mineralization at Horne (Gibson et al., 2000). The porphyritic cryptodomes of intermediate composition, which are locally amygdular, breached the western side of the Upper H orebody and caused significant remobilization of sulfides. They also contain xenoliths, including some that comprise massive sphalerite and pyrite (Kerr and Mason, 1990). The mafic dikes, thought to represent up to three generations of intrusions, are more prevalent in the upper mine levels (close to surface) and form a complicated network that follow structural elements or bedding contacts in the Horne Block. Many dikes crosscut the succession with little regard for the structure of the orebodies, however some have been observed to crosscut along structural features containing massive sulfide orebodies (Price, 1934). Price (1934) also

suggested that many of these dikes have been altered and replaced by sulfide in the ore zones, leading him to the conclusion that the dikes were emplaced during and after the formation of massive sulfides. Elevated gold grades occur locally on both sides of dikes that crosscut massive sulfide orebodies (Price, 1934). Similar remobilization of gold has been noted along syenite dikes which have been emplaced subsequent to tilting and initial deformation of the volcanic pile (Kerr and Mason, 1990).

3. Geology of the Horne West Succession

The volcanic succession of the study area corresponds to the West 3913 member (Figure 4) as described by Gibson et al. (2000). The study area comprises the western portion of the felsic volcaniclastic rock-dominated, wedge-shaped and fault-bounded Horne Block and is located 1 km west of the Horne Mine (Figure 5). The outcrops host at least two distinct zones of gold and sulfide mineralization referred to as the New Zone and West Zone.

3.1 Structural and stratigraphic setting

The study area is bounded by subvertical faults, the Andesite Fault located to the south and the Horne Creek Fault located to the north, which converge toward the west (Figure 5). The Andesite Fault separates the Horne Block from andesitic rocks to the south. Rocks within the fault zone range in character form quartz-veined, foliated, and brecciated to sharp, and it locally hosts 1 m-thick aphyric mafic intrusions with sharp margins. Northeast-trending splay faults defined by loose breccia intervals branch from of the Andesite Fault at the south margin of the Horne West stratigraphy (see below). The Horne Creek Fault is located approximately 100 m to 150 m north of the northernmost exposed Horne West outcrop and separates coherent aphyric rhyolite of similar appearance on either side (Figure 5). The Horne Creek fault is characterized by a zone up to 10 m thick comprising sheared and foliated rocks, with clay mineral-rich rubble intersections in drill core representing faults. In addition, localized quartz veining and/or a series of sheared zones and faults less than 10 m thick may occur over a span of more than 75 m around the main fault or instead of the fault. The locally spherulitic aphyric rhyolite that is observed up to at least 250 m north of the Horne Creek fault at shallow depths is commonly faulted, veined by quartz and intruded by or mixed with a quartz-feldspar porphyry.

The Horne West study area hosts tabular lithic-dominated sandstone beds in the eastern portion of Horne West outcrop, which are oriented at approximately 284/88. Bedding contacts observed to the west of these tabular beds in outcrop are oriented at approximately 176/83, indicating that some deformation has occurred along the western margin of the succession (Figure 6).

A subvertical fault, oriented at roughly 175/89, cuts the succession. A maximum of 15 m sinistral displacement and vertical movement of lithological units and the West Zone gold zone is inferred to occur along the fault. This fault is observed in the upper portion of the Horne West succession in drill core and is inferred to crosscut the entire Horne Block (see below). The fault is defined by a rubble zone commonly occurring adjacent to and within mafic intrusions. Its orientation was determined from three drill-core intersections with the fault. Small-scale folds with 10 cm limbs have been observed in drill core (Holes HW-07-04, 215 m and HW-07-06, 363 m), and possible localized inversion of stratigraphic top in beds has been observed close to the surface and at depth (Holes HW-07-06 and HW-07-05). However, the typical sequence of lithofacies is preserved throughout the stratigraphic succession despite these local structural elements (see below). The small-scale folds observed in drill core are defined mainly by the deformation of beds and also by deformation of a well-defined fabric in the rock. This fabric, defined principally by the shape of chlorite clasts but also phyllosilicate minerals and other lithic fragments, is observed over the entire outcrop in volcaniclastic rocks and is oriented consistently east-west regardless of the orientation of beds in surface outcrop. This suggests that the formation of this fabric post-dated any deformation that is observed on the outcrop but pre-dates late small scale folds observed in drill core (Figure 6). It cannot be confirmed that this fabric is either related to deformation at the western margin of the succession or represents an axial planar

cleavage. This East-West trending fabric within the Horne Block was likely initially developed during deformation and compaction concomitant with low grade metamorphism of the BRG at which time beds within the Horne Block were tilted so that they are now dipping vertically. The fabric within the Horne Block is well developed compared to neighbouring rocks of the Noranda mining camp due to its proximity to the Cadillac Break as well as its increased susceptibility to deformation as a result of the intense phyllosilicate alteration present in the rocks. However, sulfide mineralization and associated alteration are discordant, as in other pipe like alteration systems in the camp, and are not associated to later transposing structural features.

The Horne West succession contains two distinct types of sulfide occurrence; Clastic sulfides, derived from the breakup of a massive or semi-massive sulfide body, are observed within clastic units in the central portion of the volcanic succession along two principal stratigraphic horizons (see below). The volcanic succession, including these sulfide clasts, has been overprinted by a second generation of hydrothermally introduced disseminated and stringer sulfides which are associated with the widespread chlorite and sericite alteration.

3.2 Lithofacies Description and Interpretation

Eleven lithofacies for the Horne West Succession have been identified in drill core and in outcrop. The lithofacies are separated based on mappable character and are described below in their general order of appearance from stratigraphic base to top. Nomenclature used to describe the facies follows that of McPhie et al. (1993). Angularity and visual classification of clast sorting follow the nomenclature of Powers (1953) and Harrell (1984). The descriptions below are based on core logs for 20 drill holes comprising 5500 m of core (Appendix A).

3.2.1 Quartz-phyric rhyolite

Quartz-phyric rhyolite units have an aphanitic groundmass and are coherent with sharp irregular external contacts (figure 7-1). The one rhyolite interval observed in drill core is 10 m thick. The quartz phenocrysts are approximately ~0.7 mm in diameter and are typically no larger than 1mm, with a two dimensional concentration of approximately 5 phenocrysts per square centimetre.

The quartz-phyric rhyolite is interpreted to be an intrusive rhyolite. Supporting this is the sharp contacts at the top and base of the drill core intersection.

3.2.2 Amygdular clast-bearing lithic breccia

Amygdular clast-bearing lithic breccia (Figure 7-1) contains cobble- to pebble-sized clasts and comprises poorly sorted medium to very thick beds of lithic breccia consisting principally of angular to subrounded clasts of aphyric rhyolite (with more than 5% angular to subrounded, irregular, or wispy amygdular aphyric rhyolitic fragments). The amygdular clasts commonly contain submillimetre- to millimetre-size subparallel elongate amygdules or amygdule-rich zones (tube pumice), or spaced submillimetre rounded or irregular amygdules. The amygdular clast-bearing lithic breccia contains abundant wisps and shards and less common quartz-phyric rhyolite clasts, flow-banded rhyolite, sandstone or granule breccia intraclasts, massive sulfide clasts (typically less than 1cm in diameter) and partly sulfide-replaced clasts up to 10 cm in diameter. Beds typically have a massive non-graded base with a normally graded top, but may also be normally graded throughout, more commonly so in medium or thickly-bedded beds. Beds comprising this facies commonly have accumulations of more dense lithic fragments close to the base and more amygdular fragments and shards in the upper portion. The thickest

and coarsest amygdular clast-bearing breccia beds are up to 10 m thick and locally have lithic boulders up to 32 cm and amygdular clasts more than 12cm in length.

The amygdular clast-bearing lithic breccia is interpreted to have been deposited subaqueous mass flows of pumice and vesicular rhyolite clasts. The character of the flows ranged from concentrated to hyperconcentrated density flows or grain flows and these were generated by transport of debris in a subaqueous environment following volcanic eruptions (Mulder and Alexander, 2001). Bed character, including very thick bedding with lithic clast accumulations at the bases of beds and relatively higher concentrations of amygdular clasts and wispy clasts or shards at the tops, as well as the incorporation of intraclasts, are consistent with resedimented, deep (below wave base) subaqueous, syn-eruptive volcaniclastic deposits as identified by McPhie et al. (1993). A variety of clast types (i.e., Quartz-phyric rhyolite, sulfide clasts, intraclasts, flow banded rhyolite, aphyric rhyolite, and vesiculated rhyolite fragments) likely represent accidental, cognate and accessory materials generated by the volcanic eruption and subsequent mass-flow events.

3.2.3 Aphyric coherent rhyolite

Aphanitic aphyric coherent rhyolite (Figure 7-2) was observed in drill core but also at the base of the Horne West outcrop. The rhyolite is locally spherulitic. Flow banding and perlitic fractures close to the external contacts are also locally observed. Intersections of aphyric rhyolite range from 10s of centimetres to locally greater than 100 m in thickness at the top of the succession. The contacts between the rhyolite and adjacent volcaniclastic rocks vary from sharp and irregular at both the upper and lower contacts to gradational toward monomictic breccia with rotated clasts at the upper contact. Aphyric coherent rhyolite may also terminate against in situ

jigsaw-fit rhyolite breccia or sediment-matrix rhyolite breccia. Polygonal fracture patterns, commonly with 10 to15 cm spacing between fractures, are observed in the rhyolite in drill core locally.

The character of the contacts between aphyric coherent rhyolite and adjacent facies varies widely depending on location in the stratigraphic succession. At the base of the stratigraphic succession rhyolite intervals with sharp upper contacts are interpreted to be intrusive whereas those with upper contacts that juxtapose monomictic breccia with rotated clasts may be extrusive. At the top of the stratigraphic package, the upper contact is not observed and the emplacement mechanism of the rhyolite cannot be constrained, however, it is likely that this is an intrusive rhyolite given the large thicknesses observed lacking autoclastic breccia related to extrusion.

3.2.4 Monomictic breccia with rotated clasts

Monomictic breccia with rotated clasts (Figure 7-3) comprises irregular, angular, shard-like, and curviplanar clasts of rhyolitic material that have been rotated prior to deposition. Beds are commonly very poorly sorted, reverse-graded (locally form 3 mm clasts up to 30 cm clasts), and are thickly to very thickly bedded (up to at least 3 m). Massive or weakly normally graded beds are also observed locally. Beds typically have sharp contacts with overlying volcaniclastic rocks but gradational contacts with the underlying aphyric coherent rhyolite. Clasts are commonly blue-black in drill core and are darker than the surrounding fine-grained irresolvable matrix. The largest clasts are up to 30 cm in diameter and may be subround to subangular. Rounded lithic fragments, flow-banded clasts, and amygdular-clasts are rare.

Monomictic breccia with rotated clasts is closely associated with intervals of aphyric coherent rhyolite intervals near the base of the stratigraphic succession, where aphanitic aphyric coherent rhyolite is locally spherulitic, commonly flow banded or contains perlitic fractures. The monomictic breccia with rotated clasts is typically underlain by an interval of aphyric coherent rhyolite which grades into either reverse- or normally-graded breccia. At least two separate aphyric coherent rhyolite intervals have been observed in drill core that share this relationship with the clast-rotated monomictic breccia. The lower contacts of the aphyric rhyolite associated to the monomictic breccia are typically sharp and interfinger with underlying volcaniclastic materials.

The clast-rotated monomictic breccia is interpreted to be resedimented hyaloclastite formed by quench fragmentation of subaqueously extruded rhyolite equivalent to, and genetically related to, the intrusive aphyric coherent rhyolite but may also represent quench fragmented breccias observed locally at the top and base of intrusive rhyolite bodies. The rotated clasts with curviplanar margins and common reverse-graded beds observed in the clast-rotated monomictic breccia are features that are consistent with resedimented hyaloclastite (cf. McPhie et al. 1993). The local gradational transition from coherent rhyolite to clast-rotated monomictic breccia is also consistent with this interpretation (McPhie et al. 1993). The dark color of the clastic fragments in the clast-rotated monomictic breccia, most likely indicating chlorite content, may reflect post depositional alteration of glass formed by the quench fragmentation process.

3.2.5 Wispy clast-rich breccia and granule breccia

Wispy clast-rich breccia (Figure 7-4) is characterized by an abundance of irregular to angular shard- or flame-like wisps that are typically homogeneously mixed throughout the bed

and are moderately well sorted with respect to each other. These wisps have a preferred orientation (typically bedding-parallel) that defines a fabric. They are dominantly chloritic in composition but are composed of white mica locally. Typically, beds of this facies can be divided into two principal zones: a coarser granule- to cobble-rich base and a coarse clast-poor wisp-dominated top. This facies has been further divided into three subfacies based on bed character and clast content. Together these subfacies occur in a fining-upward normally graded succession in the central portion of the section.

Sulfide clast-bearing subfacies

The sulfide clast-bearing subfacies is characterized by its abundant wisps and massive sulfide clasts that commonly accumulate at the base of the beds, forming poorly sorted to very poorly sorted beds. They are typically normally graded with respect to all clast types but commonly reverse-graded in the few tens of centimetres at the base. Entirely reverse-graded beds are uncommon. The sulfide clast-bearing breccias form broadly channelized or otherwise tabular beds with widths greater than 10 m and thicknesses up to 20 m locally.

The chlorite wisps in this subfacies range in size from very small (sand-sized or less) up to 7 cm at the base of coarse beds, but are commonly ~1.5 cm. The aphyric, non-amygdular, rhyolite fragments range up to 25 cm in diameter and may be normally graded throughout the bed, but the largest rhyolite clasts accumulate at the base of the beds along with dense sulfide fragments. These clasts are angular to subangular and have moderate sphericity (equidimensionality). Rarely, aphyric rhyolite clasts are flow-banded. Uncommon subrounded to subangular quartz-phyric rhyolite clasts up to 30 cm (more commonly 10 cm) are observed and sometimes possess a distinct brown-mauve alteration color due to sulfide disseminations.

Massive sulfide clasts composed of pyrite (some with traces of sphalerite and chalcopyrite) range in size from sand-sized particles to boulders 55 cm across; however, clasts typically do not exceed 20 cm in length in drill core and are more commonly on the order of 5-10 cm. Sulfide clasts are concentrated at the base of beds and are abruptly normally graded relative to other clast types. Smaller sulfide clasts, typically on the millimetre scale but ranging up to outsized clasts of 2 cm, are also observed within the upper wispy clast-dominated portion of normally graded beds. All sulfide clasts are angular to subrounded and have irregular shapes. In addition to massive sulfide clasts, partly sulfide-replaced clasts have been observed. These include rare irregularly shaped sulfide-impregnated sandstone and wispy clast-rich granule breccia intraclasts up to at least 25 cm in length, partly sulfide-replaced coherent rhyolite fragments up to 25 cm, and rhyolite fragments with intense sulfide dissemination or veins that terminate at the clast margin (Figures 9-1 to 9-3). Framboidal pyrite growth occurring in intraclasts, rhyolite clasts, and quartz-phyric rhyolite clasts, is also observed.

Sulfide clast-poor subfacies

The sulfide clast-poor subfacies comprises beds that are texturally equivalent to the tops of the sulfide clast-bearing subfacies and is similarly characterized by abundant evenly distributed, homogeneously mixed chlorite, wisps. It contains granule- to cobble-sized lithic fragments locally at the base of beds; however sulfide clasts or partly sulfide-replaced clasts are rare or absent and the coarse basal portion of the beds are reduced in thickness compared to the sulfide clast-bearing subfacies or may be absent. Bed thickness varies from thin to more commonly very thick. Beds are typically normally graded but may be reverse-graded and locally alternate between intervals rich in wispy clasts and intervals rich in sand-sized particles close to

the tops. Wispy clasts in this subfacies commonly range from 1 to 30 mm, with a maximum size of 5 cm. Lithic fragments are angular to subrounded, up to 10 cm in diameter, and are composed of aphyric rhyolite.

Amygdular clast-bearing subfacies

This subfacies comprises a series of medium- to very thickly bedded sulfide clast-poor, wispy clast-rich breccia beds that contain amygdular clasts. The beds are poorly sorted, normally graded and contain abundant evenly distributed, homogeneously mixed chlorite wisps and subangular to angular aphyric rhyolite fragments up to a maximum of 5 cm in length. Rarely, these beds are normally graded with wisp-poor, lithic clast-dominated tops.

The wispy clast-rich breccia is interpreted to represent resedimented syn-eruptive volcaniclastic deposits (cf. McPhie et al. 1993) formed by mass-flow events generated by subaqueous volcanic eruption. It forms compositionally uniform successions comprising thick mass-flow deposits, beds that have lithic clast-rich bases, shard-rich tops, and intraclasts near the base. The beds are dominated by texturally unmodified juvenile clasts. These characteristics and the doubly-graded structure are consistent with resedimented syn-eruptive volcaniclastic deposits according to McPhie (1993). The wispy clasts are interpreted to be glassy juvenile fragments produced by explosive fragmentation of lava, which have undergone subsequent alteration. Other lithic clasts include massive-sulfide clasts, partly sulfide-replaced volcaniclastic material and rhyolite, quartz phyric rhyolite fragments, and unmineralized intraclasts. These may be accessory, accidental, or cognate pyroclasts generated by the explosive eruption or incorporated by erosion at the base of the flows. The wispy clast-rich breccia was deposited by subaqueous concentrated or hyperconcentrated density flows (depending on structure of individual beds), the

dominant particle support mechanisms being grain-to-grain support and flow turbulence, and grain-to-grain support, respectively (cf. Mulder and Alexander, 2001).

The volcanic clasts in the breccia sometimes have different alteration styles and sulfide replacement characteristics. The heterogeneity suggests that these altered clastic materials were mineralized or altered prior to their deposition and might have originated from separate source areas or an area that has a heterogeneous substrate.

3.2.6 Xenolith-bearing coherent rhyolite

This facies comprises aphyric and aphanitic coherent rhyolite, locally with perlitic texture, that contains mafic xenoliths (Figure 7-5). The contacts between the xenolith-bearing rhyolite and adjacent rocks are typically sharp and irregular, rarely with a chilled or darkened margin. Flow banding and decimetre thick in situ jigsaw-fit breccia are also observed locally at the top or basal contacts. Flow banding is also observed within the rhyolite adjacent to the mafic xenoliths. The xenoliths range from dark green to black in color and commonly have a peppery granular or phaneritic texture. The xenoliths commonly have highly irregular margins and range in size from 2 to 60 cm in length in drill core but are more commonly ~10 cm. Xenoliths are principally distributed in the central "core" portion of the rhyolite, have a normally graded distribution where observed in outcrop (Monecke et al., 2008) and commonly occur together in groups; other portions of the rhyolite may be free of xenoliths. Jointing, in which fractures that are oriented perpendicular to the contact between the rhyolite and volcaniclastic materials, is also observed in outcrop. On surfaces perpendicular to the contacts the interconnecting fractures form polygonal fracture patterns that are 10 to 15 cm in diameter.

The xenolith-bearing rhyolite is interpreted to be intrusive (Monecke, et al., 2008) based on the sharp upper contacts with localized flow banding and breccia. The rhyolite occurs adjacent to, and cuts across, different facies that may have otherwise formed part of a continuous stratigraphic succession.

The existence of texturally similar xenolith-bearing rhyolite clasts in the overlying quartz-phyric rhyolite clast- and sulfide clast-bearing lithic breccia suggests that xenolith-bearing rhyolite, was locally extrusive or exposed at the surface nearby by a fault scarp and was caught up in other units as accessory or accidental fragments. However this exposure did not occur within the study area as the textural evidence suggests that the xenolith bearing rhyolite was intrusive wherever it has been observed in drill core or in outcrop. The origin of the mafic xenoliths is not known.

3.2.7 Lithic clast-dominated breccia and sandstone

The lithic clast-dominated breccia and sandstone (Figure 7-6) comprise beds dominated by angular to subrounded lithic fragments. This facies has been divided into two subfacies; one composed entirely of sandstone and another composed entirely of granule- to cobble sized breccia fragments. The lithic clast-dominated breccia and sandstone can be separated from other facies based on the quantity (>50 vol.%) of subrounded lithic particles in the matrix, the lack of intact juvenile volcanic rock fragments, and in certain cases by bed structure and thickness and clast sorting, which can range from poorly sorted to moderately well sorted. Although the end members are commonly separated, single beds that contain both subfacies and are abruptly or, less commonly, gradually normally graded from cobble-, pebble- or granule-sized fragments to medium-grained sand-sized particles are observed in drill core and in outcrop. Combinations of

these lithic clast-dominated beds locally form accumulations that are 20 m thick (Figure 10). Where observed in outcrop the lithic-clast-dominated breccia and sandstone are tabular in shape and are laterally continuous over distances greater than 5m.

Breccia subfacies

The lithic clast-dominated breccia subfacies (Figure 7-6) comprises beds formed by cobble- to granule-sized fragments. Many clast types have been observed in the breccia including lithic fragments, wispy clasts, rare quartz-phyric rhyolite clasts, single quartz crystals, amygdular grains, and massive sulfide clasts up to a maximum of 10 cm. The clasts range from subrounded to angular. Beds, that may include a sandstone top, range from thinly bedded to, more commonly, very thickly bedded, but they do not typically exceed 2 m in thickness. The beds are poorly sorted and normally or reversely graded, or rarely not graded at all, and tend to contain clasts that reflect the composition of stratigraphically adjacent clastic units. Erosive scours up to approximately 25 cm deep are observed at the basal contact of coarse-grained breccia beds in outcrop.

Sandstone subfacies

Individual beds of lithic clast-dominated units composed entirely of sand-sized particles (Figure 7-6; very coarse upper to upper-fine sandstone) range from very thinly bedded up to thickly bedded (most commonly thin- to medium-bedded) with planar lamination defined by grain distribution. Sandstone dominated intervals with rare intermittent granule- to pebble-breccia horizons can reach thicknesses of up to 10 m (Hole HW-07-05). The sandstone typically contains greater than 70 vol.% lithic fragments, although they may contain chloritic wisps or

fragments of wisps, similar to those found in the wispy clast-rich breccia. Individual 1 mm equidimensional quartz crystals have been observed locally. The sandstone beds are poorly to moderately well sorted. Angular to subrounded sulfide clasts up to 1.5 cm composed primarily of pyrite are rarely observed at the base of the beds.

The lithic clast-dominated sandstone and breccia are interpreted to be deposits formed by redeposition of volcaniclastic materials through turbidity flows and concentrated density flows (cf. Mulder and Alexander 2001). Materials in the deposits may have been generated by mass wasting of unstable terrain upslope and thus reflect the composition of the source material. However, thick sequences of tabular sandstone with localized breccias may also represent overbank deposits (overbank turbidity flows and/or concentrated density flows) generated by nearby channelized flows. This seems likely where the lithic clast-dominated facies overlies or underlies coarser deposits such as quartz-phyric rhyolite clast- and sulfide clast-bearing lithic breccia (see below). The incorporation of clast types related to the quartz-phyric rhyolite- and sulfide clast-bearing lithic breccia, as well as the relatively high degree of sorting are consistent with this interpretation. In particular, the relatively high degree of sorting, the presence of subrounded volcanic clasts, and the paucity of intact juvenile fragments are features that are consistent with post-eruptive resedimentation processes (cf. McPhie et al. 1993). The predominance of mass-flow bedforms and medium- to very thickly bedded tabular beds, as opposed to those dominated by traction current bedforms, is consistent with deposition in a deep subaqueous setting (McPhie et al. 1993).

3.2.8 Quartz-phyric rhyolite clast- and sulfide clast-bearing lithic breccia

The quartz-phyric rhyolite clast- and sulfide clast-bearing lithic breccia (quartz-phyric rhyolite clast breccia; Figure 7-7) is a pebble to boulder breccia that contains more than 50 vol.% lithic fragments, consisting of aphyric rhyolite, quartz-phyric rhyolite, and sulfide clasts. This facies is distinguished from Facies 3.2.7 based on sorting, heterogeneity of clast types, grainsize, and relative abundance of quartz-phyric rhyolite clasts and sulfide clasts. The beds are dominated by lithic fragments, are poorly sorted to very poorly sorted, and are commonly normally graded with granule breccia and sandstone tops equivalent to the lithic clast-dominated breccia and sandstone described for Facies 3.2.7 above. Less commonly they are massive and structureless, and may be thickly bedded or very thickly bedded, up to 6 m. The bottom few tens of centimetres are commonly reversely-graded, and the lower 2 m of a bed may contain up to 50 vol.% massive sulfide clasts and/or partly replaced sulfide clasts. As much as 50 cm of erosion occurred locally by scouring at the base of beds in outcrop (Monecke et al., 2008). Sulfide clasts that are more than 20 cm in diameter commonly create loading structures such as indents, depression, or deformation of the sediment below, where they are deposited along the basal contact of the beds.

The quartz-phyric rhyolite clasts in this facies range up to 1 m in length but are more commonly close to 15 cm. Massive sulfide clasts are up to 1.05 m in length in drill core but are typically no larger than 20 cm in length. This facies also contains a large number of other materials including flame-like wispy clasts, typically no longer than 2 cm, amygdular wisps and/or lithic fragments up to 15 cm in length, aphyric rhyolite clasts up to 45 cm in length, and rare xenolith-bearing rhyolite clasts that are texturally similar to the underlying xenolith-bearing

rhyolite. Flow-banded aphyric rhyolite clasts up to10 cm across and, rarely, mafic clasts similar to the mafic xenoliths in the xenolith-bearing coherent rhyolite are also observed.

In addition to the massive sulfide clasts this facies contains a large number of clasts that are partly replaced by sulfides, including quartz-phyric rhyolite or aphyric rhyolite clasts, locally with colloform pyrite or pyrite rims (see below). Intraclasts and partly sulfide-replaced intraclasts of lithic clast-dominated breccia and sandstone and chlorite wisp-rich breccia are also observed. Most clast types range from subrounded to angular in shape but are more commonly angular. Lithic clasts, sulfide clasts and quartz-phyric rhyolite are subspherical to lozenge-shaped, predominantly with bedding-parallel long-axis orientations.

The quartz-phyric rhyolite- and sulfide clast-bearing lithic breccia occurs in channelized or tabular beds. Beds commonly occur together in groups in drill core and outcrop and are deposited on top of, or are intercalated with, lithic-clast-dominated sandstone and breccia. The lack of compositional uniformity and the presence of some unabraded juvenile fragments, such as the flame-like wispy clasts, are consistent with resedimented syn-eruptive deposits (cf. McPhie et al. 1993). Alternatively, they may be deposited during post-eruptive resedimentation involving mass wasting of unstable volcanic rocks upslope. The presence of a wide variety of volcanic and non-volcanic clast types of variable composition and the rounding of volcanic clasts are features consistent with volcanogenic sedimentary mass flow deposits as outlined by McPhie et al (1993). The mass-flow bedforms are also consistent with a deep subaqueous (below wave base) setting (McPhie et al. 1993). The normally graded beds with sandstone tops may have been formed by concentrated density flows which have grain-to-grain support, and flow turbulence as their dominant particle support mechanisms (cf. Mulder and Alexander, 2001). Some of the thicker ungraded structureless beds may record deposition of subaqueous hyperconcentrated

density flows (or grain flows) which are predominantly grain-to-grain supported and which are common in steep-slope environments (Mulder and Alexander, 2001).

The heterogeneity of sulfide replacement, host materials, and even alteration style of sulfide-enriched clasts suggests that they were altered and mineralized prior to their deposition, and that they might originate from separate source areas or a heterogeneous substrate. Clasts were incorporated into the beds most likely as a combination of mass wasting of previously mineralized rocks near hydrothermal vents or a massive sulfide mound or by erosion at the base of the flows. Volcano-tectonic processes, such as doming or earthquakes, may have played a role in triggering these mass-flow events.

3.2.9 Suspended intraclast and cobble-boulder breccia

The suspended intraclast and cobble-boulder breccia (Figure 7-8) is only observed in drill core and comprises boulders, rafts, and intraclasts suspended in sand- to granule- sized sediment matrix up to 35 m thick. Intraclasts and rafts commonly have distorted bedding and are composed of wispy clast-rich breccia and lithic clast-dominated sandstone and breccia. Intraclasts and lithic fragments may also be chloritized and/or sericitized and contain sulfide disseminations or laminations. Quartz-phyric-rhyolite clasts up to 9 cm and sulfide clasts have been observed. Aphyric rhyolite clasts up to 70 cm, some with sulfide veining, are also commonly observed in drill core (Holes HW-07-06 and HW-07-07)

This facies is interpreted to have been deposited by a cohesive debris flow in which the dominant support mechanism during transport was matrix strength (cf. Mulder and Alexander, 2001). Many of the distorted intervals of sedimentary material are interpreted to be large intraclasts and rafts. Very poor sorting overall, outsized clasts in a finer matrix, and intraclasts

and rafts with distorted bedding, indicate that little mixing occurred during transport and that the intraclasts were not completely lithified. In common with the wispy clast-rich breccia and the quartz-phyric rhyolite clast breccia, the heterogeneous sulfide enrichment and alteration supports the concept that the clastic materials were altered and/or mineralized prior to deposition.

3.2.10 In situ jigsaw-fit rhyolite breccia

In situ jigsaw-fit breccia (Figure 7-8) comprises angular clast-supported aphanitic aphyric rhyolite breccia that occurs within or at the margins of coherent rhyolite. The breccia consists of tightly packed, angular, monomictic clasts that have undergone little or no rotation or movement. Clast sizes range from sand-sized particles to boulders but are commonly to 5 to 10 cm across. Flow-foliated clasts are also locally observed. In drill core intersections of in situ jigsaw-fit breccia up to 7 m but ranging down to decimetre scale are observed, commonly at the contacts of the aphyric coherent rhyolite or xenolith-bearing coherent rhyolite intervals.

The in situ jigsaw-fit breccia is interpreted to have formed by quench fragmentation at the lower and upper contacts of intrusive rhyolite.

3.2.11 Sediment-matrix rhyolite breccia

Sediment-matrix breccia (Figure 7-9) comprises aphyric rhyolite breccia fragments, commonly ranging from 2 to 15 cm in size, hosted within and supported by sand- to granule-sized volcaniclastic material. The fragments are subangular to subrounded, and some have curviplanar margins. The sediment matrix breccia occurs adjacent to, and locally grades into, aphyric coherent rhyolite with thicknesses ranging from 10 cm up to 10 m. The coherent aphyric rhyolite in contact with the sediment-matrix breccia may be flow-banded and has sharp or

irregular margins that may be chilled at both the upper and lower contacts. Inclusions of sedimentary material ranging up to 20 cm in length are commonly observed in the coherent rhyolite close to the contact with sediment-matrix breccia.

The sediment-matrix rhyolite breccia is interpreted to be formed by intrusion and intermingling of rhyolite into unconsolidated, wet volcaniclastic material. This type of breccia is commonly referred to as peperite (Skilling et al., 2002).

3.3 Mafic intrusions

Mafic intrusive rocks observed in drill core range from aphanitic to phaneritic in texture with less than 1 mm-sized blocky- to blade-like crystals of pyroxene and plagioclase, and commonly grade from a chilled margin toward increasing grain size away from the contacts of the basalt (Figure 8). The contacts between the mafic intrusions and the wall rocks are commonly sharp with a glassy margin less than 5 cm thick occurring in the intrusion and chloritization occurring in the adjacent wall rock. Separate centimetre-scale lobate bodies of mafic material intermixed with volcaniclastic material are observed locally at the contacts, most commonly in the wispy clast-rich breccia. This suggests that at least some of the mafic intrusions intruded into unconsolidated volcaniclastic material. Carbonate-epidote-quartz veins are commonly observed in the mafic intrusions.

3.4 Sulfide-bearing clasts

Sulfide-bearing clasts occur mainly along two stratigraphic horizons: at the base of the fining-upward normally graded succession of wispy clast-rich breccia and within quartz-phyric rhyolite- and sulfide clast-bearing lithic breccia (Figures 10-1 to 10-4). However, less abundant

sulfide-bearing clasts are also observed throughout the central portion of the succession in volcaniclastic rocks, including in the sulfide clast-poor wispy clast-rich breccia and in the lithic clast-dominated sandstone and breccia. The following section focuses on examples from the two principal horizons (Figures 9-1 to 9-3).

Sulfide-rich clasts in the Horne West succession include clasts with less than 5% sulfide to massive sulfide clasts (typically composed of more than 90% sulfide with some quartz). Sulfides occur within or replace quartz-phyric rhyolite, aphyric rhyolite, or volcaniclastic material, which may have been cemented together by sulfides (Figures 9-1 to 9-3). A wide variety of characteristics are observed in these partly sulfide-replaced clasts. Examples include clasts with disseminated or stringer sulfides, including some with stringers that terminate at the margin of the clasts. These clasts have chlorite-rich rims adjacent to the sulfide veins and sericitization occurring throughout in the remainder of the clast. Some clasts of quartz-phyric or aphyric rhyolite also contain sulfide disseminations to semi-massive sulfide. These commonly have a mauve-brown colour, presumably caused by finely disseminated pyrite and sphalerite. Some partly sulfide-replaced clasts are composed of clastic material (including different types of clasts) cemented by pyrite. Similar intraclasts or clasts with little sulfide mineralization but with alteration that differs from in situ hydrothermal mineralization (see below) are also locally observed. These include intraclasts of chloritized wispy clast-rich breccia that contain other sulfide clasts and pinkish to strongly sericitized clasts.

The massive sulfide clasts include massive recrystallized granular aggregates of pyrite with quartz distributed throughout, or colloform pyrite crusts that have quartz-rich zones between the colloform pyrite. In some sulfide clasts there is a mixture of porous pyrite and massive granular pyrite texture within the same clast. Clasts with yellow to white coloured

sericitic portions between the granular or massive pyrite are also observed. Fractures in the massive pyrite are common and are most commonly filled with quartz.

Petrographic analysis of the massive sulfide clasts reveals that the massive pyrite commonly contains minor amounts to traces of sphalerite and chalcopyrite occurring along fractures or as inclusions in the pyrite grains (Figure 9-4). Rarely they contain no sphalerite or chalcopyrite. Euhedral pyrite crystal faces ranging up to 1 mm in size are commonly in contact with quartz within quartz filled voids or fractures. Inclusions and irregularly shaped blebs of sphalerite and chalcopyrite are typically 0.05 mm in diameter. In some massive sulfide clasts the chalcopyrite and sphalerite make up to 25% of the clasts and are concentrated in the core zones of the massive pyrite. Chalcopyrite or sphalerite blebs commonly occur in quartz filled fractures or voids and are typically absent from the adjacent euhedral pyrite that appears to have been recrystallized. Irregular blebs of chalcopyrite in the quartz and in fractures are commonly larger (up to more than 1mm across) than the small inclusions found in the pyrite mass, probably reflecting local remobilization and recrystallization. Some clasts contain rounded to subhedral sphalerite grains typically 0.1-0.2 mm but ranging up to 1 mm, with clusters of very finely disseminated pyrite occurring in the core of the grains. Rarely, 40 um or smaller elongated chalcopyrite inclusions are observed within sphalerite in some clasts (resembling chalcopyrite disease). Some sphalerite is transparent under plane polarized light and is yellow-brown in colour. Sphalerite may also occur as submillimetre-scale bands in colloform pyrite crusts. These textures are interpreted to reflect primary deposition in the volcanogenic massive sulfide environment, as no obvious fabric or evidence of recrystallization is observed there.

Some massive sulfide clasts contain granular quartz masses, with grains typically no larger than 0.02 mm, that resemble fine-grained volcaniclastic material outside of the clast.

However this probably reflects the presence of a volcaniclastic matrix in the massive sulfide from which the clasts were derived. Quartz-filled fractures are commonly observed cutting the clasts; they may contain localized masses (up to 4 mm across but typically less than 1 mm) of bladed to subhedral chlorite (typically less than 0.05 mm) with pale blue extinction under crossed polarizers. Late carbonate veins (1mm) locally crosscut the clasts. Quartz crystals at the margins of the massive pyrite (1 mm or smaller) are commonly aligned perpendicular to the pyrite mass, reflecting infilling of open fractures. Small masses of chlorite are observed locally between the pyrite masses.

Interpreted origins of the sulfide clasts

Several observations clearly distinguish the clastic sulfides from hydrothermally introduced sulfides in the matrix of the volcanic rocks (described below). Sulfide-bearing clasts commonly have alteration that is not consistent with the matrix, and/or of many other clasts, in the host bed (such as mauve-coloured pyrite and sphalerite, or sericite alteration). Clasts within a single bed commonly have a variety of sulfide replacement textures ranging from sulfide stringers to evenly distributed disseminations to massive sulfide. Most of the sulfide clasts are located in beds that have a large average grain size (cobble to boulder) and also contain easily recognizable clast types. The beds that host sulfide-bearing clasts, and that do not occur in strongly hydrothermally altered zones lack sericite or chlorite alteration surrounding the sulfides in the matrix of the bed (strong sericite-chlorite alteration of the matrix is typically only observed near hydrothermally emplaced sulfide disseminations or stringers). As a result these clastic units contain a disproportionate amount of sulfide relative to alteration in the matrix.

Abundant very small (<1 cm), pyrite-rich fragments are commonly found in beds that contain massive sulfide clasts. This rubble may be difficult to distinguish from hydrothermally precipitated disseminated sulfide in the matrix. However, much of this sand- to pebble-sized pyritic material can be attributed to the breakdown of massive sulfide or partly sulfide-replaced clasts during transport. Rarely direct evidence that a sulfide rich portion of a clast has been eroded during transport is observed (Figure 9-2).

The variety of sulfide clasts, ranging from pyrite-dominated to sphalerite-rich to chalcopyrite- and sphalerite-rich, implies that the clasts were sourced from different parts of an eroding massive sulfide body. The variety of associated alteration and host lithologies indicate that the source included a variety of volcanic lithofacies, including quartz phyric rhyolite, aphyric rhyolite, and volcaniclastic rocks (e.g., wispy clast-rich breccia) that were part of the host strata of the parent sulfide deposit. The presence of wispy clast breccia intraclasts in the uppermost horizon of sulfide-clast bearing lithofacies may indicate that transport and deposition of the sulfide clasts was coincident with local volcanic eruptions or that wispy clast-rich material was exposed at the source of the mass flows.

The characteristics of the massive sulfide clasts observed in thin section (i.e., chalcopyrite and sphalerite rich core zones and euhedral pyrite rims and the occurrence of chalcopyrite blebs in the adjacent quartz-rich zones) suggests that there has been at least one episode of recrystallization and local remobilization of sulfide minerals at grain margins and along fractures. However, many of the primary sulfide textures have been preserved. In thin section, chlorite, observed locally within quartz-filled fractures, appears to be a remnant of the original alteration associated with the formation of the massive sulfides. A later generation of quartz was emplaced during the recrystallization of the massive sulfide clasts.

3.5 Stratigraphic architecture

3.5.1 Subsurface architecture

Schematic subsurface representations of the stratigraphy of the Horne West succession are shown in plan view and cross section in Figures 10-0 to 10-4, which were constructed using drill core data. The logged core encompasses a corridor that covers a broad zone close to the surface and a narrower zone (one hole) down depths of more than 600 m (Figures 5, 6 and 11). Two drill cores also were logged from holes located west of the Horne West outcrops (Holes HW-07-02, HW-07-03). The main features of the stratigraphic succession as well as lateral facies changes and relationships, are described in this section.

The base of the stratigraphic succession in the Horne block is dominated by amygdular clast-bearing lithic breccia, in a series of beds up to at least 10 m in thickness. This unit increases in thickness toward the west from less than 5 m to more than 20 m, as seen in plan view at shallow depths. Individual beds also increase in thickness to the west from approximately 5 m to 15 m. This part of the stratigraphic succession was intruded by a 10 m-thick quartz phyric rhyolite, a xenolith-bearing rhyolite intrusion approximately 10 m thick (Hole S-574), and also hosts monomictic breccia with rotated clasts.

Stratigraphically overlying these rocks are localized aphyric coherent rhyolite and monomictic breccia with rotated clasts produced by extrusion onto the seafloor and more abundant aphyric coherent rhyolite emplaced by subsequent intrusion of similar rhyolite into buried volcanic rocks. The thickness of the aphyric coherent rhyolite may be up to 40 m (Hole S-613) but is locally thinner in the central portion of the study area at shallow depths (Hole S-614). Aphyric coherent rhyolite together with monomictic breccia were deposited in at least two stratigraphic intervals by separate extrusive events (Hole S-613), and may be laterally continuous

over more than 100 m locally (Figure 10-1). Monomictic breccia with rotated clasts and in situ jigsaw-fit breccia, produced by autoclastic brecciation at the top or base of intrusive rhyolite, occur in intervals up to 3 m in thickness locally. This lower portion of the stratigraphic succession, including the aphyric rhyolite intrusions, is cut out by the Andesite fault along strike to the east and at depth.

Above these rocks is a fining-upward succession of very thickly bedded, normally graded wispy clast-rich breccia that dominates the central part of the succession. Individual beds have a tabular or broadly channelized geometry spanning more than 100 m in width and may be upwards of 30 m thick (Figure 10-1). The overall thickness of this facies type is up to75 m in some locations. Several successive beds of wispy clast-rich breccia with abundant sulfide clasts dominate the basal portion of this succession, whereas sulfide clast-poor breccia dominates the top. Wispy clast-rich breccia is not observed in the far western portion of the study area. Instead, amygdular clast-bearing lithic breccia and intrusive aphyric coherent rhyolite is observed there (Figure 10-1). The wispy clast-rich breccia is partly cut out by the Andesite Fault at depth and toward the east, but it maintains a similar thickness overall in the eastern part of the study area.

Above the wispy clast-rich breccia is a 50 m-thick succession of lithic clast-dominated sandstone and breccia intercalated with beds of quartz-phyric rhyolite clast breccia. This succession increases in thickness slightly at depth and towards the eastern extent of the study area. Near the base of this succession, suspended intraclast and cobble-boulder breccia is observed but only in the deep eastern portions of the drilled section. Beds of quartz phyric-rhyolite clast breccia are commonly stacked in groups, but individual beds are difficult to correlate with confidence. Two groups of stacked quartz-phyric rhyolite clast breccia are stratigraphically separated by a succession of lithic clast-dominated breccia and sandstone and

can be tentatively correlated (Figure 10-3). The uppermost group is rich in amygdular clasts; the lower group has a higher abundance of quartz-phyric rhyolite and dense massive sulfide clasts. The lower group can be further subdivided into a shallower portion that contains more abundant massive sulfide clasts and quartz-phyric rhyolite clasts and a deeper eastern portion that contains more intraclasts and wispy fragments. Beds that have the greatest abundance of quartz-phyric rhyolite clasts and dense massive sulfide clasts are observed in the shallow west portion (Holes S-574, S-716), shallow east (Hole S-632), and central portions (Hole HW-07-05) of the explored area. The thickest intersection of these rocks is observed in the deep eastern extent of the study area (Hole HW-07-06).

A 10 m-thick interval of xenolith-bearing coherent rhyolite occurs within wispy clast-rich breccia beds and another interval, up to 25 m thick, occurs above within and adjacent to the lithic clast-dominated units. The upper xenolith-bearing coherent rhyolite extends at least 200 m laterally and pinches out towards the east (Figure 10-1). The relationship between the xenolith-bearing rhyolite and aphyric coherent rhyolite, which occurs in abundance along the western extent of the study area, is unclear and they may be related to each other. The xenolith-bearing rhyolite is thicker and is observed at a higher stratigraphic position in the shallower western extent of the study area than in the deeper eastern extent (Figures 10-1 and 10-2). Xenolith-bearing coherent rhyolite occurs in the immediate footwall of quartz-phyric rhyolite clast breccia which contains clasts of the xenolith-bearing rhyolite, indicating that the coherent rhyolite was emplaced prior to the deposition of some of the overlying volcaniclastic rocks.

Above the sandstone, quartz-phyric breccia, and xenolith-bearing coherent rhyolite, is a second sulfide clast-poor wispy clast-rich breccia that is up to of 25 m thick locally, together with beds of amygdular clast-bearing lithic breccia that are up to 10 m thick. The amygdular

clast-rich breccia occurs above the lithic clast-dominated sandstone and breccia and quartz-phyric rhyolite clast breccia in the shallow western portion of the study area (Figure 10-1). In the shallow eastern part of the study area, wispy clast breccia occurs above these units. Both the amygdular clast-rich lithic breccia and the wispy clast-rich breccia at this stratigraphic level pinch out at depth in the section. Sandstone beds followed by amygdular clast-bearing lithic breccia lie above the quartz-phyric rhyolite clast breccia in the deeper parts of the section (Holes HW-07-05, HW-07-06). Finally, the succession is capped by aphyric coherent rhyolite, which is at least 100 m thick locally. Sediment-matrix breccia and in situ jigsaw-fit breccia is commonly observed along the margin of the coherent rhyolite. This rhyolite obscures the distribution of the uppermost volcaniclastic units.

Notable east-west facies changes occur at a location west of the subvertical fault where deformation is observed in outcrop (Figure 10-1). This far western part of the study area is dominated by amygdular clast-bearing lithic breccia and intrusive aphyric coherent rhyolite (Figures 10-1 and 10-2, and Holes HW-07-02, HW-07-03), whereas monomictic breccia, wispy clast rich breccia, lithic clast-dominated sandstone and breccia, and quartz-phyric rhyolite breccia are observed to the east. The zone along which these changes occur is characterized by a change in the bedding orientation from beds oriented east-west in the east to beds to with a north-south orientation in to the west, as well mafic intrusions and late faulting.

3.5.2 Mafic intrusions

Mafic intrusions occur throughout the studied section, including within the Andesite fault locally and within the thick succession of aphyric coherent rhyolite that occurs at the top of the stratigraphic succession. They are more abundant at shallow depths and close to the area in

which late faulting has occurred (Figure 10-1). East-west trending mafic intrusions are commonly observed along bedding contacts in the wispy clast-rich breccia but also crosscut beds that have a north-south (176/83) bedding orientation observed in outcrop (Figure 10). Both subvertical north-south oriented mafic intrusions and east-west oriented intrusions crosscut the volcanic stratigraphy. Sills and dikes are also commonly observed adjacent to and within the xenolith-bearing coherent rhyolite at shallow depths. Subvertically oriented mafic dikes in the central portion of the study area host late faults that are characterized by rubble zones (Figure 10-1). These mafic intrusions could possibly represent several generations of intrusions. Some are intruded after the observed bedding changes in outcrop.

3.5.3 Depositional history and paleo-environment

The explored sections of the Horne West block are part of a complicated volcaniclastic rock-dominated environment dominated by a wide variety of mass-flow deposits, numerous rhyolite intrusions, and localized extrusive rhyolite flows. None of the mass flow deposits show signs of hot deposition. The volcaniclastic stratigraphy can be divided into two main styles of deposition. Thick deposits of wispy clast-rich breccia and amygdular clast-bearing lithic breccia are interpreted to have formed following voluminous explosive volcanic eruptions in the subaqueous environment. Lithic clast-dominated breccia and sandstone and quartz-phyric rhyolite clast breccia were deposited by mass flows related to mass wasting of rocks or sediments upslope or, to a lesser extent, resulting from small volcanic eruptions. The thick deposits formed by explosive volcanism dominate the top and base of the stratigraphic succession, whereas the central part is dominated by mass-flow deposits related to mass wasting or small explosive eruptions.

The sulfide clasts in the succession were derived from at least one massive sulfide body located somewhere along the paleo-seafloor and were deposited along two principal stratigraphic intervals in the lower and central portions of the stratigraphic succession. The lowermost interval of sulfide clasts occurs along the base of a fining-upward succession of normally graded wispy clast-rich breccia, and the uppermost sulfide clasts are hosted in quartz-phyric rhyolite clast breccia.

The increase in the number of quartz-phyric rhyolite clast breccia beds, the decrease in the abundance and size of dense massive sulfide fragments and associated quartz-phyric rhyolite clasts along the same corridor, the thickening of interstratified sandstone beds, and the paucity of intrusive or extrusive rhyolite, towards the deep eastern extent of the study area, suggests that there was a shift from a proximal constructive high to a more distal environment at depth. This is also supported by the presence of cohesive debris flow deposits at depth (suspended intraclast and cobble-boulder breccia, Holes HW-07-06 and HW-07-07) which can have long runout distances and typically come to rest on relatively shallow slopes (cf. Mulder and Alexander, 2001). These facies relationships suggest that the transport direction was down-plunge, from close to the present day surface toward deeper portions of the study area and that the clastic materials originated from areas that are now eroded.

Paleo environmental and topographic reconstruction of the Horne Block by Barrett et al. (1991) places the Horne stratigraphy on the slope of a volcanic edifice with radial, and concentric, synvolcanic faults that host the Horne massive sulfide deposits. The axial faults of the Horne graben have been suggested to represent cauldron margin radial faults, whereas the graben cross faults represent concentric ring structures (Kerr and Mason, 1990; Barrett et al., 1991). It was proposed that the Horne stratigraphy, which is now dipping vertically, was

deposited on the northward slope of the volcanic edifice such that it would be facing the Noranda Cauldron if it where righted without rotation (Barrett et al. 1991). Evidence used to support this reconstruction includes the transition of facies from rhyolite flows and flow breccia at the base of the succession to clastic rhyolitic rocks at the top (in section), as well as the transition from massive rhyolite to breccias to tuffs toward depth (along strike) which reflects transition from a proximal to distal setting relative to a rhyolitic extrusive center (Barrett et al. 1991; Roobol and Hackett, 1987). Observations at Horne West are in agreement with the findings of these authors and record changes down-plunge from proximal to distal relative to a rhyolite extrusive center near the present day surface (Figures 10-7 and 10-8). The distribution of facies and sulfide fragments at Horne West is thus broadly similar in style to the No. 5 Zone, although most likely at a lower stratigraphic interval (older) than the Horne deposit. The upslope massive sulfides, which were the source of the sulfide clasts, have most likely been eroded.

The relative timing of the intrusion of the xenolith-bearing coherent rhyolite has been constrained to the same period in which the succession of lithic clast-dominated sandstone and breccia and quartz-phyric rhyolite clast breccia was being deposited. This is supported by the occurrence of clasts of xenolith-bearing rhyolite in overlying quartz-phyric rhyolite clast breccia. The xenolith-bearing rhyolite is intrusive in character wherever it is observed in drill core and in outcrop, meaning that it was extrusive or was exposed at the seafloor by synvolcanic faults in an area that is not currently mapped. Most likely the exposure or extrusion of xenolith-bearing rhyolite occurred up-dip close to the massive sulfide mineralization at a location that has been eroded.

The aphyric rhyolite intrusions at the base of the succession may have been emplaced following the extrusion of rhyolite onto the sea floor, the latter producing the observed facies

association of curviplanar fragment monomictic breccia with rotated clasts and coherent aphyric rhyolite. This change in style of emplacement likely occurred after the effusive rhyolite was buried by wispy clast-rich breccia. The intrusion of rhyolite into the succession may have caused a doming of the stratigraphy locally, affecting the distribution of overlying volcaniclastic material. These intrusions are closely associated with hydrothermal alteration and mineralization locally (see below).

Discontinuities in facies from east to west may be explained by synvolcanic faulting, or alternatively by folding, as suggested by bedding orientation changes in outcrop. Synvolcanic faulting is consistent with the large thickness changes of wispy clast-rich breccia, lithic clast-dominated sandstone and breccia, and quartz-phyric rhyolite clast breccia from east to west. However, the zone where these changes seem to have occurred is poorly represented in drill core. The mafic intrusions that occur in this part of the succession post-date the felsic volcanic rocks and may have intruded along previously existing syn-volcanic faults. Textures observed locally, such as intermingling of mafic intrusion with sediment, suggest that at least some of the mafic intrusions were emplaced when the succession was not completely consolidated. Potential synvolcanic faults have also been identified in outcrop (Thomas Monecke, personal communication, 2008). Synvolcanic faults previously identified in the Horne stratigraphy are individually of limited vertical extent and are rarely intruded by mafic dikes (Kerr and Gibson, 1993).

Summary of the depositional events

The following is a summary of the relative timing of geological events related to the construction of the Horne West stratigraphy, based on facies relationships and other geological observations in this study.

1) Clast-rotated monomictic breccia (hyaloclastite) related to a nearby, but not observed, extrusive coherent rhyolite was deposited at the base of the succession.

2) Amygdular clast-bearing lithic breccia (resedimented syn-eruptive mass-flow) was deposited, most likely in response to a nearby volcanic eruption.

3) Rhyolite was extruded onto the sea floor on top of the amygdular clast-bearing lithic breccia, producing aphyric coherent rhyolite and associated overlying clast-rotated monomictic breccia.

4) Quartz-phyric rhyolite intruded into the volcanic pile (timing uncertain).

5) Up to 75 m of sulfide clast-bearing wispy clast-rich breccia (these are the first beds rich in sulfide clasts) and sulfide clast-poor wispy clast-rich breccia and sandstone were deposited onto the sea floor in a fining-upward, normally graded succession as mass flows triggered by a series of nearby volcanic eruptions.

6) Aphyric coherent rhyolite intruded into the volcanic stratigraphy at the base of the wispy clast-rich breccia.

7) Tabular sandstone and breccia beds, possibly generated as overbank facies locally, were deposited adjacent to and coevally with beds of quartz-phyric rhyolite clast breccia (these are the second set of beds rich in sulfide clasts).

8) The xenolith-bearing rhyolite was intruded into the pile and locally extruded or was exposed, possibly by synvolcanic faulting. This is demonstrated by the presence of clasts of xenolith-bearing coherent rhyolite in stratigraphically-overlying quartz-phyric rhyolite clast breccia. Older

beds of quartz-phyric rhyolite clast breccia are locally crosscut or lie stratigraphically beneath the maximum stratigraphic level of the xenolith-bearing rhyolite.

9) Tabular lithic clast-dominated sandstone and breccia beds were deposited adjacent to and coevally with quartz-phyric rhyolite clast breccia that locally directly overlies the xenolith-bearing rhyolite (these are part of the second set of beds rich in sulfide clasts).

10) Amygdular clast-bearing lithic breccia, amygdular clast-bearing and sulfide clast-poor wispy clast-rich breccia, and lithic clast-dominated sandstone are deposited at the top of the succession.

11) Aphyric coherent rhyolite was emplaced within unconsolidated volcaniclastic material producing sediment-matrix breccia and in situ jigsaw-fit breccia along contacts locally. This rhyolite caps the volcanic succession defined by the limits of the study area.

4. Alteration and Gold Mineralization

Gold mineralization is spatially associated with two separate stratigraphic intervals or zones, referred to as the New Zone and West Zone (Figure 10). The New Zone lies stratigraphically below the West Zone. Gold assay data from 90 drill cores that penetrate the western Horne Block were used to construct long sections of the mineralized zones (Figures 11-1 and 11-2). Detailed records of the geology, sulfide mineralization, and alteration, from 20 of these drill cores have been used to interpret the origins of the mineralized zones (Appendix A).

4.1 New Zone

Mineralization in the New Zone is situated near the base of the volcanic succession and is roughly conformable with bedding, striking at approximately 281 degrees. In long section (Figure 11-1) the New Zone pinches out at depth and is faulted locally by late splay faults off the Andesite fault (Figure 10). The western limit of the New Zone is poorly constrained from drill core but appears to coincide with important facies changes and/or bedding orientation changes observed in outcrop (Figure 10). To the east, the New Zone and the host stratigraphy are truncated by the north-dipping Andesite Fault (Figure 10).

Gold mineralization in the New Zone occurs mainly within, but not limited to, intrusive or extrusive aphyric coherent rhyolite, and is associated with pyrite-rich veins or stringers up to 1 cm wide (commonly 1 to 3 mm), disseminated euhedral pyrite (up to 1 cm but commonly less than 1mm) and vein-like blebs or masses of granular or fine-grained pyrite (Figures 12-1 to 12-6). Gold-bearing pyrite veinlets also occur in the volcaniclastic rocks adjacent to the coherent rhyolite, including in monomictic breccia with rotated clasts and wispy clast-rich breccia. The pyrite veinlets have a chlorite-rich alteration rim up to 10 mm wide and a sericite halo that

occurs abruptly outside the chlorite and grades away from the margin of the vein or saturates the adjacent wall rock. Chlorite also occurs surrounding the disseminated sulfides, in patches and within the matrix of the host rocks.

At a broader scale, a 10 m-thick zone of moderate to strong sericitization is associated with the New Zone gold mineralization (Holes S-614 and S-575, Figure 12-9). Sericitization occurs as matrix replacement in coherent rocks and within the matrix between clasts in volcaniclastic rocks. Chlorite is less abundant at this scale, as matrix and clast replacement adjacent to and within aphyric coherent rhyolite.

4.2 West Zone

In long section the West Zone comprises two separate areas of high gold concentration with little overlap (Figures 11-1 and 11-2). The first is best developed at surface and pinches out at an elevation of 5125 m; the other occurs at a higher stratigraphic level below an elevation of 5150 m. The true boundaries of the zone have not yet been delimited. The gold zones are not confined to any one bed but occur as broadly conformable intervals within xenolith-bearing coherent rhyolite, lithic clast-dominated breccia and sandstone, quartz-phyric rhyolite clast breccia, and wispy clast-rich breccia (Figure 10).

Sulfide mineralization and alteration in the xenolith-bearing coherent rhyolite is similar to that of the New Zone, with pyrite-rich veins up to 10 mm thick (more commonly from 1 to 3 mm). Narrow rims of chlorite-rich alteration (up to 10 mm wide) and a sericite halo decreases away from the veins (Figure 12-1 to 12-6, Appendix A). Some pyrite veins are associated with chlorite only. Gold-enriched, fine-grained pyrite veins up to 30 mm wide and with sharp margins also occur in volcaniclastic rocks (Hole HW-07-05). In wispy clast-rich breccia, below the

xenolith-bearing coherent rhyolite, the pyrite is mainly disseminated, euhedral to subhedral, and fine-grained (blebs up to 10 mm) with chlorite alteration haloes. Stringers are more common in the coherent rhyolite. Gold is also enriched in sulfide disseminations and within sulfide laminae in lithic clast-dominated sandstone locally (Holes HW-07-06, S-572).

Drill core data reveal a potential spatial relationship between certain mafic intrusions in the West Zone and the incidence of high gold grades. The highest gold grade intersections for the West Zone occur (e.g., Holes S-573, HW-07-04, S-715, S-575, S-716, S-714) in proximity to, and most notably stratigraphically below, certain mafic intrusions in the shallow western portion of the study area (Figure 4). Sulfide mineralization, chloritization and elevated gold grades are also observed adjacent to mafic dikes away from the high grade mineralization in the center of the West Zone (Holes S-631 and S-632, Appendix A). Traces of sulfides occur in mafic intrusions occurring close to zones of relatively strong sulfide mineralization and alteration (Hole S-573). However, mafic intrusions that are observed either within or outside of the gold zones typically have minimal sulfide mineralization and do not possess the same sericitization and chloritization observed throughout the succession. Unlike the hydrothermal alteration associated to gold in the volcanic succession (see below), the mafic intrusions typically have carbonate-epidote-quartz veins. Euhedral to subhedral pyrite cubes up to 4 mm in diameter, occur locally in these mafic intrusions in the groundmass or along quartz-carbonate veins. Mafic dikes with brecciated contacts containing sulfide mineralization and carbonate-epidote-quartz veining are observed locally above a gold zone in Hole S-716. Some of the mafic sills and dikes are altered (sericite +/- silica) to light green-grey or brown color. However, most are unaltered, and there is no correlation between alteration of the dikes and proximity to the gold mineralization zone.

4.3 Alteration

Alteration has been logged based on a relative scale from 0 to 5 (none, traces/weak, moderate, moderate-to-strong, strong, intense) (Appendix A). Sericite and chlorite alteration are observed throughout the Horne West succession. However more intense zones of sericitization and chloritization are observed locally, including some that are associated with specific intrusive rhyolite bodies (Figures 10-5 and 12-9). The observed distribution suggests that there are two principal styles of alteration, namely chloritization and sericitization associated with parts of specific synvolcanic rhyolite intrusions in the western portion of the study area and more widespread background chloritization +/- sericitization.

The most clearly defined alteration in drill core is centered on the xenolith-bearing coherent rhyolite and the coherent aphyric rhyolite that occurs near the base of the stratigraphic succession. Chloritization can be mapped out over the extent of the xenolith-bearing coherent rhyolite intrusion in the West Zone (Figure 10-5). It is strongest in a central area at shallow depths (e.g., Hole S-572), where the rhyolite is altered to dark grey to black. Chloritization decreases outwards towards the east, west and at depth. Sericitization is more closely linked to sulfide mineralization in the xenolith-bearing rhyolite, and occurs with higher intensity towards the margin of the rhyolite intrusion, commonly extending into the adjacent volcaniclastic rocks (Holes S-716, S-714, S-575). Similar patterns are observed in the aphyric coherent rhyolite and associated breccia in the New Zone. Sericite, sulfide, and chlorite alteration and gold mineralization decrease over several tens of metres from the contact with the coherent aphyric rhyolite into the overlying wispy clast-rich breccia (Hole HW-07-04). The alteration surrounding the xenolith-bearing coherent rhyolite and the coherent aphyric rhyolite that occurs near the base of the stratigraphic succession can be summarized this way; Alteration is most intense in areas

with elevated gold grades in the shallow portion of the West Zone and New Zone. Chloritization is stronger than sericitization in the center of the rhyolite bodies, with more abundant sericitization at the margins and in adjacent volcaniclastic rocks. This relationship is observed in S-575 at the New Zone and the West Zone. In S-572 the center of the xenolith-bearing rhyolite is strongly chloritized but contains almost no sulfide mineralization, whereas the margins are strongly sericitized (with chloritization occurring only at the margins of pyrite veins) and contain abundant sulfide mineralization as well as gold (Appendix A).

In the stratigraphically highest part of the West Zone intersected down-plunge, background sericitization is the dominant alteration style and occurs as matrix or clast replacement in the host volcanic rocks. Background chloritization dominates in the wispy clast-rich breccia in the shallow portions of the study area. These rocks also locally contain rare chalcopyrite stringers (Figures 10-5 and 12-3a).

Several intersections (up to 4 m in drill core) of volcaniclastic rocks and coherent rhyolite in the upper portion and lower portion of the stratigraphic succession contain abundant brown, orange, or pink spots comprising epidote and carbonate and/or garnet that are typically 1 mm or less in size (Figure 12-9). This spotted alteration occurs consistently above at least one interval of the West Zone mineralization or below the New Zone. A brightly coloured zone of alteration comprising white mica +/- epidote +/- calcite with traces of hematite occurs at approximately the same stratigraphic interval. This alteration is observed in rocks on both sides of the late subvertical fault. White mica +/- epidote +/- calcite +/- hematite alteration in the aphyric coherent rhyolite at the top of the stratigraphic succession occurs primarily along polygonal fractures but also commonly as background alteration that permeates the rock. Both the spotted alteration and the brightly coloured alteration are patchy and are not easily correlated from hole

to hole but they occur in a consistent stratigraphic position relative to West Zone and New Zone mineralization (Holes S-631, S-714, S-572, S-574, S-576, HW-07-04). Additionally, they are better defined in the shallow western portion of the study area near the surface. This mimics the general distribution of chlorite observed in the xenolith-bearing coherent rhyolite. Although they are spatially associated with mineralization, the white mica +/- epidote +/- calcite +/- hematite and spotted alteration zones are devoid of gold.

4.4 Petrography of sulfides

Stringer veins

Sulfide-rich stringer veins occur throughout the central part of the Horne West succession. They represent approximately 45% of the total sulfides (excluding sulfide clasts) observed in outcrop and drill core. Stringers are most prominent in the aphyric coherent rhyolite as well as the xenolith-bearing coherent rhyolite in the central portion of the succession (Appendix A) but also occur in the central part of the succession as more diffuse stringers in volcaniclastic rocks. Rare chalcopyrite-rich stringers have been observed below the intrusive rhyolite bodies in chloritized or sericitized volcaniclastic rocks (Hole S575, 135 m and Hole S576, 15 m).

The pyrite stringers in the Horne West succession variably contain minor sphalerite and chalcopyrite (Figures 12-3 and 12-4). Stringers are commonly crudely zoned with a pyrite- and/or chalcopyrite-rich core. Crystalline quartz (commonly with length oriented perpendicular to the pyrite faces), muscovite, and sphalerite occur toward the margins of individual veins. Fine-grained masses of chlorite with a blue-black extinction or green bladed crystals commonly occur toward the margin of, or adjacent to, the stringer.

Sulfide laminations

Sulfide laminations are commonly observed in planar-laminated sandstone beds within the stratigraphic succession (Figure 7-6, Appendix A). They represent approximately 10% of the total sulfides (excluding sulfide clasts) observed in outcrop and drill core. In thin section the sulfide laminations are defined by intervals rich in pyrite grains or crystals and quartz, intervals rich in sphalerite grains, and also zones of lozenge-shaped grains or semi-continuous bands and patches up to 2 mm thick that are composed of quartz, pyrite, sphalerite, rare chalcopyrite, and white mica (Figures 12-7 and 12-8). Within these semi-continuous quartz-rich patches, irregular sphalerite grains (up to 0.5 mm) and blebs of chalcopyrite (up to 0.25 mm) are observed, including some sphalerite with fine grained chalcopyrite inclusions (chalcopyrite disease) in the central portion of the grain. Pyrite grains typically have some euhedral crystal faces; irregular or ragged shaped pyrite grains are also observed. Porous pyrite grains with core zones containing voids as well as sphalerite and chalcopyrite blebs, similar to what are observed in massive sulfide clasts, are observed locally throughout. The concentration of pyrite grains sometimes appears to be greatest at the base of individual laminae, gradually decreasing towards the top or more rarely towards the base. Horizons that are rich in sphalerite grains are more diffuse, forming vague laminations (1-2 mm). The sphalerite grains rarely contain inclusions of pyrite or fine-grained chalcopyrite, and the central parts of sphalerite grains are commonly transparent under plane polarized light. The matrix of the sandstone beds that host the sulfides is typically composed of quartz, white mica and variable amounts of chlorite.

While some sulfide laminations appear to represent sulfide impregnation of more permeable layers, some of the sulfide laminations could locally be clastic sulfides. In particular, the sand-sized grains of sphalerite in the sandstone and some porous pyrite grains are interpreted

to represent sulfide-bearing clastic material. This is supported by the similarity of the mineralogy in the laminations and in the massive sulfide clasts, including the presence of sphalerite- and chalcopyrite-inclusion-rich zones in pyrite grains. The fine-scale grading commonly observed might also suggest deposition as fine-grained detrital layers (e.g., caused by density separation of pyrite grains during the formation of planar lamination). Kerr and Gibson (1993) observed fine-grained clastic sulfides in the lithic clast dominated breccia and sandstone. At least one episode of recrystallization has altered and/or obscured the primary textures, so it is difficult to say with confidence to what extent the laminae represent original clastic textures. Sulfide laminations are interpreted to have been hydrothermally emplaced when they have a crude, stringer-like distribution of pyrite and quartz and/or sphalerite and the laminae may have formed preferentially along planar laminations characterized by higher fluid permeability.

Sulfide disseminations

A variety of sulfide dissemination textures occur at Horne West (Figures 12-5 and 12-6). They represent approximately 45% of the total sulfides (excluding sulfide clasts) observed in outcrop and drill core throughout the succession. The most common sulfide dissemination textures include granular aggregates and masses of euhedral pyrite crystals surrounded by green chlorite and quartz. Others, typically those within strongly sericitized zones, lack chlorite around their margins. Mixtures of disseminated pyrite and sphalerite with associated chlorite-rich haloes are also rarely observed. The chlorite, which is most commonly brownish blue or purple under crossed polarizers (similar to what is observed in the stringers), typically occurs as fine grained masses or may be composed of visible bladed crystals ranging up to 0.025 mm in size. Quartz typically forms euhedral crystals perpendicular to the margins of pyrite grains (especially in

pressure shadows), however randomly oriented rice-shaped grains of quartz with uneven or ragged margins are observed locally within the chloritized zone. Small patches of epidote and carbonate also have been observed associated with some disseminated sulfides within the epidote alteration zone that occurs locally above the West Zone. Pyrite or sphalerite within the disseminations are commonly overprinted by bladed intersecting muscovite crystals that can range up to greater than 1mm in length, or smaller chlorite crystals that can range up to 0.025 mm. However, the association with fine-grained chlorite and large bladed crystals of muscovite is thought to be characteristic of hydrothermal sulfide disseminations and clearly distinguishes this style of mineralization from clastic sulfides.

Occurrence of Gold

Native gold has been observed in thin section within disseminated and stringer sulfides, interpreted to have formed by in situ hydrothermal sulfide mineralization, in both the New Zone and the West Zone (Figure 12-2, Appendix A). Samples in which gold has been observed have well defined hydrothermal chlorite and sericite alteration. The gold occurs in euhedral to subhedral pyrite grains or masses of grains and is consistently observed within fractures and in pyrite inclusions, locally together with sphalerite and/or chalcopyrite. The gold grains range in size up to 0.05 mm.

4.5 Geochemistry

Samples taken for whole rock geochemical analysis of the Horne West succession were obtained from drill holes S-714, S-715, S-716, S-573, and S-574. Samples of representative rock, 30 to 50 cm long, were taken at intervals with a typical spacing of approximately 10 m. Sulfide fragments were avoided in order to assess the effects of hydrothermal alteration throughout the succession. Samples were powdered and analyzed at Actlabs for various elements using instrumental neutron activation analysis (INAA), fusion followed by acid digestion and inductively coupled plasma mass spectrometry (FUS-MS), fusion followed by acid digestion and induced coupled plasma emission spectrometry (FUS-ICP), four-acid digestion followed by inductively coupled plasma mass spectrometry (TD-MS), nitric acid and peroxide digestion followed by induced coupled plasma mass spectrometry (NP-MS), coulometry and other infra red measurement techniques (COUL, IR), fire assay with an atomic absorption spectrometry finish (FA-AA), and cold vapour atomic absorption spectrometry (FIMS). The results of the whole rock data are given in Table 1 (Appendix B). The data obtained have been used to characterize intrusive units within the succession, aid in the interpretation of alteration, and to construct geochemical and metal zonation profiles of the typical Horne West volcanic succession. Assay data (Appendix A) provided by Xstrata Copper Canada and Alexis Minerals were also examined.

4.5.1 Least-altered rhyolite composition and discrimination diagrams

The least-altered Horne West rhyolite is an aphyric coherent rhyolite in the upper portion of the succession (e.g., Hole S-572, 151 m, Hole S-716, 22 m). This rhyolite caps the volcanic succession and occurs up to, and possibly beyond, the Horne Creek Fault in drill core. This least-

altered rhyolite (5 samples) was selected based on a comparison with major element and trace element geochemistry of least-altered Horne and Quemont rhyolites in Maclean and Hoy (1991), calculated AI and CCPI alteration indices with cut off values of <20 and <50 respectively, and low S content (Tables 1 and 2). The 5 least-altered rhyolite samples originate from the same aphyric rhyolite body at the top of the succession which is sericitized compared to least altered Horne and Quemont rhyolite (Figure 13-1b). Least-altered Horne West rhyolite plots within the FIIIa rhyolite field similar to Horne and Quemont rhyolite (Figures 13-2a). Rare earth element plots of Horne West rocks are comparable to those of Horne and Noranda-wide REE profiles outlined in Kerr and Gibson (1993), suggesting that the rhyolites have a similar origin (Figure 13-2b). Horne rocks show REE depletion compared to typical Noranda rhyolite (Fig 13-2b) and have a wide variation in Eu values (Figures 13-3 to 13-6). The unusual positive Eu anomalies, which occur more commonly in intrusive rhyolite are unlikely to represent primary igneous chemistry but instead may reflect subsequent alteration by circulating hydrothermal fluids. Eu enrichment in the fluids may originate from the destruction of Plagioclase and Clinopyroxene throughout the succession and within the footwall rocks. Alternatively the positive anomalies may be attributed to the incorporation or a small amount of mafic material into the melts that later produced these lithofaces. This may be explained in part by the observation of mafic Xenoliths in some of the rhyolite, and is supported by the relative REE depletion in the majority of samples with positive Eu anomalies. The Horne West rhyolites form a broadly coherent group that is likely related to least-altered Horne and Quemont rhyolite (Figures 13-7 and 13-8). Figure 13-7 shows evidence that the Horne West rhyolite is equivalent to Horne and Quemont least-altered rhyolite but that it may have undergone mass loss relative to the latter, as the immobile Al_2O_3 and TiO_2 are present at higher concentrations. Horne West rhyolite plots within the in-

plate field of Gorton and Schandl (2000) reflecting the association with ensimatic crust, as observed in many other Archean rocks of the Abitibi subprovince and in the Main Camp (Figure 13-9).

4.5.2 Major element geochemistry

At Horne West CaO and Na_2O are notably depleted in altered rocks in the middle of the succession, within and between the West Zone and New Zone (Figures 14-1), whereas K_2O is enriched throughout the sampled section relative to least altered rhyolite, decreasing slightly toward the top of the succession. MgO values are highest at the base and central parts of the succession and lowest at the top. The distribution of Na_2O and CaO partly reflects depletion in the central part of the succession due to hydrothermal alteration (replacement of feldspars by sericite). K_2O enrichment reflects sericitization that is present throughout the succession and MgO likely reflects chloritization in the most intensely mineralized or altered zones as well as the abundant chlorite wisps in the wispy clast breccia. SiO_2 ranges from 60 to 75 wt% throughout the succession with the highest values in rhyolite intrusions and at the top of the succession, reflecting silicification (Figure 14-2). The local enrichment of CaO reflects the occurrence of calc-silicate alteration at the top and bottom of the succession, possibly caused by metamorphism of a carbonate alteration assemblage. Carbonate is present at the top and base of the succession only (Figure 14-2) and is also likely related to calcite stringers associated with the calc-silicate alteration assemblage that is observed in this part of the succession. S is most abundant in the central part of the succession with lower concentrations at the top and base; the highest values (8 wt. %) occur within the West Zone and New Zone (Figure 14-3), reflecting the distribution of hydrothermal sulfide (clasts were not included in the samples). Fe_2O_3 enrichment occurs within

the mineralized zones and in the wispy clast-rich breccia that dominates the central portions of the succession (where MgO remains low). The enrichment is attributed to pyrite associated with mineralization, but also suggests that the abundant chlorite contained in the wisps may be a Fe-rich end member (Figures 14-7 and 14-8, Table 1).

A Chlorite-Carbonate-Pyrite Index (CCPI, Large et al., 2001) and Ishikawa Alteration Index (AI, Ishikawa et al., 1976) box plot (Figure 14-5), as well as a sericitization plot (Figure 14-6) were constructed for the Horne West succession. These reveal a relatively abrupt transition from least-altered rocks toward strongly sericitized and chloritized samples most closely associated with mineralization. The aphyric coherent rhyolite at the top of the succession does not show the same degree of sericitization and chloritization that is observed in the other intrusive rhyolites in the succession, supporting the suggestion that it was emplaced into the volcanic pile late relative to hydrothermal mineralization. Profiles showing CCPI and AI for the Horne West succession show that alteration is strongest in the middle of the succession (Figures 14-7 and 14-8).

4.5.3 Trace element geochemistry

Metals, such as Zn, Cu, Pb, Mn, As, and Ba reflect the hydrothermal mineralization and alteration of the host rhyolite and volcaniclastic rocks; clasts were avoided in the sampling. Pb and As have similar distributions with high values occurring at the margins of the gold zones (Figure 14-3). There is a consistent metal zonation within the West Zone, with Cu at the stratigraphic base of the zone followed by elevated Au values and then Zn toward the top (Figure 14-4). The data available suggest that this zonation may be reversed within the New Zone, with Zn towards the stratigraphic base followed by Au and Cu at the top. The distribution of metals is

roughly symmetrical about the middle of the studied succession which is the most intensely altered. Zn and Cu are related to sulfide stringers and disseminations. Cu enrichment, in particular, is explained in part by the occurrence of rare chalcopyrite-dominated stringer veins that are observed only at shallow depths in the chloritized central portion of the wispy clast-rich breccia between the two zones of gold mineralization (Figure 12-3a). Mn is enriched at the base of the stratigraphic succession relative to the top (e.g., concentrations greater than 1 wt.% at the base of S-574) and both at the top and base of the stratigraphic package in holes in the western portion of the study area (e.g., holes S-574 and S-716). Mn enrichment is associated with calc-silicate alteration and likely reflects the presence of manganiferous carbonate and garnet. Ba is distributed symmetrically about the central portion of the succession and roughly mimics the distribution of Cu. Ba enrichment could be associated with sericitization, and likely reflects the presence of Ba-rich muscovite in the sericitized volcanic rocks.

4.5.4 Gold

Whole rock samples have gold concentrations between nil and >3 g/t Au with values typically higher than 0.5 g/t Au within the gold zones. Assay data provided by Xstrata Copper Canada and Alexis Minerals (Appendix A) suggest that sulfide clasts may be slightly enriched in gold relative to background gold levels. Beds with coarse sulfide clasts that occur outside of the West Zone and New Zone locally have gold grades higher than 1 g/t Au (Appendix A). However, whole rock data indicate that disseminated sulfides have grades greater than 3 g/t Au; the highest grade in stringers reported was 1.3 g/t Au. K_2O, Fe, S, Cu, Zn, and Cd correlate with gold in whole rock data but Cu and Zn do not correlate with Au on a sulfur-normalized basis (Table 3). Ag, Cd and In are the metals that best correlate with gold when normalized to sulfur.

4.6 Interpretation

Moderate to strong sericitization is most closely associated with gold mineralization in both mineralized zones, although less intense in the West Zone. The typical features associated with increased gold concentration in volcaniclastic or coherent rocks are a combination of sericitization and disseminated and/or stringer pyrite with chlorite at the margins of the sulfide veins or disseminations (Figure 12-1). Sulfide clasts are not the source of gold enrichment nor do they contribute significantly to gold grade within the mineralized zones, as revealed in assay data (Appendix A). However, small quantities of gold in beds containing massive sulfide clasts (Holes S-575, S-574, S-576) may indicate minor enrichment in the source or local overprint by gold-rich veins and disseminated sulfide.

The gold mineralization in the West Zone and New Zone is attributed to broadly synvolcanic circulation of gold-rich hydrothermal fluids through the volcanic pile. Supporting this is the spatial relationship of alteration and mineralization to the body and margins of the xenolith-bearing coherent rhyolite and aphyric coherent rhyolite intrusive bodies. The latter suggests that gold mineralization may have occurred coevally with intrusion of the rhyolite. However, these synvolcanic intrusive rhyolite bodies are not mineralized everywhere and the gold is commonly hosted in nearby volcaniclastic rocks. Thus, the intrusions may have acted as conduits for fluids locally or may have remobilized gold if they intruded across mineralized zones or disrupted zones of active hydrothermal fluid circulation along synvolcanic faults. The changes in bedding orientation and facies at the western margin of the New Zone and West Zone may be related to synvolcanic faulting which could have restricted rising hydrothermal fluids responsible for the gold mineralization and also controlled the location of intrusive rhyolite. The fact that gold mineralization is distributed along or below stratigraphic intervals that contain

abundant pyrite-dominated sulfide clasts suggests that gold mineralization could have been coeval with the development of massive sulfide mineralization along strike at the same paleo-seafloor position. However, the gold mineralization is clearly linked to hydrothermally introduced stringers and sulfide disseminations in the matrix and not the sulfide clasts.

The relationship between mafic intrusions and the localized distribution of gold and sulfide, particularly in the West Zone, is attributed to late remobilization of the sulfides and gold by mafic dikes that crosscut or intruded along gold-enriched zones, possibly along synvolcanic faults. These dikes are interpreted to be late synvolcanic and/or post-volcanic in origin. That the original source of gold is not associated to the mafic intrusions is supported by the lack of consistent alteration or gold mineralization in other similar dikes found throughout the succession, distinctly different alteration (quartz-carbonate-epidote veining) in the mafic dikes compared to the mineralized zone, and a general lack of alteration in the majority of mafic intrusions.

Enrichment of Ca, Na, Mn, and carbonate at the top and base of the stratigraphy (above the quartz-phyric rhyolite and sulfide clast-bearing lithic breccia and below intrusive coherent aphyric rhyolite) correlate with the observed white mica-carbonate-epidote and hematite calc-silicate alteration as well as the zones of pink, orange, or brown epidote and carbonate and/or garnet spots. The pervasive sericite and chlorite alteration within the succession is interpreted to be associated with more widespread synvolcanic hydrothermal upflow through the volcanic package. Manganese enrichment toward the base of the stratigraphic succession may represent part of a footwall alteration zone related to a massive sulfide forming hydrothermal system nearby (cf. Dubé et al., 2007). For example there are distinct similarities between the Mn enrichment at Horne West and a zone of quartz-biotite-garnet alteration with associated Mn

enrichment at the nearby La Ronde Penna deposit (Dubé et al., 2007). Garnet alteration at LaRonde is characterized by high Mn content and is attributed to metamorphism of Noranda-type chloritic alteration assemblages, in which garnet stability is promoted by the high Mn. Dubé et al. (2007) have suggested that this Mn enriched zone, which represents the proximal footprint of VMS footwall alteration, could be used as a marker for exploration efforts.

The lack of correlation between Cu and Au on a sulfur-normalized basis is consistent with observations by Price (1934) and Barrett et al. (1991) who noted that Au and Cu grades were not, or not consistently, correlative spatially in the Horne deposit. This may have resulted from the segregation of Cu and Au due to a thermal gradient present at the time of mineralization, introduction of Au during a late phase of mineralization, or remobilization of Au along with Zn during a phase of metamorphism. Cu within the Horne deposit is typically localized close to the stratigraphic base of the massive sulfides which is consistent with what has been observed in the West Zone. The metal zonation within the West Zone, from Cu at the base to Zn at the top, is also consistent with previous observations by Gibson and Kerr (1993), who noted manganese and zinc enrichment in the hangingwall of the West Zone, with gold and copper more enriched in the footwall of the West Zone (Gibson and Kerr, 1993). Alternatively, the Cu-rich central portion of the succession possibly reflects a high temperature zone at the core of an area of lateral hydrothermal fluid flow, with Zn and Au occurring at the cooler fringes of this zone. This is consistent with the observed distribution of the most intense alteration noted in Figures 10-5, 14-5 and 14-6. The distribution of the alteration and metals supports the hypothesis that rhyolite intrusions within the succession locally acted as barriers that confined the flow and/or introduced hydrothermal fluid by crosscutting and/or blocking previously established hydrothermal upflow.

5. Summary and Conclusions

Lithostratigraphy

The explored sections of the Horne West block are part of a complicated volcaniclastic rock-dominated environment characterized by deposition of a wide variety of mass-flow deposits, numerous rhyolite intrusions, and localized extrusive rhyolite flows. Changes in the facies assemblages down-plunge (toward depth) are interpreted to reflect a transition from a proximal to distal volcanic slope environment. These changes include a decrease in the abundance of coarse sulfide clasts and an increase in intraclasts and suspended cobble-boulder breccias deposited by cohesive debris flows. This transition supports indications from previous authors that the Horne rocks were emplaced on the slope of a volcanic edifice (Kerr and Gibson, 1993; Barrett et al., 1991).

Two principal sulfide clast-bearing horizons are observed in central portion of the succession. The lowermost occurs near the base of a fining-upward succession of normally graded wispy clast-rich breccia; the uppermost occurs within quartz-phyric rhyolite clast breccia and lithic clast-dominated sandstone and breccia. Subsurface mapping shows that the lower portion of the stratigraphy including the lowermost intrusive rhyolite and sulfide clast-bearing horizon are truncated at depth and toward the east by the Andesite Fault, whereas the uppermost sulfide clast-bearing horizon extends down to a depth greater than 400 m. Sulfide clasts in both of these horizons were produced by volcanic disruption or mass wasting of a massive sulfide body that was forming at the sea floor along strike. The characteristics of the clasts show that sulfide replacement and other alteration occurred at the source of the clasts in a variety of host rocks including aphyric rhyolite, quartz phyric rhyolite, and volcaniclastic rocks. Scour structures at the base of lithic clast-dominated breccia in outcrop have steeply dipping beds that

suggest the direction of paleoflow was roughly in the up dip-down dip direction (Monecke et al., 2008). This, in conjunction with the interpreted transition from a proximal system at shallow depths to a more distal environment down-plunge, suggests that the massive sulfide which produced the clasts is eroded.

The lithofacies changes in the central portion of the outcrop, namely a transition form wispy-clast rich breccia to quartz-phyric rhyolite clast breccia and lithic clast-dominated sandstone and breccia, reflects a transition from mass flows generated by voluminous volcanic eruptions to mass flows related to mass-wasting. The quartz-phyric rhyolite clast breccia and lithic clast-dominated breccia and sandstone facies may represent rocks that were deposited over a relatively long period of time compared to underlying and overlying volcaniclastic rocks, allowing for a period of hydrothermal upflow and synvolcanic mineralization. Successive shallowly emplaced synvolcanic rhyolite intrusions (aphyric rhyolite and xenolith-bearing rhyolite, respectively) occur beneath the two principal sulfide clast-bearing horizons and form an important host rock for gold and in situ hydrothermal sulfide mineralization.

Observations by Kerr and Gibson (1993) concerning Horne West concur with the findings of this study, including the switch from volcaniclastic rocks deposited by eruption to predominantly epiclastic rocks and the presence of massive sulfide clasts and sulfide bearing intraclasts along multiple stratigraphic horizons.

Deformation and/or important facies changes have been noted along the western portion of the succession described above, although drill hole information is limited in this area. Amygdular clast-bearing lithic breccia and coherent rhyolite dominate the succession west of the deformed zone and the mineralized zones. In outcrop the cleavage orientation remains consistent across this area and has not yet been linked to any major folds. The cleavage predates later small-

scale folds observed in drill core, thus the bedding changes observed along the western margin of the outcrop predate the formation of the cleavage and other late structural changes. These abrupt along-strike changes in lithofacies in the western portion of the study area are attributed to synvolcanic faulting, folding or a combination of both of these.

Gold mineralization and alteration

Gold mineralization occurs with sericite and chlorite alteration and disseminated and stringer sulfides at two stratigraphic intervals within or below the sulfide clast-bearing units. The gold-rich disseminated and stinger sulfide mineralization at Horne West are interpreted to have formed in spatial and temporal association with the near-seafloor massive sulfides that were the source of the sulfide clasts. However, sulfide clasts do not contribute significantly to gold grade at either of these stratigraphic intervals. The New Zone, at the base of the succession is hosted within intrusive aphyric coherent rhyolite, rhyolite breccia, and the extrusive coherent rhyolite and monomictic breccia with rotated clasts facies association. Gold mineralization is observed down to a depth of 200 m (where drilled) but is truncated by the Andesite Fault toward the east and pinches out at depth with the host stratigraphy. The West Zone occurs stratigraphically above the New Zone and is hosted by xenolith-bearing coherent rhyolite and adjacent beds of lithic clast-dominated breccia and sandstone and quartz-phyric rhyolite breccia. The West Zone steps up stratigraphically into lithic clast-dominated breccia and sandstone and quartz-phyric rhyolite breccia down to depths of 400 m along the drilled corridor. A swarm of mafic intrusions in the shallow western portion of the study area has caused local remobilization of gold. The highest grade portions of both gold zones occur where abrupt facies changes and bed deformation occur at the western flank of the study area. There is a distinct spatial relationship

between alteration and mineralization and the body and margins of the shallowly intrusive synvolcanic xenolith-bearing rhyolite and aphyric coherent rhyolite bodies, particularly at shallow depths. These synvolcanic intrusions may have acted as a conduit for hydrothermal fluids locally or may have remobilized gold if they intruded across mineralized zones or zones of active hydrothermal fluid circulation.

Geochemical observations from downhole sampling show that the base of the New Zone contains anomalously high concentrations of Mn. The distribution of Cu, Au, Zn and other elements is broadly symmetrical about to the central portion of the succession. Localized calc-silicate alteration (epidote, white mica, and garnet) occur above the West Zone and below the New Zone and correlate with Ca, Na, and Mn enrichment, whereas the central portion of the study area is dominated by sericite and chlorite alteration. The strong Mn enrichment and garnet alteration at the base of the succession may be part of the metamorphosed equivalent of proximal chlorite alteration similar to what is observed at LaRonde (Dubé et al., 2007). Alteration, including footwall Mn enrichment, epidote and carbonate and/or garnet spots, as well as chloritization and sericitization in intrusive rhyolite bodies, increase towards the shallow western margin of the succession. This suggests that the source of hydrothermal fluids and more proximal volcanic environment were located close to the surface in the western part of the property.

Observations based on drill core are consistent with the surface mapping of Monecke et al. (2008), which indicate that Horne West represents the fringe of a stacked hydrothermal system. Gold, sulfide mineralization and alteration occurred coevally with the formation of massive sulfide (represented by the sulfide clasts) and with the emplacement of multiple rhyolite

intrusions that were separate but broadly spatially and temporally associated with formation of the nearby giant Horne deposit.

Economic potential

If the above interpretations are correct, the Horne West succession remains prospective for disseminated gold and zinc mineralization, including possible massive sulfide deposits at depth along the western portion of the study area. The chance of finding the original massive sulfide from which the sulfide clasts originated is not prospective as most evidence suggests that it has been eroded. However, the important stratigraphic changes in the western portion of the study area may represent a zone of synvolcanic faulting that remains to be explored. An area of increased gold mineralization occurs at depth in the West Zone, the western flank of which has not been explored. This area, which is stratigraphically elevated relative to the West Zone at surface may represent a separate zone of hydrothermal upflow along a shared structural feature, and may thus be prospective for massive sulfide mineralization. However, the significance of abrupt facies changes in the western portion of the outcrop remains uncertain. Clarification of relationships along the western margin of the study area will help to resolve the possibility of synvolcanic structures extending to unexplored areas in the deeper portions of the West Zone.

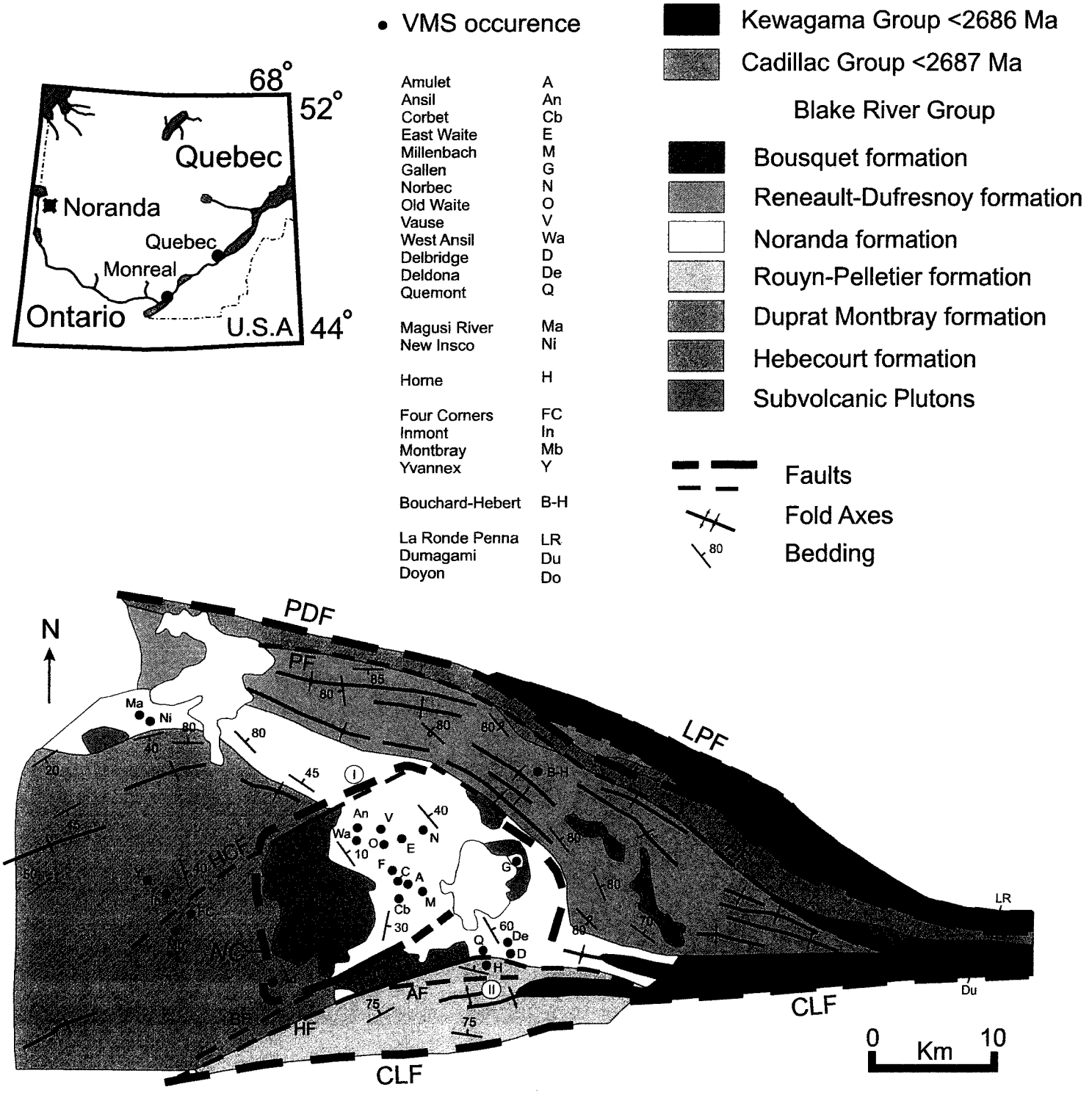

Figure 1. Stratigraphic subdivision and structure of the Blake River Group showing the location of the Noranda Cauldron and VMS deposits (modified from Gibson and Galley, 2007). PDF = Porcupin Destor Fault, PF =Parfouru Fault, LPF = La Pause Fault, CLF = Cadillac Larder Lake Fault, HCF = Hunter Creek fault, BF Beauchastel Fault, HF, Horne Creek Fault, AF = Andestite Fault, *NC* inferred structural margin of the Noranda Cauldron. FPIC (F) (P) signifies the Flavrian and Powell segments of the Flavrian-Powell Intrusive Complex.

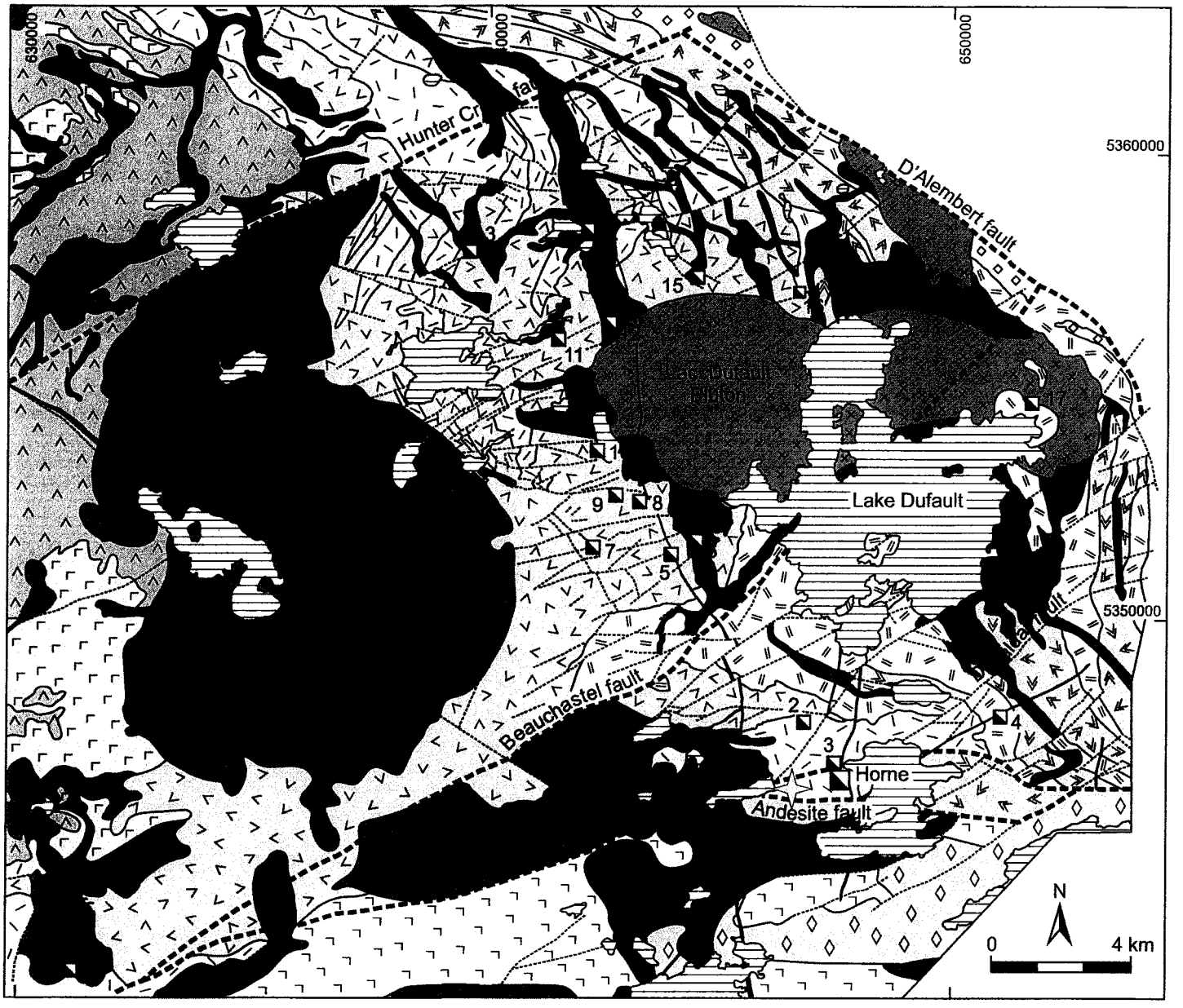

VMS deposits: 1=Aldermac, 2=Joliet, 3=Quemont, 4=Delbridge, 5=D68, 6=Millenbach, 7=Corbet, 8=Amulet A, 9=Amulet C, 10=Amulet F, 11=Old Waite, 12=East Waite, 13=Ansil, 14=Vauze, 15=Norbec, 16=Newbec, and 17=Gallen

ARCHEAN EXTRUSIVE ROCKS

Undifferentiated
- Rhyolite
- Basalt/andesite

Cycle 1+2
- Rhyolite
- Basalt/andesite

Cycle 3
- Rhyolite
- Basalt/andesite

Cycle 4
- Rhyolite
- Basalt/andesite

Cycle 5
- Basalt/andesite

ARCHEAN INTRUSIVE ROCKS
- Syenite
- Granodiorite
- Trondhjemite, tonalite
- Gabbro, quartz diorite

PROTEROZOIC INTRUSIVE ROCKS
- Diabase
- Major fault
- Minor fault
- Deposit
- Horne West

Figure 2. Generalized geological map of the Noranda camp, showing structural elements and distribution of extrusive and intrusive rocks.The locations of VMS deposits are indicated (modified from Santaguida, 1999).

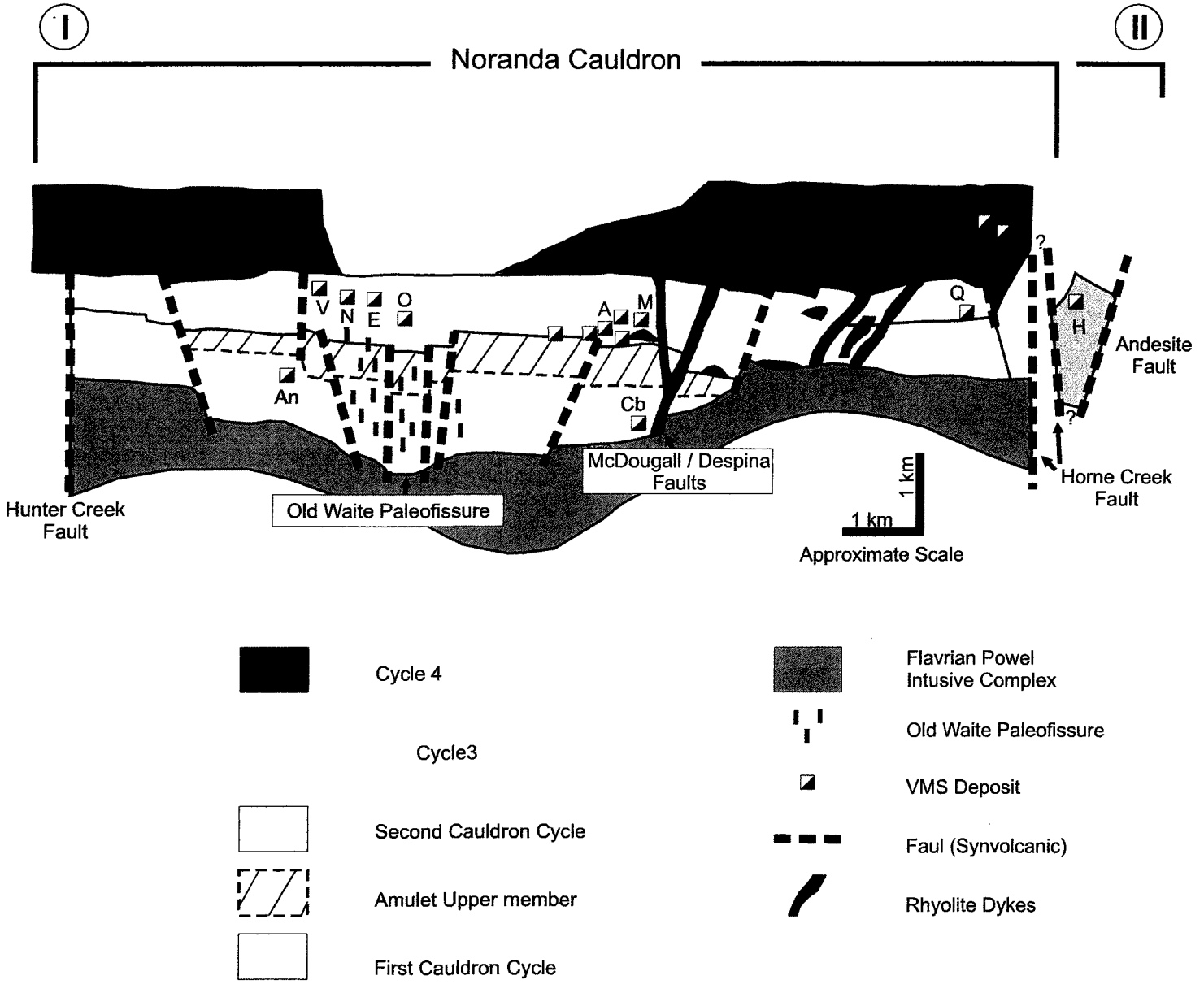

Figure 3. Reconstruction of a north-south cross section through the noranda cauldron in the central portion of the Blake River group showing distirbution of VMS deposits and structural controls. Refer to Figure 1 for trace of the section and for abbreviations used to denote the VMS deposits (modified from Gibson and Galley, 2007).

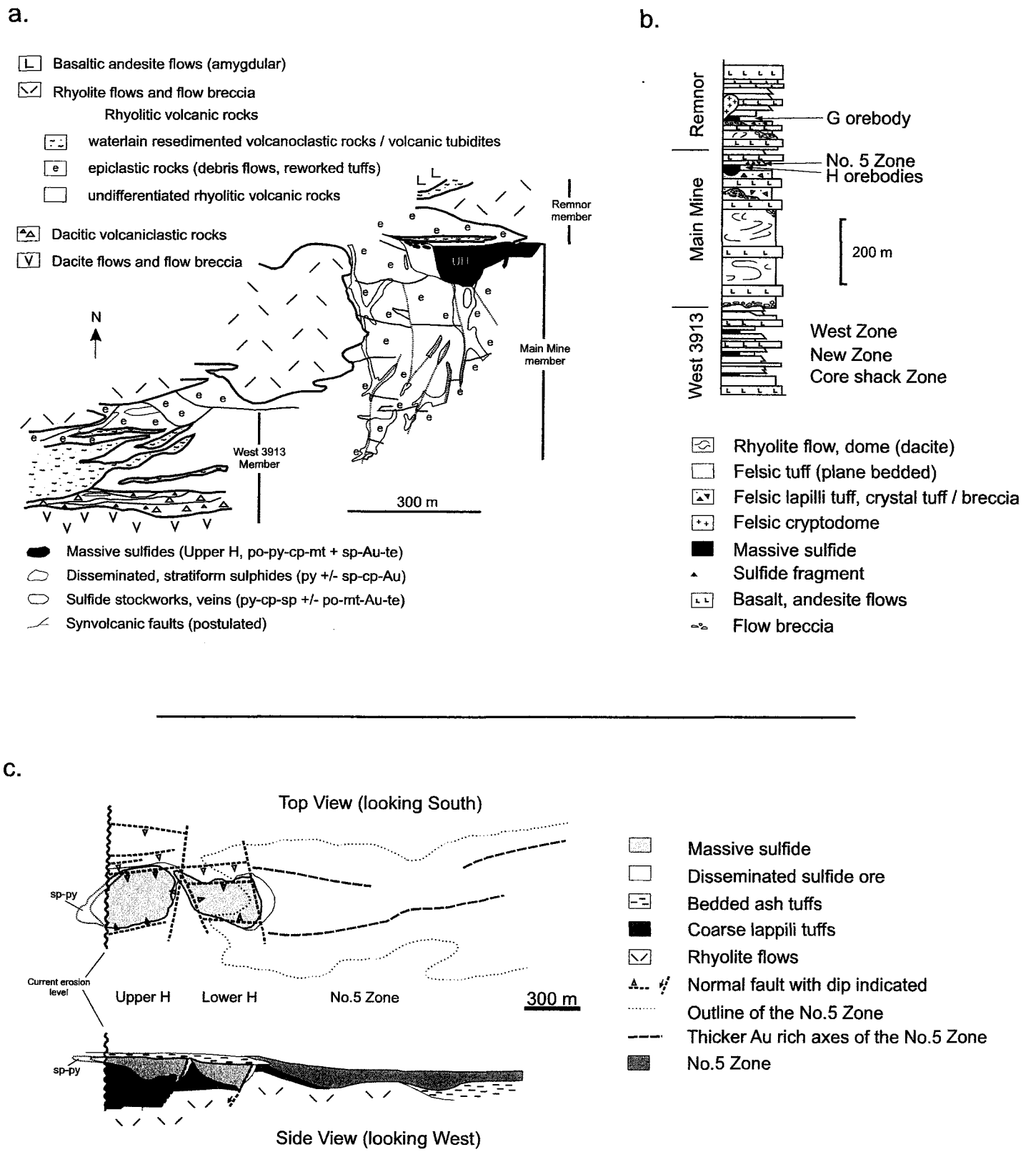

Figure 4. a) Section of the Horne mine sequence based on the geology of the 975ft level (modified from Kerr and Gibson, 1993). b) Simplified and idealized Horne stratigraphy (modified from Gibson et al. 2000). c) Map and section of the Horne orebodies in plan view and in cross-section showing the Horne paleo-graben (modified from Gibson and Kerr, 1990).

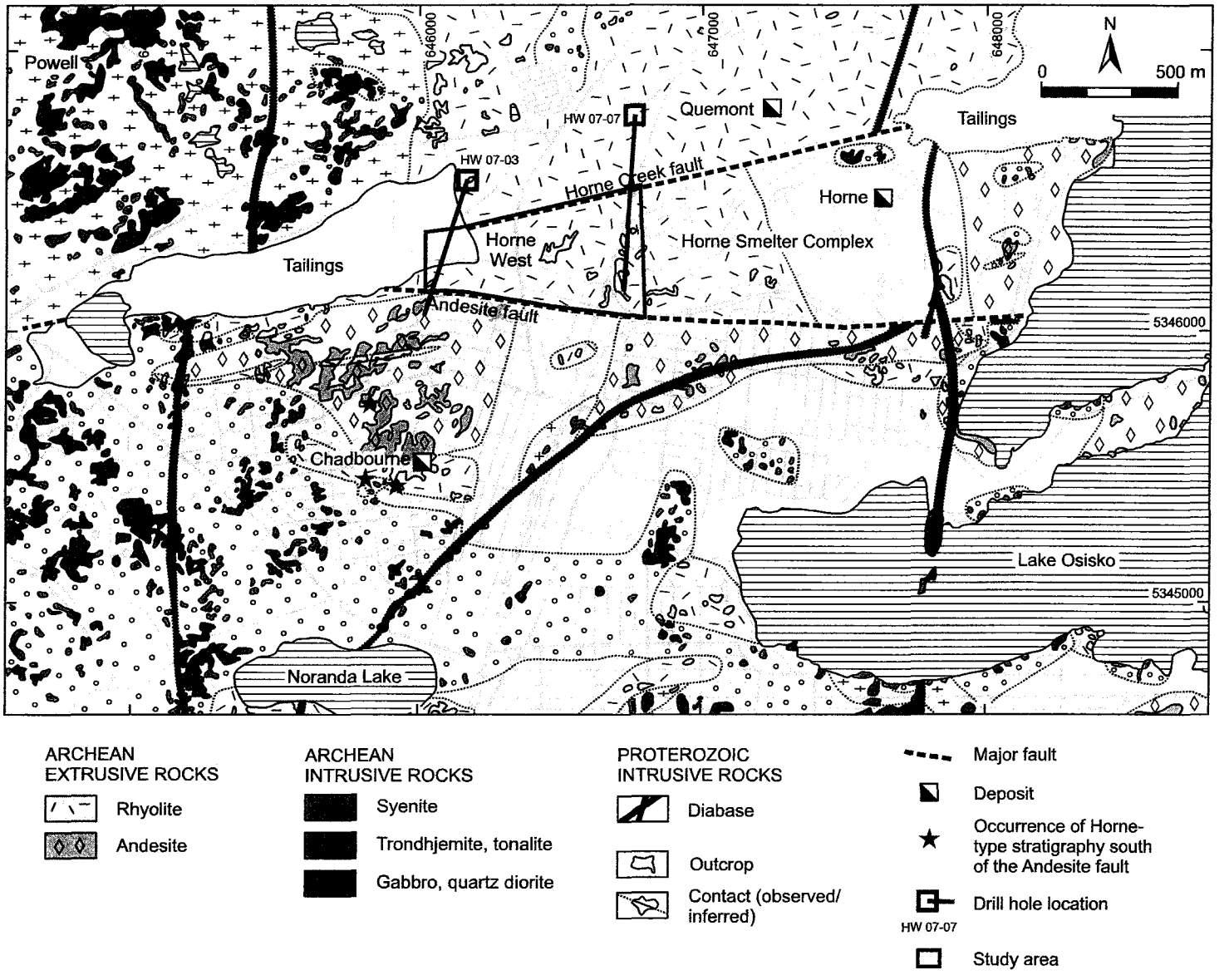

Figure 5. Location of the Horne West outcrops relative to the Horne mine (modified from Wilson, 1941). (drawing courtesy of Thomas Monecke)

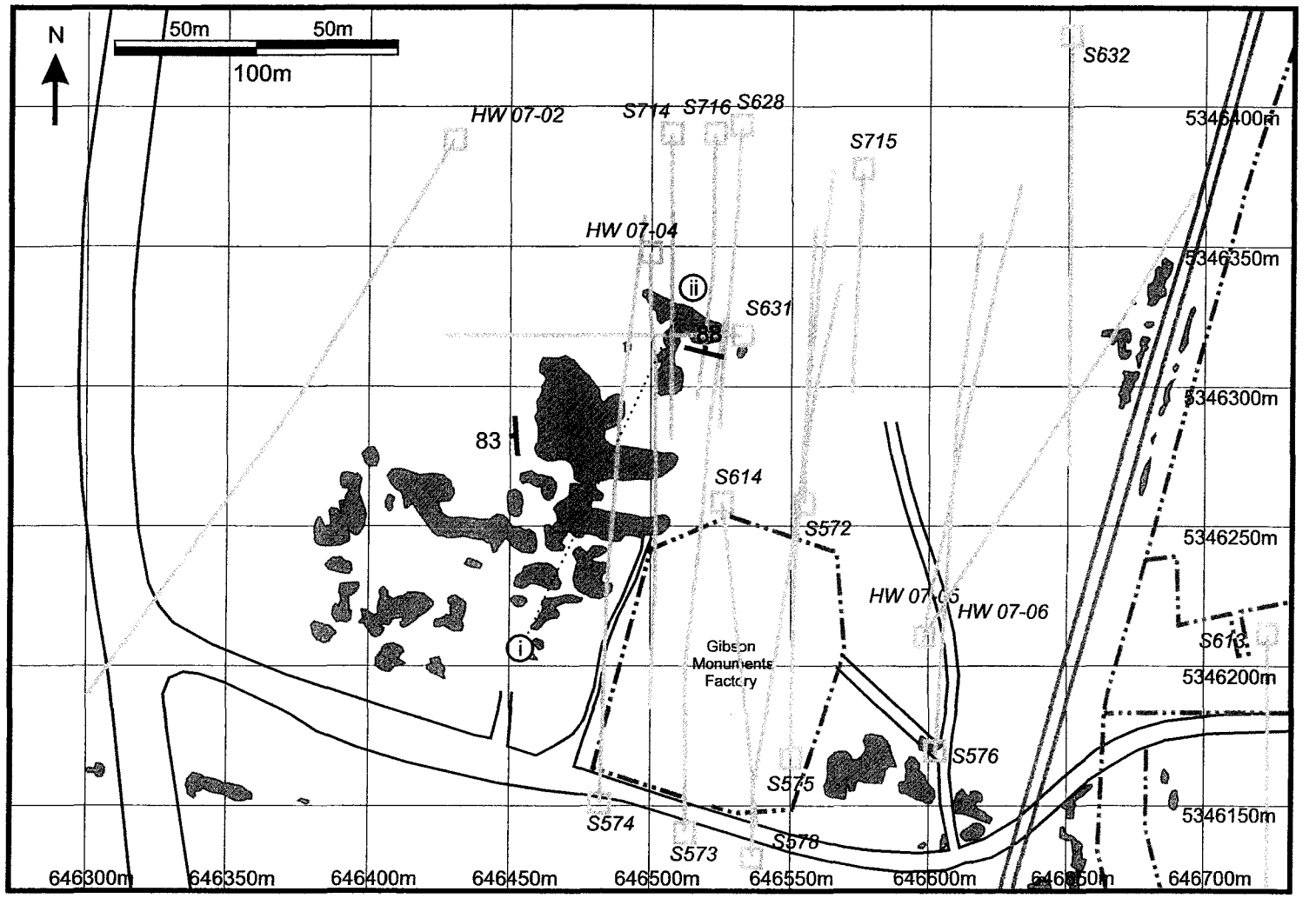

Legend

- Surface projection of drill hole
- S714 Drill hole collar location
- Swamp/Marsh
- Outcrop
- Road
- Fence
- Railroad
- 88 Bedding orientation

Cleavage orientation

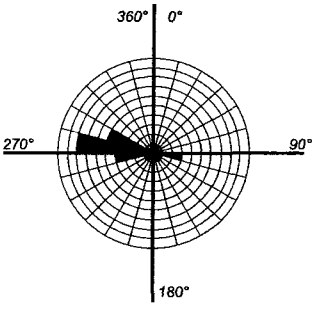

290/90	285/90
280/84	110/82
282/89	290/89
276/88	280/90
270/84	96/77
256/86	100/60
101/87	85/80
262/90	278/65
301/85	272/89
286/88	264/88
290/86	270/90

Figure 6-1. Horne West outcrops and surface projection of most logged drill core. The structural fabric, defined principally by the shape of chlorite clasts but also phyllosilicate minerals and other lithic fragments, remains consistent over the extent of the outcrop despite localized bedding orientation changes, which suggests that the fomation of this fabric post-dated any deformation of beds in surface outcrop. The cleavage measurements were obtained from locations covering the central portion of the outcrop including areas with differing bedding orientation. The stratigraphic succession observed in outcrop (i to ii) is shown in Figure 6-2.

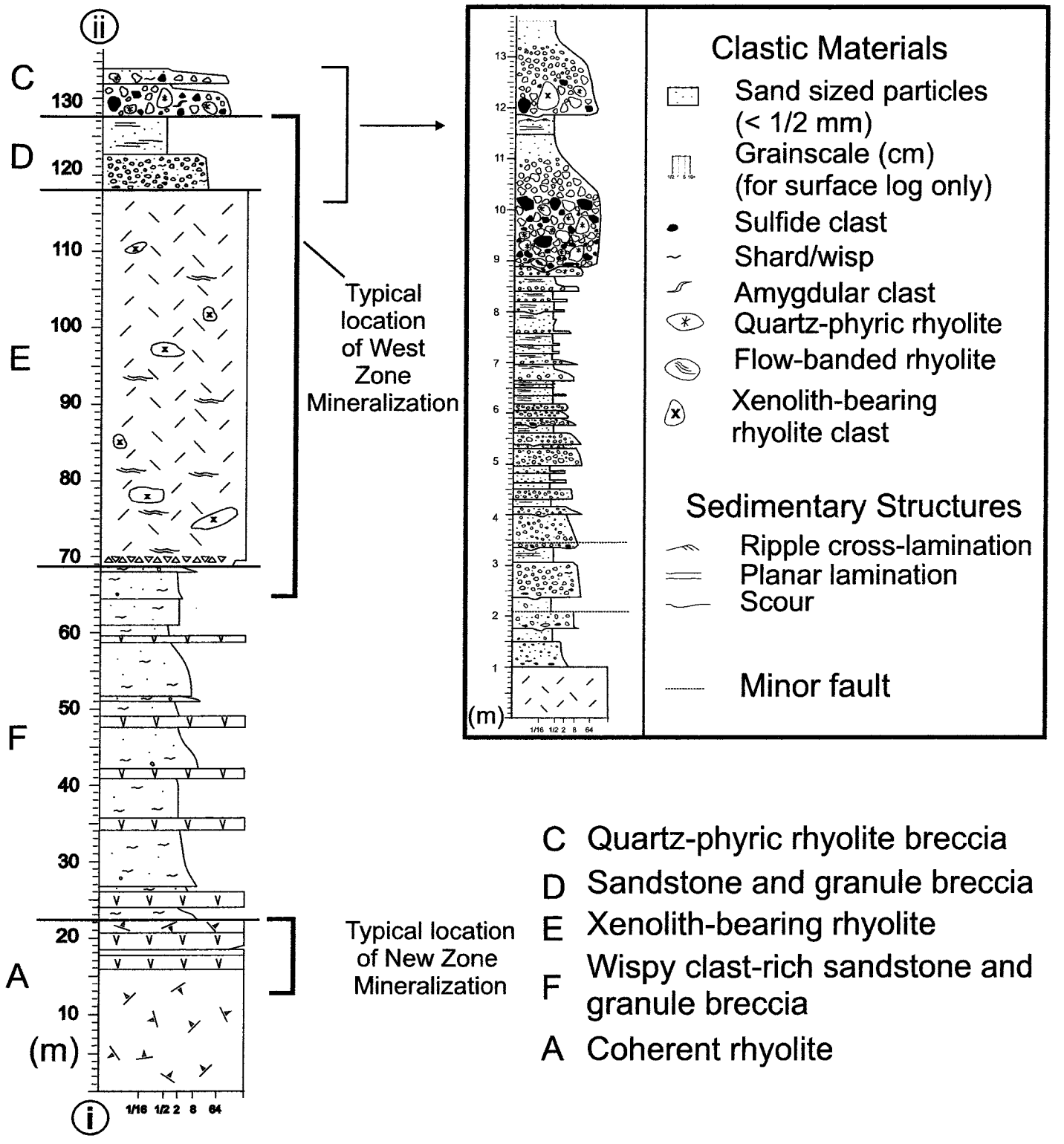

Figure 6-2. The geological succession observed in outcrop at Horne West corresponding to observations from i to ii in Figure 6-1 showing a detailed reconstruction of the uppermost part of the outcrop.

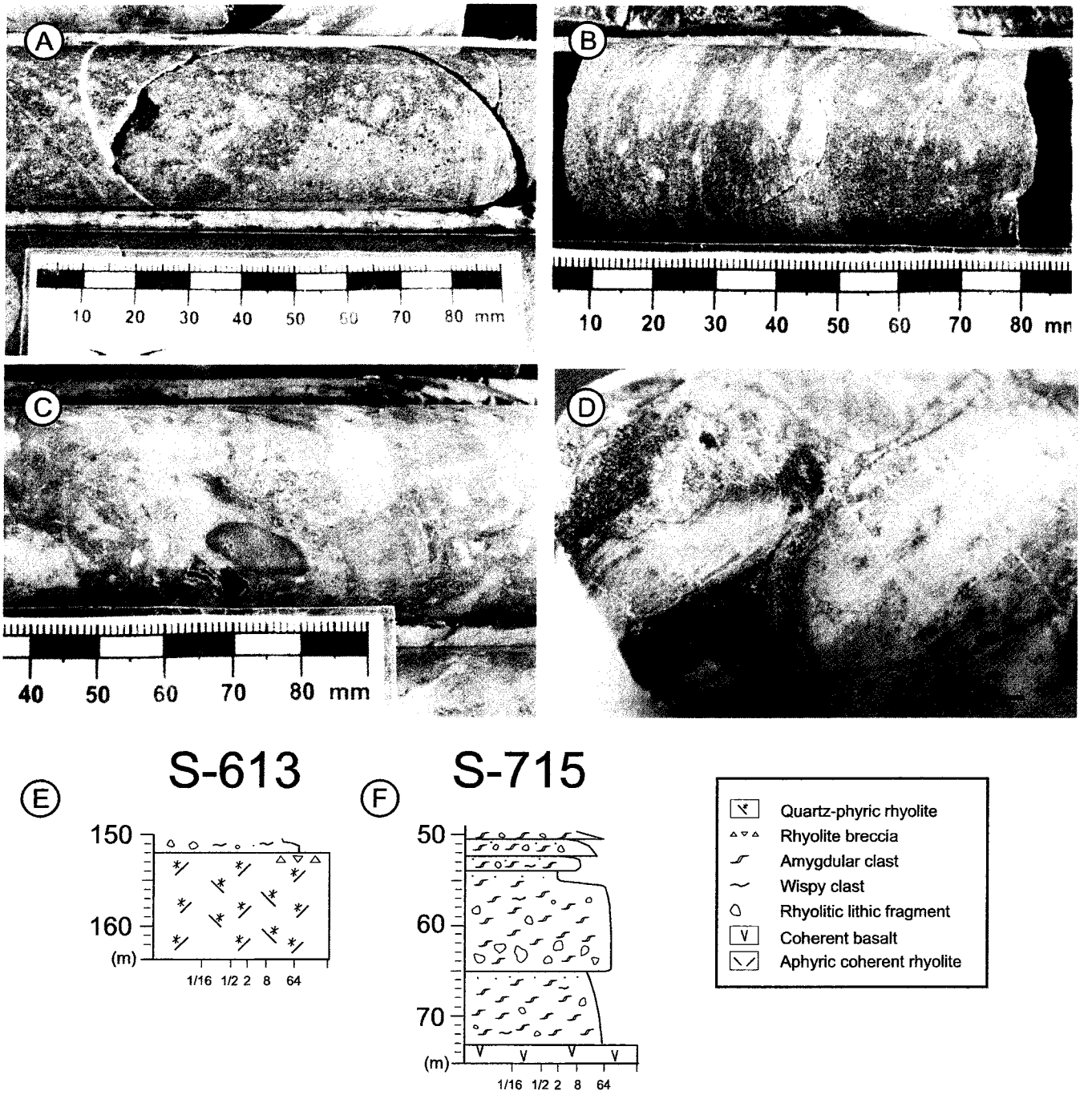

Figure 7-1. A) Coherent quartz-phyric rhyolite (S-613, 160 m). B) Sulfide stringers occuring near the top contact of the quartz-phyric rhyolite intrusion (S-613, 152 m). C) Amygdular clast-bearing lithic breccia (S-714, 64 m). D) Amygdular clasts in amygdular clast-bearing lithic breccia showing elongated amygdules (outline of clasts in pencil) (S-574, 245 m). E) F) Representative drill core log of quartz-phyric rhyolite and amygdular clast-bearing lithic breccia, respectively.

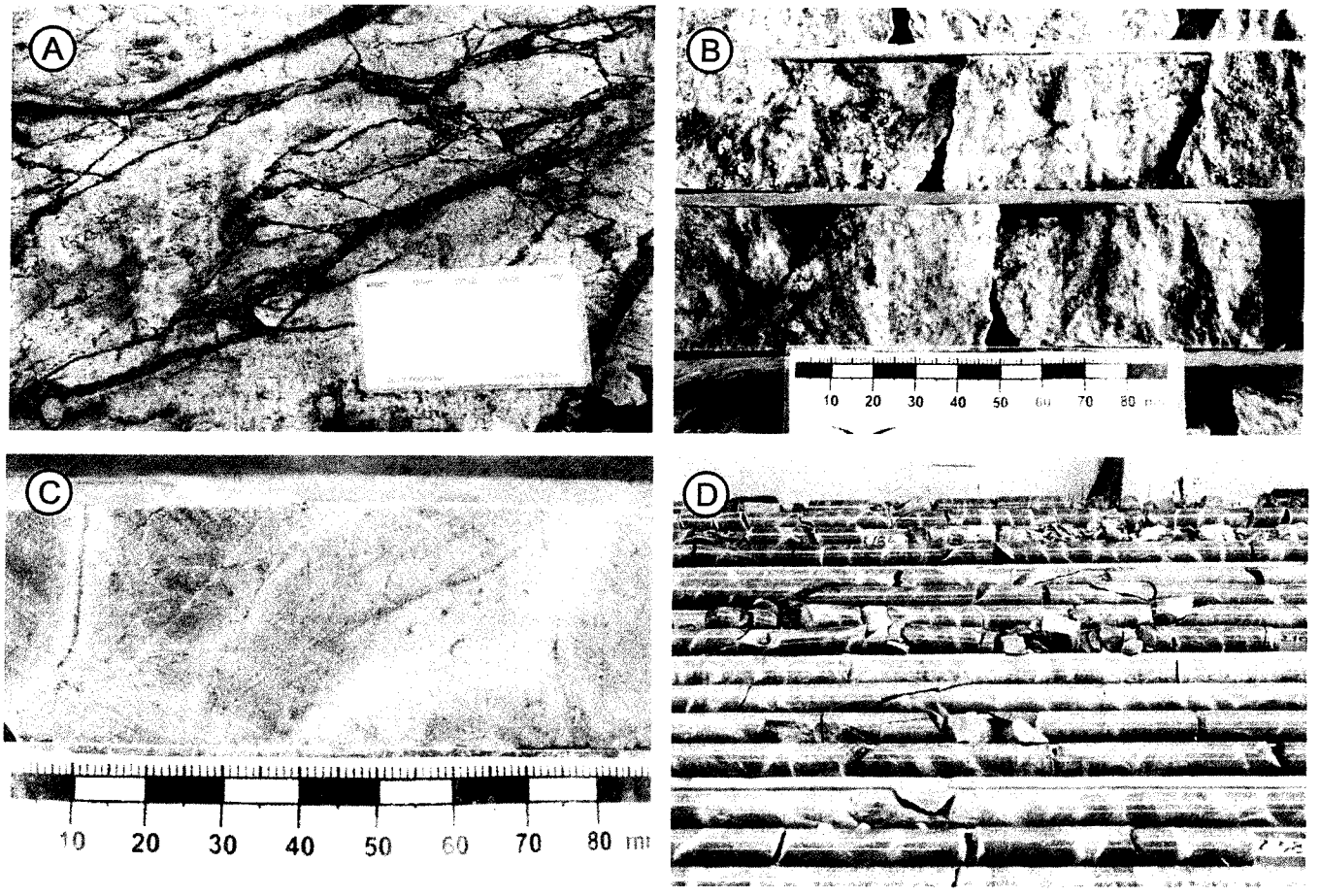

Figure 7-2. Aphyric coherent rhyolite. A) sulfide stringers in aphyric coherent rhyolite in outcrop. B) Aphyric coherent rhyolite with sulfide stringers and disseminations. (S-614, 195 m). C) White mica and hematite alteration in aphyric coherent rhyolite (S-716, 24 m). D) Regularly spaced white mica-altered fractures in aphyric coherent rhyolite, for scale core is 36.5 mm in diameter (S-628, 60 m). E) Representative drill core log of aphyric coherent rhyolite.

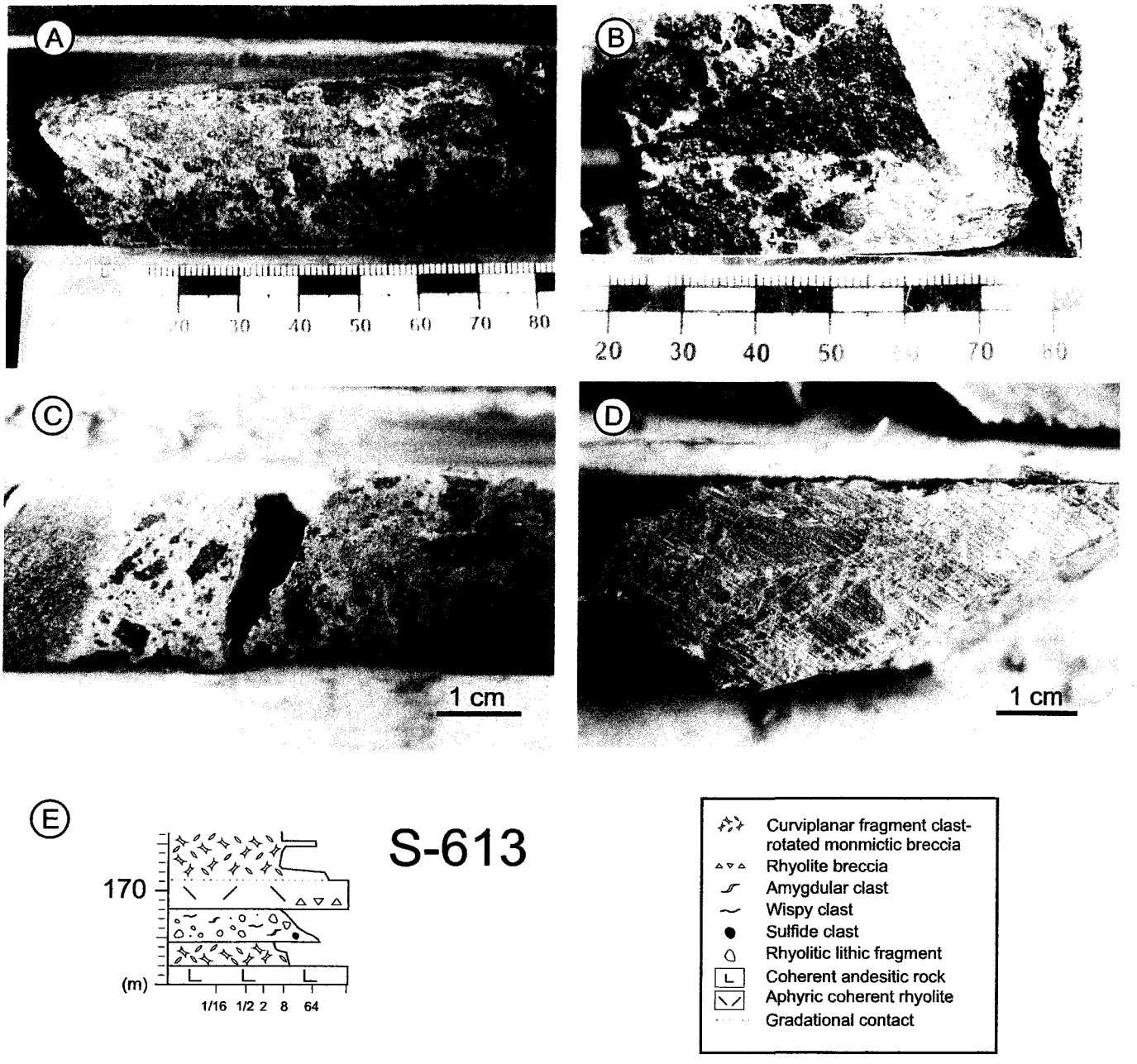

Figure 7-3. Clast-rotated monomictic breccia. A) B) Clast-supported clast-rotated monomictic breccia with chlorite-rich fragments (S-613, 85 m). C) Matrix-supported clast-rotated monomictic breccia (S-613, 96 m). D) Clast-supported clast-rotated monomictic breccia with siliceous fragments (S-613, 183 m).

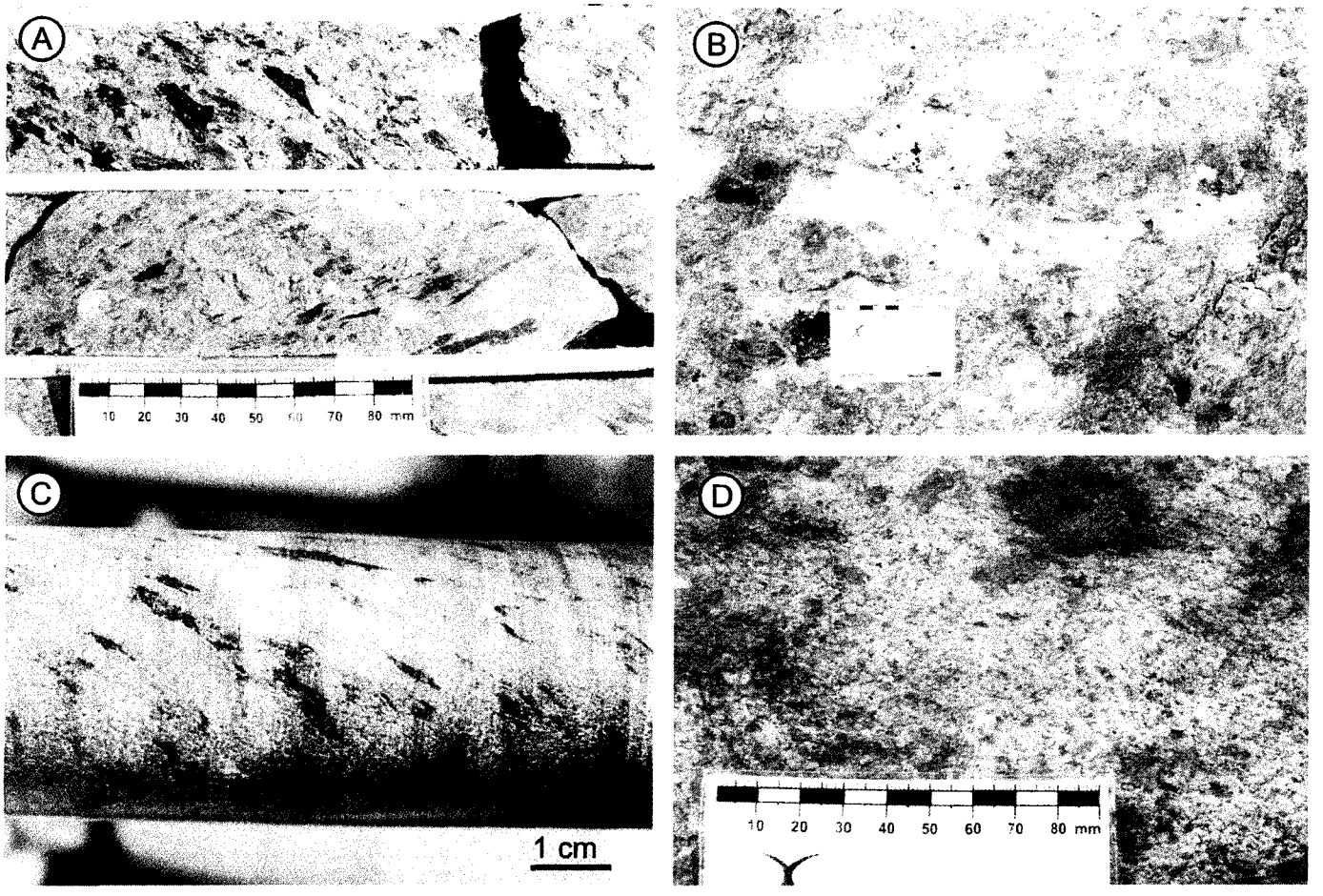

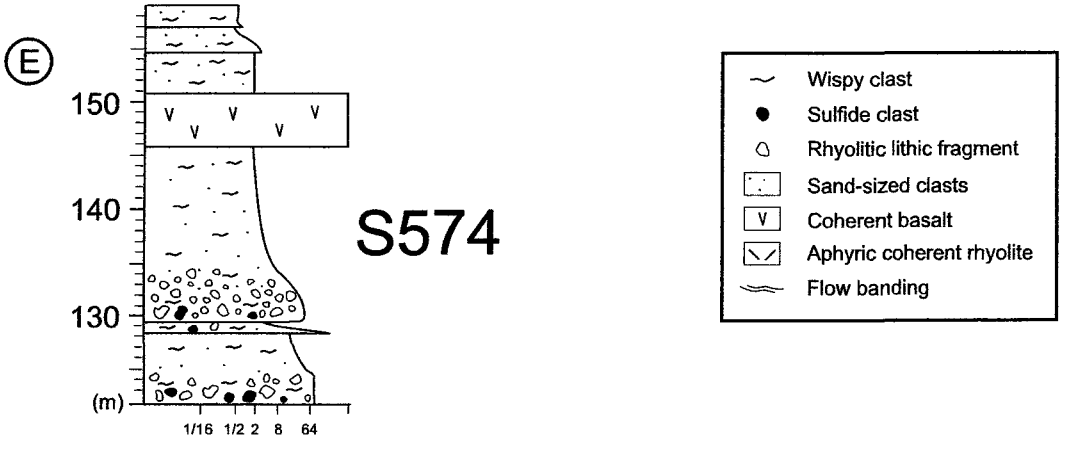

Figure 7-4. Wispy clast-rich breccia. A) Pebble-sized breccia in drill core with sulfide fragments (HW-07-06, 42 m). B) Wispy clast-rich breccia with small sulfide clasts in sand-blasted outcrop. C) Sulfide clast-poor wispy clast-rich granule breccia (S-628, 222 m). D) Wispy clast rich breccia in outcrop. E) Representative core log of a normally graded fining upward sequence of wispy clast-rich breccia with granule breccia at the top and coarse sulfide clast-bearing wispy clast-rich breccia at the base.

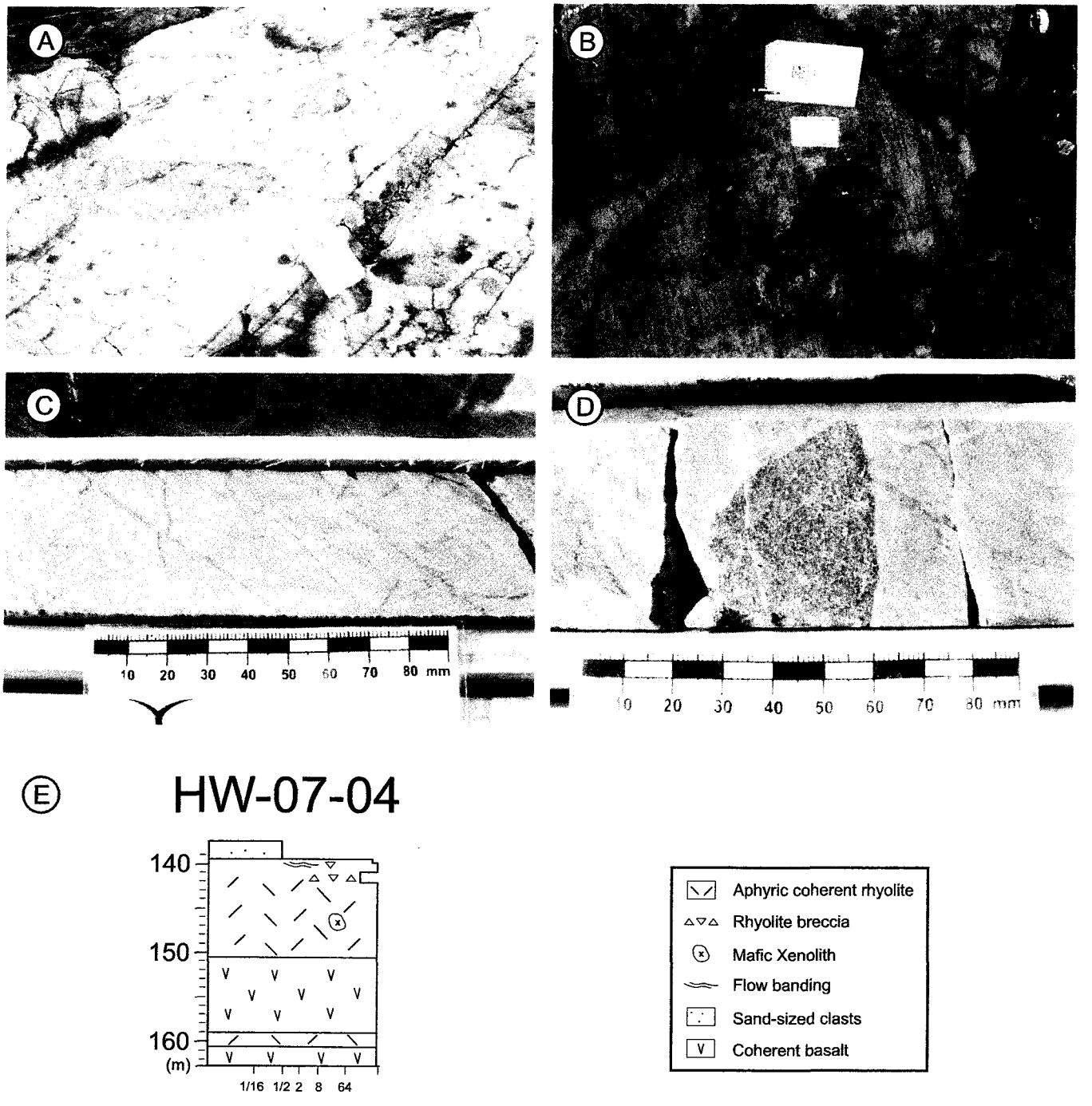

Figure 7-5. Xenolith-bearing rhyolite. A) Mafic xenoliths in flow banded rhyolite in outcrop. B) Polygonal jointing and xenolith in outcrop. C) Sulfide stringers in xenolith-bearing rhyolite (HW-07-05, 162 m). D) Mafic xenolith in the xenolith-bearing rhyolite (HW-07-05, 162 m). E) Representative drill core log of xenolith-bearing rhyolite.

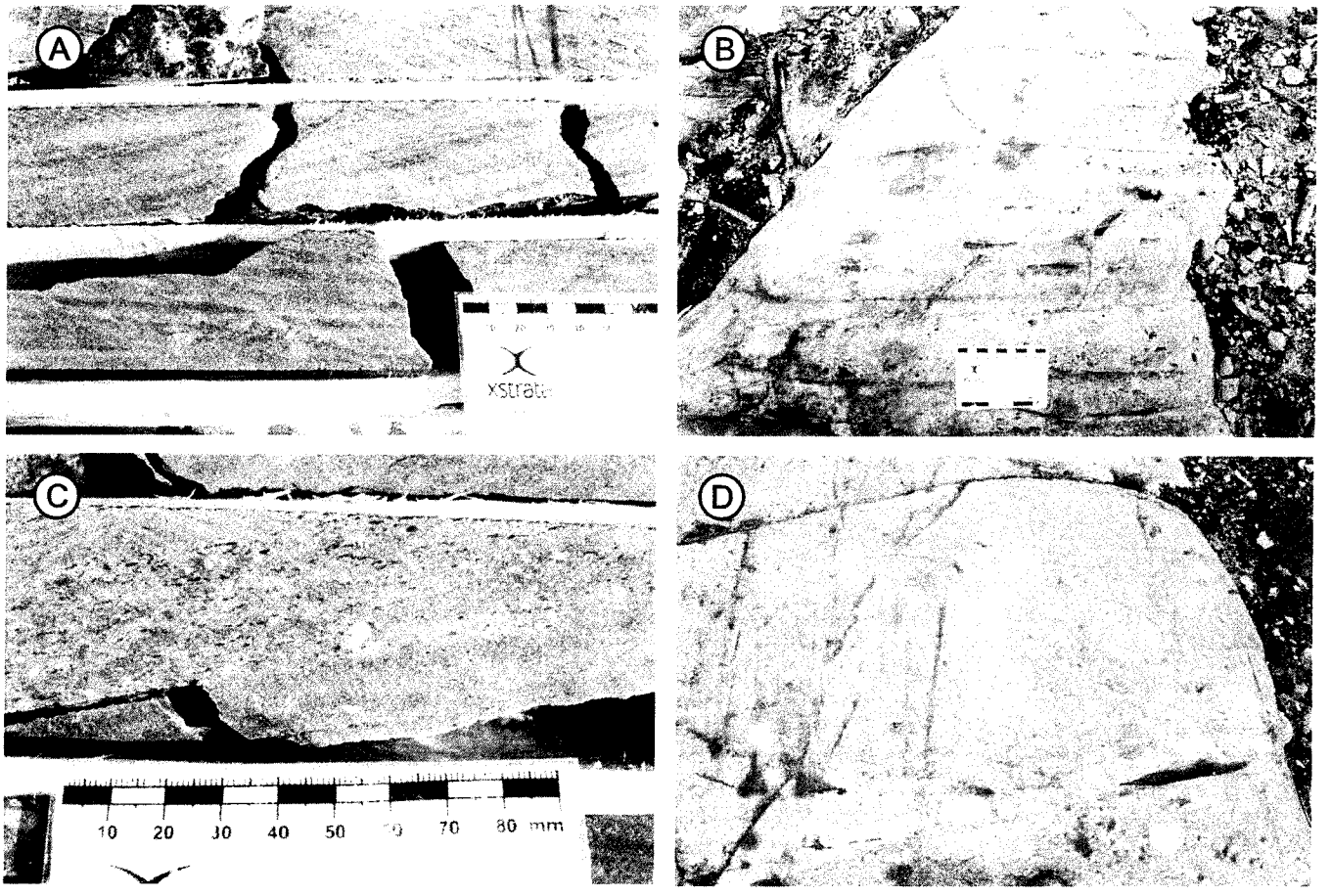

Figure 7-6. Lithic clast-dominated sandstone and breccia. A) Lithic clast-dominated sandstone with sulfide lamination (HW-07-05, 180 m). B) Plane-bedded and normally graded lithic clast-dominated sandstone and granule breccia in outcrop. C) Lithic clast-dominated sandstone and granule breccia (HW-07-05, 180 m). D) Normally graded lithic clast-dominated breccia with a scour structure at base in outcrop (card for scale). E) Representative drill core log of lithic clast-dominated sandstone and breccia.

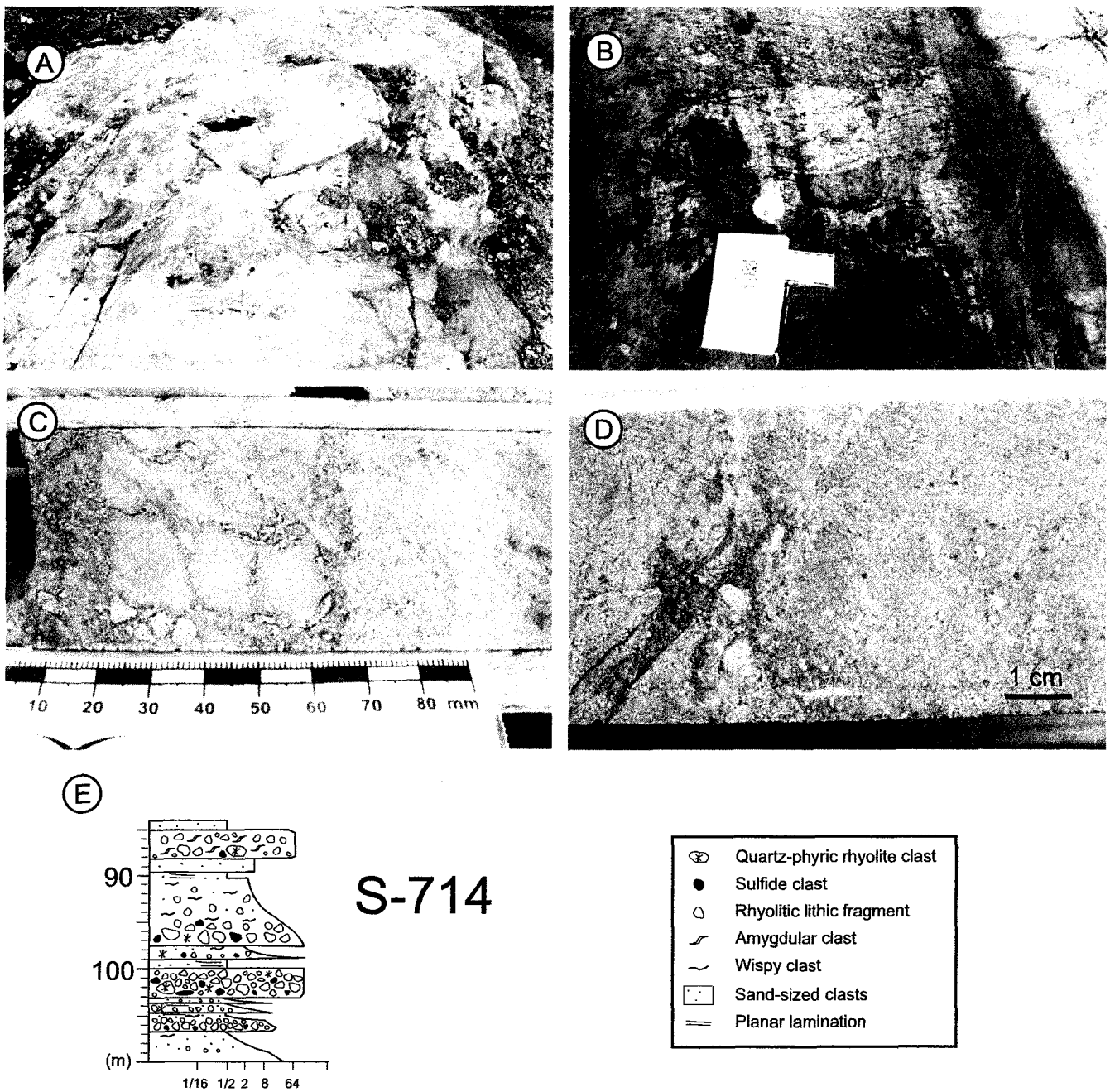

Figure 7-7. Quartz-phyric rhyolite clast- and sulfide clast-bearing lithic breccia. (quartz-phyric rhyolite breccia) A) Thick succession of quartz-phyric rhyolite breccia with scours up to 1m deep and abundant sulfide fragments in outcrop (card for scale). B) 1 m-wide clast of xenolith-bearing rhyolite contained within the quartz-phyric rhyolite in outcrop. C) Quartz-phyric and aphyric rhyolite clasts in the quartz phyric rhyolite breccia (HW-07-05, 207 m). D) Sulfide fragment and altered quartz-phyric rhyolite clast in quartz-phyric rhyolite breccia (HW-07-06, 87 m). E) Representative drill core log of quartz-phyric rhyolite breccia.

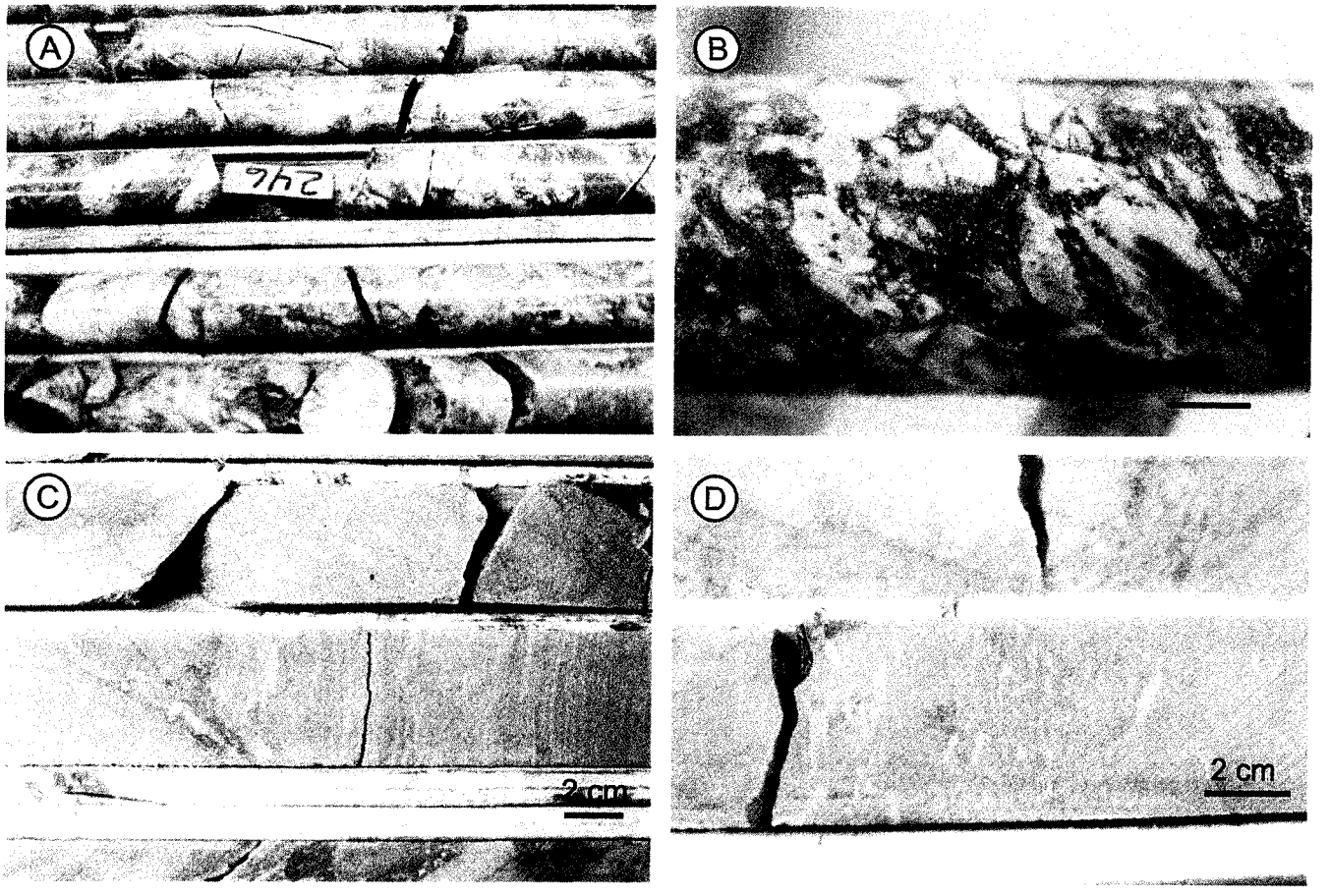

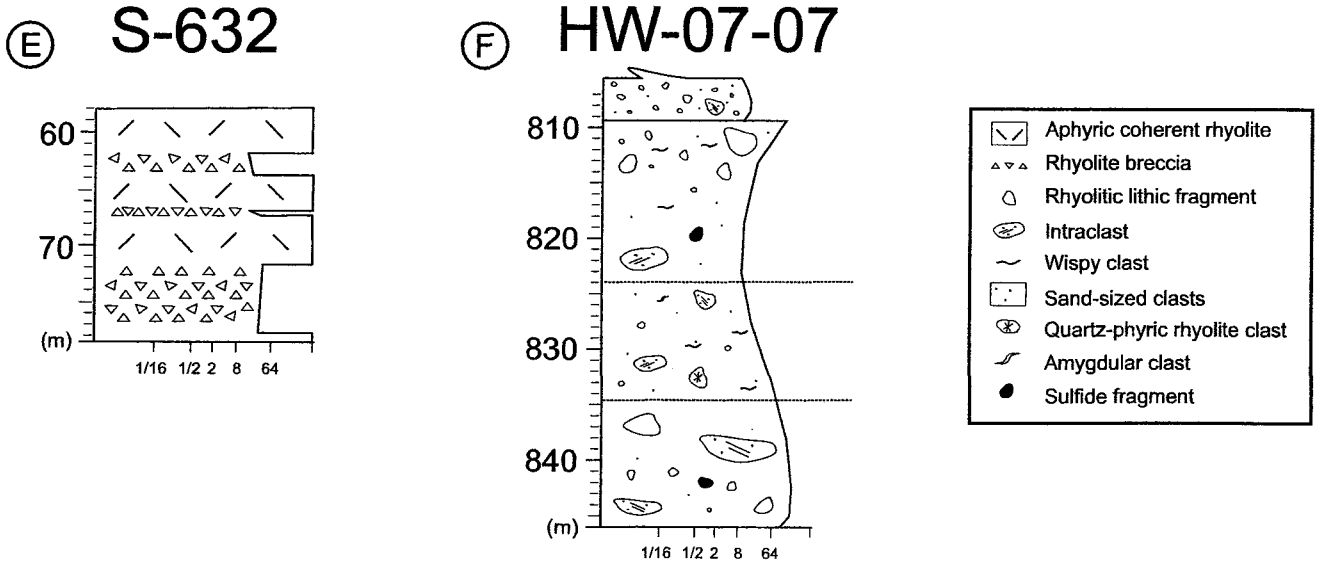

Figure 7-8. A) B) Monomictic rhyolite breccia with in situ jigsaw-fit texture occurring near the margin of aphyric coherent rhyolite. For scale core diameter is 36.5 mm (S-632, 75 m). C) Sulfide laminated sandstone intraclasts in suspended intraclast and cobble-boulder breccia. Note the change in bedding orientation between clasts and the presence of coarser rhyolite fragments adjacent to the intraclasts in the martrix (HW-07-07, ~833 m). D) An interval with coarse rhyolite fragments (top) and an interval with distorted bedding (base). Note the interval containing more wispy fragments (HW-07-07, ~833 m). E) F) Representative drill core logs containing monomictic rhyolite breccia and suspended intraclast and cobble-boulder breccia, respectively.

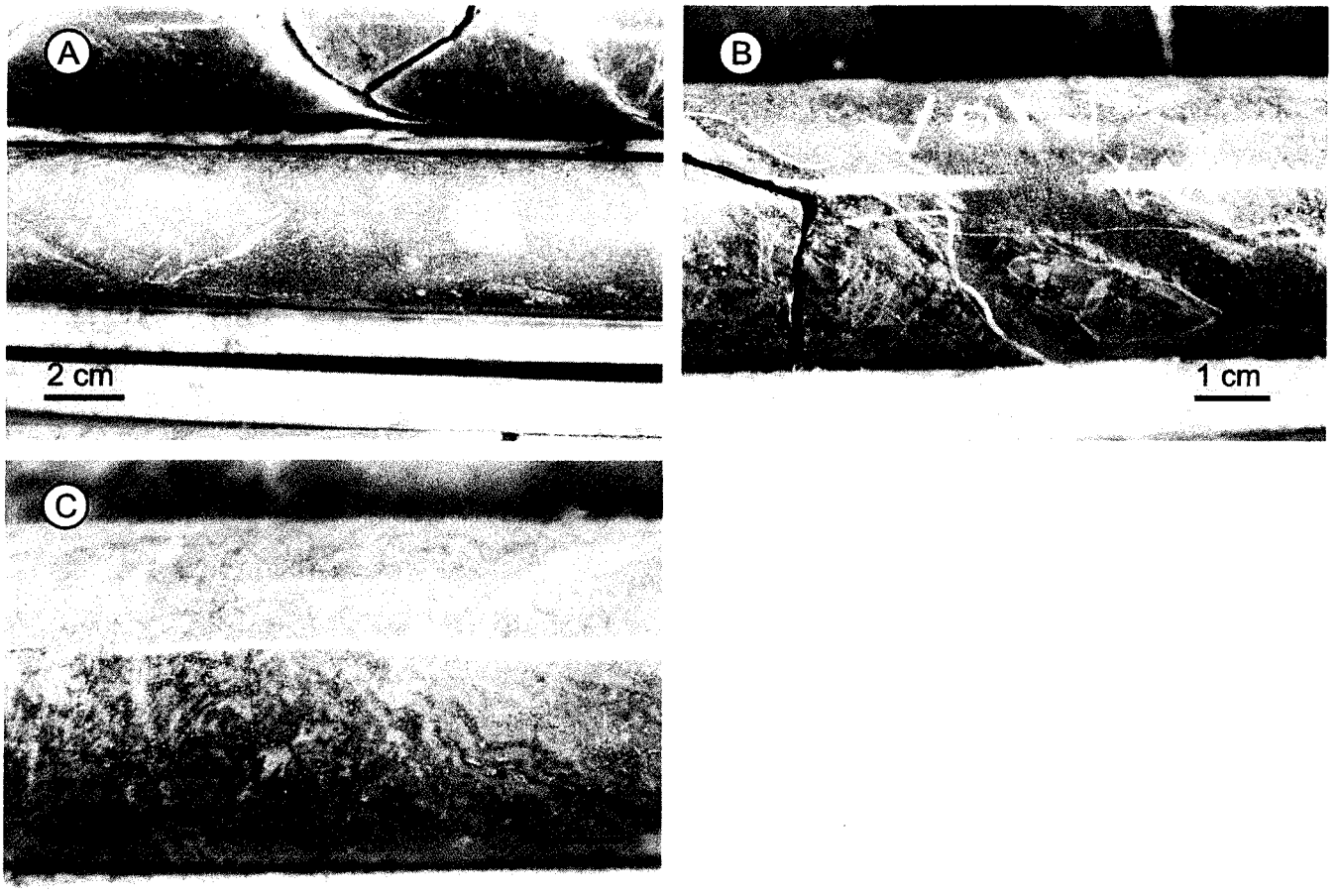

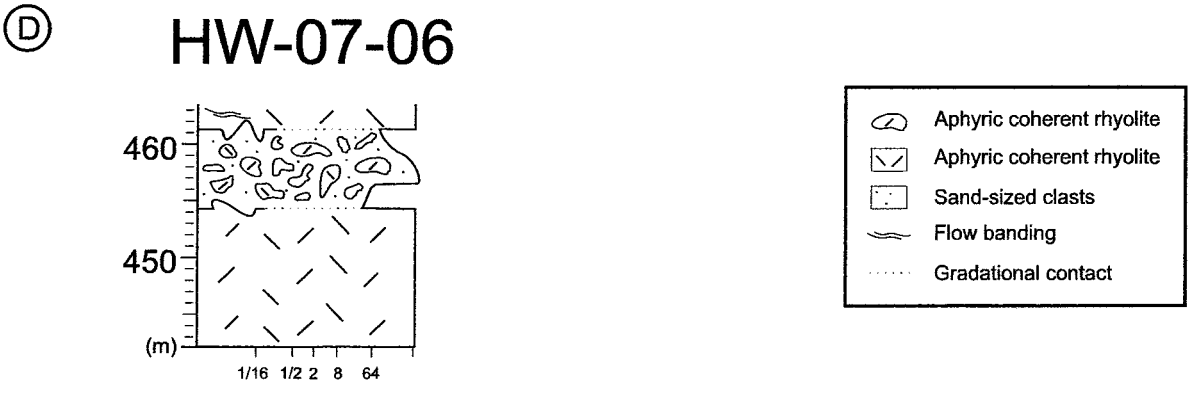

Figure 7-9. Sediment-matrix rhyolite breccia. A) B) Matrix-supported rhyolite breccia comprising fragments in sandstone adjacent to coherent rhyolite (S-628, 48 m and HW-07-05, 310 m, respectively). C) Mixture of fine rhyolite fragments and sandstone (HW-07-05, 310 m). D) Representative drill core log of sediment-matrix rhyolite breccia.

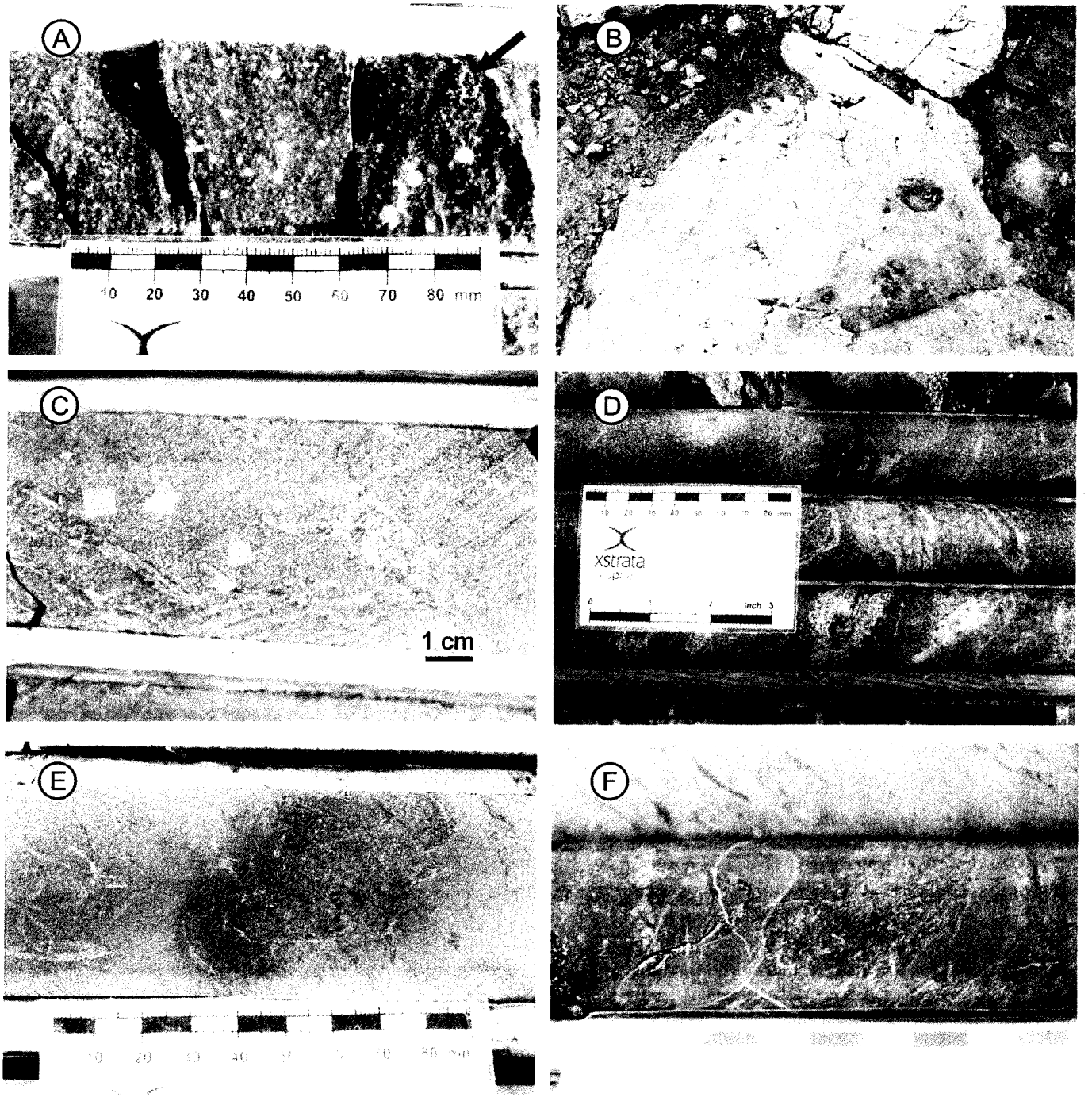

Figure 8. Basalt and syenite intrusions. A) Feldspar-phyric syenite intrusion. Note the green xenolith in the upper right hand corner (red arrow) (HW-07-06, 196 m). B) Basalt intrusion (red arrow) in wispy clast-rich breccia in sand-blasted outcrop. Note the chlorite alteration halo adjacent to the intrusion (green arrow). C) Basalt in drill core with euhedral pyrite dissemination (HW-07-05, 190 m). D) Quartz-carbonate veins with euhedral pyrite dissemination and epidote-rich veins in intrusive basalt (S-575, 210 m). E) Irregular pocket of sedimentary material incorporated near the contact of a basalt intrusion (HW-07-06 241). F) Finger of basalt intruding into volcaniclastic material (S-613, 270 m).

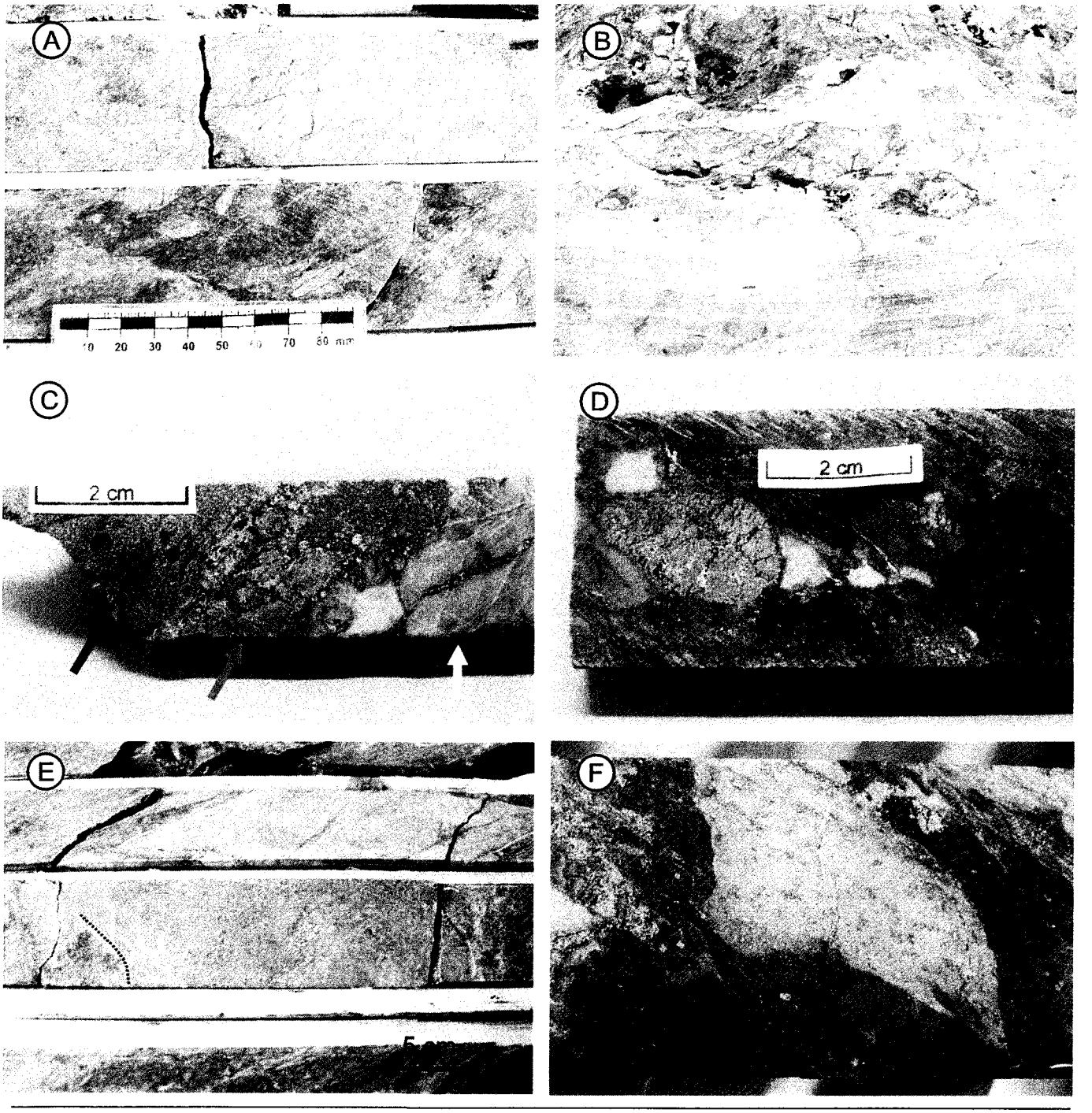

Figure 9-1. Sulfide clast textures. A) Fine-grained massive sulfide clast (top) and numerous smaller sulfide clasts in sericitized quartz-phyric rhyolite breccia (HW-07-06, 28 m). B) Massive sulfide clasts at the base of quartz-phyric rhyolite breccia in outcrop. C) Partly sulfide-replaced quartz-phyric rhyolite clast (red arrow), framboidal massive sulfide clast (green arrow), and sericitized rhyolite fragment with sulfide stringer (yellow arrow) in quartz phyric rhyolite breccia (HW-07-05 198 m). D) Rounded massive sulfide clast and siliceous clasts partly replaced by sulfides in quartz-phyric rhyolite breccia (S-714, 77 m). E) Partly sulfide-replaced and altered aphyric rhyolite clast (borders indicated) in quartz-phyric rhyolite breccia (HW-07-06, 310 m). F) Disseminated sulfide in aphyric rhyolite (center). Note that the sulfide distribution in the clast is different from that in the matrix (HW-07-05, 140 m).

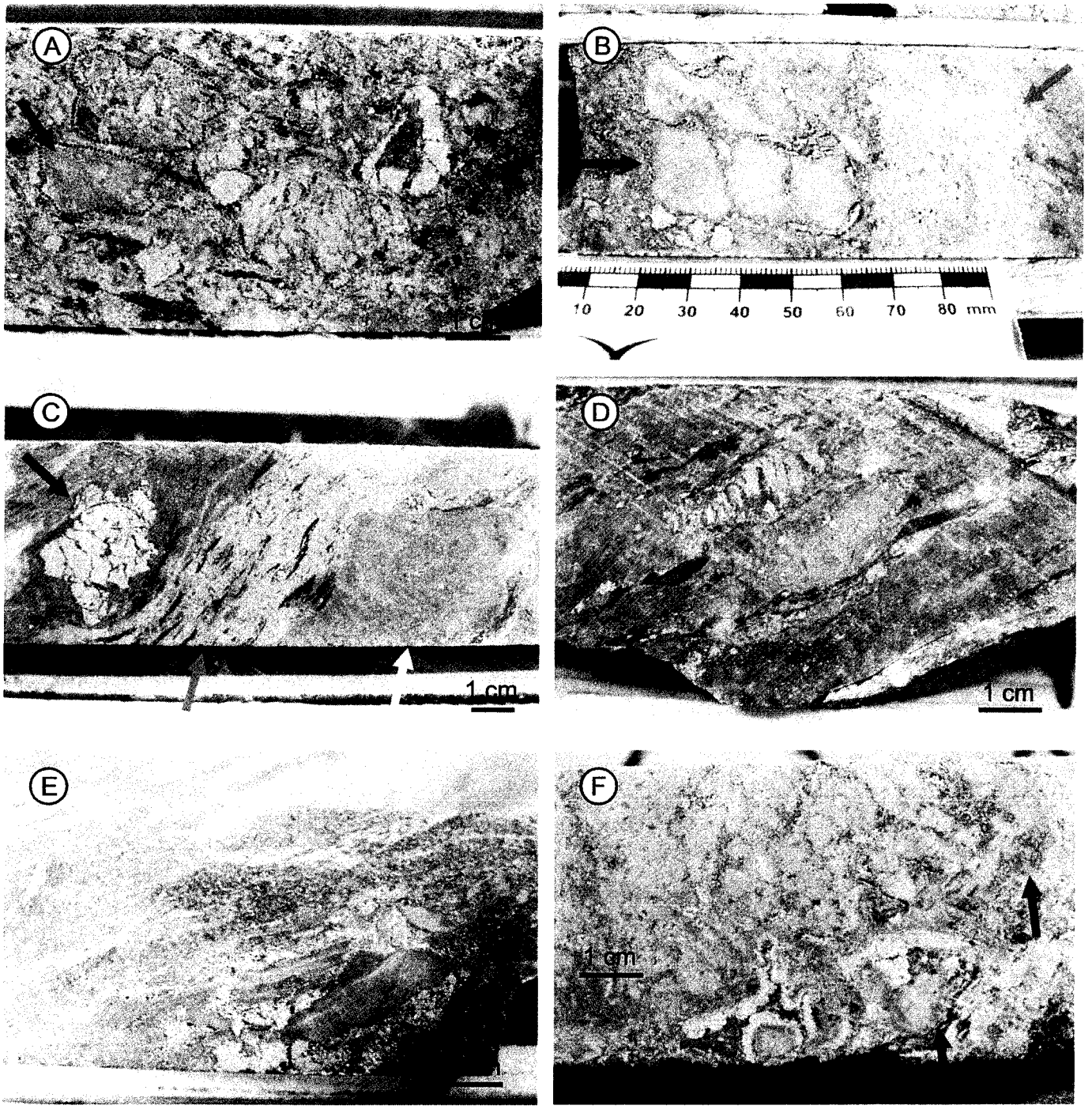

Figure 9-2. Sulfide clast textures. A) Dispersed sulfide fragments including a partly sulfide-replaced rhyolite fragment (red arrow, border indicated) in wispy clast-rich breccia (HW-07-06, 48 m). B) Aphyric rhyolite clast with sulfide in the fractures and along the margin (red arrow) and a quartz-phyric rhyolite clast with dissminated sulfides (green arrow) in quartz-phyric rhyolite breccia. Note the difference in sulfide replacement characteristics (HW-07-05, 204 m). C) Massive sulfide clast (red arrow), distorted and altered intraclast of wispy clast-rich breccia that contains small sulfide clasts (green arrow), and aphyric rhyolite with disseminated sulfides (yellow arrow) in wispy clast-rich breccia (HW-07-04, 230 m) D) Massive sulfide clasts and partly sulfide replaced rhyolite fragment in wispy clast-rich breccia (HW-07-05, 15 m). E) Partly sulfide-replaced and altered rhyolite clast in quartz-phyric rhyolite clast breccia (HW-07-06, 310 m). F) Framboidal pyrite growth occuring along a rhyolite clast in wispy clast-rich breccia. Note that the exposed areas of the clast do not have any sulfide rind, possibly as a result of abrasion during transport (HW-07-06, 87 m).

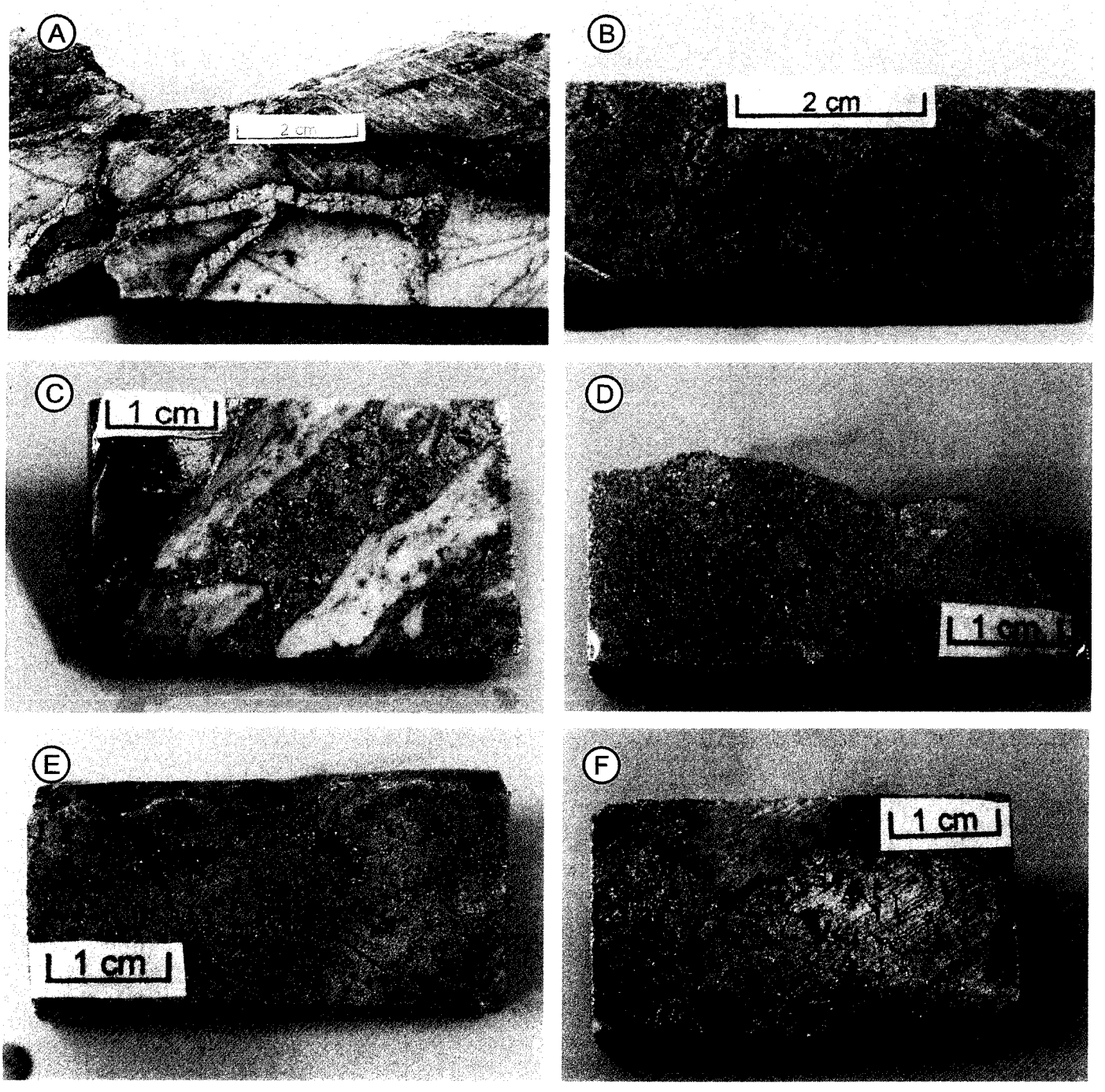

Figure 9-3. Sulfide clast textures. A) Sulfide stringers with chloritized margin in an aphyric rhyolite clast. Sulfide stringers terminate at the margin of the clast in several places (HWS-07-06, 91 m). B) Clast with massive pyrite to disseminated pyrite replacing quartz phyric rhyolite (HW-07-05, 198 m). C) Sericite-rich bands occurring in a sulfide-bearing clast (HW-07-05, 137 m). D) Granular massive pyrite intermingled with quartz and massive-textured pyrite within a single clast (S-716, 86 m). E) Concentric colloform banding of pyrite with traces of sphalerite in a massive sulfide clast (S-614, 78 m). F) Massive pyrite with traces of chalcopyrite and remaining vestiges of quartz-phyric rhyolite within a massive sulfide clast (S-631, 87 m).

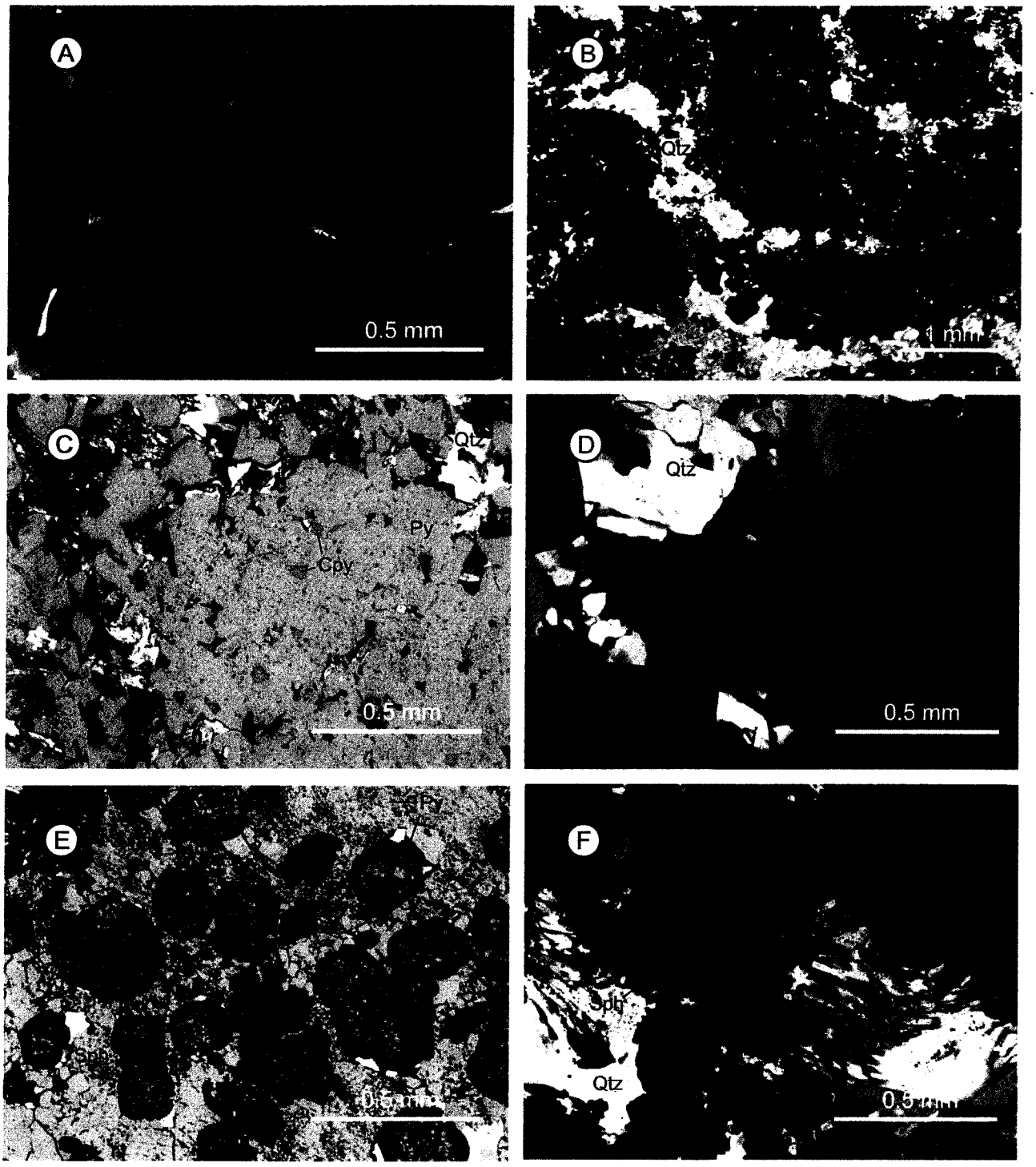

Figure 9-4. Thin section photographs of massive sulfide clasts. A) Core zones in the massive pyrite that contain chalcopyrite and sphalerite blebs along fractures. Recrystallized pyrite adjacent to fractures contain traces of these minerals (crossed polarizers and transmitted light and reflected light). B) Millimetre-scale pyrite bands spaced by crystalline quartz (plane polarized and reflected light). C) Irregular chalcopyrite blebs in massive pyrite. Euhedral pyrite faces occur commonly where the massive pyrite is in contact with quartz (crossed polarizers and reflected light). D) Massive pyrite with core zones containing inclusions of chalcopyrite and sphalerite as well as larger chalcopyrite blebs occurring outside the massive pyrite. Quartz crystals commonly have their length oriented perpendicular to the contact with the massive pyrite (crossed polarizers and reflected light). E) Subhedral sphalerite grains containing fine grained pyrite dissemination (crossed polarizers and reflected light). F) Pitted pyrite occurring adjacent to quartz with traces of sphalerite (plane polarized and reflected light).

Legend

This legend applies to figures 10-1 trough 10-5 and 10-7.


Aphyric rhyolite 2


Xenolith-bearing rhyolite


Aphyric rhyolite 1


Quartz-phyric rhyolite


Clast-rotated monomictic rhyolite breccia


Amygdular clast-bearing lithic breccia


Quartz-phyric rhyolite clast- and sulfide clast-bearing lithic breccia


Lithic clast-dominated sandstone and breccia


Wispy clast-rich sandstone and breccia with proposed bedding/scour surfaces


Andesite

Drill hole location (within +/-15m and +/-25m for cross-section and plan view respectively)

Gold zone


Syenite sill/dike


Basalt sill/dike

Andesite Fault


Minor fault/thrust fault (arrow points to downthrust block)


Fault/inferred fault (defined by a rubble zone)


Zone of gold mineralization as indicated in Figure 11.


Abrupt facies changes boundary


Sericitization +/- chloritization


Chloritization +/- sericitization

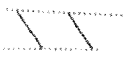
Sericite +/- epidote +/- hematite alteration


Epidote and carbonate and/or garnet spots

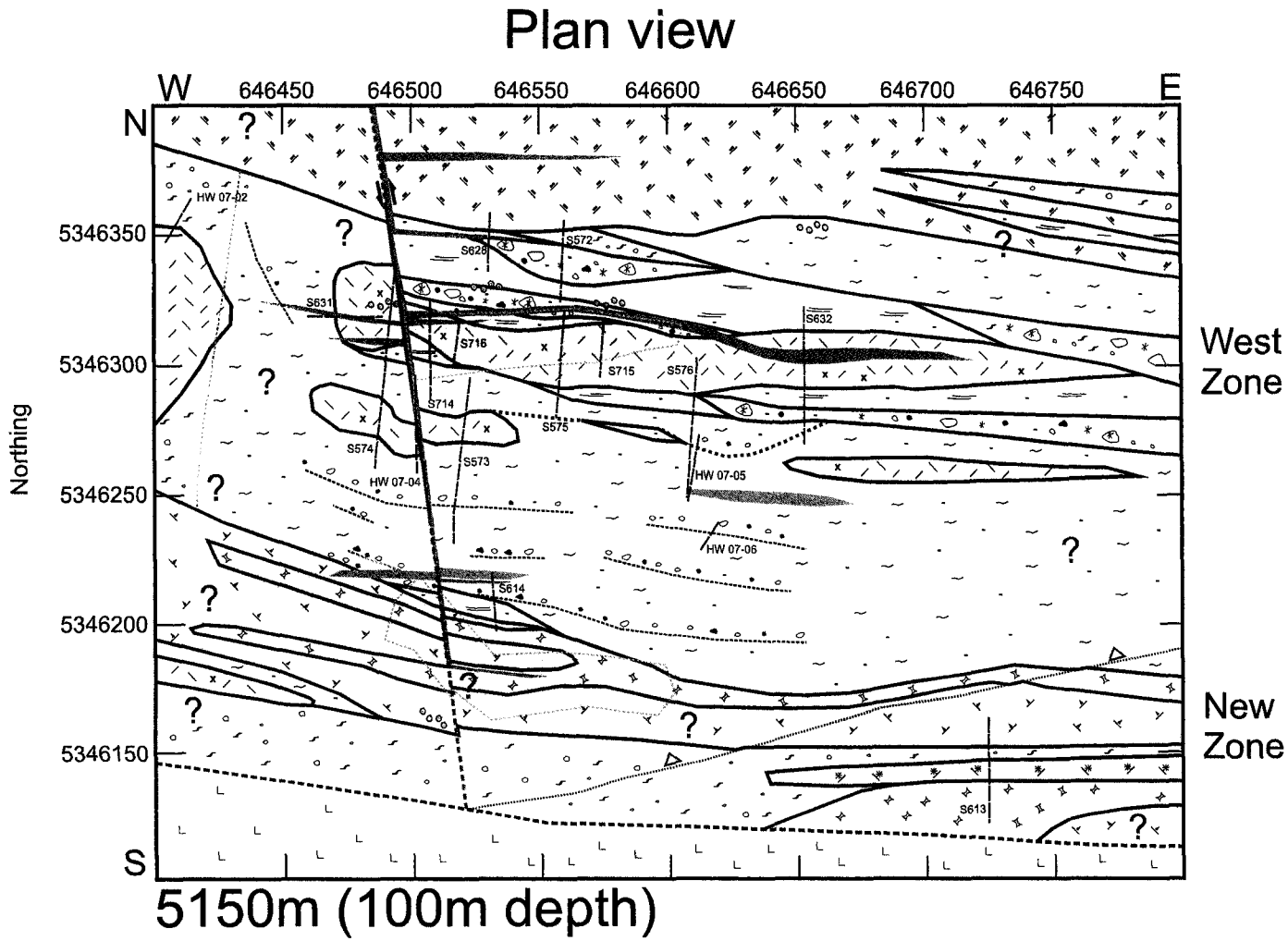

Figure 10-1. Plan view of the Horne West succession showing intervals of gold mineralization. Late faults commonly occur along mafic intrusions in the western portion of the study area. Synvolcanic faulting or slumping may have occurred at the western margin of the study area based on the abrupt facies changes and unit thickness changes from east to west.

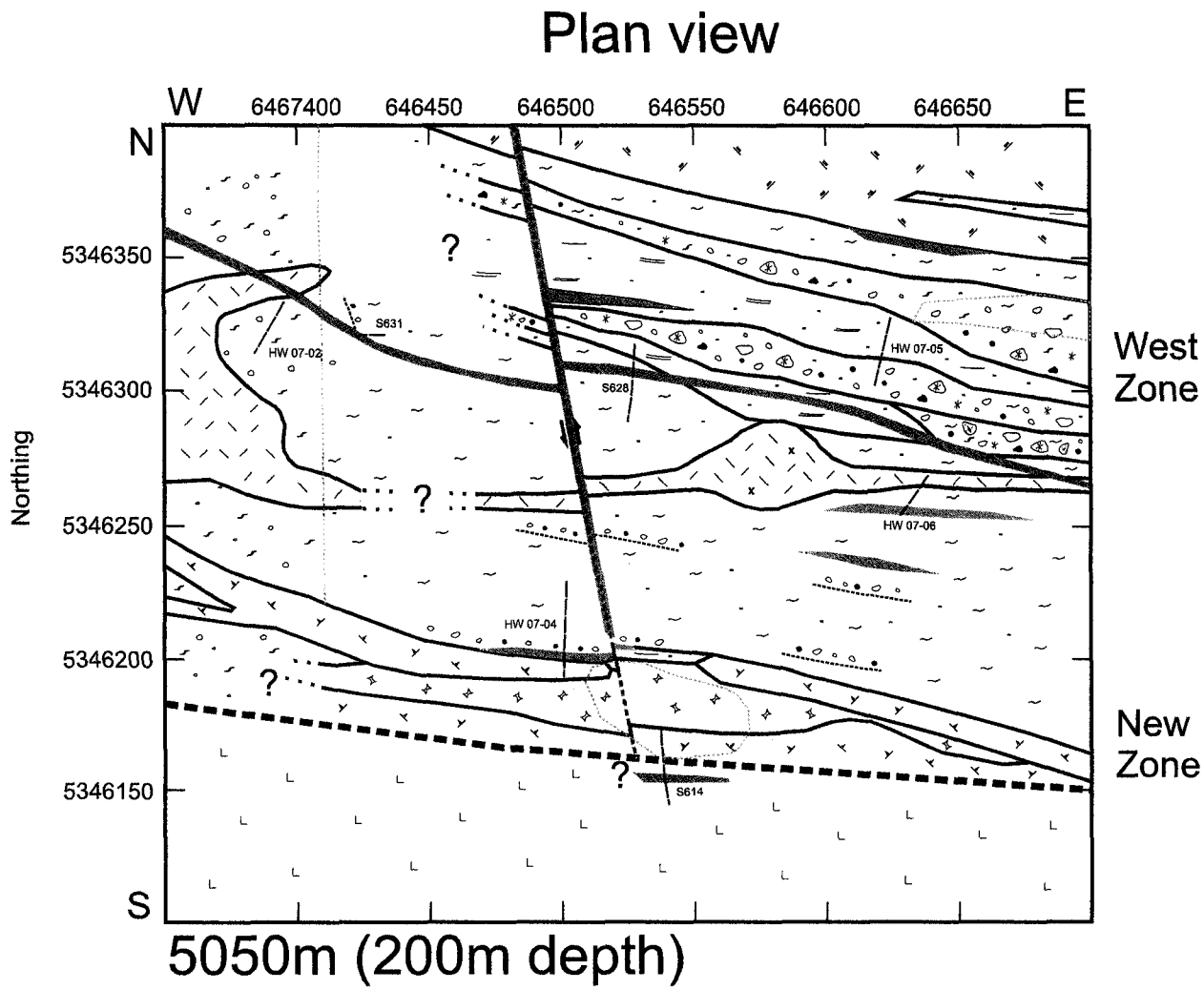

Figure 10-2. Plan view of the Horne West succession showing intervals of gold mineralization. Late faults commonly occur along mafic intrusions in the western portion of the study area. Synvolcanic faulting or slumping may have occurred along the western margin of the study area based on abrupt facies changes and unit thickness changes from east to west.

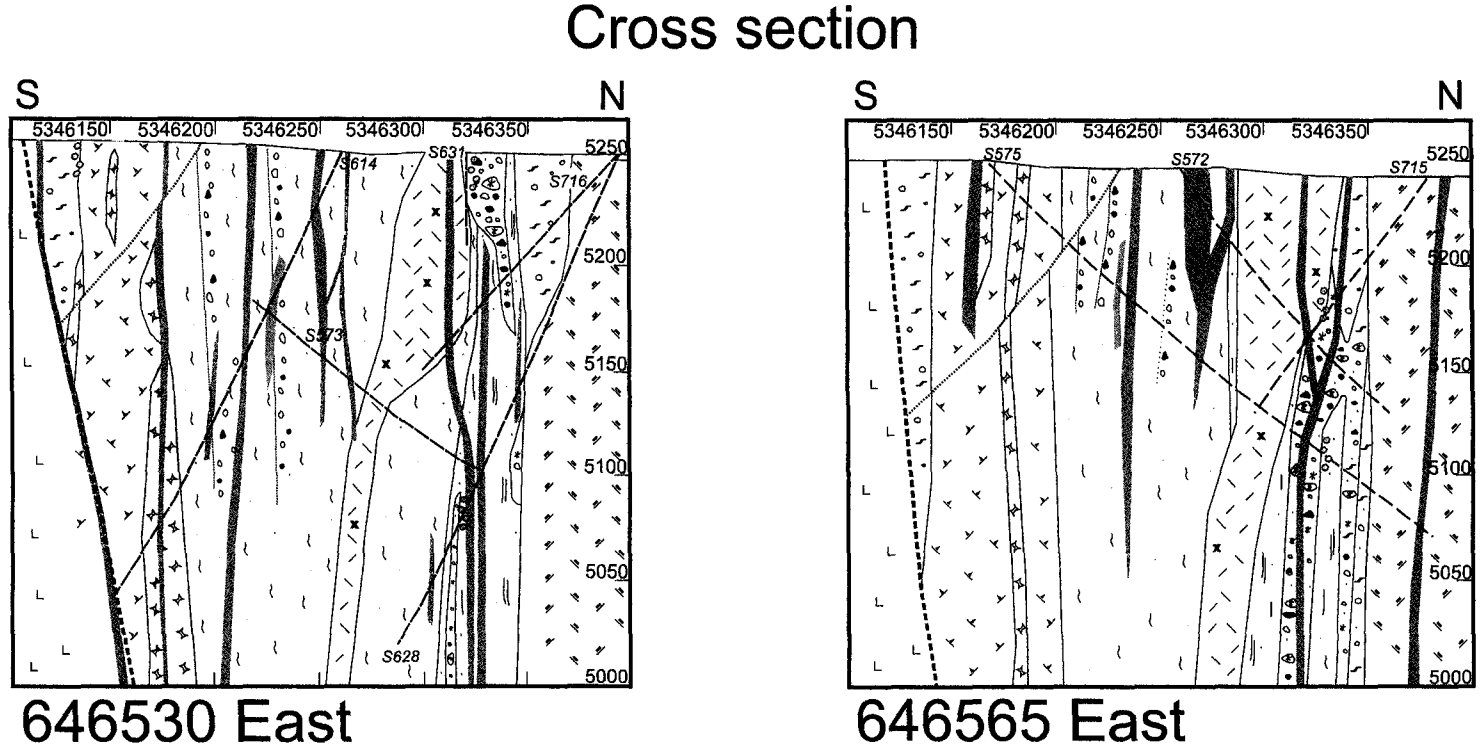

Figure 10-3. Cross sections of the Horne West succession showing intervals of gold mineralization.

Cross section

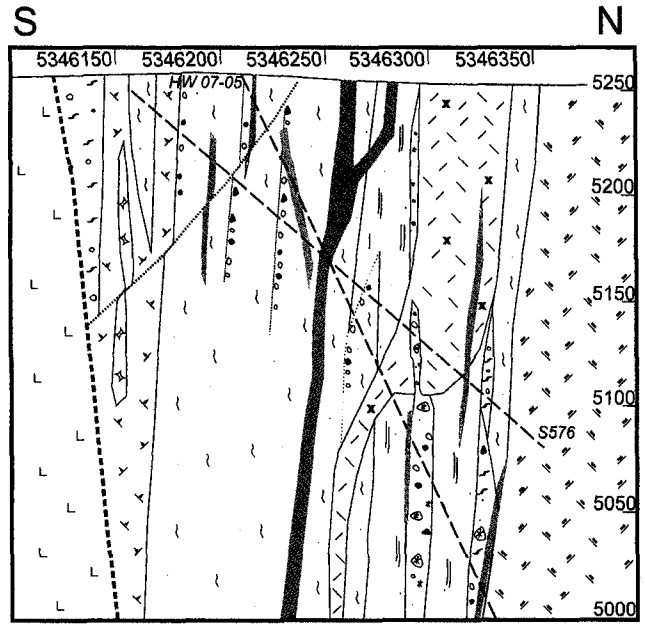

646600 East

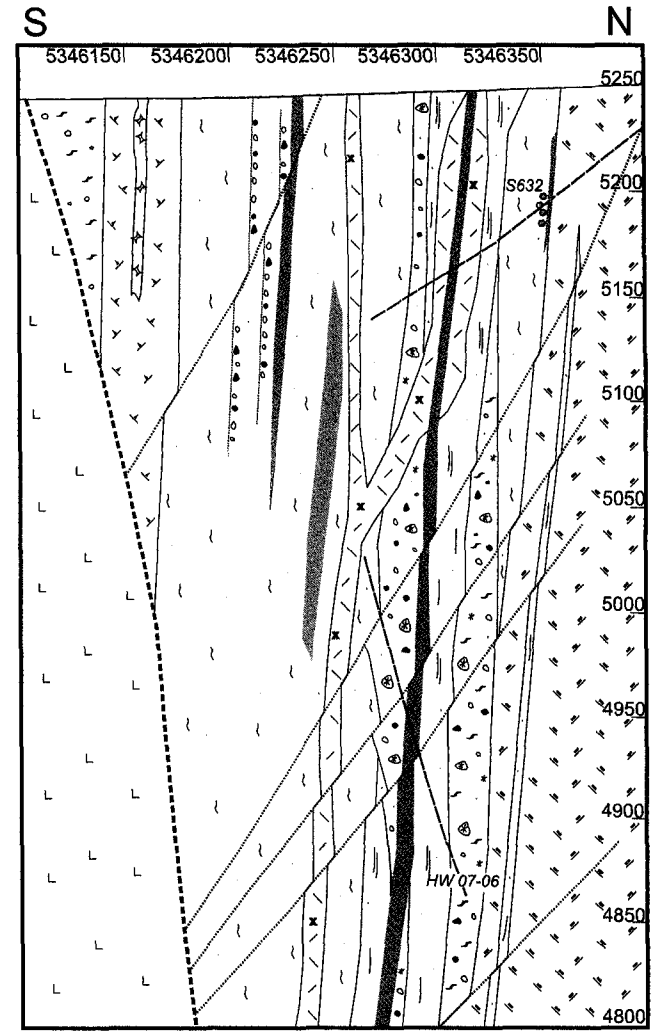

646650 East

Figure 10-4. Cross sections of the Horne West succession showing intervals of gold mineralization.

Alteration in cross section

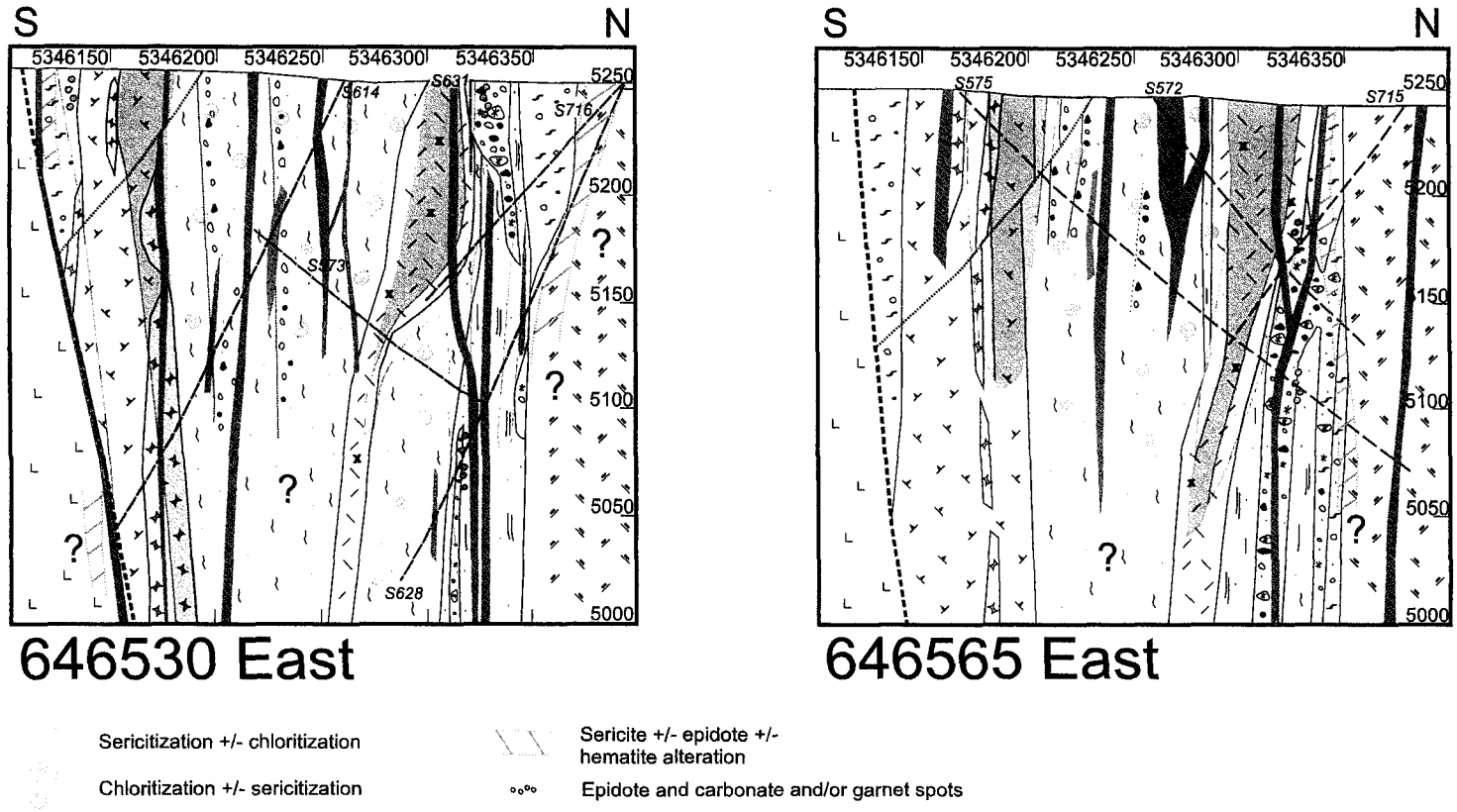

Figure 10-5. Alteration styles recognized in the Horne West succession. Alteration is typically strongest in the western and central parts of the Horne West property and is best defined in synvolcanically-emplaced rhyolite which hosts the gold mineralization.

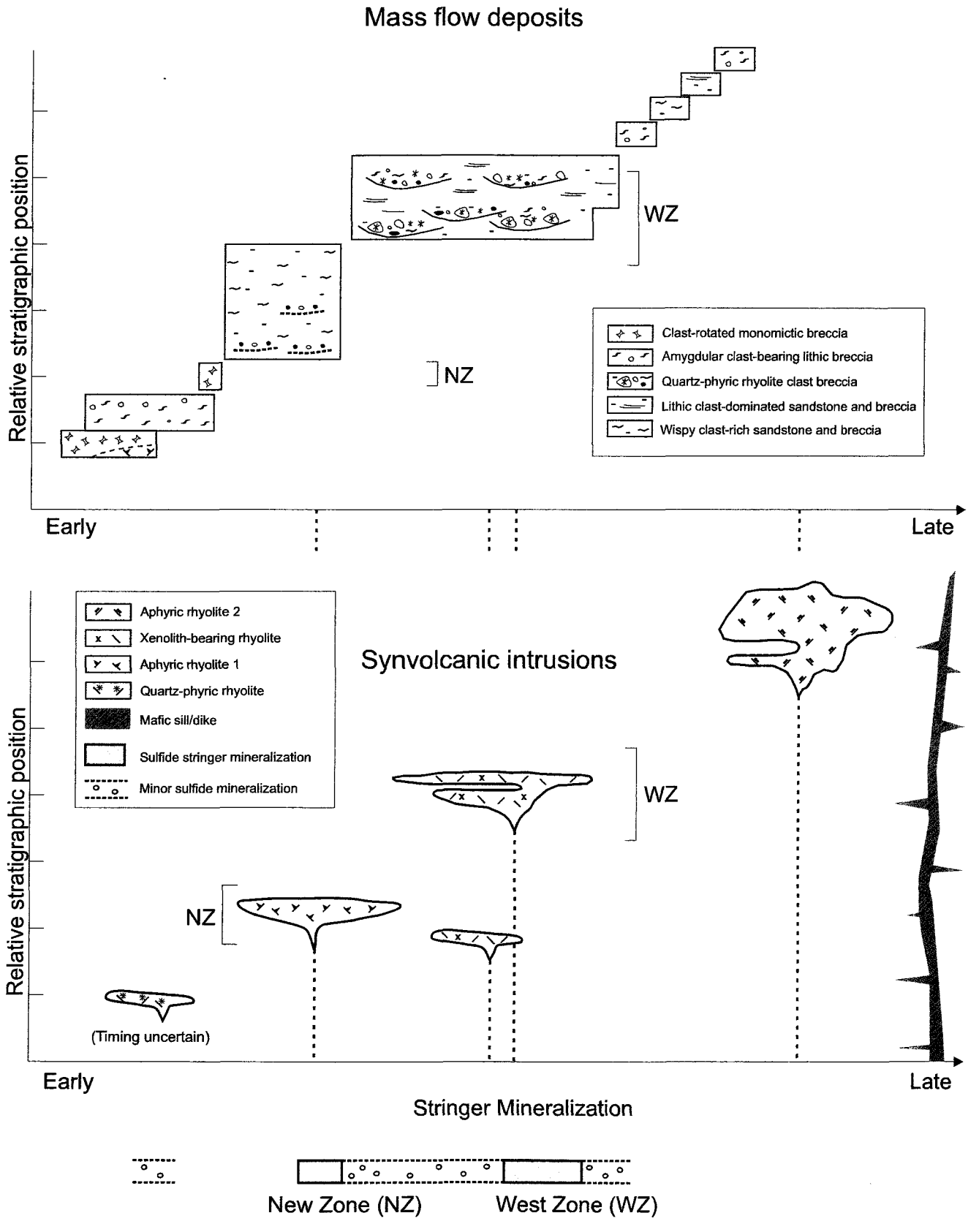

Figure 10-6. Proposed timing for depositional and intrusive events and gold-bearing sulfide stringers. Intrusive facies and gold zones are shown in their relative stratigraphic positions. The New Zone and West Zone are observed close to intrusive rhyolite bodies in the central portion of the succession.

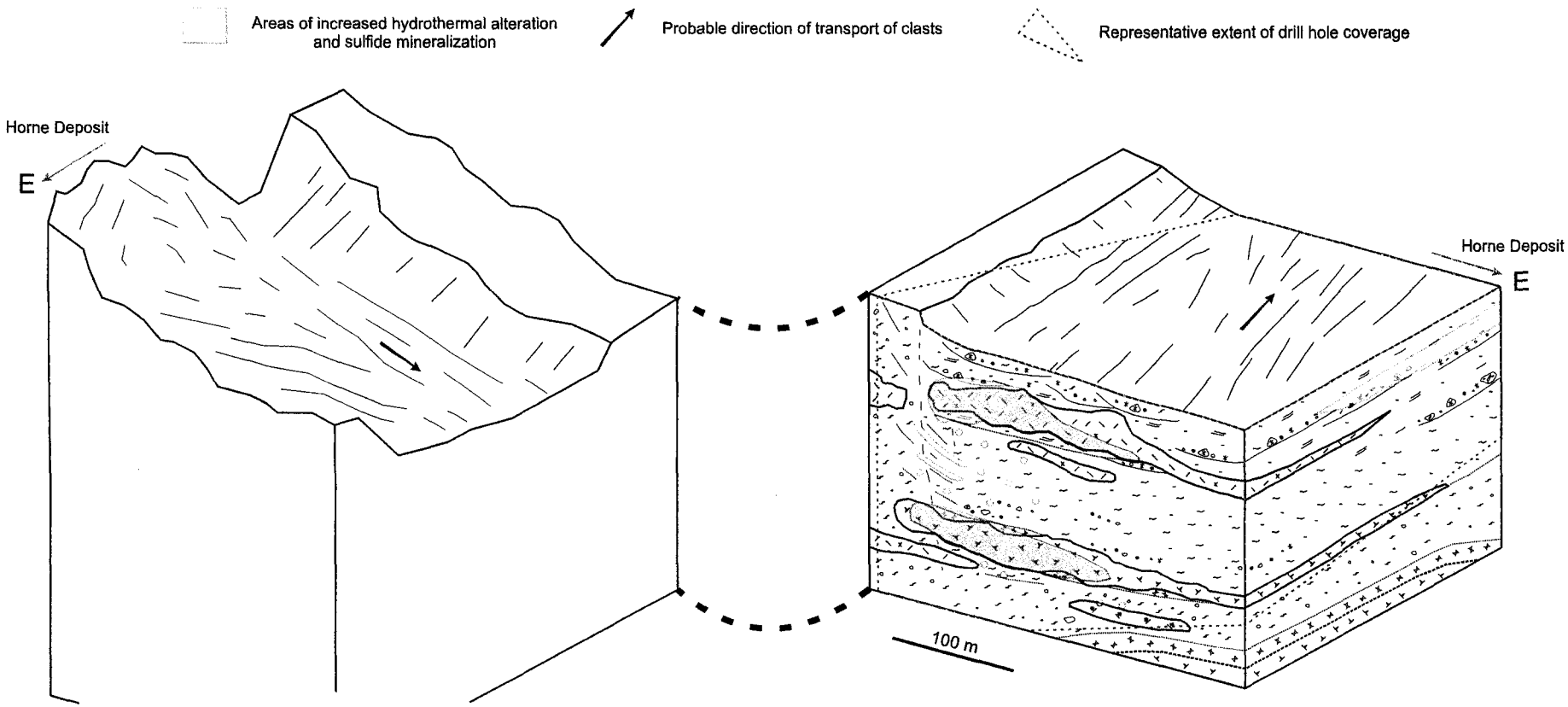

Figure 10-7, Paleotopographic reconstruction of the Horne West Succession shown after the deposition of quartz-phyric rhyolite and sulfide clast-bearing lithic breccia. Chloritization, sericitization, sulfide stringers and gold mineralization occur principally at the western margin of the study area in proximity to a zone along which syn-volcanic faulting and slumping may have occurred. This reconstruction places Horne West in a synvolcanic half-graben that is parallel to the stike of the Horne deposit and the No. 5 Zone. Horne West mineralization may pre-date the Horne orebodies and the No. 5 Zone.

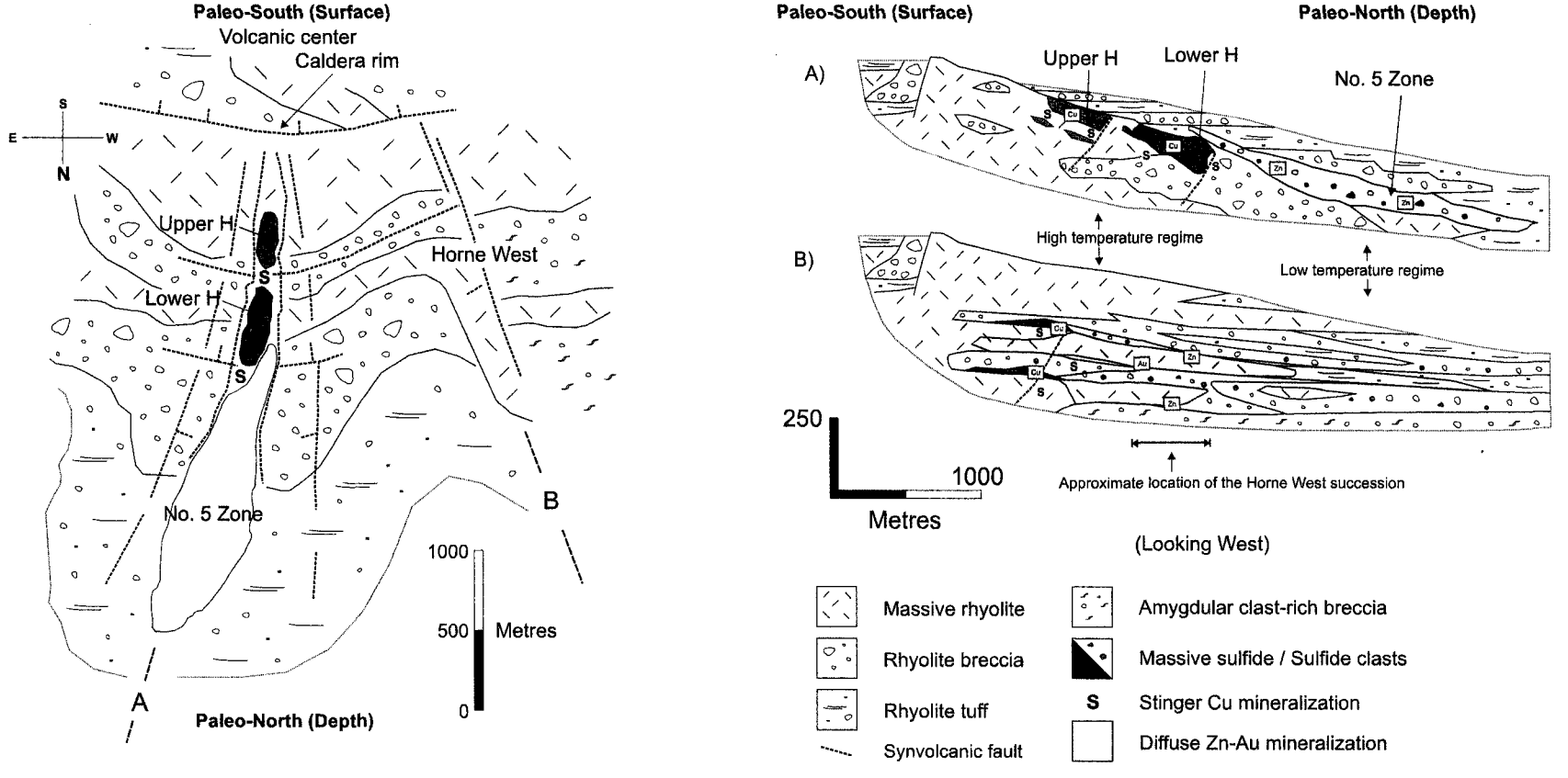

Figure 10-8. Proposed paleo-reconstruction of the Horne Block stratigraphy showing the Horne West succession situated in a half graben to the West of the Horne massive sulfides (modified from Barrett et al.1991). Paleo-cardinal directions are indicated assuming that the Horne stratigraphy is righted without rotation. Facies changes and metal zonation reflect position relative to a topographically elevated effusive rhyolitic center with concentric and radial synvolcanic faults and depressions that host massive sulfide deposits. The Horne West succession occurs within the footwall of the Horne massive sulfides and is principally characterized by Zn-Au rich lenses along intrusive rhyolite bodies and within sulfide clast-bearing rocks.

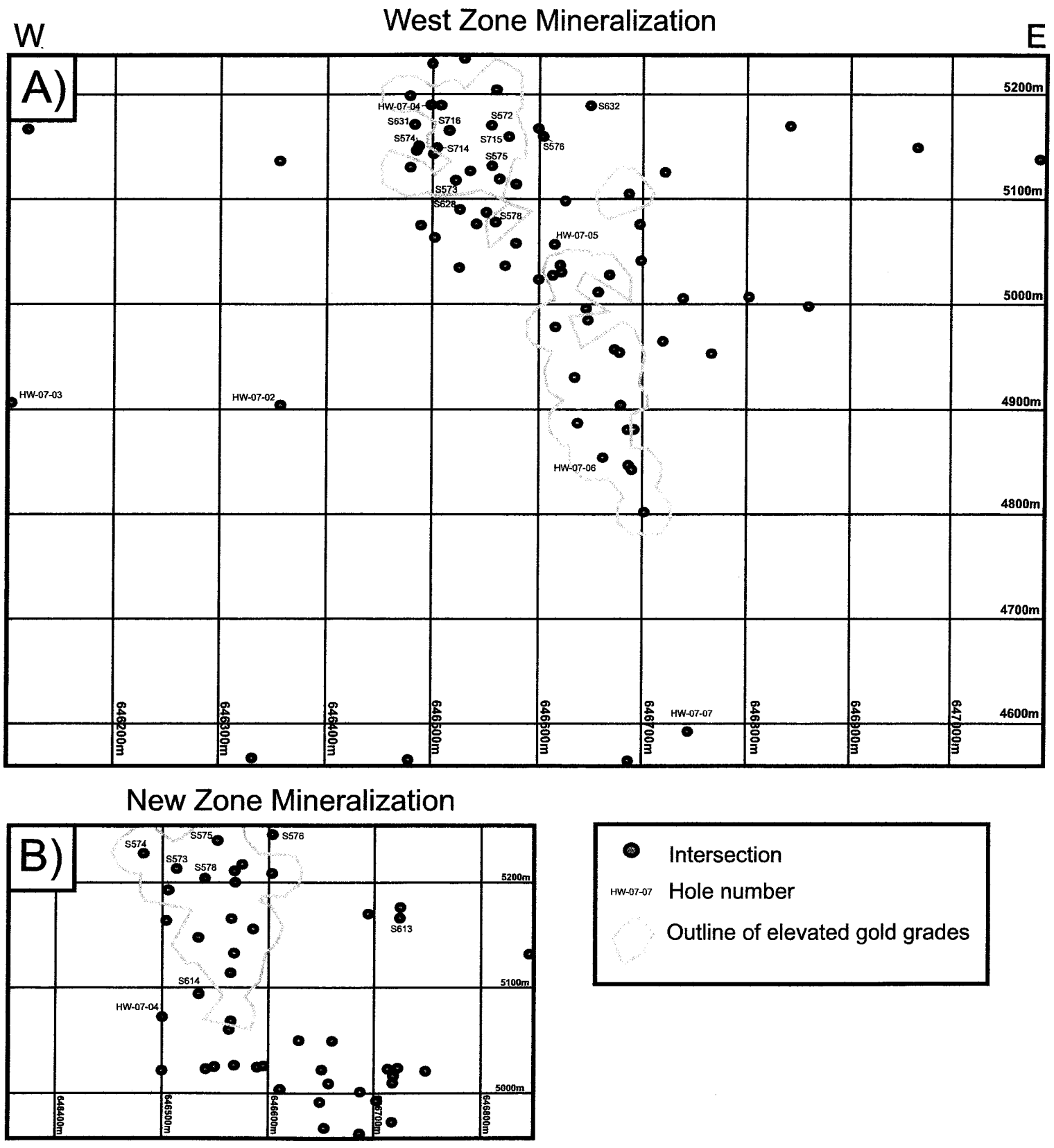

Figure 11-1. Long sections through the Horne West property showing the location of drill holes and the envelope of gold mineralization based on grade, minimum mining width, and with a maximum polygon extension of 25m toward unexplored areas:
A) West Zone B) New Zone.

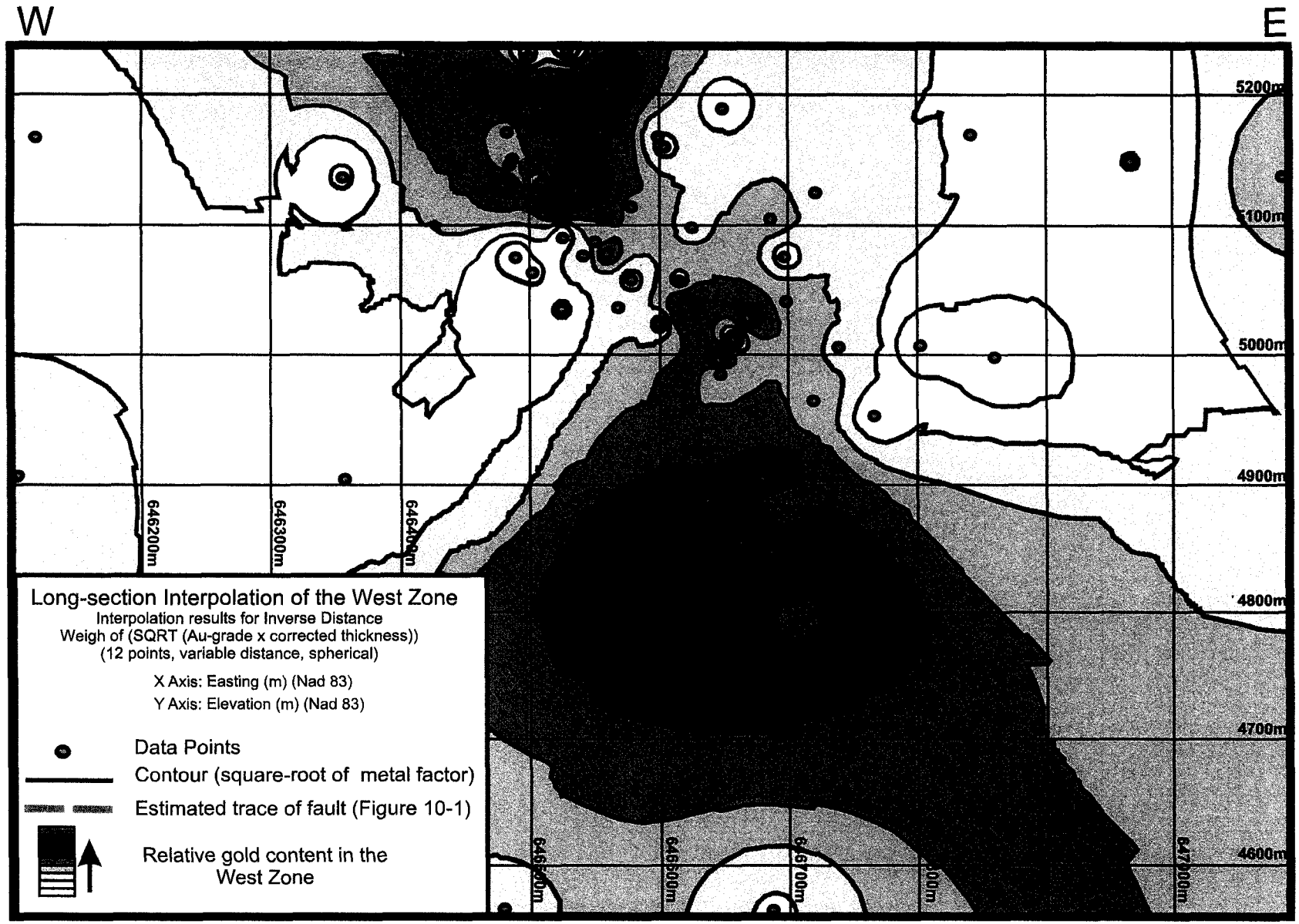

Figure 11-2. West Zone composite long-section looking North and showing inverse-distance-weight Au values (square-root-grade length) for the most significantly mineralized portions of new and historic drill core. Viewed from stratigraphic base to top (from south to North). The plot shows relative gold content in the ground which has a distinct trend and occurs principally in two zones that may represent separate upflow zones.

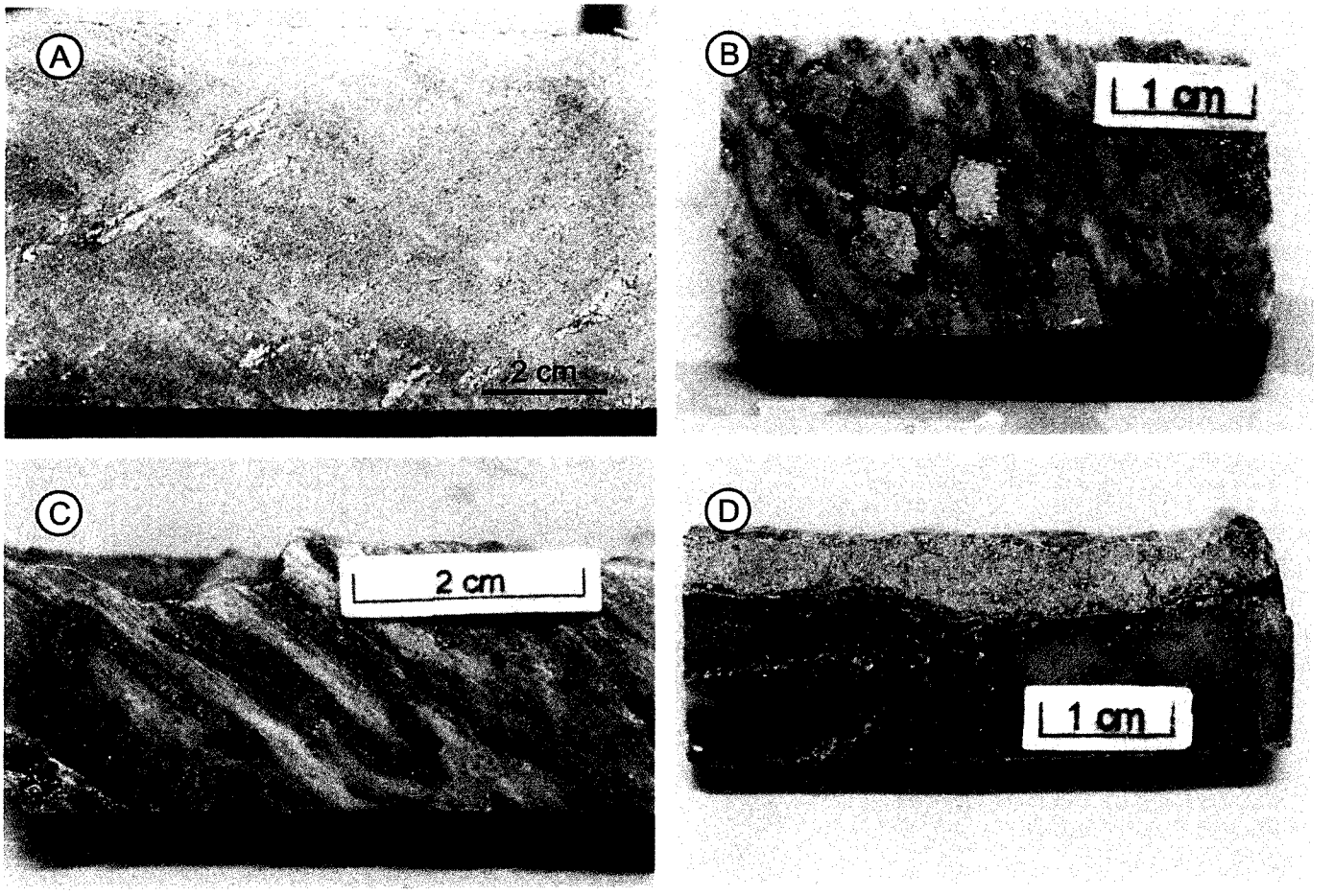

Figure 12-1. Textures related to gold mineralization. A) Disseminated sulfide, possibly replacing wispy clasts in the West Zone (HW-07-04, 96 m). B) and C) Subhedral to stringer-like blebs and disseminations in strongly sericitized rocks within the New Zone (S-574, 53 m, and S-614, 200 m, respectively. D) Sulfide stingers with associated chlorite and sericite alteration in xenolith-bearing coherent rhyolite in the West Zone (S-715, 116 m).

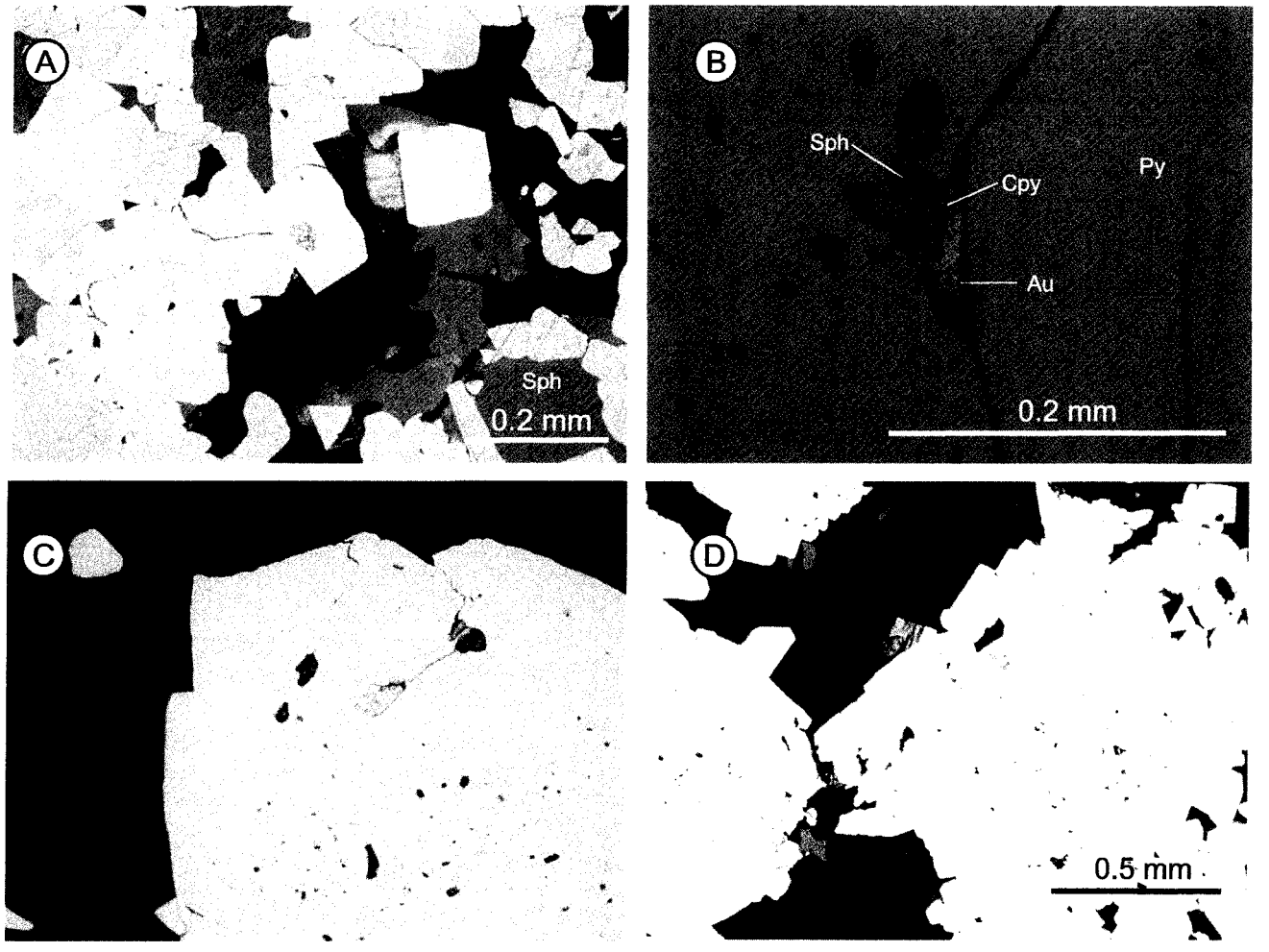

Figure 12-2. Gold observed in thin section. A) A rounded gold grain occuring in euhedral pyrite within a stringer vein (S715, 116 m, reflected light). B), C) and D) Gold occurs locally with chalcopyrite and/or sphalerite and is hosted within pyrite disseminations. It may also occur along fractures (S-614, 200 m, reflected light).

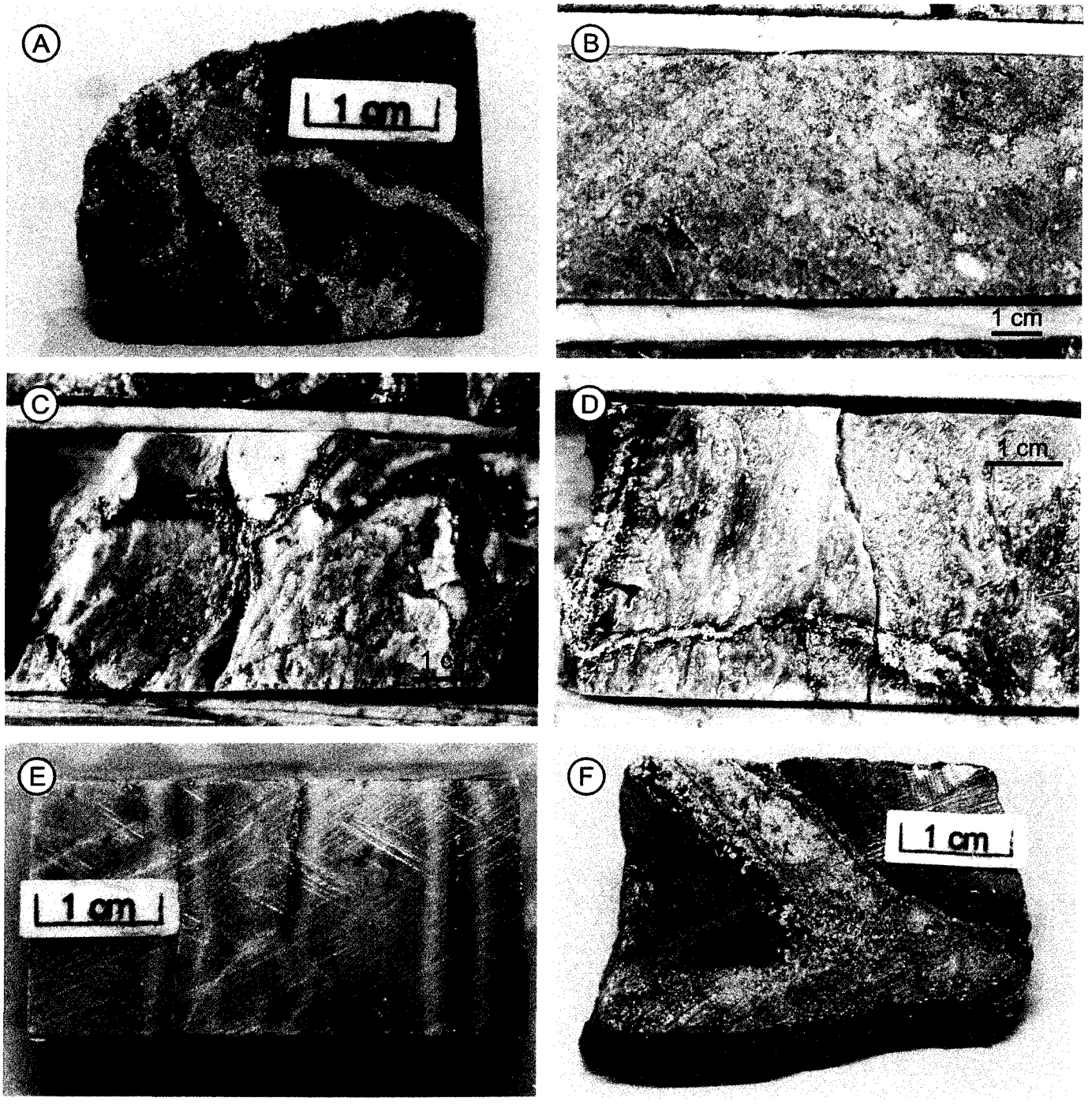

Figure 12-3. Stringer vein sulfide mineralization. A) Rare chalcopyrite stringers observed below in wispy clast rich breccia (S-575, 135 m). B) Diffuse pyrite dominated stringers are commonly observed in volcaniclasitc rocks (HW-07-05, 515 m). C), D), E), and F) Pyrite stringers with traces of sphalerite and chalcopyirte in xenolith-bearing coherent rhyolite; stringers in coherent rhyolite typically have sharp margins and may have strong chloritization occurring adjacent to the vein (S-714, 123 m, S-575, 162 m, HW-07-05, 160 m, and S-632, 148 m, respectively).

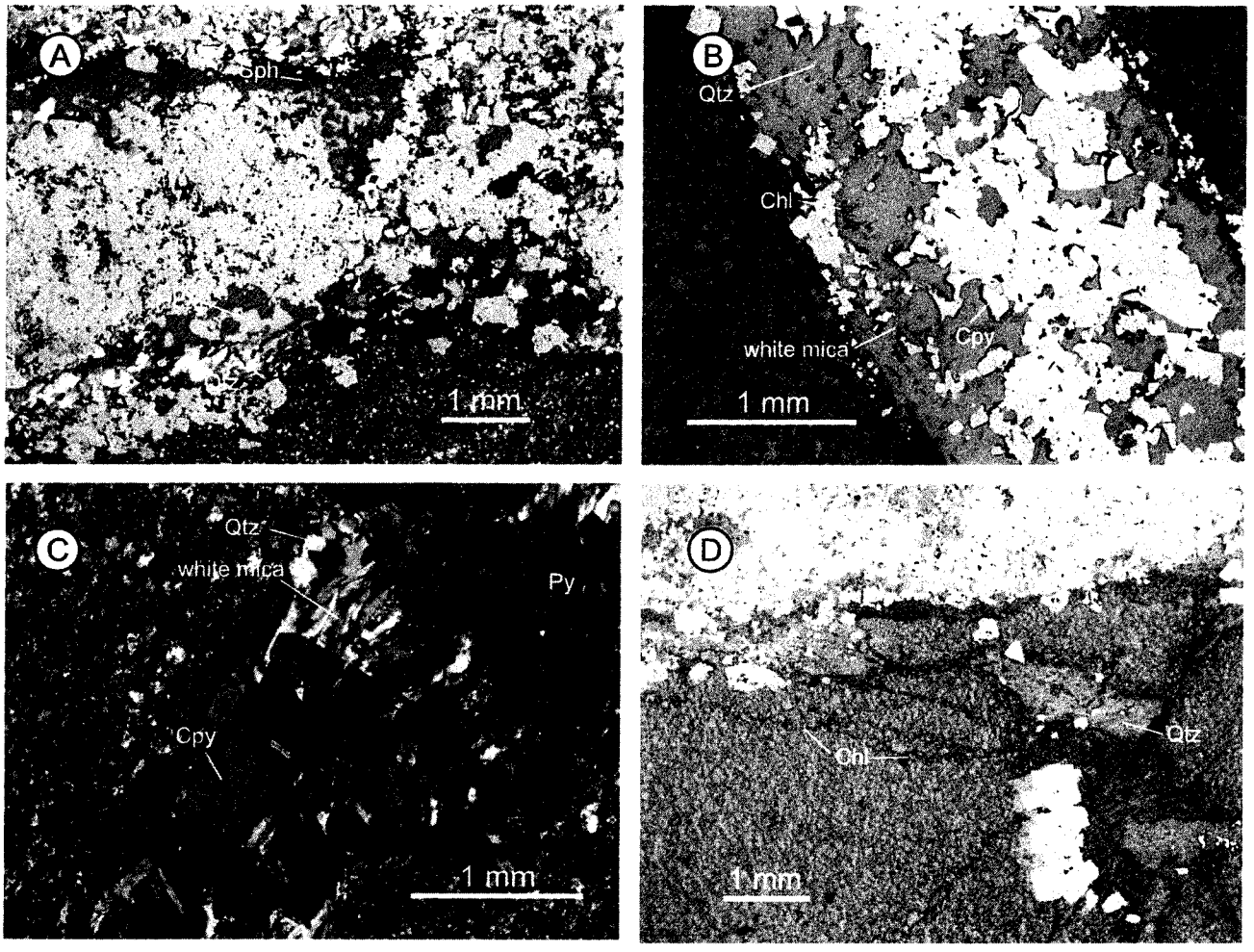

Figure 12-4. Photomicrographs of sulfide stringers in rhyolite. A) and B) Stringer veins with pyrite-rich core and sphalerite or chalcopyrite and quartz occurring toward the margin (S-632, 148 m, crossed polarizers and reflected light, and S-573, 180 m, plane polarized light and reflected light, respectively). C) and D) Stringer veins with associated white mica and chlorite (HW-07-05, 160 m, crossed polarizers and reflected light, and S-715, 116 m, plane polarized light and reflected light).

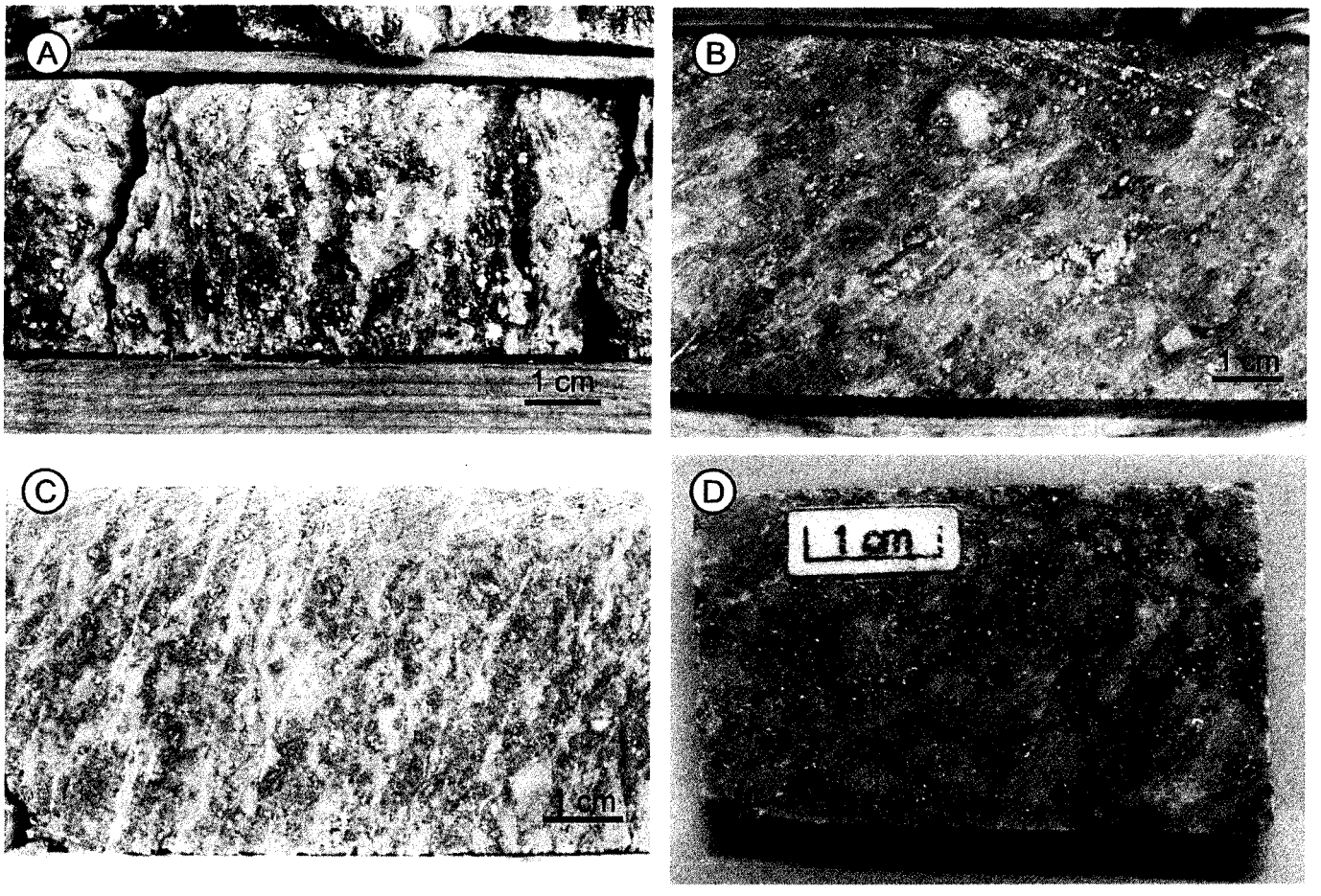

Figure 12-5. Sulfide disseminations. A), B), and C) Euhedral to anhedral pyrite in sericitized and silicified wispy clast-rich breccia (S-575, 145 m, HW-07-05, 120 m, and HW-07-06, 51 m, respctively. D) Sulfide disseminations and blebs in aphyric rhyolite (HW-07-04, 273 m).

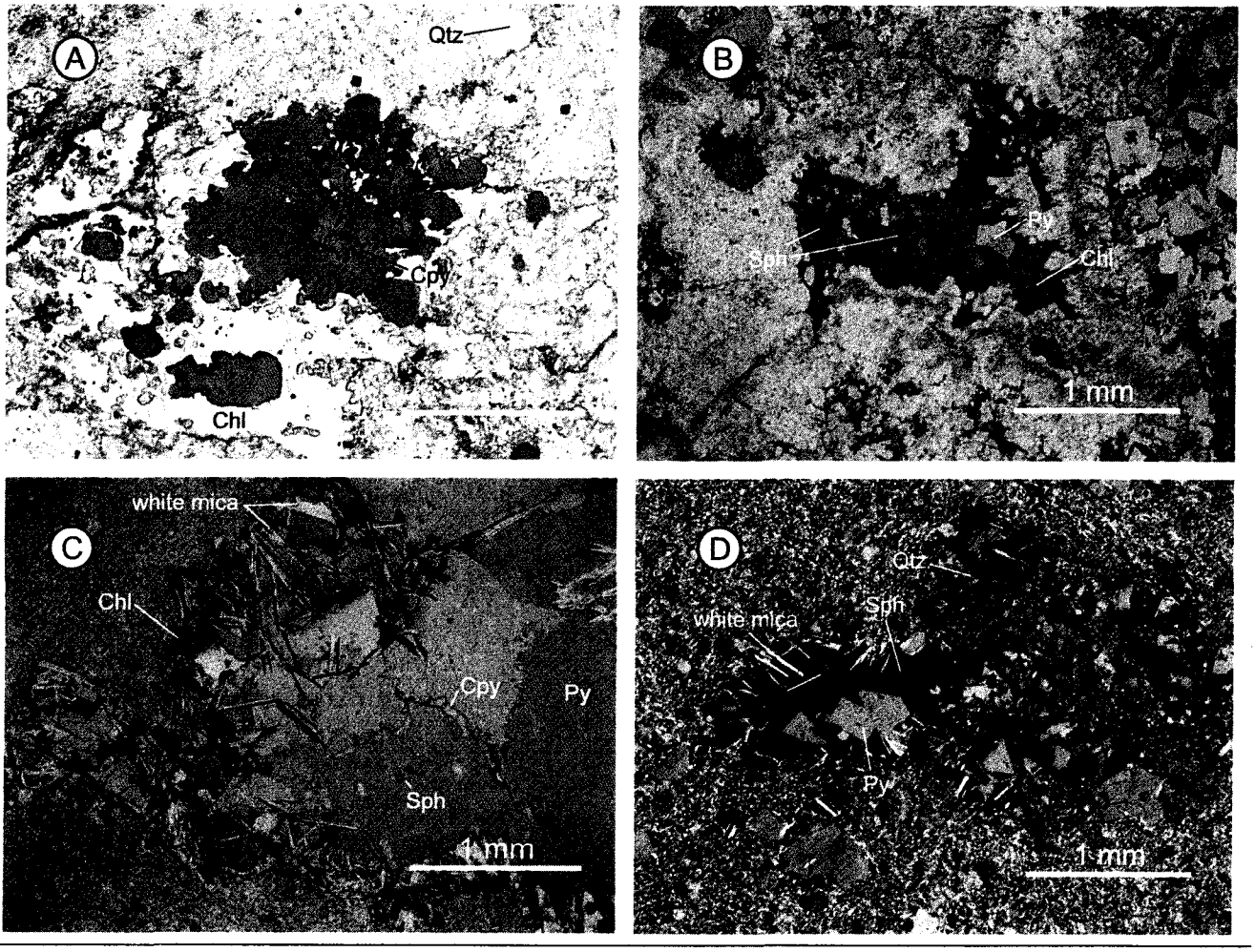

Figure 12-6. Photomicrographs of sulfide disseminations in clastic rocks. A) Chalcopyrite-rich dissemination surrounded by a fine-grained mass of chlorite with dark blue extinction under crossed polarizers (S-613, 17 m, plane polarized light and reflected light). B) Euhedral to subhedral pyrite with irregular sphalerite, surrounded by a chlorite halo (S-628, 186 m, plane polarized light and reflected light).C) Large diameter dissemination with bladed white mica crystals along the margins (S-714, 147 m, plane polarized light and reflected light).
D) Sphalerite and pyrite dissemination with white mica in sericitized host rock (S-614, 200 m, crossed polars and reflected light).

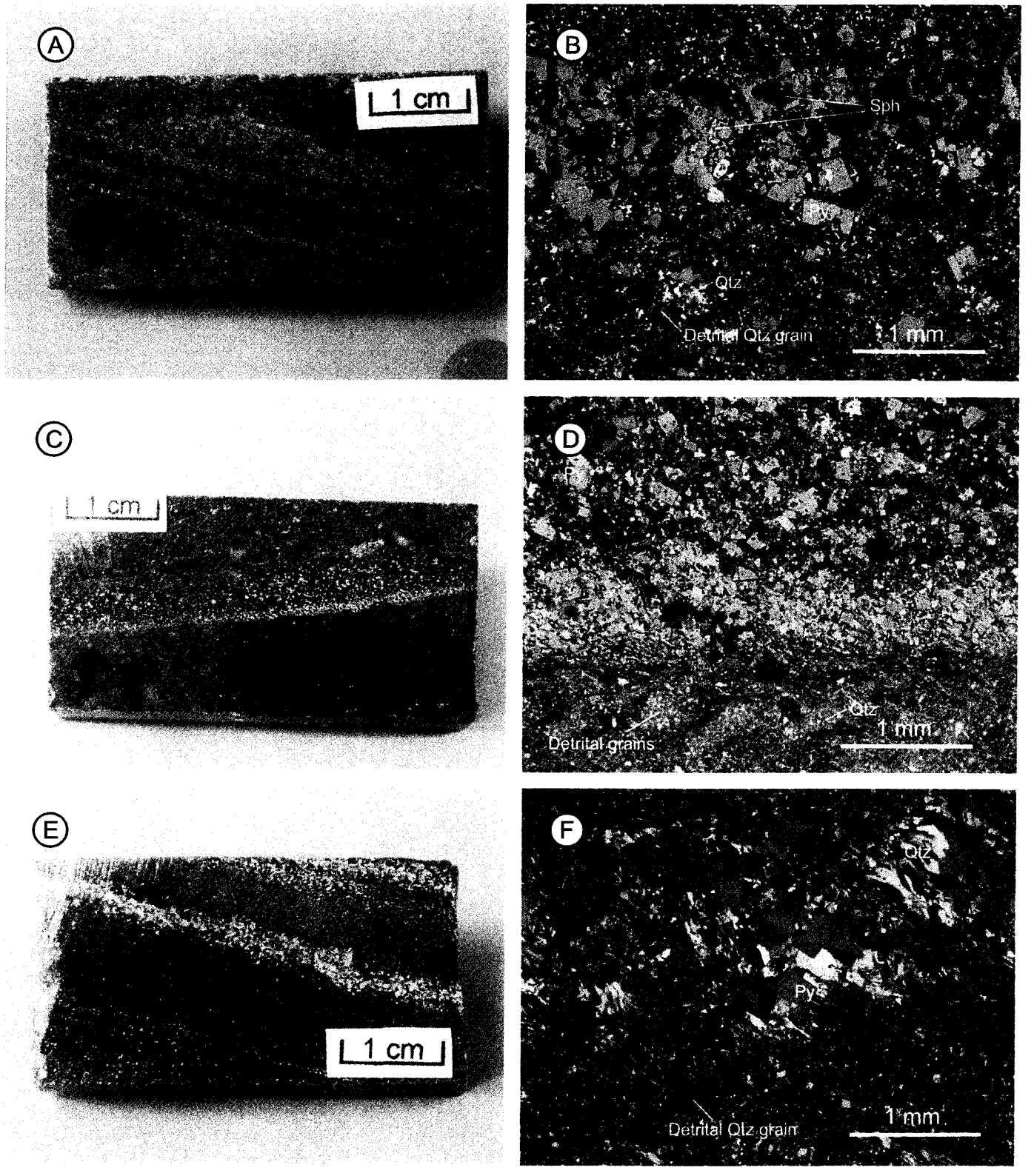

Figure 12-7. Sulfide laminations in sandstone (thin sections are under crossed polarizers and reflected light). A) and B) Laminae containing abundant sphalerite and euhedral to subhedral pyrite grains (HW-07-04, 38 m). C) and D) Euhedral to subhedral pyrite is concentrated towards the base of a fine grained interval between two coarser grained intervals in sandstone (HW-07-05, 181 m). E) and F) Sulfide laminae with abundant crystalline quartz that contrasts with nearby rounded detrital quartz grains (HW-07-06, 358 m).

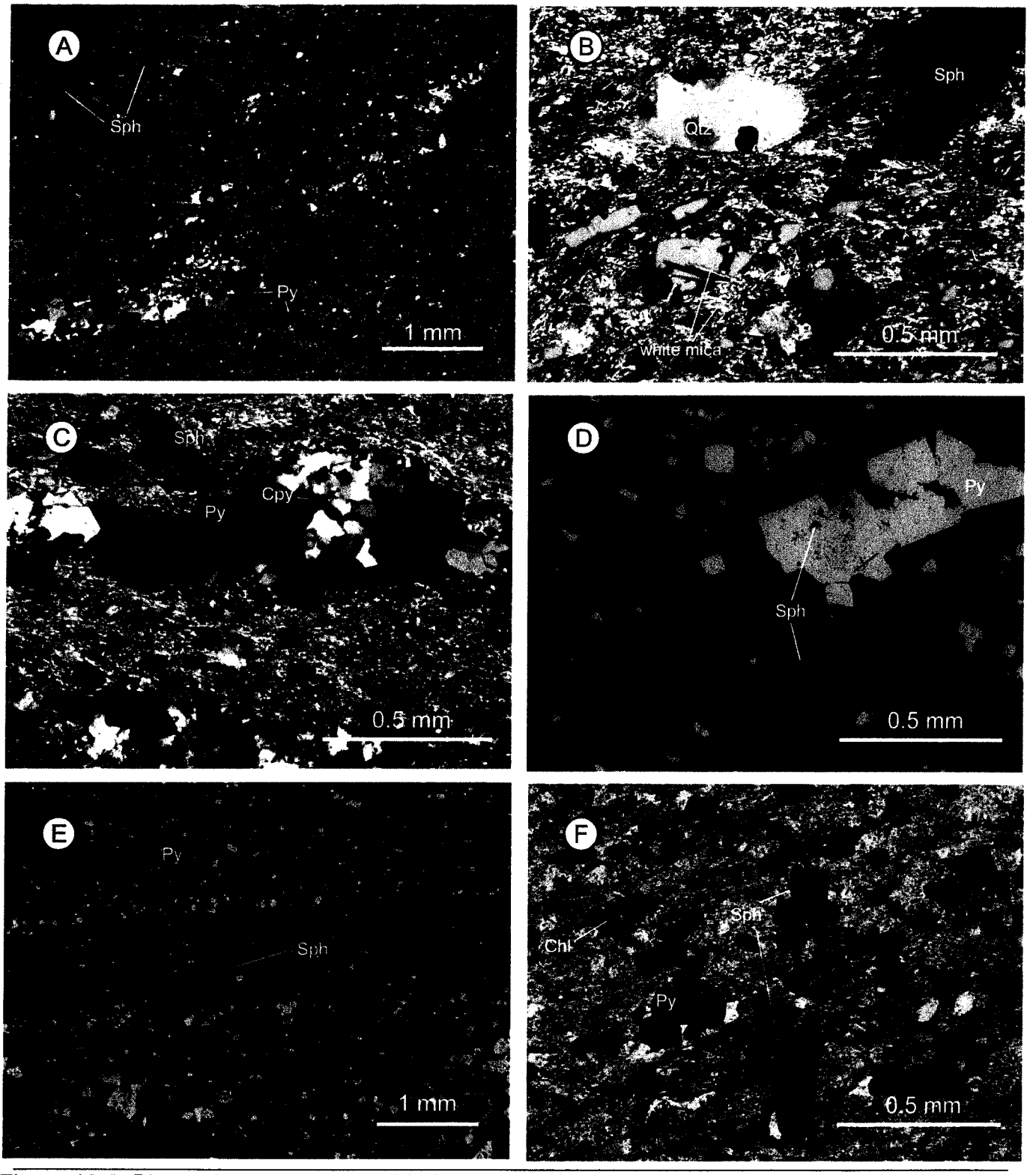

Figure 12-8. Photomicrographs of sulfide lamination in sandstone. A) Semi-continuous bands of quartz, pyrite, sphalerite and locally chalcopyrite commonly define laminae (reflected and transmitted light). B) Detrital quartz next to pyrite and sphalerite (crossed poalrizers and reflected light). C) and D) Core zones with voids or sphalerite and chalcopyite blebs in pyrite within quartz rich zones (crossed polarizers and reflected light, respectively). E) Distriburion of pyrite grains in laminae (reflected light). F) Distribution of chlorite around pyrite grains and sphalerite grains (transmitted and reflected light).

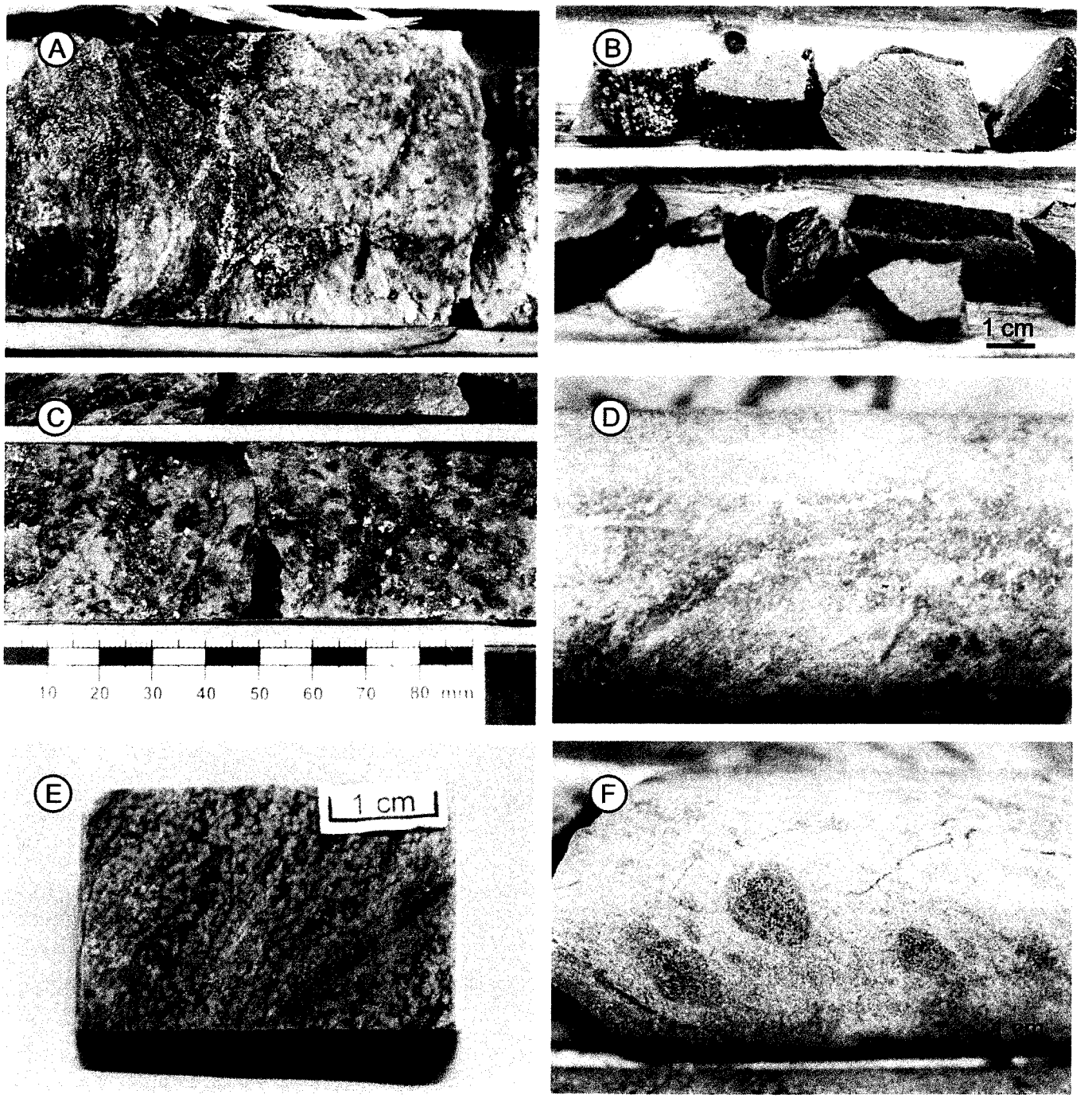

Figure 12-9. Alteration styles A) and B) Chloritized rhyolite with minor sericite and sulfide mineralization (S-573, 180.4 m, and S-574, 162 m, respectively). C) Strongly sericitized and chloritized rhyolitic breccia (S-614, 200 m). D) Epidote, hematite, and carbonate alteration in rhyolite (S-715, 108 m). E) and F) Epidote and carbonate and/or garnet spots in xenolith-bearing coherent rhyolite and in wispy clast-rich breccia volcaniclastic rocks, respectively (S-715, 88.4 m and HW-07-04, 59 m respectively).

a)

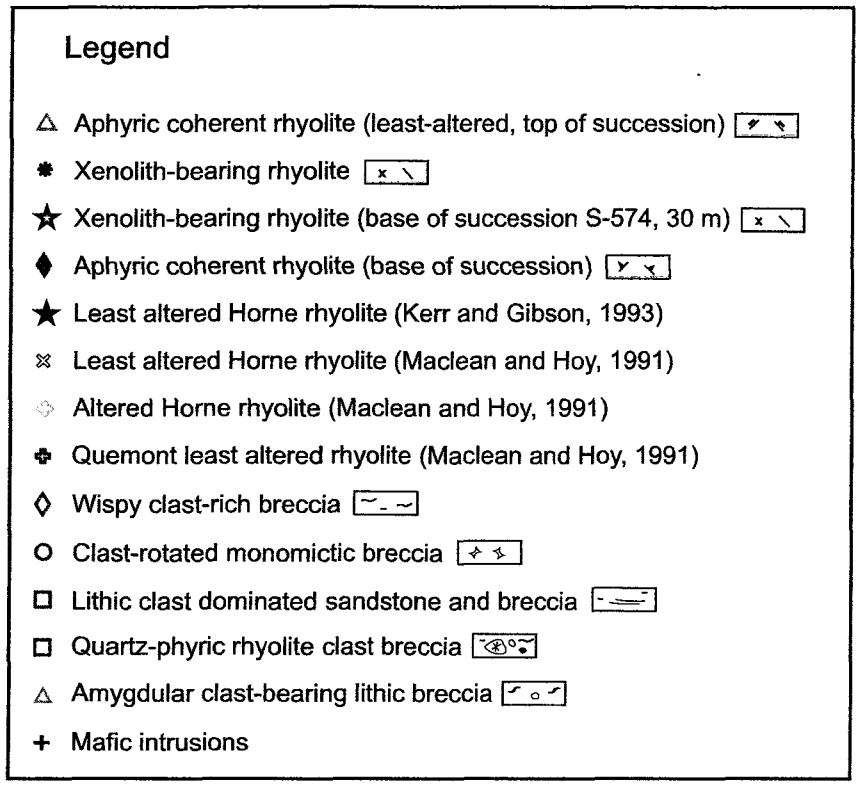

b)

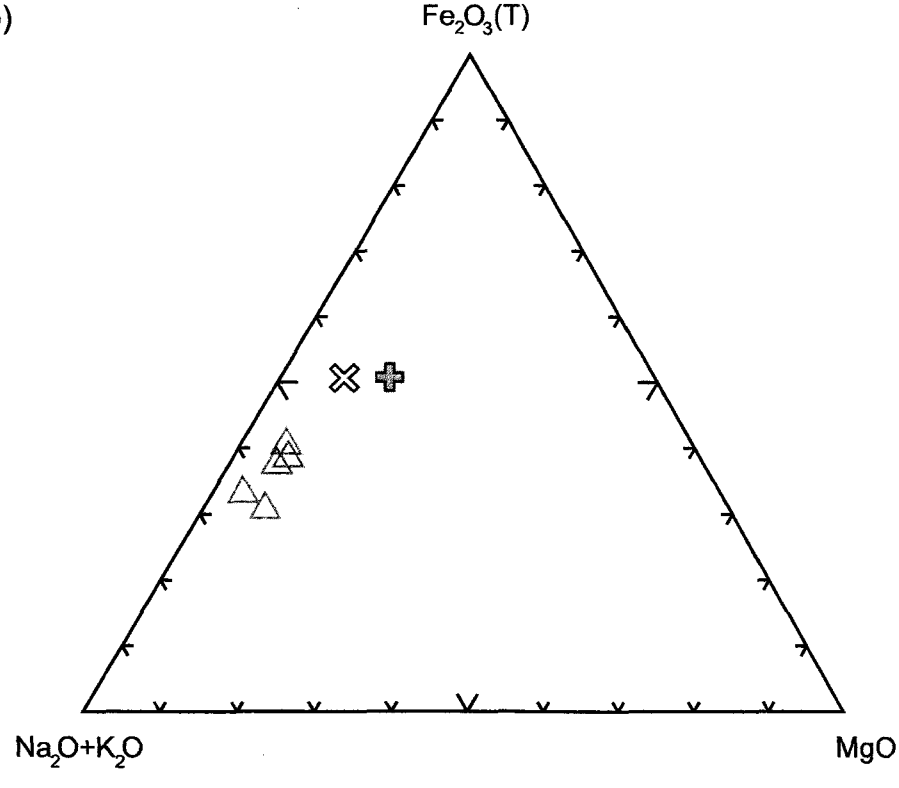

Figure 13-1. a) Legend for figures 13-1 through 13-9 and 14-6 to 14-7 showing the equivalent symbol used for facies in Figure 10). b) AFM plot of the least altered coherent rhyolite from Horne West and least altered Horne and Quemont rhyolite from MacLean and Hoy (1991). The least altered Horne and Quemont rhyolites are less altered than those at Horne West which show enrichment in alkalis most likely due to sericitization.

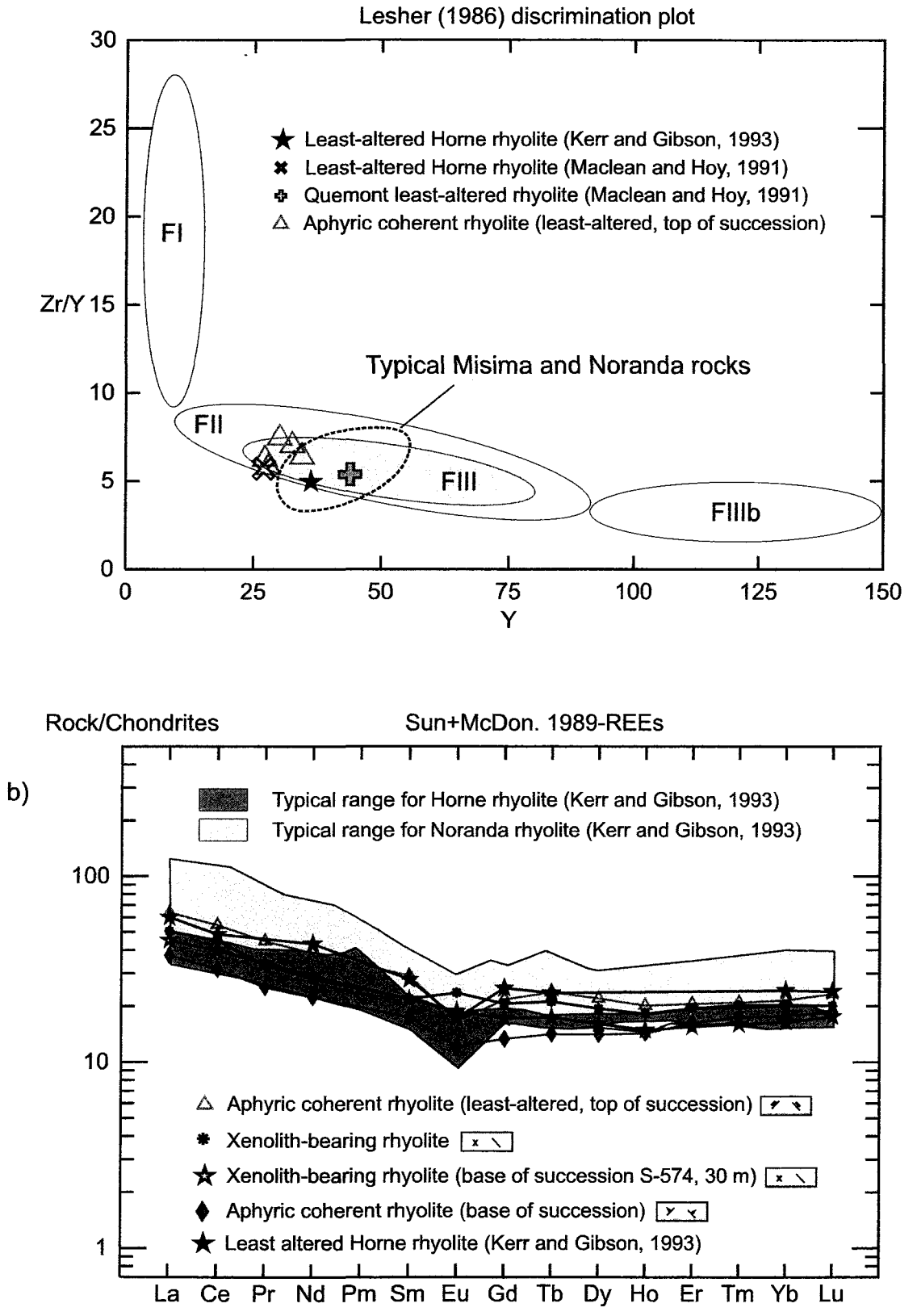

Figure 13-2. a) Zr/Y vs. Y plot with least altered Horne, Horne West, and Quemont rhyolite. b) Rare earth element profiles for representative Horne West rhyolite compared to Horne rhyolite from Kerr and Gibson (1993).

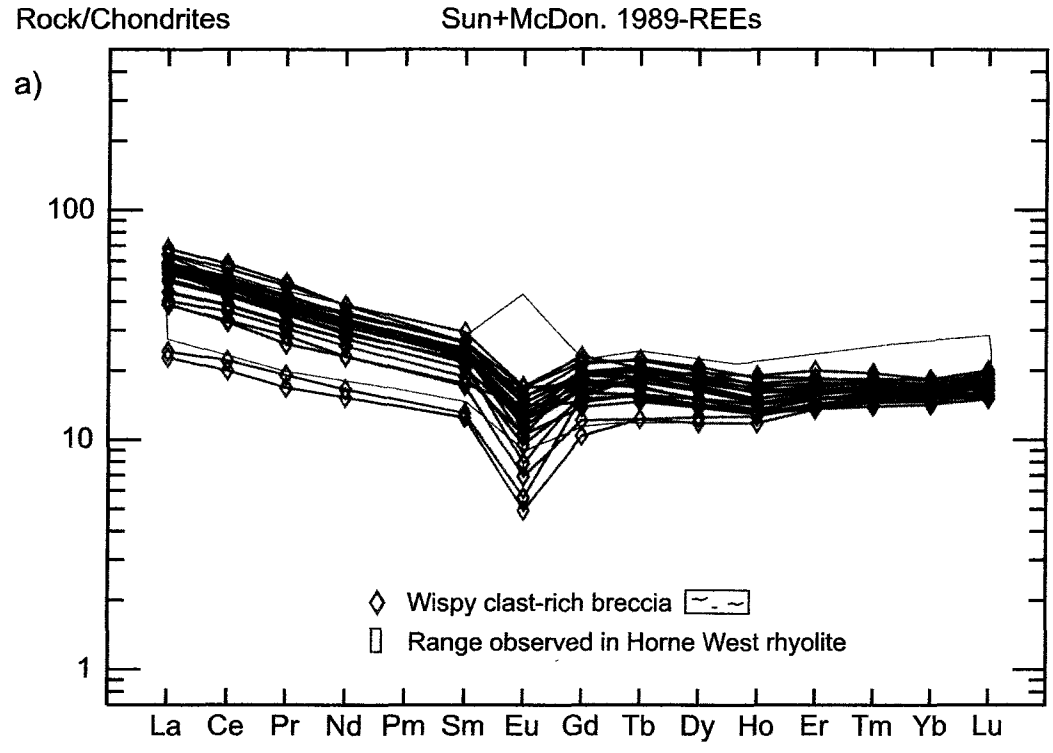

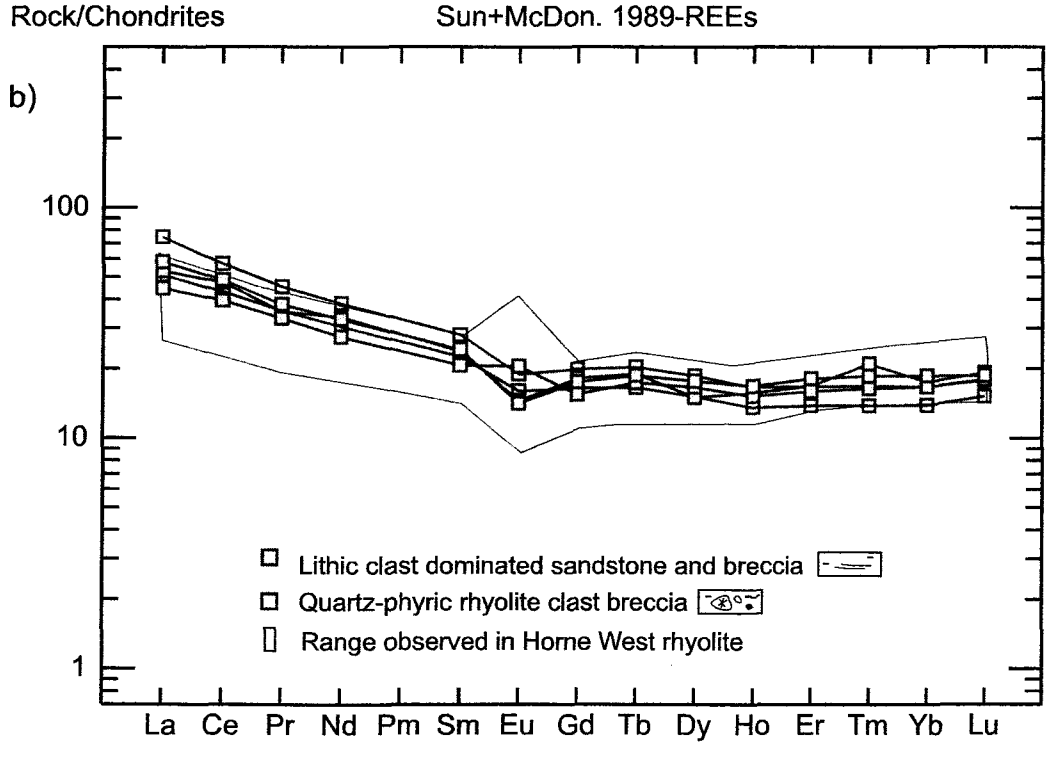

Figure 13-3. REE profiles for a) wispy clast-rich breccia b) lithic clast-dominated sandstone and breccia, and quartz-phyric rhyolite clast breccia.

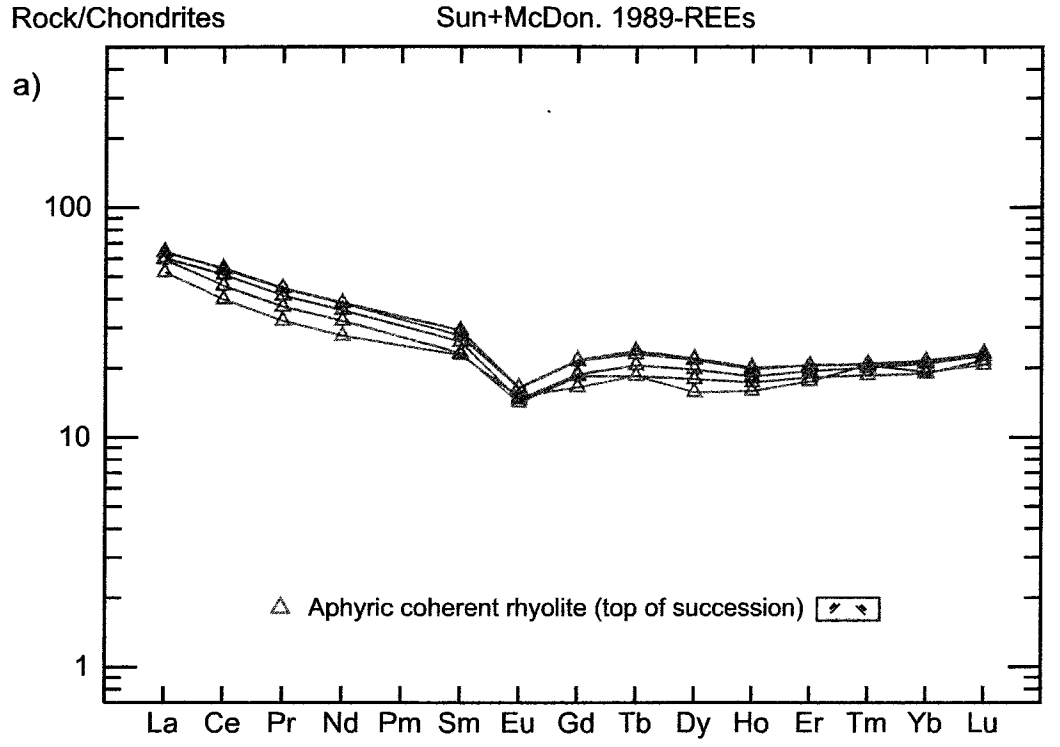

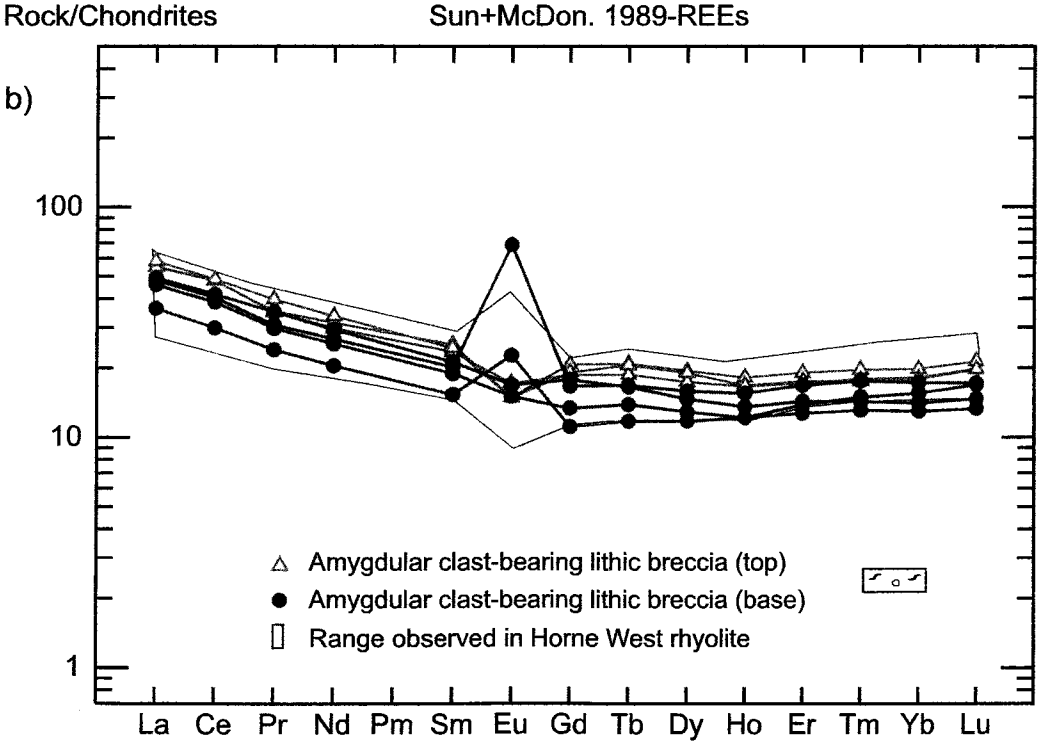

Figure 13-4. REE profiles for a) Coherent rhyolite (2) at the top of the stratigraphic succession and b) amygdular clast rich breccia at the base and top of the succession. Samples at the base commonly have a positive europium anomaly.

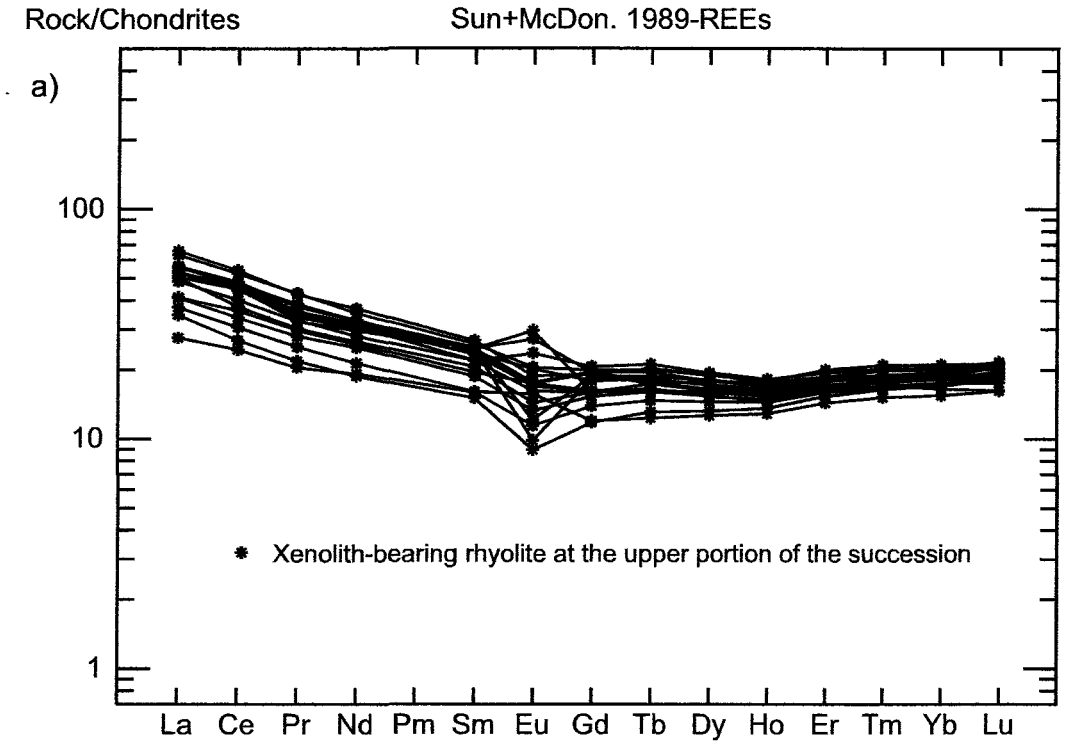

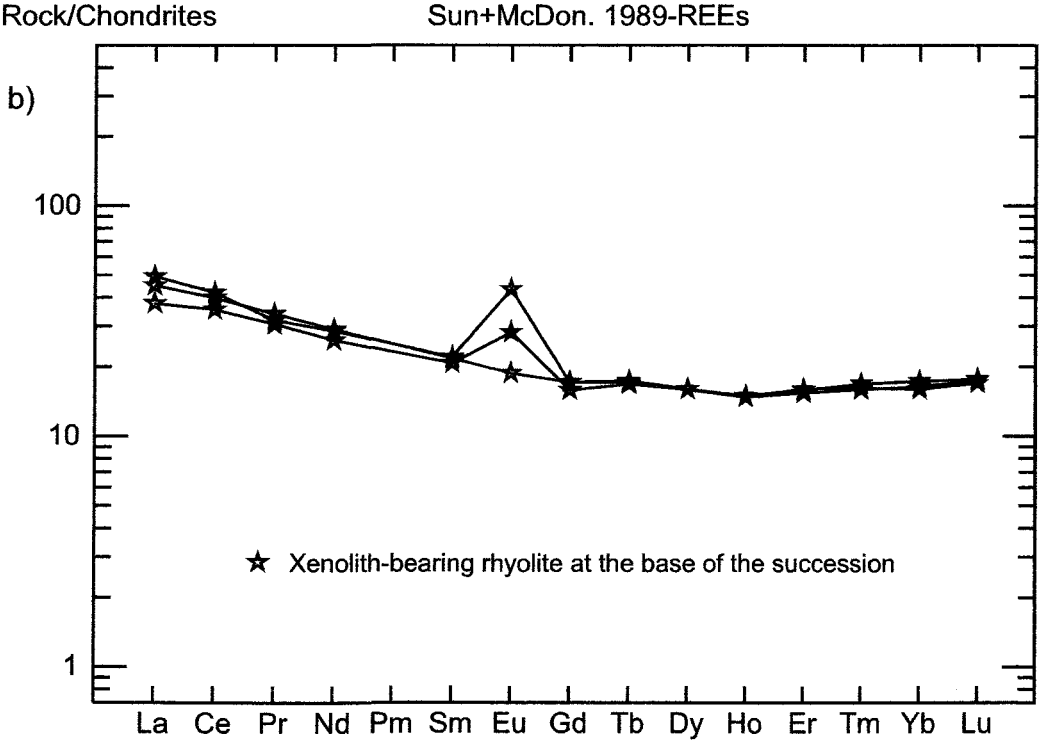

Figure 13-5. REE profiles for xenolith-bearing rhyolite at the top and center (a) and base (b) of the succession. Positive europium anomalies may be caused by the assimilation of mafic rocks that are present as xenoliths.

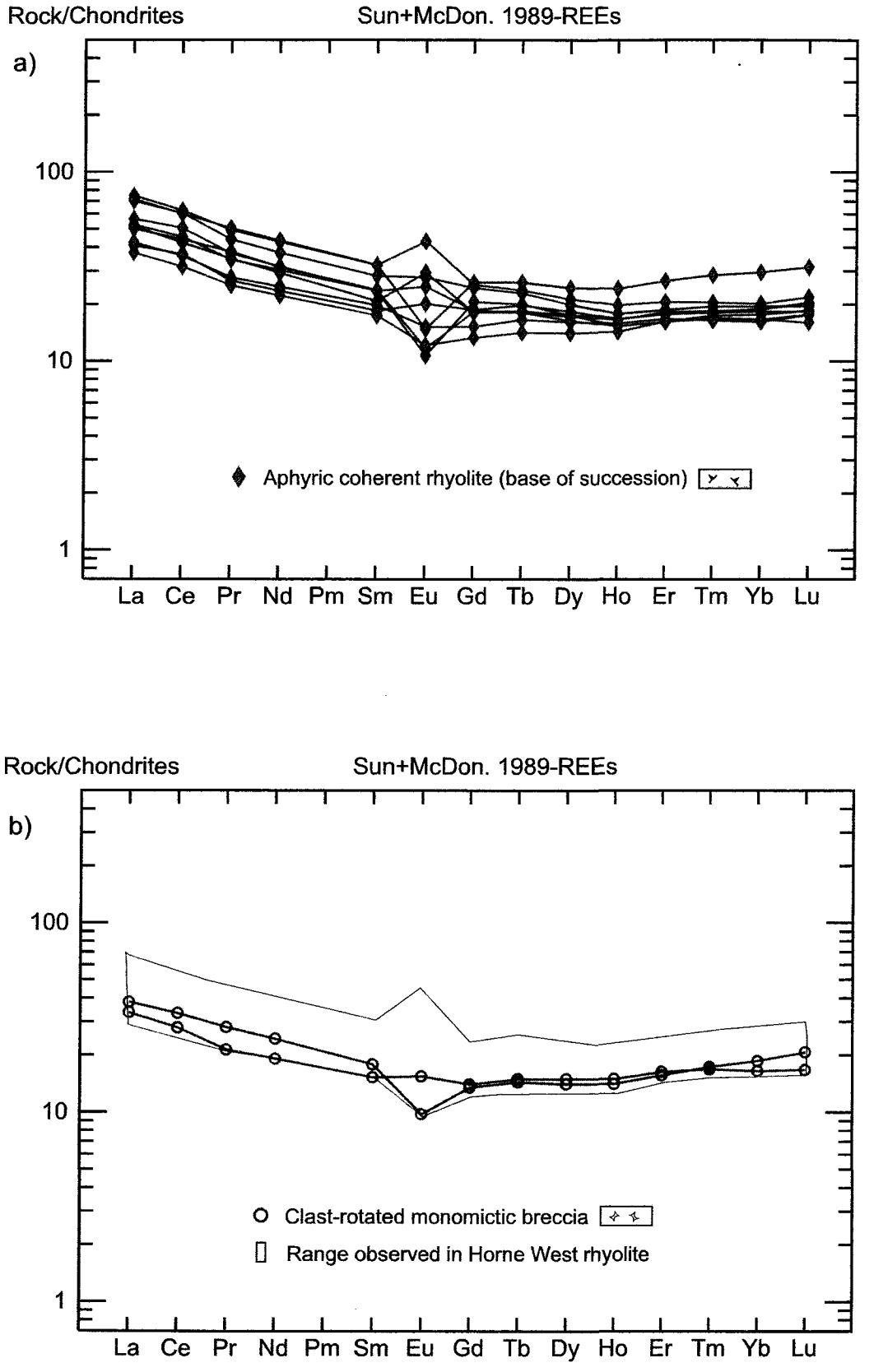

Figure 13-6. REE profiles for a) aphyric coherent rhyolite at the base of the succession and b) Clast-roated monomictic breccia.

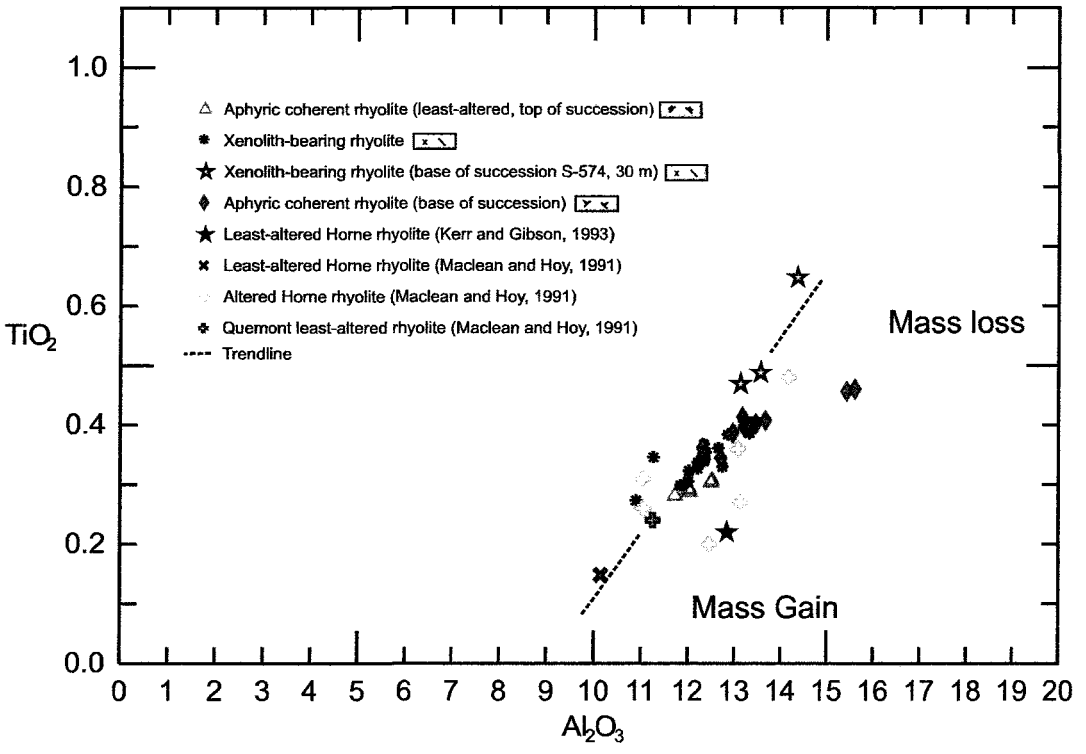

Figure 13-7. Immobile element TiO_2 vs. Al_2O_3 plot of Horne and Horne West rhyolite showing that Horne West and altered Horne rhyolites may be enriched in TiO_2.

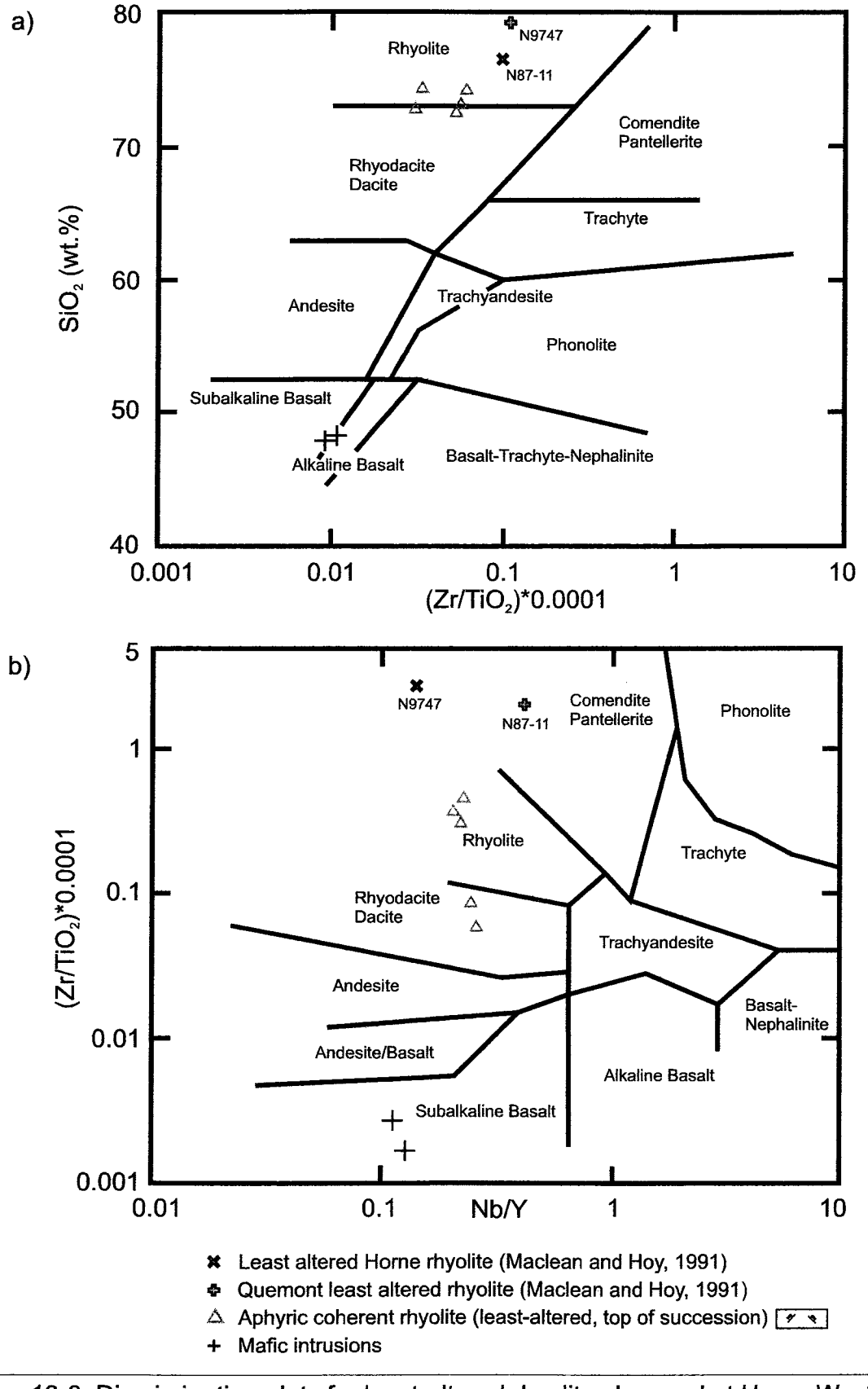

Figure 13-8. Discrimination plots for least-altered rhyolite observed at Horne West, Horne, and Quemont as well as mafic intrusive rocks from Horne West. Modified from Winchester and Floyd (1977).

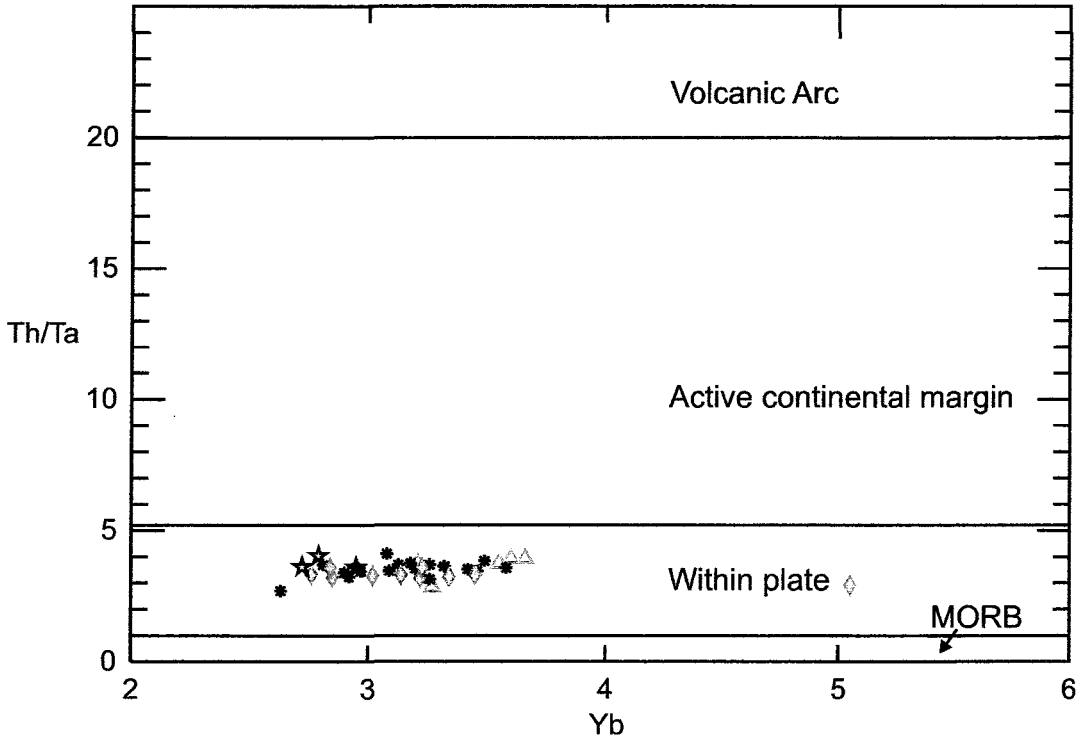

Figure 13-9. Th/Ta vs. Yb tectonic discrimination diagram of Gorton and Schandl (2000) showing the distribution of Horne West rhyolite and mafic intrusions.

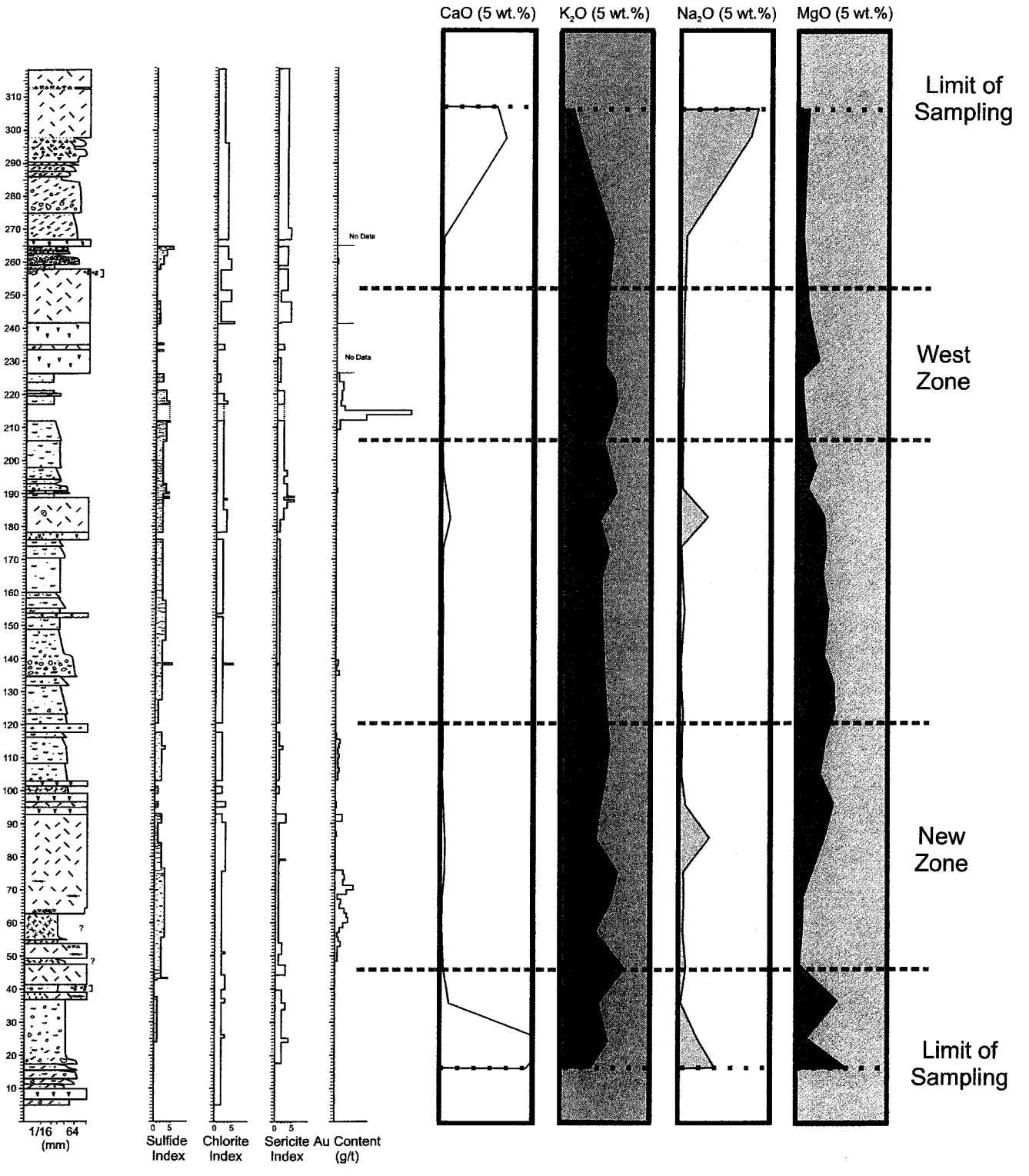

Figure 14-1. Geochemical profile of the Horne West succession. Data is shown against a compilation of holes S-715 and S-573 (For legend see Appendix A). The maximum of each scale is indicated in brackets.

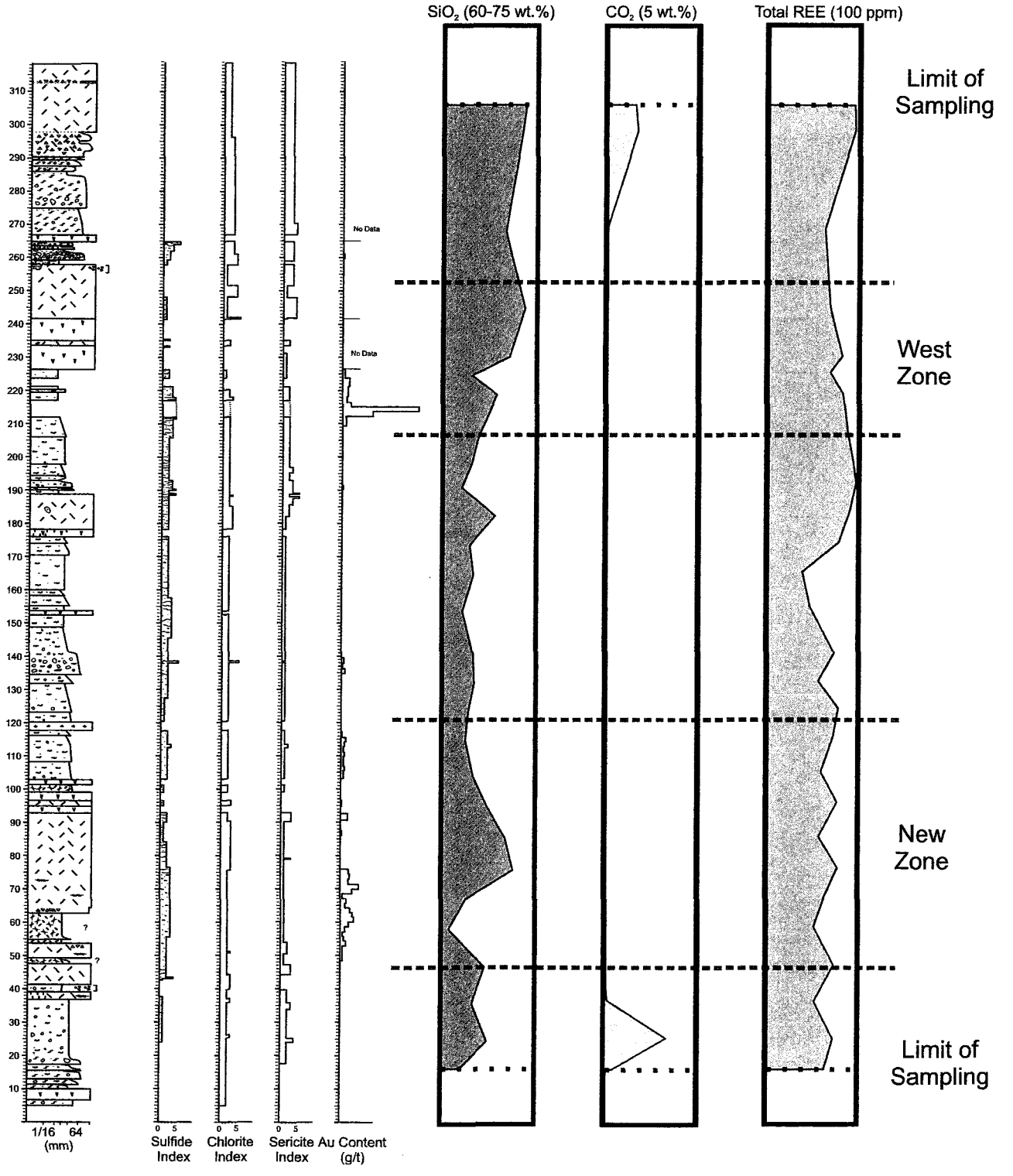

Figure 14-2. Geochemical profile of the Horne West succession. Data is shown against a compilation of holes S-715 and S-573 (For legend see Appendix A). The maximum of each scale is indicated in brackets.

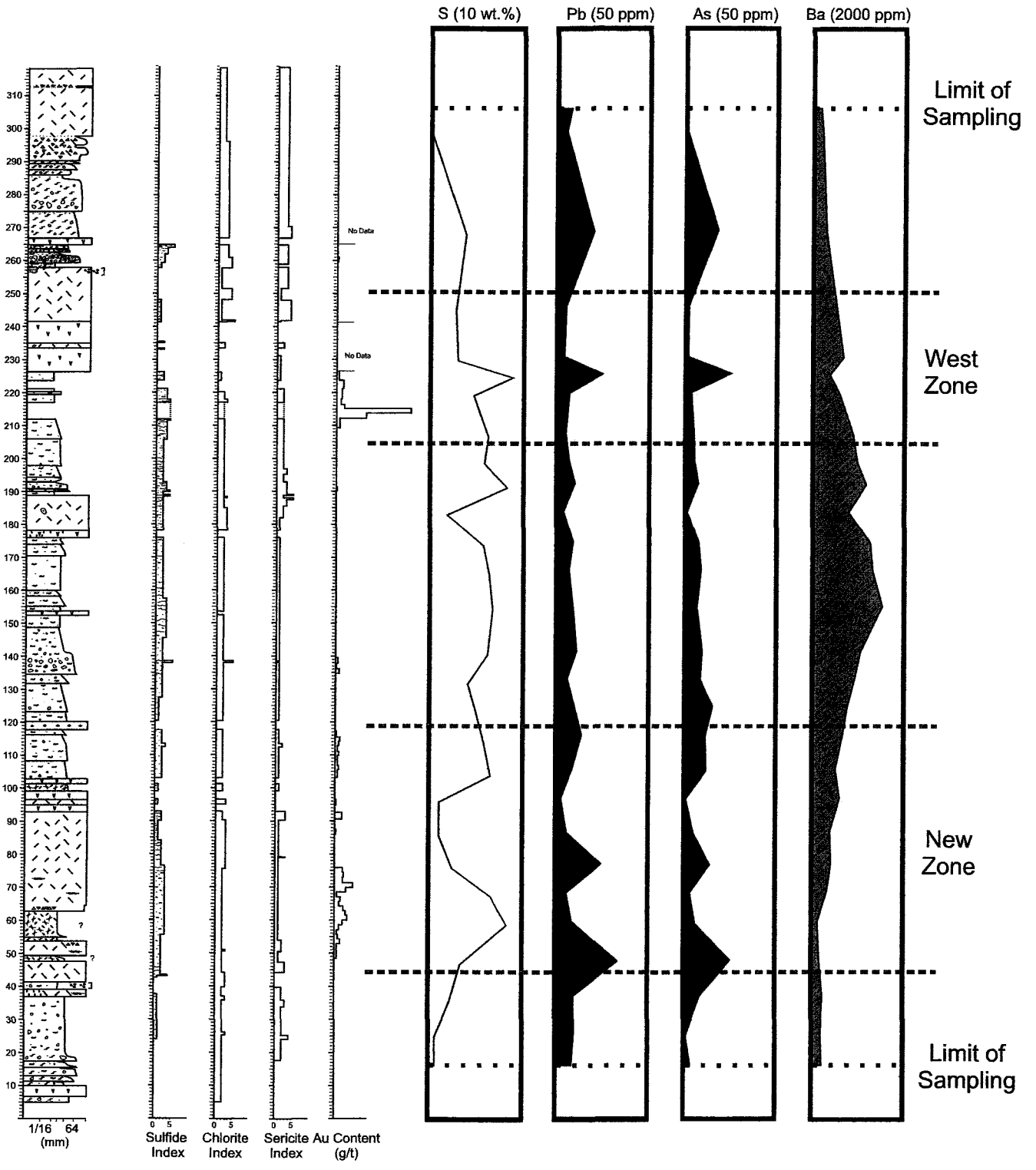

Figure 14-3. Geochemical profile of the Horne West succession. Data is shown against a compilation of holes S-715 and S-573 (For legend see Appendix A). The maximum of each scale is indicated in brackets.

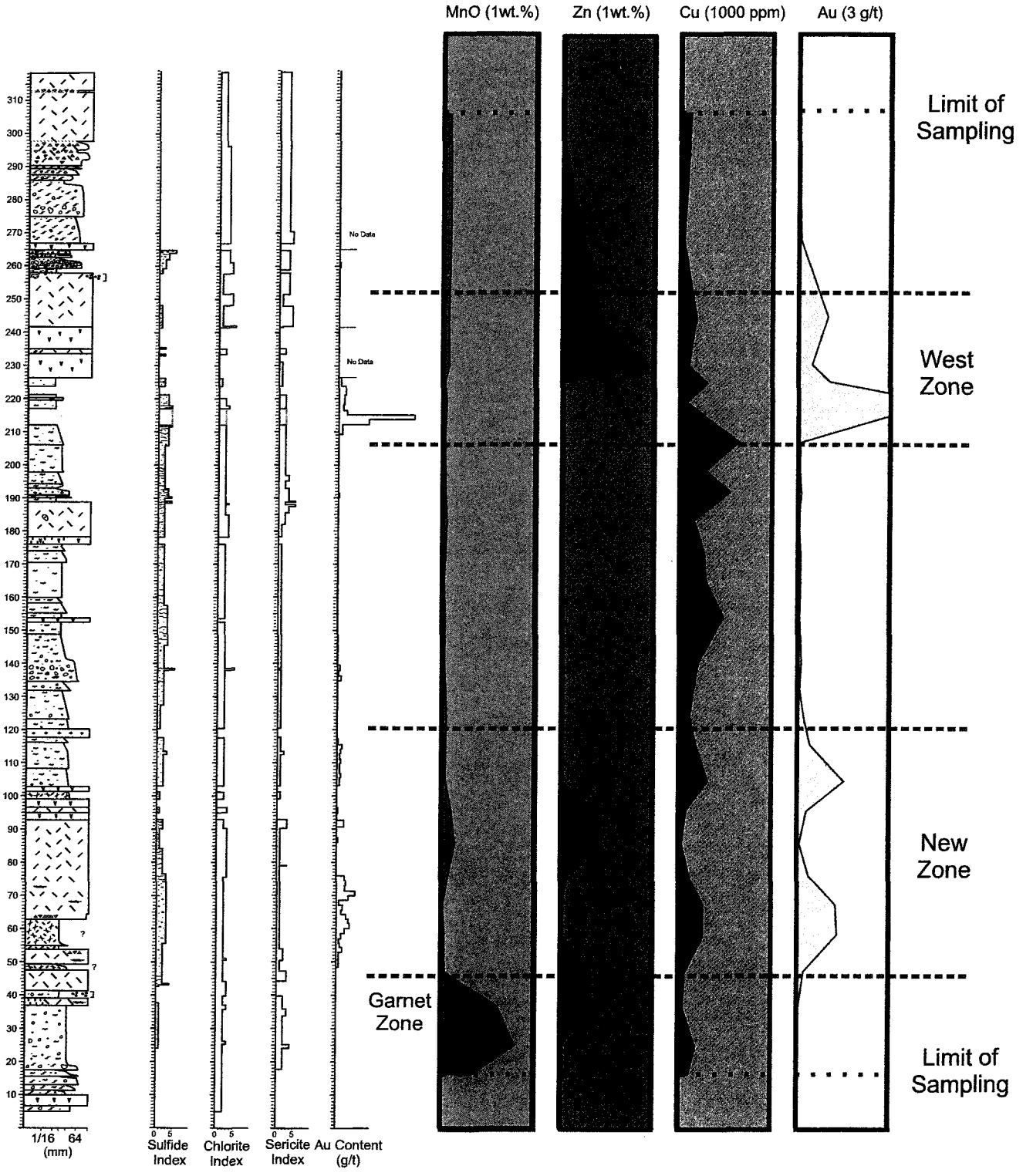

Figure 14-4. Metal zonation and geochemistry of the Horne West succession. Data is shown against a compilation of holes S-715 and S-573 (For legend see Appendix A). The maximum of each scale is indicated in brackets. The garnet zone indicated shows where garnets have been positively identified within the Mn enriched zone.

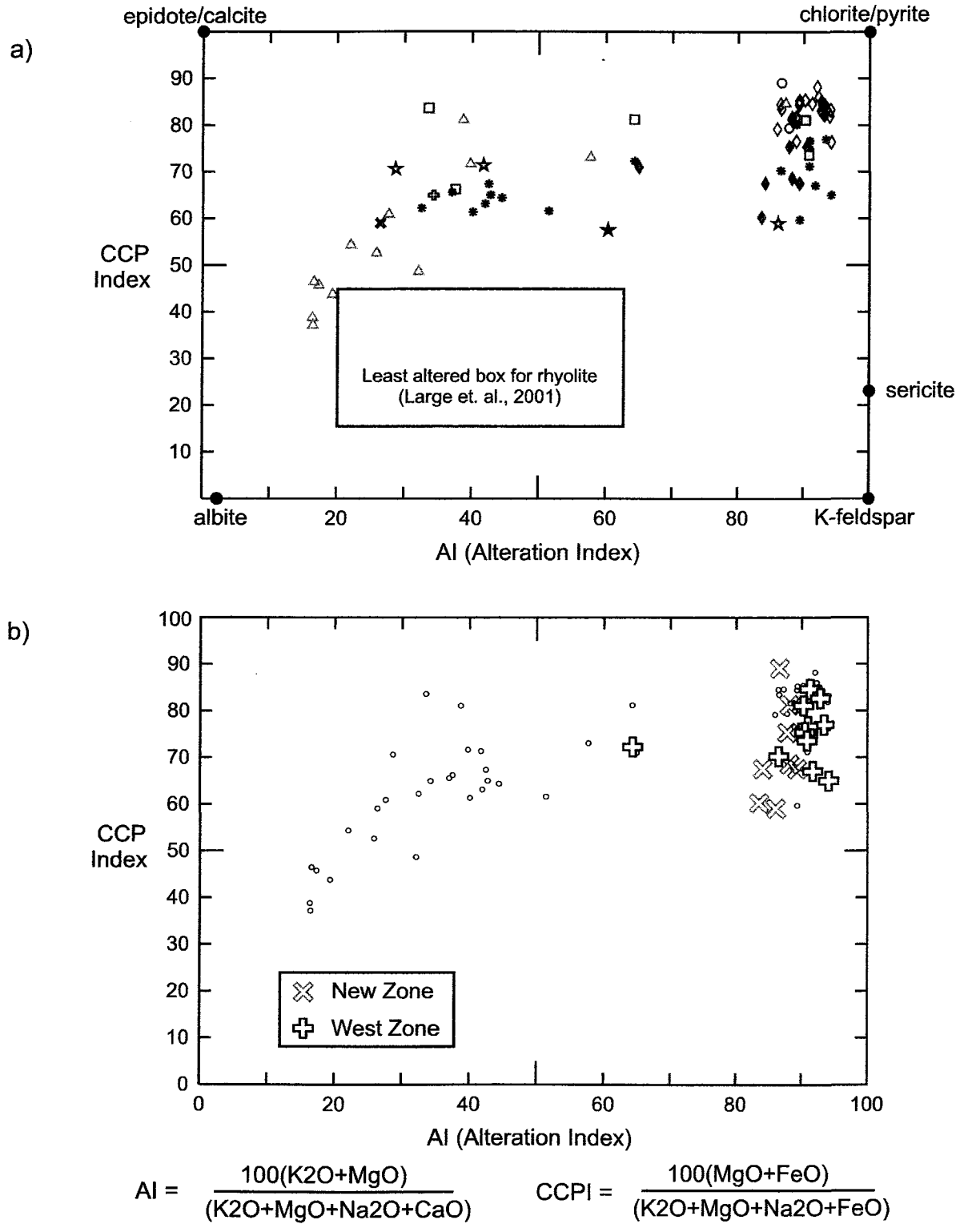

Figure 14-5. a) Alteration box plot (after Large et al., 2001) with all lithofacies types (for legend see Figure 13-1). Intense sericite +/- chloirte +/- pyrite alteration is observed locally in the uppermost intrusion of xenolith-bearing rhyolite and the aphyric rhyolite at the base of the succession. The aphyric rhyolite at thetop of the succession is least altered of Horne West rocks. This may be attributed in part to emplacement late relative to hydrothermal alteration in the rest of the succession. b) Distributionof samples obtained from the New Zone and West Zone. The most highly altered rocks occur within and adjacent to the gold zones or within the wispy clast-rich breccia.

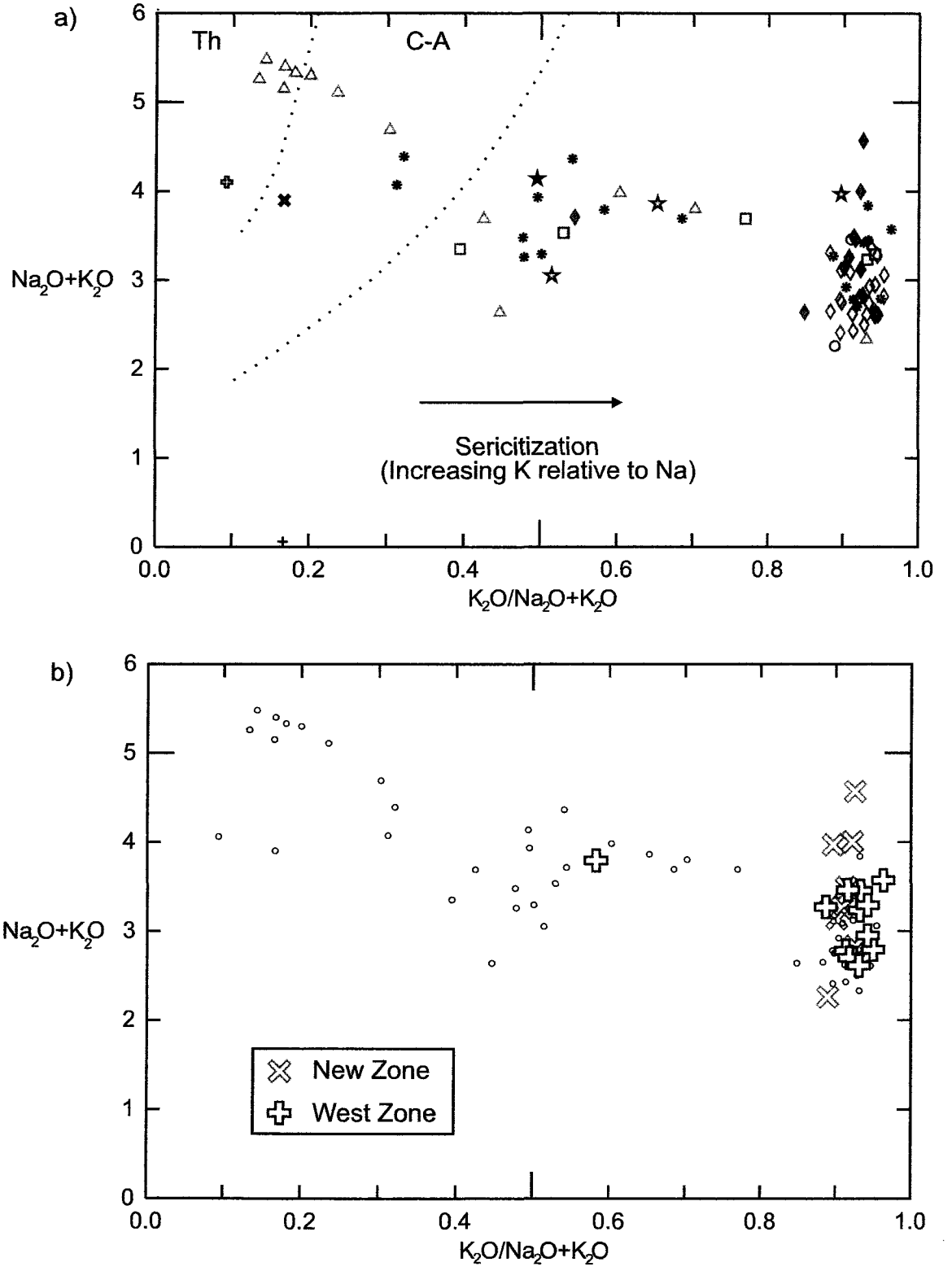

Figure 14-6. a) Sericitization plot modified from Hughes (1972) (for legend see Figure 13-1). b) Distribution of samples obtained from the New Zone and West Zone.

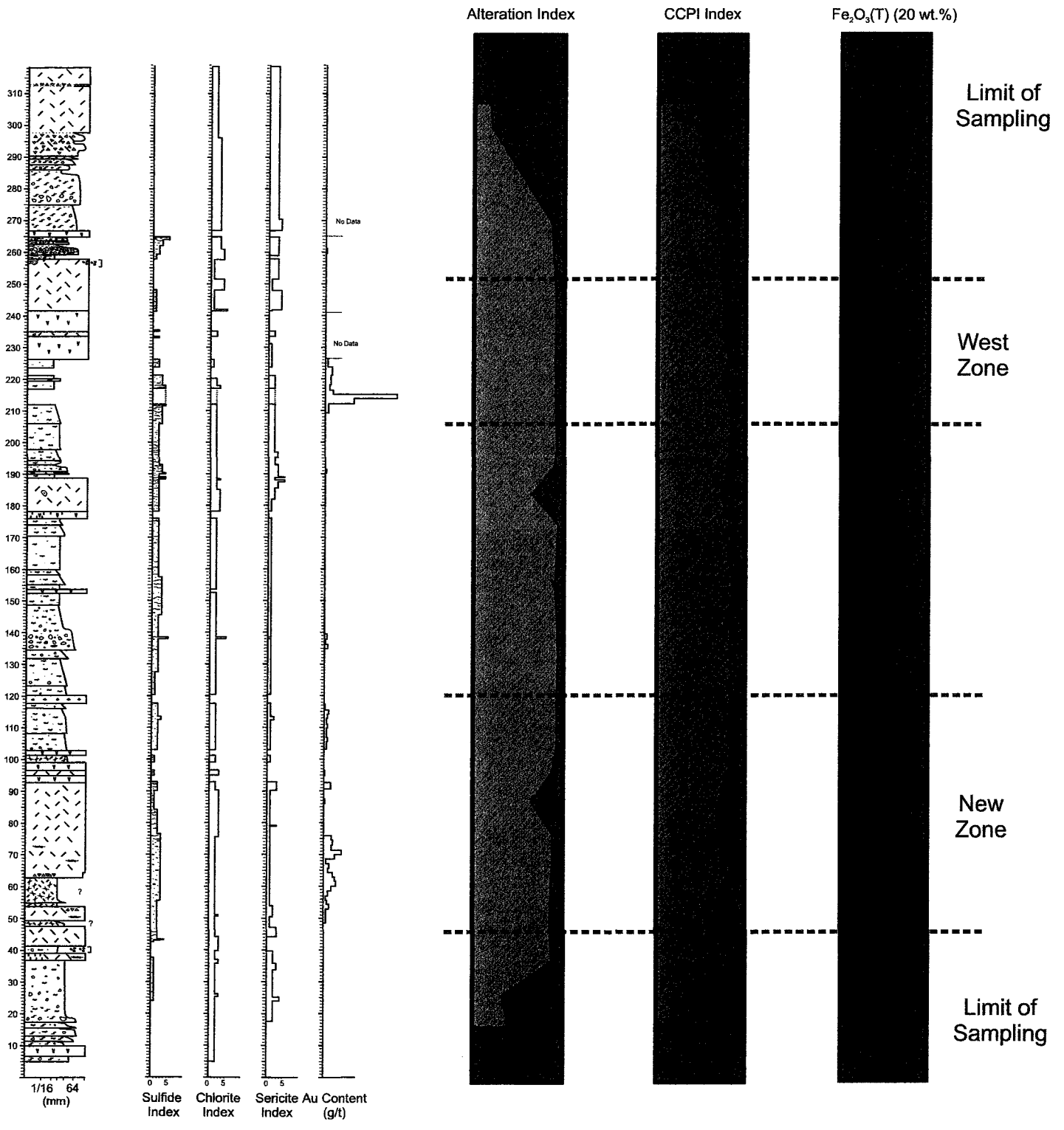

Figure 14-7. Chlorite-carbonate-pyrite (CCPI, Large et. al., 2001), Ishikawa alteration indices (AI) and total iron compared to alteration and gold mineralization at Horne West (compilation of holes S-715 and S-573, for legend see Appendix A).

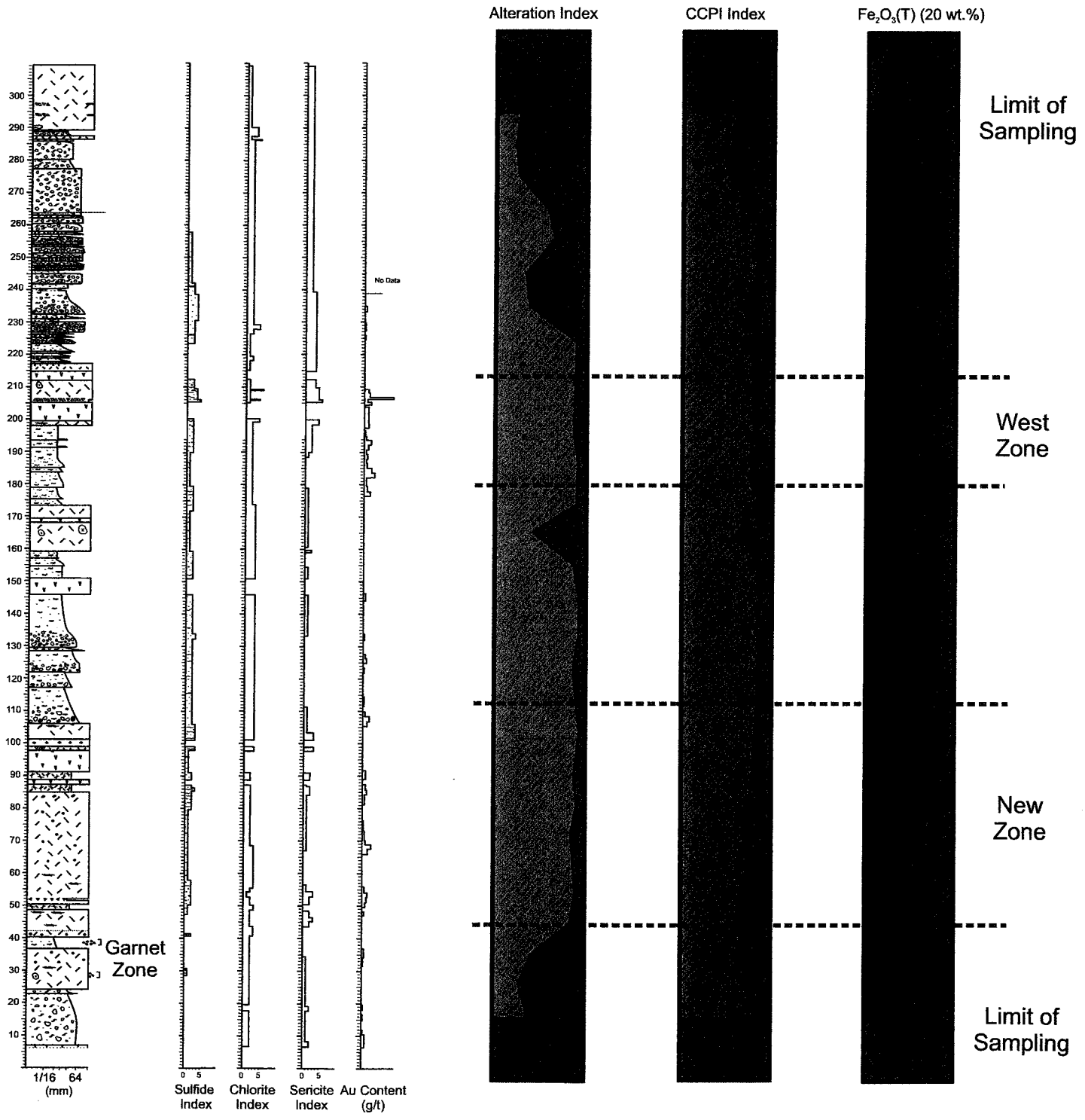

Figure 14-8. Chlorite-carbonate-pyrite (CCPI, Large et. al., 2001). Ishikawa alteration indices (AI), and total iron compared to alteration and gold mineralization at Horne West (compilation of holes S-714 and S-574, for legend see Appendix A).

Appendix A

Drill Core Data

Legend for Appendix A

Principal Lithofacies


Rhyolite and rhyolite breccia (A)


Amygdular clast-bearing lithic breccia (B)


Quartz-phyric rhyolite breccia (C)


Lithic clast dominated sandstone and breccia (D)


Xenolith-bearing rhyolite (E)


Wispy clast-rich granule breccia (F2)


Sulfide clast-bearing wispy clast-rich breccia (F1)


Clast-rotated monomictic breccia


Sediment-matrix rhyolite breccia


Suspended intraclast and cobble-boulder breccia

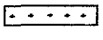
Syenite

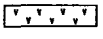
Basalt

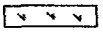
Quartz-feldspar-phyric rhyolite

Hydrothermal Sulfide Textures

: Fine grained disseminations
~ Stringer veins
·· Euheral pyrite
-- Irregular blobs and diffuse irregular stringers
= Sulfide laminations
- Replaced clasts

Symbols


Quartz-phyric rhyolite clast

Quartz-phyric rhyolite clast or quartz crystal


Sulfide clast or partly sulfide-replaced clast


Rhyolitic lithic fragment

Amygdular clast

Wispy clast


Sand-sized clasts


Intraclast or rip-up clast


Aphyric coherent rhyolite


Mafic xenolith

Flow banding

Perlitic fractures

Spherulites

Monomictic rhyolite breccia


Curviplanar clasts


Coherent andesitic rock

Minor fault

Planar lamination

Gradational contact

Scour


Spotted alteration (epidote and carbonate +/- garnet porphyroblasts)


Strong white mica +/- epidote +/- carbonate +/- hematite alteration

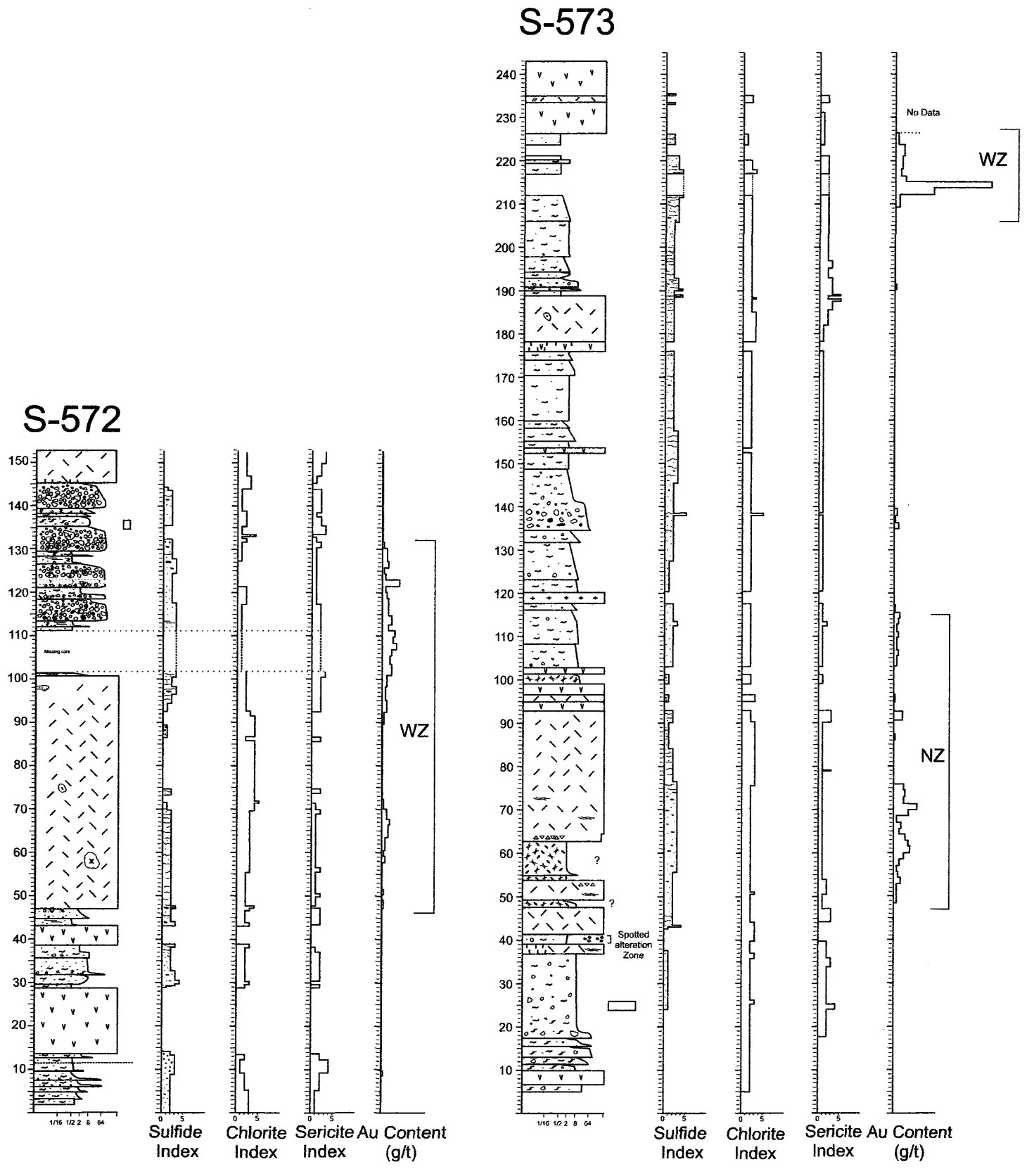
S-573
S-572
No Data
WZ
NZ
Spotted alteration Zone
Missing core
Sulfide Index
Chlorite Index
Sericite Index
Au Content (g/t)

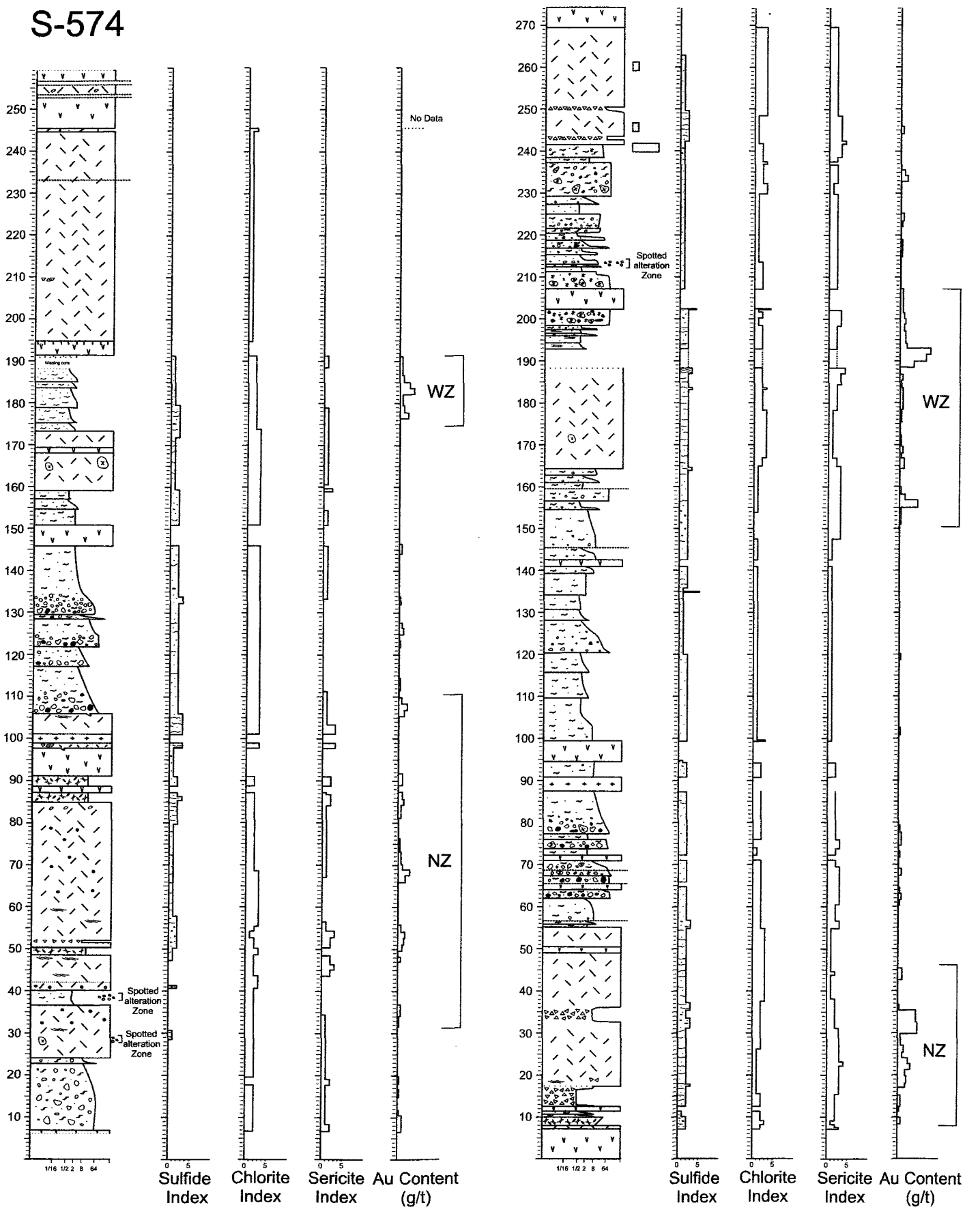
S-574
S-575
No Data
WZ
NZ
Spotted alteration Zone
Spotted alteration Zone
Spotted alteration Zone
Sulfide Index
Chlorite Index
Sericite Index
Au Content (g/t)
Sulfide Index
Chlorite Index
Sericite Index
Au Content (g/t)

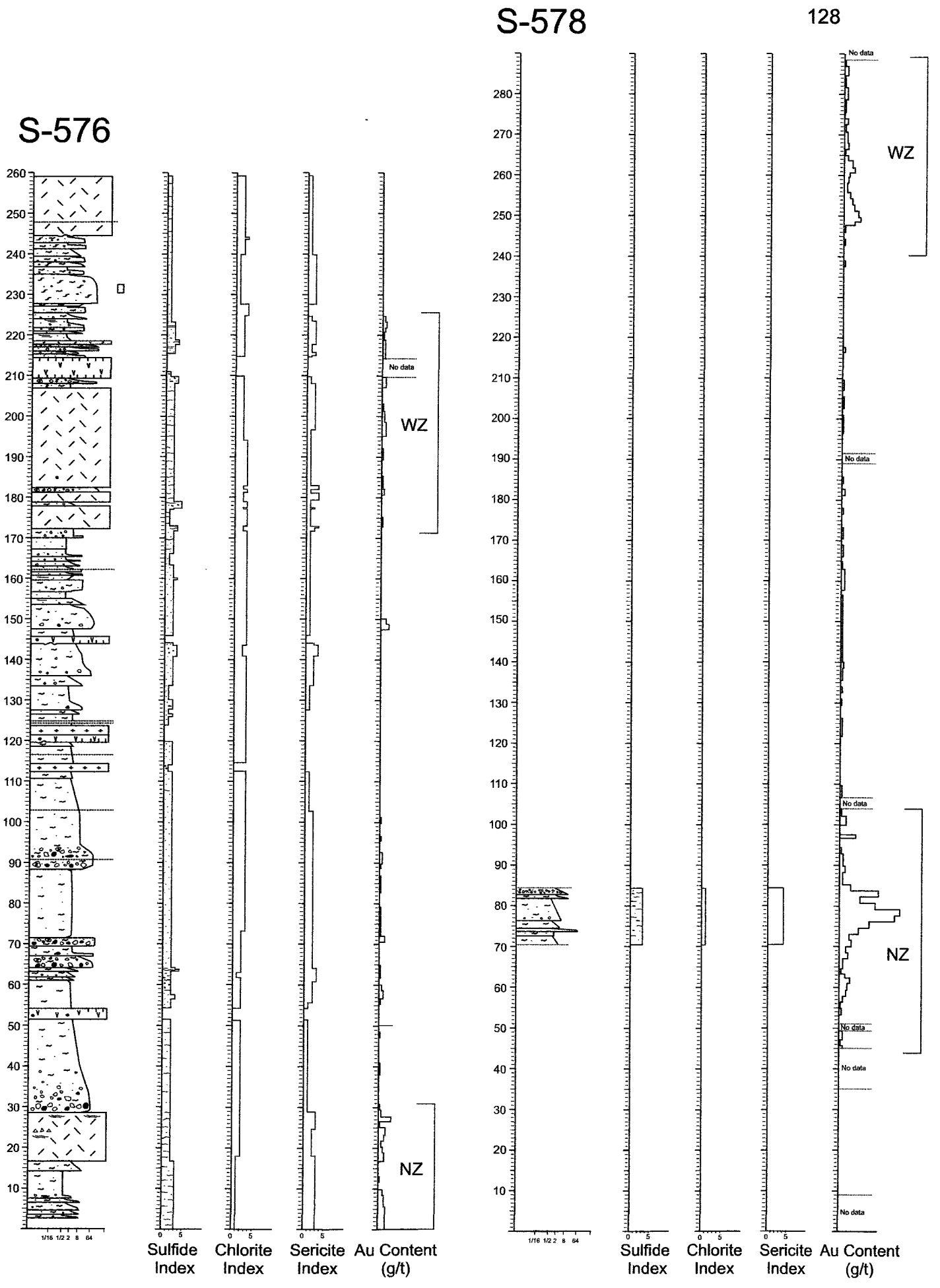
S-576
S-578
WZ
NZ
No data
Sulfide Index
Chlorite Index
Sericite Index
Au Content (g/t)

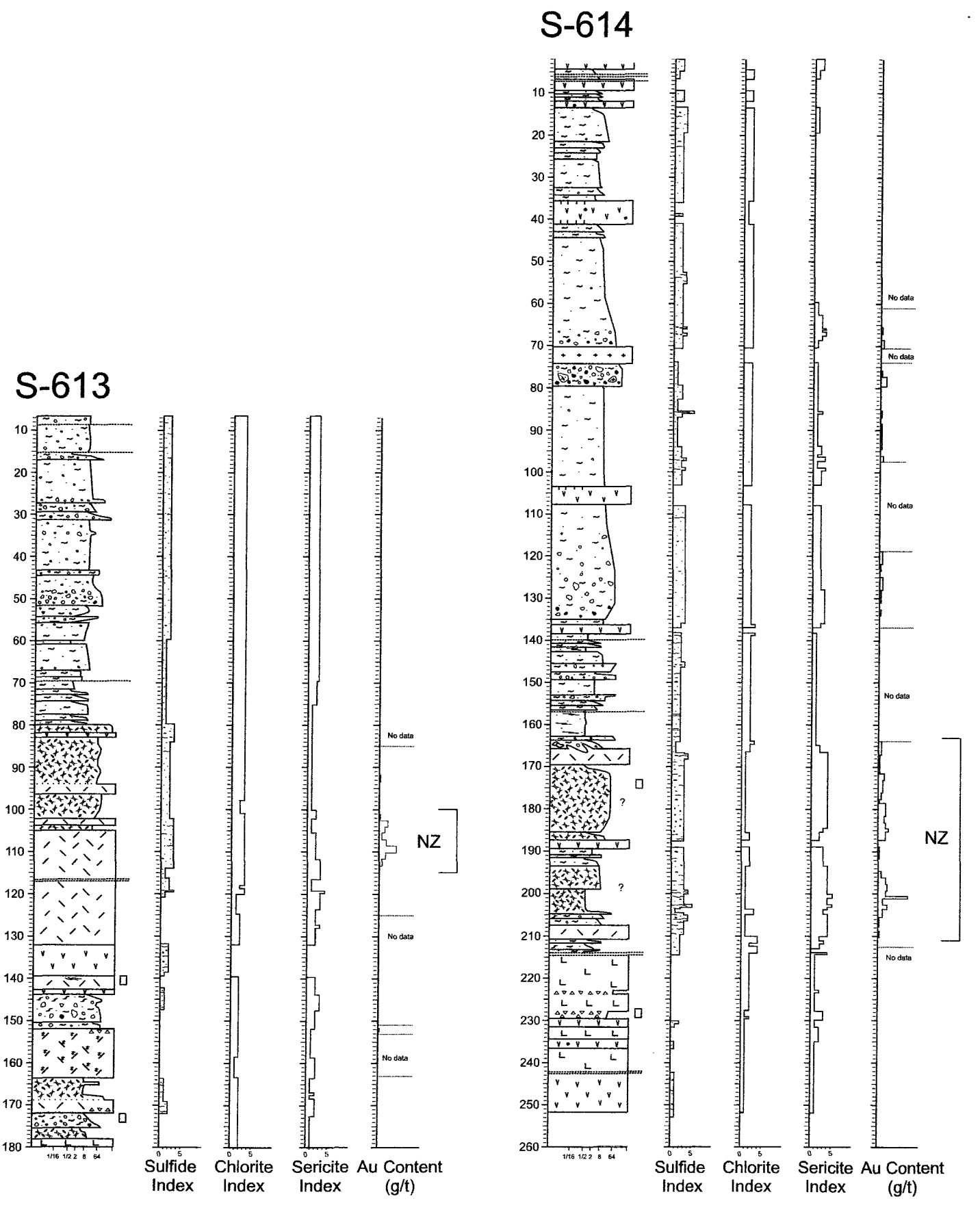
S-613
S-614
No data
NZ
Sulfide Index
Chlorite Index
Sericite Index
Au Content (g/t)

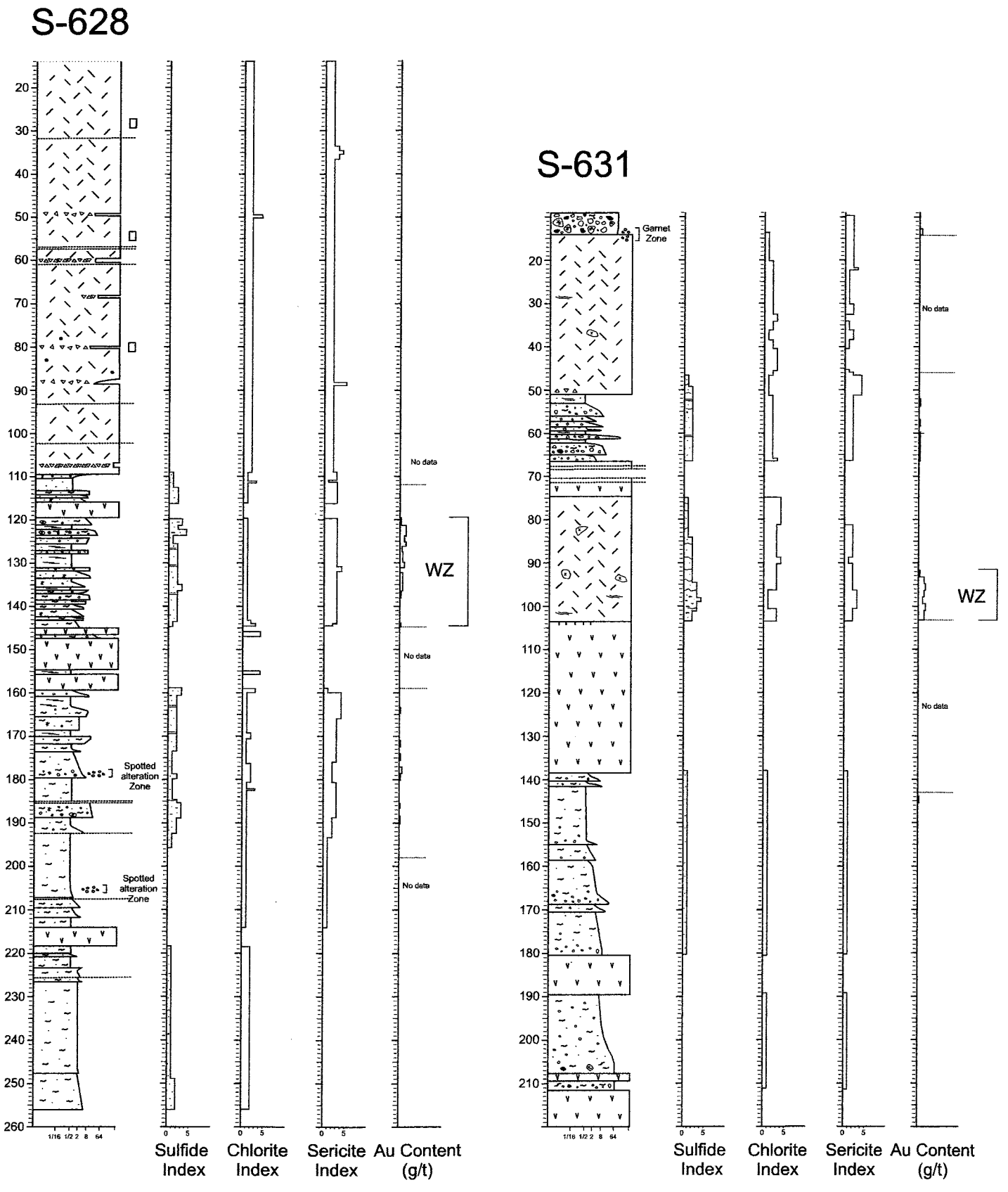
S-628
20
30
40
50
60
70
80
90
100
110
120
130
140
150
160
170
180
190
200
210
220
230
240
250
260
Spotted alteration Zone
Spotted alteration Zone
No data
WZ
No data
No data
1/16 1/2 2 8 64
0 5
Sulfide Index
Chlorite Index
Sericite Index
Au Content (g/t)
S-631
Garnet Zone
20
30
40
50
60
70
80
90
100
110
120
130
140
150
160
170
180
190
200
210
No data
WZ
No data
1/16 1/2 2 8 64
0 5
Sulfide Index
Chlorite Index
Sericite Index
Au Content (g/t)

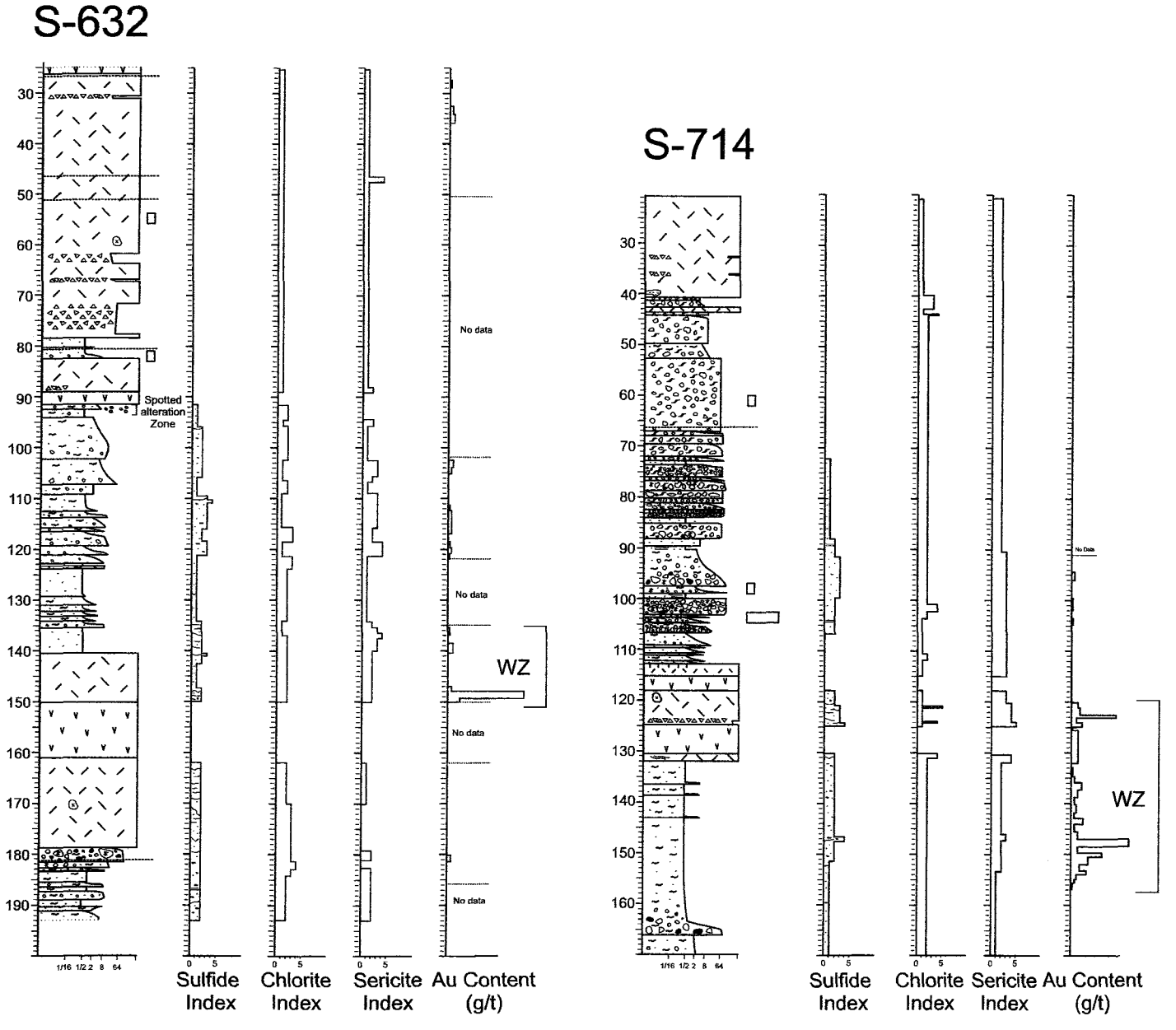
S-632
30
40
50
60
70
80
90
100
110
120
130
140
150
160
170
180
190
Spotted alteration Zone
No data
No data
WZ
No data
No data
1/16 1/2 2 8 64
0 5
Sulfide Index
Chlorite Index
Sericite Index
Au Content (g/t)
S-714
30
40
50
60
70
80
90
100
110
120
130
140
150
160
WZ
1/16 1/2 2 8 64
0 5
Sulfide Index
Chlorite Index
Sericite Index
Au Content (g/t)

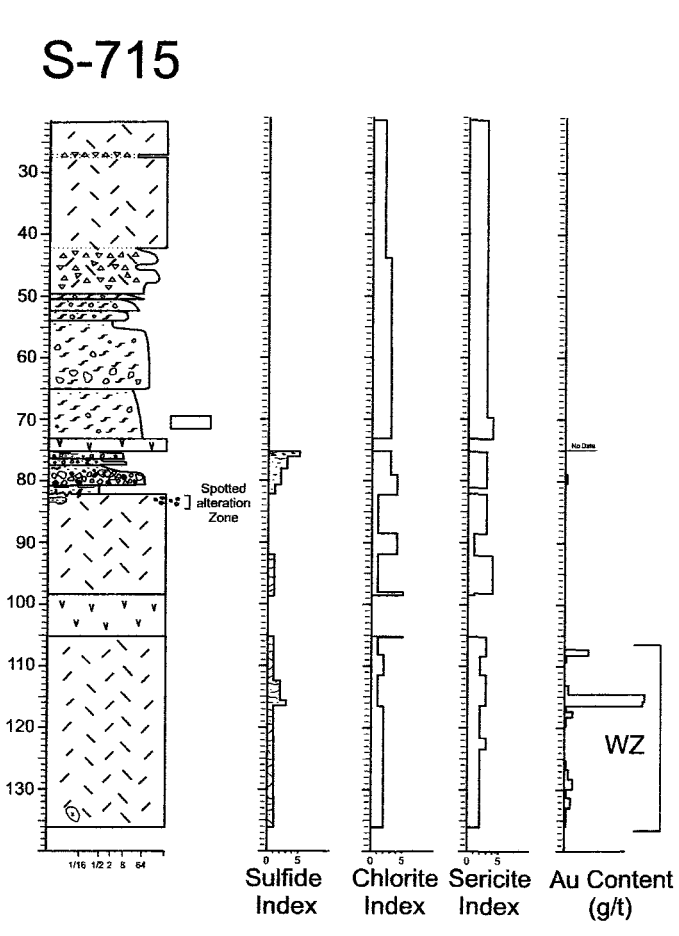
S-715
30
40
50
60
70
80
90
100
110
120
130
Spotted alteration Zone
1/16 1/2 2 8 64
0 5
Sulfide Index
Chlorite Index
Sericite Index
No Data
WZ
Au Content (g/t)

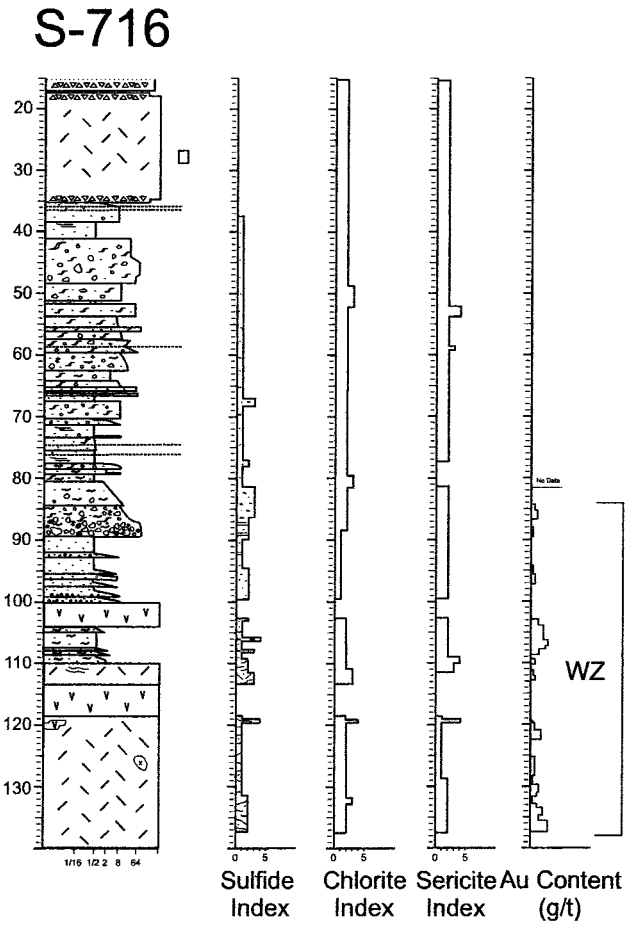
S-716
20
30
40
50
60
70
80
90
100
110
120
130
1/16 1/2 2 8 64
0 5
Sulfide Index
Chlorite Index
Sericite Index
No Data
WZ
Au Content (g/t)

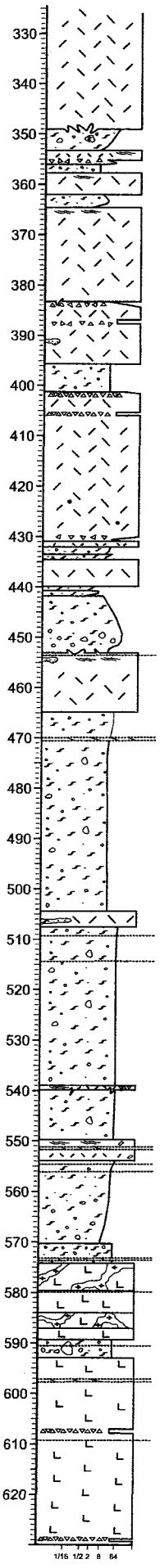

HW-07-02

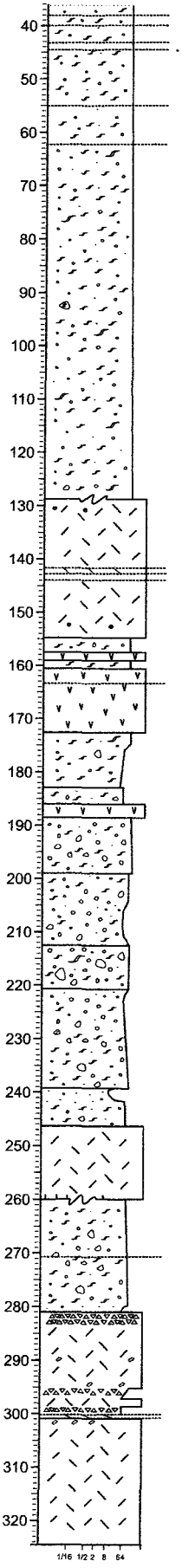

HW-07-03

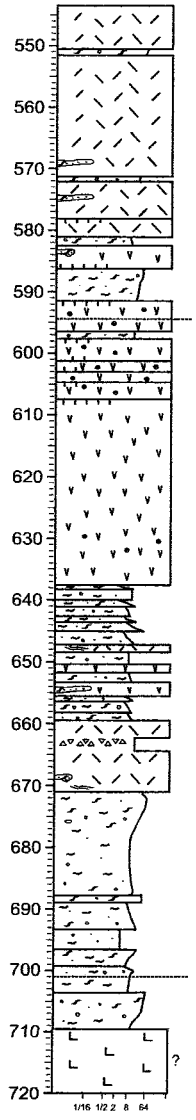

HW-07-03

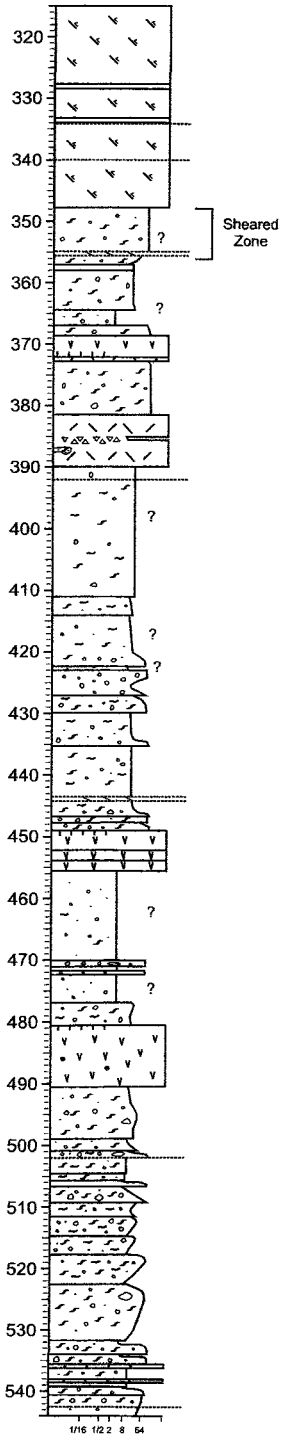

HW-07-04

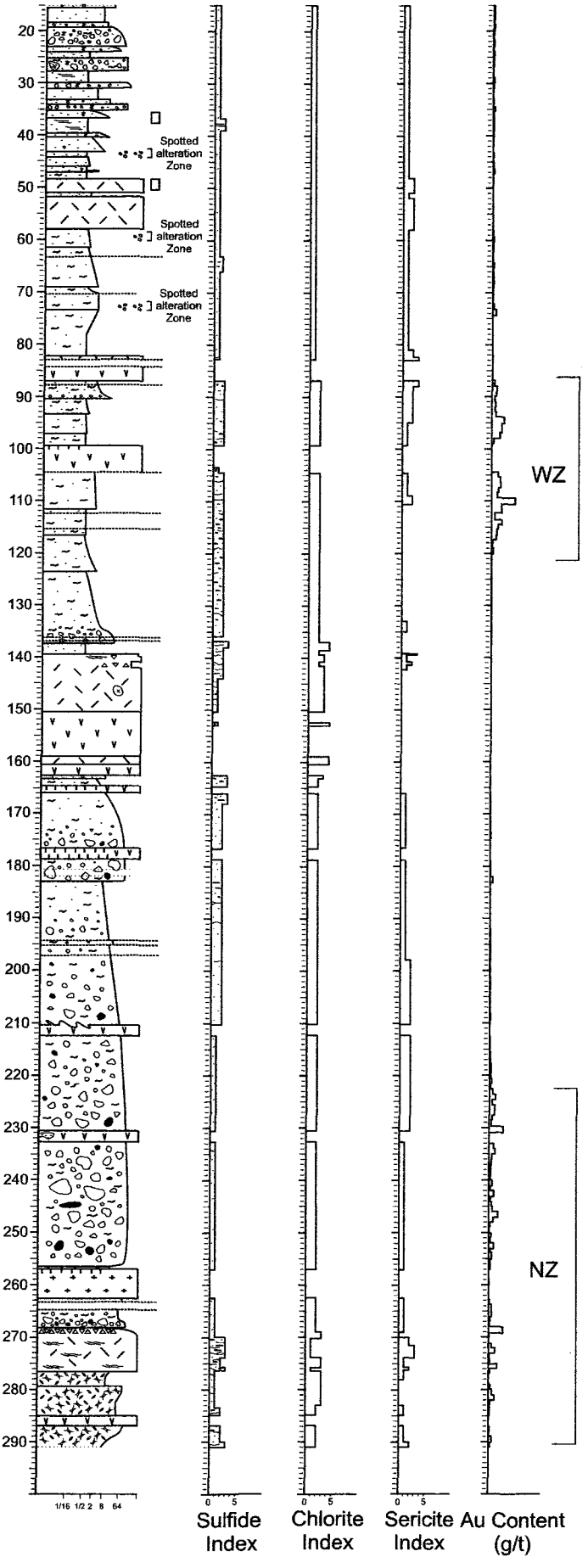
20
30
40
50
60
70
80
90
100
110
120
130
140
150
160
170
180
190
200
210
220
230
240
250
260
270
280
290
Spotted alteration Zone
Spotted alteration Zone
Spotted alteration Zone
1/16 1/2 2 8 64
0 5
Sulfide Index
0 5
Chlorite Index
0 5
Sericite Index
Au Content (g/t)
WZ
NZ

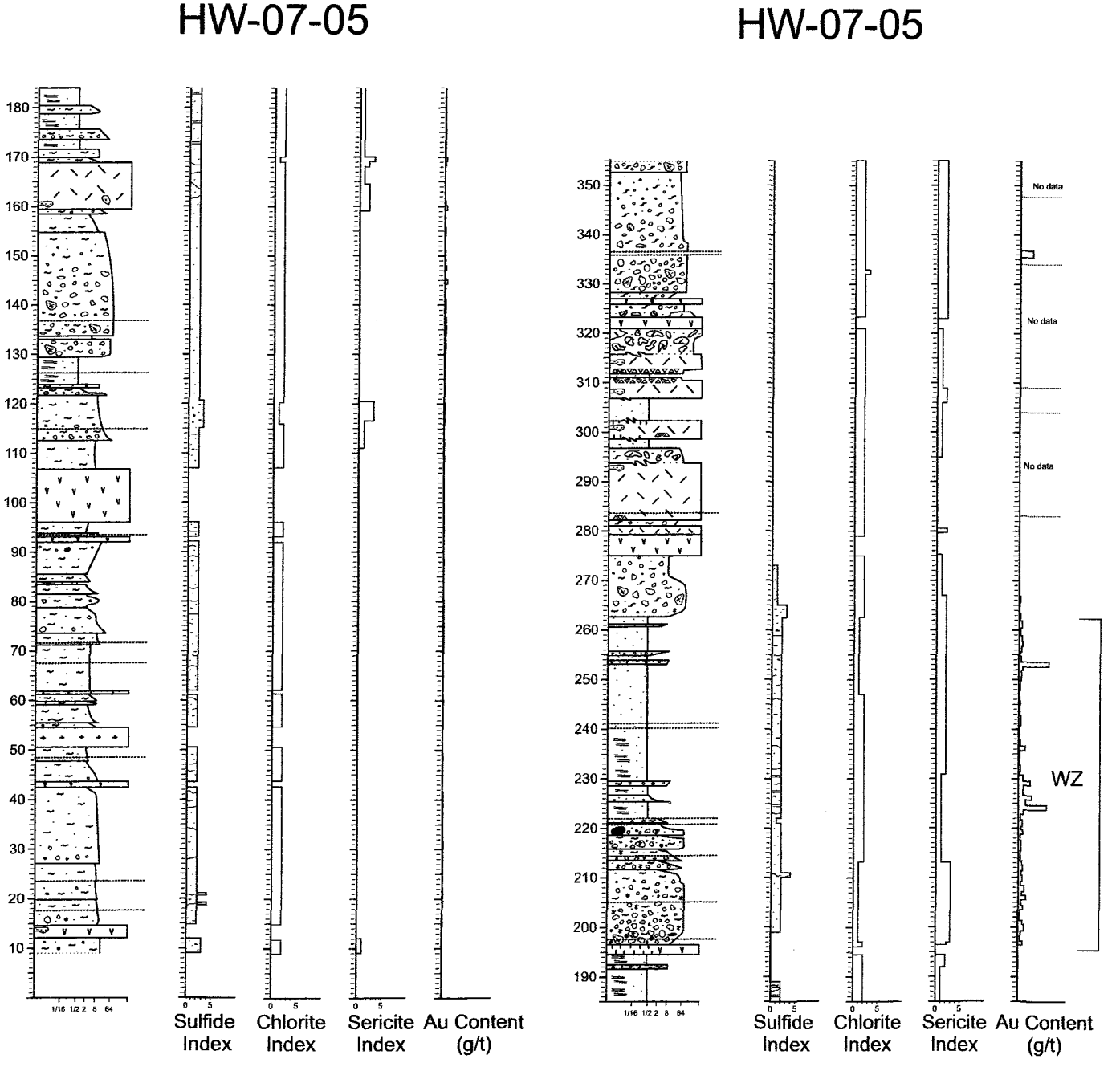
HW-07-05
HW-07-05
180
170
160
150
140
130
120
110
100
90
80
70
60
50
40
30
20
10
350
340
330
320
310
300
290
280
270
260
250
240
230
220
210
200
190
No data
No data
No data
WZ
1/16 1/2 2 8 64
0 5
Sulfide Index
Chlorite Index
Sericite Index
Au Content (g/t)

HW-07-06

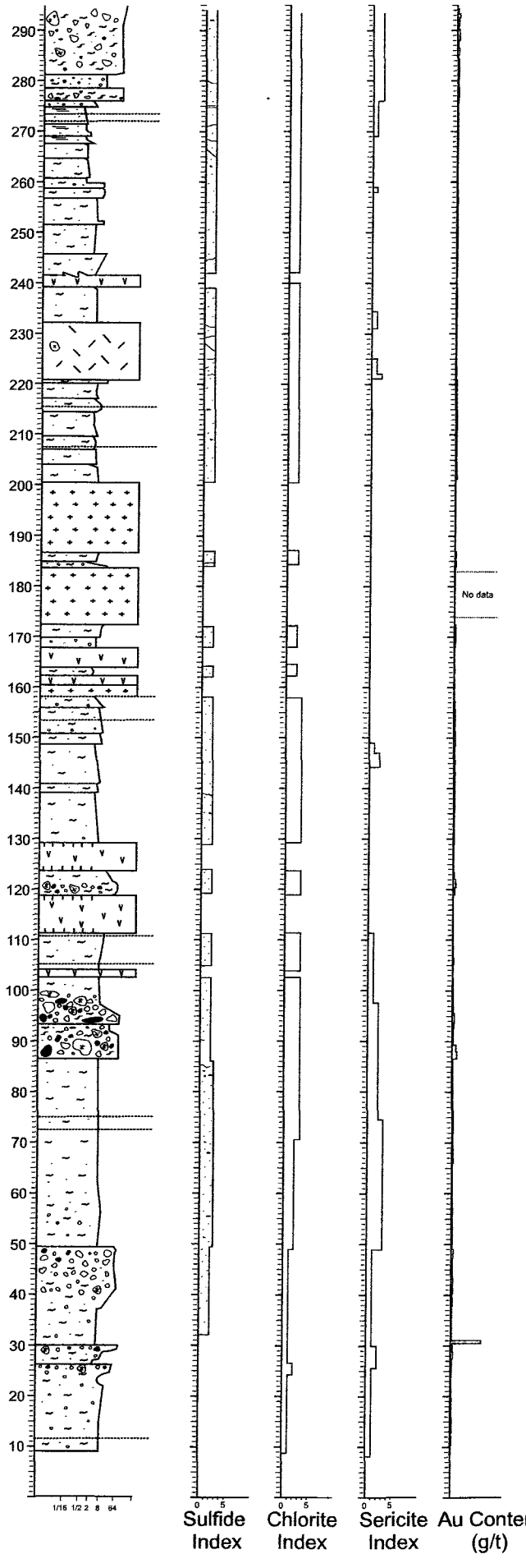

HW-07-06

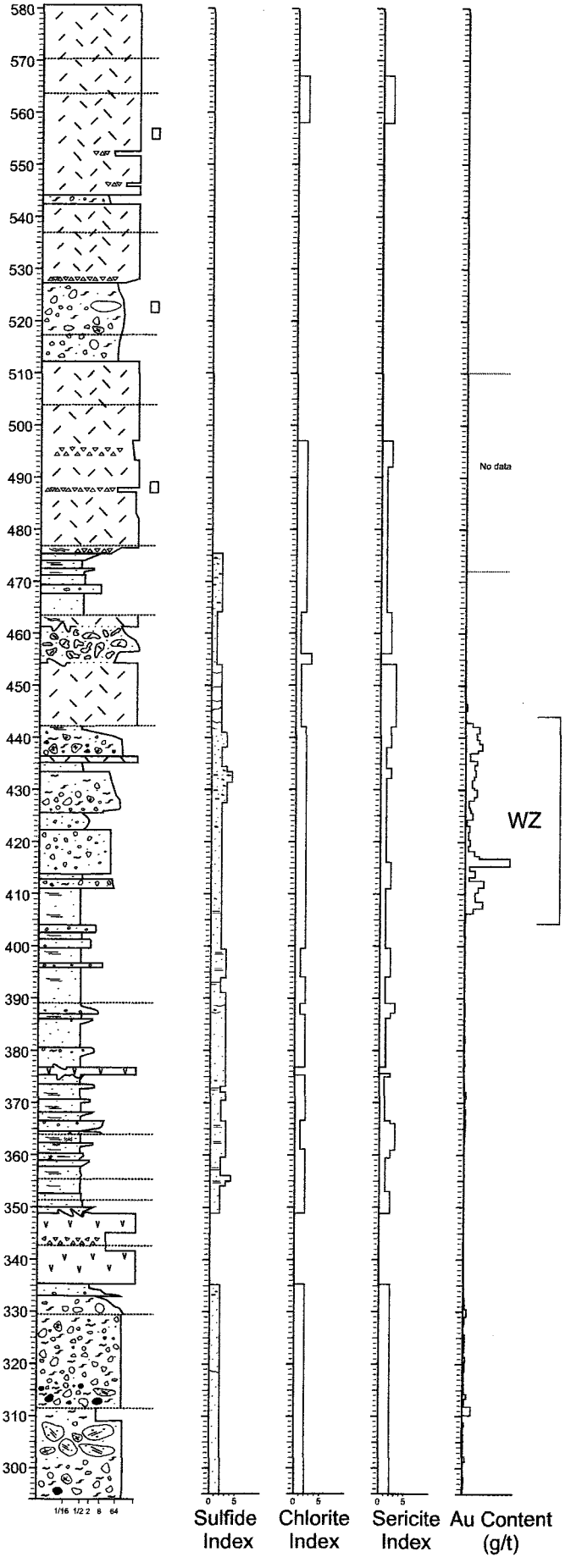

HW-07-07

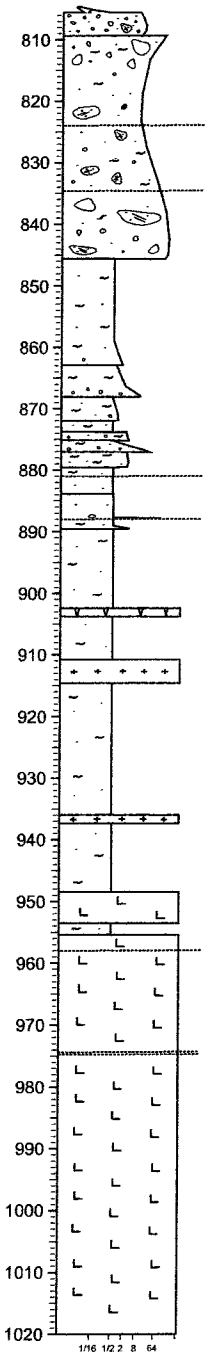

HW-07-07

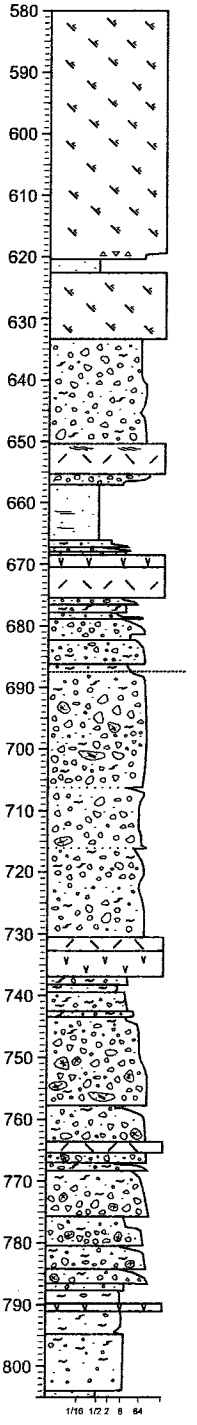

Appendix B

Tables

Table 1-A. Whole rock geochemistry of the Horne West succession

			Analyte Symbol	SiO2	TiO2	Al2O3	Fe2O3(T)
			Unit Symbol	%	%	%	%
			Detection Limit	0.01	0.001	0.01	0.01
			Analysis Method	FUS-ICP	FUS-ICP	FUS-ICP	FUS-ICP
Sample #	Hole #	Facies	Hole position (m)				
HWWR035*	S-716	Rhy2	22.20	74.51	0.292	12.03	3.97
HWWR036*	S-716	Rhy2	30.59	74.06	0.281	11.72	2.84
HWWR039*	S-715	Rhy2	24.48	73.11	0.287	12.04	3.65
HWWR040*	S-715	Rhy2	32.69	72.46	0.307	12.52	3.40
HWWR044*	S-572	Rhy2	151.94	72.70	0.303	12.50	2.74
HWWR037	S-716	XRhy	112.01	70.85	0.327	12.21	6.18
HWWR038	S-716	XRhy	127.25	69.93	0.330	12.75	8.13
HWWR042	S-715	XRhy	92.81	69.77	0.339	12.35	7.34
HWWR043	S-715	XRhy	114.15	72.83	0.273	10.90	7.58
HWWR041	S-715	XRhy	129.39	70.44	0.305	12.01	7.59
HWWR049	S-572	XRhy	93.88	73.45	0.299	11.84	6.68
HWWR048	S-572	XRhy	82.60	72.68	0.323	12.03	6.15
HWWR047	S-572	XRhy	68.58	72.69	0.337	12.21	5.30
HWWR046	S-572	XRhy	60.35	67.40	0.354	12.39	10.76
HWWR045	S-572	XRhy	49.38	71.37	0.347	12.31	8.02
HWWR088	S-574	XRhy	233.78	69.02	0.384	12.86	4.99
HWWR087	S-574	XRhy	222.81	70.50	0.368	12.35	4.94
HWWR086	S-574	XRhy	213.97	70.13	0.361	12.66	4.64
HWWR085	S-574	XRhy	204.52	67.50	0.386	13.33	4.87
HWWR084	S-574	XRhy	195.99	69.06	0.406	13.21	5.71
HWWR081	S-574	XRhy	165.20	72.47	0.342	12.37	6.20
HWWR113	S-573	XRhy	234.24	72.09	0.346	11.27	5.56
HWWR107	S-573	XRhy	182.88	68.12	0.406	13.45	8.30
HWWR068	S-574	XRhy (Base)	35.36	59.51	0.648	14.36	8.13
HWWR067	S-574	XRhy (Base)	26.21	65.33	0.488	13.56	5.88
HWWR093	S-573	XRhy (Base)	46.94	66.68	0.469	13.13	5.51
HWWR055	S-714	AmygBr (top)	46.02	66.62	0.421	13.68	6.03
HWWR056	S-714	AmygBr (top)	55.78	68.16	0.417	13.39	5.23
HWWR057	S-714	AmygBr (top)	65.23	70.39	0.418	13.56	4.69
HWWR066	S-574	AmygBr (Base)	15.54	59.73	0.681	15.02	7.92
HWWR092	S-573	AmygBr (Base)	36.27	64.69	0.465	12.95	10.46
HWWR091	S-573	AmygBr (Base)	24.69	67.10	0.403	12.87	2.98
HWWR090	S-573	AmygBr (Base)	15.54	62.45	0.620	15.16	6.49
HWWR059	S-714	QRhyBr	85.65	56.29	0.386	13.43	14.73
HWWR060	S-714	QRhyBr	95.71	56.61	0.355	11.37	16.01
HWWR058	S-714	QRhyBr	74.98	63.63	0.408	13.57	9.15
HWWR061	S-714	LBr	106.07	66.80	0.456	14.07	5.89
HWWR112	S-573	LBr	224.93	64.46	0.342	11.61	13.49
HWWR111	S-573	LBr	218.95	68.42	0.378	12.93	8.78
HWWR083	S-574	WcBr	186.84	66.22	0.407	13.00	9.84
HWWR082	S-574	WcBr	174.04	62.56	0.391	12.57	13.60
HWWR080	S-574	WcBr	155.14	65.85	0.402	13.19	14.28
HWWR079	S-574	WcBr	144.78	63.65	0.389	12.33	12.43
HWWR078	S-574	WcBr	133.81	58.83	0.397	12.39	16.30
HWWR077	S-574	WcBr	123.44	63.23	0.351	11.71	13.80
HWWR076	S-574	WcBr	113.08	63.96	0.396	12.84	12.86
HWWR110	S-573	WcBr	206.78	65.55	0.350	11.69	13.76
HWWR109	S-573	WcBr	198.33	64.40	0.385	12.38	12.94
HWWR108	S-573	WcBr	191.46	62.79	0.383	12.46	13.94
HWWR106	S-573	WcBr	173.58	64.14	0.392	12.70	11.08
HWWR105	S-573	WcBr	164.90	64.64	0.383	12.11	12.77
HWWR104	S-573	WcBr	154.08	62.97	0.369	12.13	13.65
HWWR103	S-573	WcBr	140.57	64.64	0.367	12.15	11.36
HWWR102	S-573	WcBr	132.28	64.77	0.404	13.19	10.96
HWWR101	S-573	WcBr	123.75	63.96	0.413	12.88	12.93
HWWR100	S-573	WcBr	115.21	63.50	0.396	12.86	12.73
HWWR099	S-573	WcBr	104.85	64.71	0.377	12.04	13.22
HWWR062	S-714	WcBr	134.42	65.62	0.392	13.06	10.59
HWWR063	S-714	WcBr	143.56	65.32	0.399	12.67	12.32
HWWR064	S-714	WcBr	154.53	64.77	0.403	12.30	12.88
HWWR065	S-714	WcBr	164.29	66.30	0.410	13.24	8.55
HWWR075	S-574	Rhy1 (Base)	103.94	64.75	0.414	13.17	9.07
HWWR073	S-574	Rhy1 (Base)	81.08	69.78	0.408	13.67	8.72
HWWR072	S-574	Rhy1 (Base)	71.93	66.19	0.457	15.42	7.11
[illegible]	S-574	Rhy1 (Base)	62.79	69.49	0.403	13.46	6.67
[illegible]	S-574	Rhy1 (Base)	53.64	61.98	0.461	15.60	9.04
[illegible]	S-574	Rhy1 (Base)	44.50	75.50	[illegible]	12.71	4.56
[illegible]	[illegible]	Rhy1 (Base)	[illegible]	66.92	0.497	[illegible]	[illegible]
[illegible]	[illegible]	Rhy1 (Base)	85.65	69.94	0.397	[illegible]	7.45
[illegible]	S-573	Rhy1 (Base)	75.90	71.17	0.387	12.96	6.83
[illegible]	S-573	Rhy1 (Base)	67.36	65.60	0.362	12.91	13.17
HWWR074	S-574	CrBr	90.83	64.20	0.418	13.00	12.44
HWWR094	S-573	CrBr	58.22	60.91	0.320	10.87	18.01
HWWR089	S-574	Mafic intrusive	247.19	48.32	0.737	14.38	9.35
HWWR114	S-573	Mafic intrusive	243.61	47.90	1.094	13.39	12.85

* Least altered rhyolite

Table 1-B. Whole rock geochemistry of the Horne West succession

Analyte Symbol	MnO	MgO	CaO	Na2O	K2O	P2O5	LOI	Total	Total S	CO2
Unit Symbol	%	%	%	%	%	%	%	%	%	%
Detection Limit	0.001	0.01	0.01	0.01	0.01	0.01		0.01	0.01	0.01
Analysis Method	FUS-ICP	FUS-ICP	FUS-ICP	FUS-ICP	FUS-ICP	FUS-ICP	FUS-ICP	FUS-ICP	IR	COUL
Sample #										
HWWR035	0.075	0.59	1.84	4.56	0.70	0.06	2.26	101.00	0.65	0.86
HWWR036	0.058	0.55	1.87	4.50	0.90	0.05	2.14	98.76	0.46	0.94
HWWR039	0.085	0.69	3.07	4.30	0.85	0.06	2.60	100.70	0.09	1.61
HWWR040	0.084	0.57	3.47	3.91	1.20	0.06	2.66	100.60	0.15	1.67
HWWR044	0.201	0.73	3.04	4.70	0.78	0.05	2.74	100.50	0.56	1.44
HWWR037	0.035	0.44	0.11	0.13	3.44	0.05	4.15	97.93	3.59	0.03
HWWR038	0.129	1.19	0.13	0.14	2.65	0.06	3.57	99.00	1.76	0.02
HWWR042	0.086	0.37	0.14	0.37	2.90	0.08	4.21	97.95	3.77	0.01
HWWR043	0.069	0.67	0.08	0.24	2.54	0.05	3.53	98.77	2.74	< 0.01
HWWR041	0.073	1.25	0.15	0.22	2.48	0.05	3.95	98.51	2.96	< 0.01
HWWR049	0.024	0.33	0.09	0.23	3.22	0.05	4.20	100.40	4.05	< 0.01
HWWR048	0.212	1.20	0.29	2.80	1.27	0.07	1.99	99.02	0.22	< 0.01
HWWR047	0.045	0.38	0.21	0.26	3.58	0.08	3.71	98.81	3.12	< 0.01
HWWR046	0.096	0.99	0.17	0.28	2.64	0.08	4.35	99.49	3.16	< 0.01
HWWR045	0.025	0.42	0.11	0.25	3.17	0.07	4.46	100.50	4.15	< 0.01
HWWR088	0.095	2.00	2.11	2.00	2.36	0.06	3.56	99.44	1.70	0.56
HWWR087	0.127	1.32	3.42	1.64	1.65	0.08	2.61	99.00	1.16	0.29
HWWR086	0.133	1.08	3.86	1.82	1.66	0.08	2.68	99.10	1.21	0.58
HWWR085	0.188	0.98	4.08	1.16	2.53	0.09	4.07	99.19	1.38	1.42
HWWR084	0.191	1.58	2.75	1.98	1.95	0.08	3.07	99.99	1.90	0.13
HWWR081	0.082	1.32	0.80	2.98	1.41	0.06	2.61	100.70	1.43	0.08
HWWR113	0.184	1.17	2.00	1.70	1.56	0.07	2.57	98.52	1.26	0.20
HWWR107	0.052	1.56	0.51	1.58	2.21	0.08	3.37	99.64	1.95	< 0.01
HWWR068	1.690	1.48	4.25	1.34	2.52	0.12	5.17	99.23	2.24	2.06
HWWR067	0.550	1.44	6.00	1.48	1.57	0.09	3.56	99.94	0.20	1.67
HWWR093	0.041	0.21	0.20	0.41	3.56	0.14	4.04	94.40	3.48	< 0.01
HWWR055	0.126	1.27	3.76	3.27	1.42	0.06	3.40	100.10	1.68	0.92
HWWR056	0.119	1.10	2.91	4.37	0.96	0.06	2.72	99.43	1.12	0.81
HWWR057	0.137	1.19	2.21	4.24	1.06	0.06	2.21	100.20	1.16	0.22
HWWR066	0.472	3.38	5.77	1.46	1.18	0.15	4.86	100.60	0.20	1.91
HWWR092	0.608	2.33	0.50	0.16	2.17	0.07	4.45	98.87	2.31	0.14
HWWR091	0.800	0.62	5.82	1.13	2.67	0.10	5.11	99.61	0.72	3.33
HWWR090	0.336	2.83	4.54	2.12	1.57	0.13	3.40	99.65	0.66	0.41
HWWR059	0.196	1.17	1.38	0.85	2.84	0.06	8.33	99.67	11.10	0.03
HWWR060	0.274	1.01	2.58	2.03	1.32	0.07	8.82	100.40	11.70	0.57
HWWR058	0.102	1.64	1.38	1.58	2.40	0.08	5.32	99.26	5.36	0.09
HWWR061	0.351	1.03	3.17	1.66	1.87	0.07	3.55	98.93	2.15	0.35
HWWR112	0.032	0.34	0.14	0.22	3.01	0.08	6.92	100.60	8.90	< 0.01
HWWR111	0.043	0.37	0.16	0.19	3.10	0.07	4.75	99.19	4.71	< 0.01
HWWR083	0.042	0.74	0.12	0.29	3.17	0.09	5.07	98.98	5.32	< 0.01
HWWR082	0.093	1.55	0.24	0.23	2.39	0.09	5.16	98.87	4.30	< 0.01
HWWR080	0.050	1.39	0.33	0.32	2.79	0.09	0.09	98.78	6.39	< 0.01
HWWR079	0.043	2.37	0.13	0.25	2.16	0.08	5.23	99.08	4.29	< 0.01
HWWR078	0.032	1.82	0.14	0.21	2.22	0.09	7.08	99.53	7.76	< 0.01
HWWR077	0.036	1.34	0.31	0.29	2.49	0.08	6.73	100.40	7.75	0.02
HWWR076	0.076	2.03	0.26	0.28	2.47	0.09	5.67	100.90	5.37	< 0.01
HWWR110	0.029	0.60	0.11	0.18	2.43	0.07	5.55	100.30	6.27	< 0.01
HWWR109	0.036	1.10	0.13	0.17	2.78	0.10	5.67	100.10	5.89	< 0.01
HWWR108	0.038	0.64	0.29	0.18	3.10	0.08	6.63	100.50	8.31	< 0.01
HWWR106	0.042	1.67	0.15	0.13	2.69	0.07	5.79	98.85	5.73	< 0.01
HWWR105	0.025	1.49	0.12	0.18	2.32	0.08	5.96	100.10	6.40	< 0.01
HWWR104	0.038	1.81	0.14	0.31	2.34	0.08	6.30	100.10	6.77	< 0.01
HWWR103	0.031	1.59	0.13	0.15	2.45	0.06	6.00	98.92	6.26	< 0.01
HWWR102	0.044	2.12	0.14	0.15	2.49	0.07	5.31	99.66	4.17	< 0.01
HWWR101	0.055	2.18	0.13	0.22	2.59	0.08	5.52	101.00	4.93	< 0.01
HWWR100	0.049	1.66	0.16	0.19	2.74	0.09	5.85	100.20	5.80	< 0.01
HWWR099	0.046	1.36	0.12	0.18	2.56	0.09	6.08	100.80	6.56	< 0.01
HWWR062	0.031	0.37	0.23	0.21	3.15	0.09	4.94	98.68	4.99	0.03
HWWR063	0.015	0.26	0.13	0.39	2.92	0.09	5.29	99.80	5.72	< 0.01
HWWR064	0.031	0.48	0.12	0.28	2.81	0.08	5.75	99.92	6.38	< 0.01
HWWR065	0.053	1.30	0.12	0.14	2.92	0.07	5.13	98.22	4.64	< 0.01
HWWR075	0.092	2.95	0.26	0.14	2.47	0.11	5.07	98.49	3.41	< 0.01
HWWR073	0.088	0.82	0.15	0.24	2.88	0.09	3.59	100.40	1.91	< 0.01
HWWR072	0.071	1.21	0.62	0.31	3.69	0.12	4.38	99.61	3.30	0.07
HWWR071	[illegible]	1.97	0.43	0.21	2.62	0.10	5.19	98.93	0.65	0.03
HWWR070	0.077	0.45	0.22	0.34	4.21	0.09	6.52	98.99	7.87	< 0.01
HWWR069	0.250	0.38	0.36	0.80	2.96	0.07	2.65	100.10	0.68	0.20
[illegible]	[illegible]	2.01	0.18	0.40	[illegible]	0.11	[illegible]	[illegible]	[illegible]	< 0.01
HWWR097	[illegible]	[illegible]	0.28	1.69	2.02	0.09	2.91	99.90	1.10	0.01
HWWR096	0.079	0.98	0.26	0.30	3.19	0.11	4.75	99.91	2.53	0.01
HWWR095	0.020	0.45	0.13	0.31	2.83	0.10	5.99	99.24	6.65	< 0.01
HWWR074	0.051	0.86	0.25	0.31	3.15	0.11	5.57	100.40	5.78	< 0.01
HWWR094	0.037	0.38	0.12	0.25	2.01	0.08	6.88	99.85	8.34	< 0.01
HWWR089	0.221	7.80	8.31	2.18	0.15	0.32	6.75	98.53	0.02	2.88
HWWR114	0.766	6.59	9.62	0.05	0.01	0.10	6.84	99.21	0.68	2.57

Table 1-C. Whole rock geochemistry of the Horne West succession

Analyte Symbol	Au	Ag	Cu	Zn	Pb	Mn	As	Sb	Cd	Bi
Unit Symbol	ppb	ppm	ppm	ppm	ppm	ppm	ppm	ppm	ppm	ppm
Detection Limit	5	0.5	0.5	0.5	2	2	0.5	0.2	0.2	0.1
Analysis Method	FA-AA	FUS-MS	TD-MS	TD-MS	TD-MS	TD-MS	NP-MS	FUS-MS	TD-MS	FUS-MS
Sample #										
HWWR115	9	< 0.5	33.4	46.9	7	501	< 0.5	< 0.2	< 0.2	< 0.1
HWWR095	< 5	< 0.5	43.5	51.5	7	401	< 0.5	< 0.2	< 0.2	0.2
HWWR091	7	< 0.5	121.0	48.1	8	584	< 0.5	< 0.2	< 0.2	0.8
HWWR090	< 5	< 0.5	30.7	35.3	5	639	< 0.5	< 0.2	< 0.2	0.3
HWWR044	8	< 0.5	19.8	32.5	5	1310	0.5	< 0.2	< 0.2	0.5
HWWR037	396	< 0.5	104.0	4290.0	8	267	3.1	< 0.2	21.8	< 0.1
HWWR038	384	< 0.5	62.5	5240.0	3	851	1.1	< 0.2	25.2	< 0.1
HWWR042	65	0.6	35.0	2190.0	20	558	17.5	< 0.2	6.3	0.1
HWWR043	959	< 0.5	298.0	3510.0	5	428	1.4	< 0.2	11.4	< 0.1
HWWR041	445	< 0.5	115.0	8580.0	4	548	1.1	< 0.2	38.7	< 0.1
HWWR049	685	< 0.5	63.4	2800.0	8	171	12.0	< 0.2	12.0	< 0.1
HWWR048	< 5	< 0.5	5.7	1830.0	2	1450	0.6	2.9	5.6	< 0.1
HWWR047	562	78.6	72.2	3450.0	8	281	1.7	0.7	18.6	0.6
HWWR046	1360	< 0.5	164.0	57.8	5	628	1.1	3.0	< 0.2	0.4
HWWR045	44	< 0.5	280.0	16.5	6	168	1.7	< 0.2	< 0.2	0.1
HWWR088	26	< 0.5	41.6	278.0	9	647	2.9	< 0.2	0.9	< 0.1
HWWR087	39	< 0.5	99.1	647.0	36	848	5.3	< 0.2	2.8	< 0.1
HWWR086	29	< 0.5	116.0	506.0	15	853	2.4	9.9	2.0	0.9
HWWR085	39	< 0.5	75.9	311.0	12	1260	2.0	1.4	1.1	3.0
HWWR084	81	< 0.5	119.0	498.0	11	1170	4.7	< 0.2	1.8	0.1
HWWR081	< 5	< 0.5	95.2	39.6	4	632	0.7	1.9	< 0.2	0.2
HWWR113	82	0.8	173.0	663.0	58	1310	2.8	< 0.2	2.1	< 0.1
HWWR107	24	< 0.5	163.0	23.9	4	392	0.9	< 0.2	< 0.2	< 0.1
HWWR068	265	2.2	94.4	154.0	13	> 10000	5.9	0.3	< 0.2	1.4
HWWR067	< 5	< 0.5	65.8	140.0	18	3690	< 0.5	0.9	< 0.2	0.7
HWWR093	214	< 0.5	70.9	3750.0	34	256	25.7	< 0.2	12.2	0.2
HWWR055	39	< 0.5	127.0	258.0	10	903	1.6	< 0.2	0.8	0.2
HWWR056	42	< 0.5	112.0	258.0	11	787	2.3	< 0.2	0.7	0.1
HWWR057	28	< 0.5	67.9	166.0	9	828	2.0	< 0.2	0.3	< 0.1
HWWR066	< 5	< 0.5	55.4	141.0	7	2860	1.2	2.3	< 0.2	< 0.1
HWWR092	33	< 0.5	78.6	2570.0	10	3910	8.5	< 0.2	11.5	< 0.1
HWWR091	24	< 0.5	8.0	61.7	10	5710	0.9	2.8	< 0.2	1.4
HWWR090	6	< 0.5	105.0	169.0	9	2400	3.3	< 0.2	< 0.2	< 0.1
HWWR059	281	2.3	423.0	664.0	27	1240	23.2	2.6	2.8	0.3
HWWR060	367	1.3	536.0	2070.0	22	1870	22.4	1.0	10.1	2.1
HWWR058	178	< 0.5	391.0	322.0	13	629	6.8	< 0.2	1.0	0.7
HWWR061	60	< 0.5	94.8	150.0	13	2320	2.1	< 0.2	< 0.2	0.2
HWWR112	1030	< 0.5	355.0	103.0	25	234	25.1	< 0.2	< 0.2	0.1
HWWR111	> 3000	< 0.5	137.0	93.8	7	291	3.0	< 0.2	< 0.2	< 0.1
HWWR083	886	1.2	214.0	7570.0	8	289	6.2	< 0.2	39.1	0.2
HWWR082	105	< 0.5	250.0	141.0	6	628	3.1	< 0.2	< 0.2	0.3
HWWR080	54	< 0.5	304.0	18.6	5	225	4.0	< 0.2	< 0.2	0.2
HWWR079	55	0.6	403.0	50.5	9	335	7.6	< 0.2	< 0.2	0.4
HWWR078	110	0.7	547.0	33.2	15	238	19.1	< 0.2	< 0.2	0.2
HWWR077	117	0.7	250.0	34.4	9	237	11.1	18.6	< 0.2	0.2
HWWR076	93	0.8	280.0	55.0	8	406	12.1	0.7	< 0.2	0.2
HWWR110	59	< 0.5	669.0	32.1	5	203	4.4	< 0.2	< 0.2	< 0.1
HWWR109	51	< 0.5	294.0	28.0	7	263	4.9	< 0.2	< 0.2	< 0.1
HWWR108	108	< 0.5	633.0	21.4	10	312	7.0	11.7	< 0.2	0.2
HWWR106	79	< 0.5	453.0	26.9	9	296	7.1	< 0.2	< 0.2	< 0.1
HWWR105	84	< 0.5	618.0	43.3	7	195	8.6	< 0.2	0.3	< 0.1
HWWR104	65	< 0.5	506.0	42.7	9	276	6.4	< 0.2	< 0.2	0.1
HWWR103	103	< 0.5	319.0	33.6	11	221	9.4	< 0.2	< 0.2	< 0.1
HWWR102	60	< 0.5	237.0	39.6	6	286	8.4	< 0.2	< 0.2	< 0.1
HWWR101	201	< 0.5	218.0	65.6	10	375	15.2	< 0.2	< 0.2	< 0.1
HWWR100	407	< 0.5	201.0	62.2	14	340	11.6	0.3	< 0.2	< 0.1
HWWR099	1530	< 0.5	319.0	56.4	9	298	11.9	< 0.2	< 0.2	0.2
HWWR062	1280	< 0.5	250.0	8900.0	8	223	1.8	< 0.2	60.4	< 0.1
HWWR063	810	< 0.5	227.0	62.0	10	102	2.4	< 0.2	< 0.2	0.3
HWWR064	1390	< 0.5	284.0	81.5	6	224	8.1	0.5	< 0.2	0.2
HWWR065	1540	11.4	270.0	5110.0	8	412	7.6	0.3	31.4	< 0.1
HWWR075	52	< 0.5	60.8	254.0	5	619	5.5	1.5	0.2	0.2
HWWR073	172	1.2	48.8	2200.0	17	595	6.1	< 0.2	10.0	< 0.1
HWWR072	396	4.9	62.4	8810.0	22	1000	19.0	< 0.2	12.1	< 0.1
HWWR071	15	1.9	57.8	5630.0	35	2740	2.0	2.1	15.2	< 0.1
HWWR070	837	< 0.5	59.5	> 10000	6	908	3.8	< 0.2	1050	< 0.1
HWWR069	27	< 0.5	95.2	1470.0	16	1520	11.1	< 0.2	5.0	< 0.1
HWWR097	302	< 0.5	42.0	2980.0	8	816	0.5	< 0.2	19.1	< 0.1
HWWR096	70	< 0.5	58.7	3970.0	50	887	4.9	< 0.2	16.9	< 0.1
HWWR095	380	2.0	123.0	819.0	25	1480	14.1	0.5	3.8	0.4
HWWR094	1250	0.7	408.0	62.5	6	165	3.0	< 0.2	< 0.2	0.4
HWWR074	1390	0.8	236.0	97.0	7	351	7.4	< 0.2	< 0.2	0.1
HWWR094	1310	< 0.5	340.0	117.0	9	242	5.9	1.0	0.2	0.1
HWWR089	< 5	< 0.5	16.7	280.0	12	1640	0.7	< 0.2	< 0.2	0.5
HWWR114	12	< 0.5	47.4	453.0	16	6330	1.8	< 0.2	0.2	0.7

Table 1-D. Whole rock geochemistry of the Horne West succession

Analyte Symbol	Co	Ni	Cr	V	Mo	Ga	In	Sn	Tl	W
Unit Symbol	ppm	ppm	ppm	ppm	ppm	ppm	ppm	ppm	ppm	ppm
Detection Limit	0.5	20	1	5	2	1	0.1	1	0.05	0.5
Analysis Method	TD-MS	FUS-MS	TD-MS	FUS-ICP	FUS-MS	FUS-MS	FUS-MS	FUS-MS	FUS-MS	FUS-MS
Sample #										
[illegible]	[illegible]	[illegible]	[illegible]	[illegible]	[illegible]	[illegible]	[illegible]	[illegible]	[illegible]	[illegible]
HWWR037	3.0	< 20	71	7	< 2	17	1.7	6	0.34	1.4
HWWR038	3.3	< 20	54	6	< 2	18	3.0	8	0.26	1.3
HWWR042	3.9	< 20	75	< 5	< 2	18	< 0.1	8	0.32	1.1
HWWR043	3.1	< 20	71	6	< 2	17	0.5	6	0.23	< 0.5
HWWR041	5.2	< 20	69	9	< 2	16	1.5	8	0.34	< 0.5
HWWR049	3.6	< 20	105	7	< 2	19	0.3	7	0.27	0.6
HWWR048	2.3	< 20	103	8	< 2	15	< 0.1	7	0.17	0.5
HWWR047	3.2	< 20	77	8	< 2	17	3.2	7	0.29	1.5
HWWR046	4.5	< 20	68	10	< 2	18	< 0.1	9	0.27	< 0.5
HWWR045	2.2	< 20	70	8	< 2	16	< 0.1	3	0.25	0.8
HWWR088	5.6	< 20	86	25	8	18	0.2	2	0.44	0.5
HWWR087	6.1	< 20	93	26	2	16	0.3	3	0.37	0.6
HWWR086	5.4	< 20	117	23	< 2	16	0.3	3	0.31	0.9
HWWR085	6.1	< 20	71	29	3	18	0.3	3	0.59	1.3
HWWR084	6.4	< 20	90	27	3	16	0.3	2	0.36	< 0.5
HWWR081	3.3	< 20	107	14	< 2	17	< 0.1	5	0.20	0.7
HWWR113	6.8	< 20	87	32	5	14	0.3	5	0.26	0.7
HWWR107	4.3	< 20	68	16	3	18	< 0.1	5	0.21	0.6
[illegible]	[illegible]	[illegible]	[illegible]	[illegible]	[illegible]	[illegible]	[illegible]	[illegible]	[illegible]	[illegible]
HWWR055	7.9	< 20	116	51	< 2	18	0.1	2	0.35	0.7
HWWR056	7.9	< 20	116	50	< 2	18	< 0.1	2	0.27	0.8
HWWR057	6.8	< 20	140	50	2	19	< 0.1	1	0.29	0.7
[illegible]	[illegible]	[illegible]	[illegible]	[illegible]	[illegible]	[illegible]	[illegible]	[illegible]	[illegible]	[illegible]
HWWR059	7.0	< 20	58	45	< 2	19	0.7	7	0.83	1.0
HWWR060	9.6	< 20	69	33	8	15	1.2	8	0.33	1.0
HWWR058	7.7	< 20	86	39	< 2	18	0.3	6	0.81	1.0
[illegible]	[illegible]	[illegible]	[illegible]	[illegible]	[illegible]	[illegible]	[illegible]	[illegible]	[illegible]	[illegible]
HWWR083	8.3	< 20	32	30	< 2	19	8.1	9	0.50	0.5
HWWR082	7.1	< 20	56	28	< 2	17	0.1	10	0.34	0.8
HWWR080	5.0	< 20	55	29	< 2	18	0.2	14	0.40	0.6
HWWR079	7.6	< 20	65	29	< 2	19	0.2	7	0.36	0.6
HWWR078	9.6	< 20	58	29	< 2	18	0.1	9	0.62	0.7
HWWR077	4.9	< 20	59	25	4	16	0.2	9	0.56	< 0.5
HWWR076	6.8	< 20	52	30	< 2	17	0.2	9	0.73	< 0.5
HWWR110	8.4	< 20	54	23	< 2	19	0.2	19	0.32	< 0.5
HWWR109	4.8	< 20	52	43	4	19	< 0.1	10	0.29	0.8
HWWR108	7.1	< 20	80	27	< 2	19	0.1	12	0.39	1.1
HWWR106	7.7	< 20	67	30	< 2	17	0.1	7	0.34	< 0.5
HWWR105	5.0	< 20	64	23	< 2	19	< 0.1	5	0.26	< 0.5
HWWR104	7.3	< 20	62	26	< 2	21	< 0.1	7	0.40	< 0.5
HWWR103	6.6	< 20	53	28	< 2	16	< 0.1	6	0.38	< 0.5
HWWR102	5.4	< 20	60	33	< 2	18	< 0.1	5	0.40	< 0.5
HWWR101	8.3	< 20	54	32	< 2	16	0.1	9	0.47	< 0.5
HWWR100	8.4	< 20	64	32	< 2	19	0.1	12	0.60	0.5
HWWR099	5.5	< 20	63	30	< 2	18	< 0.1	7	0.62	< 0.5
HWWR062	5.1	< 20	68	25	< 2	21	38.5	5	0.31	1.3
HWWR063	5.3	< 20	44	30	< 2	19	< 0.1	6	0.38	0.6
HWWR064	5.3	< 20	67	28	< 2	17	0.1	14	0.44	< 0.5
HWWR065	9.6	< 20	69	31	< 2	17	5.9	14	0.42	< 0.5
[illegible]	[illegible]	[illegible]	[illegible]	[illegible]	[illegible]	[illegible]	[illegible]	[illegible]	[illegible]	[illegible]
HWWR074	6.8	< 20	83	13	< 2	19	< 0.1	5	0.35	0.7
HWWR094	3.4	< 20	53	7	< 2	18	0.5	2	0.31	1.2
[illegible]	[illegible]	[illegible]	[illegible]	[illegible]	[illegible]	[illegible]	[illegible]	[illegible]	[illegible]	[illegible]

Table 1-E. Whole rock geochemistry of the Horne West succession

Analyte Symbol	Hg	Ba	Rb	Sr	Th	U	Sc	B	Be	Cs
Unit Symbol	ppb	ppm	ppm	ppm	ppm	ppm	ppm	ppm	ppm	ppm
Detection Limit	5	3	1	2	0.05	0.01	1	1	1	0.1
Analysis Method	FIMS	FUS-ICP	FUS-MS	FUS-ICP	FUS-MS	FUS-MS	FUS-ICP	INAA	FUS-ICP	FUS-MS
Sample #										
[illegible]	< 5	140	19	48	2.52	0.68	9	14	1	1.0
[illegible]	< 5	168	27	42	2.77	0.88	9	5	< 1	1.1
[illegible]	< 5	159	21	55	2.76	0.70	10	11	< 1	1.3
[illegible]	< 5	204	30	66	2.79	0.69	11	16	< 1	1.5
[illegible]	< 5	133	27	59	1.96	0.50	10	< 1	1	1.0
HWWR037	37	329	72	9	2.38	0.68	10	9	< 1	1.5
HWWR038	41	430	49	9	1.97	0.58	10	9	< 1	0.9
HWWR042	18	289	62	22	2.44	0.70	8	23	< 1	1.0
HWWR043	12	524	49	12	2.23	0.62	7	16	< 1	0.7
HWWR041	48	666	46	14	2.42	0.67	10	11	< 1	1.1
HWWR049	19	437	69	12	2.54	0.67	9	18	< 1	1.0
HWWR048	17	233	30	13	2.54	0.68	10	13	< 1	0.5
HWWR047	50	651	76	10	2.47	0.65	10	18	1	1.4
HWWR046	6	640	51	11	2.44	0.66	10	13	1	1.2
HWWR045	8	669	51	10	1.78	0.54	10	16	< 1	0.9
HWWR088	15	481	72	74	2.32	0.68	11	23	1	2.4
HWWR087	14	309	49	78	2.11	0.57	10	12	< 1	1.6
HWWR086	12	274	47	75	2.26	0.61	10	15	< 1	1.4
HWWR085	11	341	70	59	2.40	0.67	11	14	1	1.9
HWWR084	12	424	51	50	2.00	0.55	10	10	< 1	1.3
HWWR081	6	418	31	33	2.31	0.61	10	19	< 1	0.8
HWWR113	23	296	39	40	1.85	0.51	10	13	< 1	0.9
HWWR107	11	790	43	20	2.34	0.68	12	16	1	1.0
[illegible]	9	258	67	63	1.87	0.48	17	19	1	2.0
[illegible]	< 5	173	48	91	2.10	0.67	14	12	1	1.8
[illegible]	69	179	68	22	1.81	0.72	13	29	< 1	1.0
HWWR055	14	371	49	97	2.42	0.66	13	13	1	2.2
HWWR056	10	310	34	98	2.35	0.61	12	10	1	1.4
HWWR057	< 5	296	36	95	2.48	0.68	13	10	1	1.4
[illegible]	< 5	198	32	97	1.83	0.50	18	14	1	1.0
[illegible]	86	254	45	11	1.73	0.48	13	18	< 1	1.3
[illegible]	11	201	65	83	2.08	0.56	11	22	1	2.7
[illegible]	< 5	229	45	91	1.58	0.47	18	24	1	1.5
HWWR059	34	404	71	55	2.35	0.71	11	20	1	2.4
HWWR060	58	223	32	83	1.91	0.50	9	16	1	1.2
HWWR058	12	437	64	53	2.53	0.68	11	17	1	2.1
[illegible]	9	363	56	96	2.51	0.66	13	10	1	1.7
[illegible]	12	383	66	12	2.06	0.74	9	13	< 1	1.1
[illegible]	17	598	62	14	2.14	0.61	10	13	< 1	1.2
HWWR083	55	523	68	9	2.26	0.62	11	16	< 1	1.2
HWWR082	8	750	49	8	2.11	0.57	10	15	1	1.2
HWWR080	10	1104	57	14	2.28	0.60	10	14	< 1	1.3
HWWR079	8	1100	40	11	2.05	0.56	9	14	< 1	0.8
HWWR078	18	874	43	14	2.13	0.57	10	10	< 1	0.9
HWWR077	17	945	49	17	2.05	0.54	8	13	< 1	1.2
HWWR076	12	677	48	16	2.32	0.63	10	14	1	1.0
HWWR110	14	877	47	13	2.15	0.65	9	9	< 1	0.9
HWWR109	10	965	58	11	2.07	0.68	10	9	< 1	1.1
HWWR108	20	1169	63	12	2.07	0.62	10	19	< 1	1.3
HWWR106	13	1243	50	11	1.82	0.53	10	11	< 1	1.0
HWWR105	18	1307	47	11	1.73	0.48	9	12	< 1	0.7
HWWR104	14	1522	48	11	1.97	0.71	9	11	< 1	0.9
HWWR103	18	1044	44	16	1.75	0.50	9	7	< 1	0.8
HWWR102	11	927	46	17	1.91	0.52	11	9	< 1	0.8
HWWR101	17	775	50	16	1.74	0.48	11	8	< 1	0.8
HWWR100	12	674	64	13	1.95	0.60	10	5	< 1	0.9
HWWR099	19	517	56	10	1.98	0.59	10	12	< 1	0.8
HWWR062	70	443	73	12	2.50	0.71	10	20	< 1	1.2
HWWR063	8	454	59	11	2.27	0.75	10	8	< 1	1.0
HWWR064	7	605	53	11	2.09	0.52	10	10	< 1	1.0
HWWR065	48	726	53	12	2.09	0.59	10	13	< 1	1.0
[illegible]	17	687	51	13	1.97	0.53	12	7	< 1	1.2
[illegible]	12	861	58	14	2.42	0.55	11	8	< 1	0.7
[illegible]	90	698	74	24	2.82	0.69	14	22	< 1	1.2
[illegible]	40	614	52	17	2.07	0.55	12	14	1	0.8
[illegible]	107	1001	67	29	2.45	0.67	15	23	< 1	1.3
[illegible]	31	1156	69	22	2.39	0.65	9	10	< 1	1.0
[illegible]	27	871	62	15	2.04	0.79	11	19	< 1	0.7
[illegible]	15	1104	47	21	1.90	0.51	12	12	< 1	0.8
[illegible]	12	922	61	12	1.94	0.56	11	16	< 1	0.7
[illegible]	15	942	63	14	2.30	0.65	11	14	< 1	0.9
HWWR074	10	1134	66	12	2.10	0.54	12	17	< 1	1.1
HWWR094	12	145	45	12	1.62	0.49	10	15	< 1	0.7
[illegible]	< 5	99	3	458	3.93	1.00	41	8	2	0.8
[illegible]	14	7	2	77	0.40	0.13	46	11	1	0.8

Table 1-F. Whole rock geochemistry of the Horne West succession

Analyte Symbol	Li	Ta	Hf	Nb	Zr	Y	Ge	La	Ce	Pr
Unit Symbol	ppm	ppm	ppm	ppm	ppm	ppm	ppm	ppm	ppm	ppm
Detection Limit	1	0.01	0.1	0.2	1	0.5	0.5	0.05	0.05	0.01
Analysis Method	TD-MS	FUS-MS	FUS-MS	FUS-MS	FUS-MS	FUS-MS	FUS-MS	FUS-MS	FUS-MS	FUS-MS
Sample #										
HWWR035	8	0.67	4.6	11.1	170	27.2	0.8	14.10	28.00	3.52
HWWR036	5	0.74	5.2	11.5	224	30.1	0.9	14.30	31.50	3.93
HWWR040	8	0.70	5.1	11.9	220	34.5	1.2	15.30	33.00	4.22
HWWR039	7	0.78	5.5	12.1	229	32.6	1.1	15.10	33.40	4.23
HWWR044	9	0.69	4.5	11.9	161	27.9	1.1	12.40	24.40	3.05
HWWR037	6	0.70	4.1	11.2	197	22.1	1.3	6.55	15.00	1.95
HWWR038	12	0.61	4.5	11.9	168	23.9	1.0	8.21	16.50	2.08
HWWR042	8	0.69	4.6	11.7	166	24.7	1.4	9.77	20.70	2.67
HWWR043	7	0.62	4.2	10.1	153	23.9	1.1	11.90	23.10	2.88
HWWR041	13	0.70	4.3	11.4	207	26.2	0.9	13.40	29.50	3.59
HWWR049	3	0.70	4.9	11.3	171	28.5	1.0	13.40	28.50	3.62
HWWR048	12	0.81	4.6	11.2	170	26.4	1.3	12.50	28.80	3.29
HWWR047	3	0.67	5.0	11.3	212	26.0	1.0	9.80	22.20	2.83
HWWR046	12	0.66	4.6	11.4	204	28.7	1.1	13.30	29.00	3.68
HWWR045	5	0.66	4.3	11.3	152	22.0	0.9	8.86	18.80	2.40
HWWR088	14	0.65	5.1	11.1	212	31.3	1.4	12.50	27.60	3.39
HWWR087	18	0.60	4.5	10.3	193	31.6	1.6	15.60	33.20	4.05
HWWR086	10	0.55	4.6	9.0	179	27.8	1.5	13.20	29.00	3.42
HWWR085	10	0.64	4.8	10.1	190	26.8	1.6	12.60	28.00	3.24
HWWR084	9	0.58	4.5	9.6	177	26.9	1.3	12.70	27.20	3.31
HWWR081	10	0.67	4.1	11.2	168	29.6	1.5	12.00	27.60	3.14
HWWR113	10	0.50	3.9	8.6	159	25.2	1.9	11.50	24.70	3.10
HWWR107	14	0.61	5.0	11.8	208	28.4	1.2	15.00	32.20	4.10
HWWR068	13	0.52	3.8	10.0	173	23.4	1.8	8.95	21.70	2.91
HWWR067	13	0.52	4.1	8.9	178	24.3	2.3	10.70	24.40	3.23
HWWR093	3	0.50	3.9	8.0	152	24.0	0.7	11.70	25.70	3.03
HWWR055	10	0.76	4.5	10.9	171	29.1	1.8	13.80	30.80	3.50
HWWR056	9	0.69	4.3	10.4	158	25.9	1.4	13.10	29.30	3.32
HWWR057	8	0.82	4.6	10.8	171	29.3	1.7	13.00	29.30	3.35
HWWR066	30	0.63	3.2	8.8	135	23.0	1.3	11.70	25.60	3.33
HWWR092	22	0.49	4.0	8.4	161	20.6	1.3	8.62	18.30	2.28
HWWR091	9	0.53	4.3	8.4	169	26.0	1.5	11.40	24.80	2.93
HWWR090	17	0.48	3.1	8.7	130	21.9	1.2	10.90	23.70	2.89
HWWR059	11	0.61	4.5	11.0	196	27.3	1.8	17.70	34.90	4.31
HWWR060	13	0.47	3.5	9.2	158	20.9	2.8	12.10	26.40	3.39
HWWR058	17	0.67	4.8	11.3	207	28.3	1.4	13.80	29.70	3.77
HWWR061	12	0.75	4.5	10.6	168	25.5	1.4	12.60	29.00	3.35
HWWR112	5	0.53	4.4	10.3	179	25.8	1.4	10.60	24.20	3.14
HWWR111	6	0.58	4.5	10.1	190	29.5	1.7	13.80	29.70	3.61
HWWR083	5	0.57	4.4	11.0	192	26.6	1.3	11.90	26.30	3.46
HWWR082	17	0.53	4.0	10.0	177	24.3	1.4	13.30	29.40	3.81
HWWR080	8	0.58	4.2	10.6	190	25.2	1.3	13.70	30.20	3.96
HWWR079	21	0.53	4.0	9.6	170	20.3	1.3	9.59	22.20	2.91
HWWR078	18	0.55	4.1	10.1	181	27.1	1.4	11.60	26.60	3.46
HWWR077	13	0.52	3.9	9.3	171	20.2	1.5	10.50	23.80	3.10
HWWR076	13	0.56	4.2	10.4	192	26.7	1.7	13.50	29.60	3.78
HWWR110	8	0.55	4.8	10.8	205	30.1	1.5	14.00	31.30	4.05
HWWR109	11	0.53	4.4	10.7	183	25.3	1.3	15.30	34.10	4.47
HWWR108	8	0.53	4.2	10.8	175	29.4	1.2	16.20	35.80	4.61
HWWR106	12	0.53	3.9	9.0	161	23.2	1.6	13.20	28.70	3.52
HWWR105	10	0.51	3.6	8.7	154	24.1	1.6	5.43	12.30	1.61
HWWR104	15	0.51	4.6	9.9	193	31.3	1.5	5.78	13.60	1.82
HWWR103	13	0.53	3.8	8.8	156	24.3	1.4	12.80	26.90	3.35
HWWR102	12	0.53	4.0	9.5	169	22.1	1.5	9.27	20.00	2.49
HWWR101	15	0.49	3.7	9.0	157	24.1	1.7	13.60	29.20	3.61
HWWR100	12	0.53	4.1	10.1	174	25.1	1.9	11.60	25.90	3.34
HWWR099	9	0.52	4.1	10.3	175	25.6	1.8	9.22	20.30	2.71
HWWR062	4	0.71	4.9	11.0	177	28.8	1.4	15.10	29.80	3.71
HWWR063	9	0.56	4.3	10.3	183	27.9	1.2	12.70	28.40	3.72
HWWR064	6	0.53	3.9	9.9	172	25.8	1.3	10.40	23.60	3.05
HWWR065	12	0.60	4.1	9.9	196	23.0	1.5	12.50	28.00	3.49
HWWR075	23	0.61	3.9	10.3	156	23.7	3.3	13.40	31.00	3.54
HWWR073	9	0.64	4.1	10.7	165	27.5	1.2	9.73	22.60	2.54
HWWR072	9	0.73	4.9	12.3	227	30.7	1.1	17.80	38.40	4.69
HWWR071	14	0.64	4.0	10.8	155	26.8	1.2	16.20	37.10	4.09
HWWR070	9	0.64	4.9	12.0	214	40.5	<0.5	17.10	36.90	4.81
HWWR069	8	0.75	4.4	10.7	197	30.3	1.0	10.30	25.60	3.32
HWWR098	11	0.57	4.5	11.0	196	28.6	1.7	11.90	28.00	3.61
HWWR097	10	0.55	4.9	9.8	175	25.0	1.2	9.80	19.40	2.40
HWWR096	7	0.51	4.8	8.4	168	24.1	0.8	12.50	27.90	3.28
HWWR095	8	0.57	4.2	8.6	150	25.4	0.9	10.10	22.10	2.64
HWWR074	8	0.54	4.4	10.4	189	21.3	1.0	9.06	20.40	2.67
HWWR094	9	0.45	3.5	7.3	135	27.1	0.6	7.98	17.10	2.03
HWWR089	22	0.23	2.5	4.5	97	32.0	2.6	22.90	47.60	5.96
HWWR114	24	0.22	2.0	4.5	76	24.3	3.3	5.54	14.60	2.09

Table 1-G. Whole rock geochemistry of the Horne West succession

Analyte Symbol	Nd	Sm	Eu	Gd	Tb	Dy	Ho	Er	Tm	Yb
Unit Symbol	ppm	ppm	ppm	ppm	ppm	ppm	ppm	ppm	ppm	ppm
Detection Limit	0.05	0.01	0.005	0.01	0.01	0.01	0.01	0.01	0.005	0.01
Analysis Method	FUS-MS	FUS-MS	FUS-MS	FUS-MS	FUS-MS	FUS-MS	FUS-MS	FUS-MS	FUS-MS	FUS-MS
Sample #										
HWWR035	15.00	3.56	0.822	3.79	0.69	4.54	0.98	3.02	0.476	3.21
HWWR034	16.70	3.99	0.849	3.86	0.77	5.01	1.04	3.22	0.518	3.457
HWWR033	17.90	4.34	0.950	4.42	0.86	5.57	1.12	3.42	0.517	3.60
HWWR040	18.00	4.37	0.961	4.46	0.89	5.58	1.14	3.41	0.536	3.66
HWWR044	12.90	3.49	0.875	3.39	0.69	3.99	0.90	2.91	0.526	3.27
HWWR037	8.99	2.44	0.662	2.85	0.55	3.69	0.82	2.65	0.422	2.90
HWWR038	8.77	2.30	0.519	2.42	0.49	3.36	0.77	2.54	0.420	2.92
HWWR042	11.70	2.86	0.770	3.14	0.60	4.00	0.89	2.83	0.460	3.20
HWWR043	12.40	3.15	0.834	3.28	0.61	4.04	0.87	2.75	0.433	2.95
HWWR041	15.30	3.71	1.010	3.97	0.65	4.12	0.91	2.85	0.453	3.09
HWWR049	15.40	3.73	0.570	3.76	0.70	4.59	0.97	3.06	0.483	3.32
HWWR048	14.50	3.81	1.580	4.00	0.66	4.18	0.93	2.95	0.480	3.26
HWWR047	12.10	2.99	1.010	3.33	0.61	4.04	0.89	2.82	0.449	3.13
HWWR046	15.30	3.82	0.700	3.87	0.70	4.56	0.96	2.96	0.470	3.26
HWWR045	10.00	2.46	0.910	2.46	0.46	3.21	0.73	2.38	0.387	2.63
HWWR088	14.70	3.56	0.986	3.29	0.65	4.50	1.01	3.31	0.535	3.58
HWWR087	17.30	4.10	1.090	3.94	0.76	4.83	1.00	3.09	0.508	3.42
HWWR086	14.90	3.77	1.020	4.03	0.73	4.54	0.96	2.96	0.470	3.08
HWWR085	14.20	3.62	1.170	3.68	0.68	4.37	0.93	2.95	0.482	3.18
HWWR084	14.40	3.35	0.939	3.26	0.62	3.89	0.84	2.69	0.436	2.97
HWWR081	13.10	3.36	1.370	4.24	0.79	4.93	1.03	3.22	0.517	3.46
HWWR113	13.90	3.79	1.720	3.28	0.60	3.91	0.83	2.65	0.434	2.81
HWWR107	16.50	3.97	1.190	4.09	0.75	4.81	1.03	3.23	0.514	3.49
HWWR068	12.20	3.18	1.640	3.26	0.63	4.06	0.84	2.63	0.432	2.95
HWWR067	13.60	3.33	1.090	3.53	0.65	4.08	0.84	2.56	0.408	2.79
HWWR093	13.40	3.38	2.520	3.52	0.64	4.08	0.85	2.65	0.414	2.72
HWWR055	16.80	3.89	1.030	4.26	0.80	4.24	0.99	3.06	0.562	3.18
HWWR056	13.90	3.60	0.994	3.84	0.70	4.42	0.94	2.85	0.459	3.09
HWWR057	14.70	3.87	0.864	4.27	0.78	4.94	1.03	3.16	0.501	3.37
HWWR065	13.70	3.26	0.989	3.67	0.62	3.74	0.77	2.38	0.366	2.40
HWWR092	9.56	2.35	1.320	2.29	0.44	2.99	0.69	2.30	0.383	2.65
HWWR091	12.50	3.10	3.990	3.44	0.63	4.04	0.88	2.79	0.450	2.95
HWWR090	11.90	2.90	0.875	2.76	0.52	3.28	0.69	2.11	0.335	2.21
HWWR059	17.90	4.30	1.100	4.09	0.76	4.74	0.94	2.77	0.430	2.84
HWWR060	14.20	3.46	0.929	3.39	0.62	3.85	0.77	2.29	0.353	2.36
HWWR058	15.70	3.73	0.863	3.94	0.77	4.84	0.95	2.90	0.448	3.05
HWWR061	15.60	3.65	0.849	3.74	0.71	3.82	0.89	2.79	0.536	2.98
HWWR112	12.80	3.17	1.190	3.18	0.65	4.23	0.86	2.64	0.419	2.84
HWWR111	15.30	3.71	0.821	3.60	0.70	4.50	0.95	3.00	0.474	3.17
HWWR083	14.60	3.51	0.980	3.63	0.71	4.50	0.92	2.83	0.453	2.96
HWWR082	16.50	4.06	0.836	4.07	0.70	4.21	0.83	2.53	0.397	2.75
HWWR080	16.80	4.10	0.900	3.92	0.70	4.27	0.86	2.66	0.427	2.94
HWWR079	12.00	2.88	0.610	2.86	0.55	3.54	0.74	2.32	0.370	2.58
HWWR078	14.50	3.64	0.602	4.06	0.78	4.82	0.94	2.75	0.436	2.92
HWWR077	12.90	3.13	0.553	3.11	0.58	3.63	0.74	2.26	0.357	2.42
HWWR076	15.70	3.82	0.837	3.98	0.76	4.61	0.91	2.71	0.441	2.87
HWWR110	16.40	4.09	0.985	4.50	0.83	5.12	0.98	2.88	0.452	2.99
HWWR109	18.10	4.51	0.990	4.77	0.77	4.38	0.86	2.66	0.423	2.78
HWWR108	18.00	4.08	0.884	4.40	0.84	5.31	1.06	3.09	0.459	2.99
HWWR106	15.00	3.73	0.660	3.56	0.64	3.81	0.77	2.48	0.412	2.78
HWWR105	7.16	1.91	0.286	2.14	0.46	3.20	0.72	2.34	0.375	2.54
HWWR104	7.76	2.00	0.326	3.16	0.71	5.01	1.08	3.32	0.499	3.13
HWWR103	13.90	3.32	0.460	3.29	0.59	3.63	0.76	2.50	0.406	2.69
HWWR102	10.80	2.63	0.403	2.50	0.46	3.02	0.67	2.25	0.396	2.72
HWWR101	15.10	3.58	0.666	3.39	0.57	3.52	0.74	2.38	0.387	2.61
HWWR100	13.50	3.44	0.754	3.62	0.67	4.17	0.83	2.50	0.396	2.67
HWWR099	10.80	2.69	0.824	3.00	0.59	3.84	0.82	2.62	0.419	2.74
HWWR062	15.50	3.84	0.723	4.05	0.75	4.84	1.00	3.04	0.471	3.11
HWWR063	15.60	3.72	0.783	3.98	0.74	4.62	0.96	2.93	0.452	2.95
HWWR064	12.90	3.13	0.706	3.38	0.67	4.21	0.86	2.71	0.423	2.83
HWWR065	15.10	3.79	0.695	3.79	0.63	3.85	0.81	2.50	0.391	2.68
HWWR075	14.80	3.59	0.621	4.25	0.75	4.46	0.87	2.67	0.434	2.85
HWWR073	11.00	2.83	1.170	3.86	0.74	4.67	0.95	2.93	0.464	3.14
HWWR072	20.00	4.95	2.500	5.24	0.89	5.42	1.12	3.41	0.523	3.45
HWWR071	17.50	4.33	1.610	5.04	0.86	5.07	1.01	3.09	0.489	3.44
HWWR070	20.50	4.94	0.859	5.38	0.98	6.12	1.27	4.00	0.751	4.05
HWWR069	13.70	3.46	1.240	3.73	0.68	4.30	0.94	3.01	0.479	3.22
HWWR066	14.70	3.69	0.680	3.97	0.69	4.47	0.95	2.95	0.468	3.03
HWWR095	10.10	2.57	0.704	2.74	0.53	3.38	0.81	2.69	0.446	3.00
HWWR096	14.20	3.61	1.440	3.83	0.66	4.16	0.87	2.69	0.428	2.84
HWWR094	11.60	3.02	0.881	3.14	0.62	4.00	0.90	2.72	0.429	2.76
HWWR074	11.40	2.74	0.567	2.78	0.54	3.58	0.80	2.60	0.443	3.18
HWWR094	8.93	2.34	0.899	2.89	0.56	3.81	0.85	2.71	0.431	2.81
HWWR089	24.10	5.86	1.510	4.99	0.82	4.87	1.01	3.11	0.490	3.23
HWWR114	9.91	2.90	1.400	3.50	0.72	4.55	0.86	2.54	0.387	2.48

Table 1-H. Whole rock geochemistry of the Horne West succession

Analyte Symbol	Lu	CCPI	AI	Na2O/K2O	Zr/TiO2	Zr/Y	Y/TiO2	Nb/Y
Unit Symbol	ppm							
Detection Limit	0.002							
Analysis Method	FUS-MS							
Sample #			·					
HWWR035	0.549	46.44	16.56	6.51	582.19	6.25	93.15	0.41
HWWR036	0.575	37.14	16.40	5.00	797.15	7.44	107.12	0.38
HWWR039	0.593	45.73	17.28	5.06	766.55	6.98	120.21	0.34
HWWR040	0.592	43.72	19.34	5.26	745.93	7.02	106.19	0.37
HWWR044	0.524	38.77	16.32	6.03	551.35	5.77	92.08	0.43
HWWR037	0.463	64.97	94.17	0.04	602.45	8.91	67.58	0.51
HWWR038	0.477	76.96	93.43	0.05	509.09	7.03	72.42	0.50
HWWR042	0.526	70.22	86.51	0.13	489.68	6.72	72.86	0.47
HWWR043	0.493	74.80	90.93	0.09	560.44	6.40	87.55	0.42
HWWR041	0.501	76.60	90.98	0.09	678.69	7.90	85.90	0.44
HWWR049	0.543	67.02	91.73	0.07	571.91	6.00	95.32	0.40
HWWR048	0.538	64.36	44.42	2.20	526.32	6.44	81.73	0.42
HWWR047	0.529	59.66	89.39	0.07	629.08	8.15	77.15	0.43
HWWR046	0.521	80.10	88.97	0.11	576.27	7.11	81.07	0.40
HWWR045	0.412	71.16	90.89	0.08	438.04	6.91	63.40	0.51
HWWR088	0.540	61.59	51.48	0.85	552.08	6.77	81.51	0.35
HWWR087	0.512	65.55	36.99	0.99	524.46	6.11	85.87	0.33
HWWR086	0.463	62.17	32.54	1.10	495.84	6.44	77.01	0.32
HWWR085	0.488	61.32	40.11	0.46	492.23	7.09	69.43	0.38
HWWR084	0.447	64.97	42.74	1.02	435.96	6.58	66.26	0.36
HWWR081	0.510	63.14	41.94	2.11	491.23	5.68	86.55	0.38
HWWR113	0.414	67.37	42.46	1.09	459.54	6.31	72.83	0.34
HWWR107	0.550	72.23	64.33	0.71	512.32	7.32	69.95	0.42
HWWR068	0.450	71.34	41.71	0.53	266.98	7.39	36.11	0.43
HWWR067	0.446	70.59	28.69	0.94	364.75	7.33	49.80	0.37
HWWR093	0.433	59.03	86.07	0.12	324.09	6.33	51.17	0.33
HWWR055	0.518	60.88	27.67	2.30	406.18	5.88	69.12	0.37
HWWR056	0.504	54.29	22.06	4.55	378.90	6.10	62.11	0.40
HWWR057	0.543	52.59	25.86	4.00	409.09	5.84	70.10	0.37
HWWR066	0.375	81.06	38.68	1.24	198.24	5.87	33.77	0.38
HWWR092	0.431	84.59	87.21	0.07	346.24	7.82	44.30	0.41
HWWR091	0.438	48.65	32.13	0.42	419.35	6.50	64.52	0.32
HWWR090	0.399	71.64	39.78	1.35	209.68	5.94	35.32	0.40
HWWR059	0.452	81.16	64.26	0.30	507.77	7.18	70.73	0.40
HWWR060	0.386	83.55	33.57	1.54	445.07	7.56	58.87	0.44
HWWR058	0.501	73.05	57.71	0.66	507.35	7.31	69.36	0.40
HWWR061	0.489	66.22	37.52	0.89	368.42	6.59	55.92	0.42
HWWR112	0.456	81.07	90.30	0.07	523.39	6.94	75.44	0.40
HWWR111	0.475	73.55	90.84	0.06	502.65	6.44	78.04	0.34
HWWR083	0.457	75.36	90.51	0.09	471.74	7.22	65.36	0.41
HWWR082	0.445	85.26	89.34	0.10	452.69	7.28	62.15	0.41
HWWR080	0.463	83.44	86.54	0.11	472.64	7.54	62.69	0.42
HWWR079	0.415	86.00	92.26	0.12	437.02	8.37	52.19	0.47
HWWR078	0.456	88.18	92.03	0.09	455.92	6.68	68.26	0.37
HWWR077	0.383	84.49	86.46	0.12	487.18	8.47	57.55	0.46
HWWR076	0.460	84.41	89.29	0.11	484.85	7.19	67.42	0.39
HWWR110	0.496	84.62	91.27	0.07	585.71	6.81	86.00	0.36
HWWR109	0.442	82.64	92.82	0.06	475.32	7.23	65.71	0.42
HWWR108	0.462	81.63	88.84	0.06	456.92	5.95	76.76	0.37
HWWR106	0.421	81.89	93.97	0.05	410.71	6.94	59.18	0.39
HWWR105	0.392	85.08	92.70	0.08	402.09	6.39	62.92	0.36
HWWR104	0.473	85.37	90.22	0.13	523.04	6.17	84.82	0.32
HWWR103	0.388	83.28	93.52	0.06	425.07	6.42	66.21	0.36
HWWR102	0.403	83.21	94.08	0.06	418.32	7.65	54.70	0.43
HWWR101	0.393	84.32	93.16	0.08	380.15	6.51	58.35	0.37
HWWR100	0.436	83.08	92.63	0.07	439.39	6.93	63.38	0.40
HWWR099	0.435	84.18	92.89	0.07	464.19	6.84	67.90	0.40
HWWR062	0.510	76.54	88.89	0.07	451.53	6.15	73.47	0.38
HWWR063	0.474	79.17	85.95	0.13	458.65	6.56	69.92	0.37
HWWR064	0.456	81.22	89.16	0.10	426.80	6.67	64.02	0.38
HWWR065	0.448	76.30	94.20	0.05	478.05	8.52	56.10	0.43
HWWR075	0.409	82.16	93.13	0.06	376.81	6.58	57.25	0.43
HWWR073	0.487	75.36	90.46	0.08	404.41	6.00	67.40	0.39
HWWR072	0.557	67.59	84.05	0.08	496.72	7.39	67.18	0.40
HWWR071	0.500	75.33	87.76	0.08	409.41	6.16	66.50	0.40
HWWR070	0.502	67.50	89.81	0.08	459.87	5.23	87.85	0.30
HWWR069	[illegible]	60.24	83.50	0.40	556.52	6.78	82.03	0.36
HWWR098	0.529	81.65	88.24	0.19	[illegible]	6.89	71.28	0.39
HWWR097	0.474	70.99	64.95	0.84	440.81	7.00	62.97	0.39
HWWR096	0.451	68.56	88.16	0.09	485.79	7.80	62.27	0.35
HWWR095	0.450	81.24	88.11	0.11	441.99	6.30	70.17	0.34
HWWR074	0.528	79.36	87.75	0.10	452.15	8.87	50.96	0.49
HWWR094	0.426	89.06	86.59	0.12	421.88	4.98	84.69	0.27
HWWR089	0.477	88.04	43.11	14.53	191.61	3.08	43.42	0.14
HWWR114	0.369	99.69	40.57	5.00	69.47	3.13	22.21	0.19

Table 1 Footnote

*Least altered rhyolite

HWWS = (Horne West Whole Rock)

CCPI = 100 (Fe2O3(Total) + MgO)/(MgO + K2O + FeO + Na2O)
AI = 100 (K2O + MgO)/(MgO + K2O + CaO + Na2O)

Facies

Rhy2 =	Aphyric coherent rhyolite (top of succession)
XRhy =	Xenolith-bearing rhyolite
XRhy (Base) =	Xenolith-bearing rhyolite (base of succession)
AmygBr (top) =	Amygdular clast bearing breccia (top of succession)
AmygBr (Base) =	Amygdular clast bearing breccia (base of succession)
QRhyBr =	Quartz phyric rhyolite clast breccia
LBr =	Lithic clast dominated breccia and sandstone
WcBr =	Wispy clast-rich breccia
Rhy1 (Base) =	Aphyric coherent rhyolite (base of succession)
CrBr =	Clast-rotated monomictic breccia
Mafic intrusive =	Mafic intrusive

Analysis performed by Actlabs
Analytical Methods:

INAA =	Instrumental neutron activation anaysis
FUS-ICP =	Fusion followed by ICP-ES
IR =	Infrared
COUL =	Coulometry
FA-AA =	Fire assay followed by atomic absorption spectrometry
FUS-MS =	Fusion followed by ICP-MS
TD-MS =	Four-acid digestion followed by ICP-MS
FIMS =	Cold vapor atomic absrption spectrometry
NP-MS=	Nitric acid and peroxide digestion followed by ICP-MS

Table 2. Selected geochemical data from the vicinity of the Horne mine

	Least altered rhyolite				Altered rhyolite						
Location	Horne	Horne	Quemont	Horne West	Horne	Horne	Horne	Horne	Horne	Horne	Horne
Sample no.	N9747	N87-22	N87-11	HWWR044	N87-17	N87-18	N87-19	N87-25	N87-28	N87-37	N422-150
Alteration	Fresh	Fresh	Fresh	Fresh	Qtz-Ser	Qtz-Ser	Qtz-Ser	Qtz-Ser	Qtz-Ser	Chl	Chl
Level	27	65	27	S-572, 151 m	9	49	49	65	15	2	6
Al	26.42	48.69	34.30	16.32	88.78	41.44	46.68	35.50	99.37	84.85	96.50
CCPI	59.03	71.99	64.94	38.77	52.59	80.59	76.73	69.03	86.60	72.99	94.63
Na_2O/K_2O	5.00	62.67	9.68	6.03	0.15	0.74	1.33	1.06	0.00	0.17	0.00
Zr/Tio2	1026.67	313.21	987.50	531.35	860.00	674.07	486.11	391.67	715.38	548.39	394.59
Zr/Y	5.70	2.91	5.39	5.77	7.82	7.28	7.00	6.48	5.47	8.50	9.13
Y/TiO_2	180.00	107.55	183.33	92.08	110.00	92.59	69.44	60.42	130.77	64.52	43.24
Nb/Y	0.22	0.26	0.59	0.43	0.73	0.52	0.52	0.52	0.50	0.60	0.56
SiO_2	79.30	61.33	76.59	72.70	80.17	75.58	70.46	70.10	75.09	75.56	31.42
TiO_2	0.15	0.53	0.24	0.303	0.20	0.27	0.36	0.48	0.26	0.31	0.74
Al_2O_3	10.15	16.81	11.25	12.50	12.47	13.14	13.08	14.17	11.05	11.05	26.80
$Fe_2O_3(T)$	4.83	8.87	5.88	2.74	3.21	5.46	9.53	5.28	8.77	9.10	27.85
MnO	0.08	0.15	0.11	0.201	0.01	0.48	0.34	0.05	0.03	0.00	0.18
MgO	0.79	5.86	1.64	0.73	0.54	1.06	1.45	1.92	2.93	0.36	10.25
CaO	0.76	0.63	0.19	3.04	0.00	2.10	1.39	4.68	0.03	0.10	0.45
Na_2O	3.25	5.64	3.68	4.70	0.44	0.67	1.90	1.66	0.00	0.50	0.00
K_2O	0.65	0.09	0.38	0.78	2.94	0.90	1.43	1.57	1.81	3.00	2.16
P_2O_5	0.02	0.08	0.03	0.05	0.02	0.04	0.06	0.09	0.03	0.03	0.16
Rb	16	5	8	27	Nd	Nd	Nd	Nd	Nd	Nd	53
Sr	51	31	24	59	26	37	53	97	15	24	21
Zr	154	166	237	161	172	182	175	188	186	170	292
Nb	6	15	26	11.9	16	13	13	15	17	12	18
Y	27	57	44	27.9	22	25	25	29	34	20	32

Modified from MacLean and Hoy (1991)

Table 3. Correlation between gold and other elements by sample at Horne West (n=75)

Raw Data		All metals normalized to sulfur (including gold)	
	Au	Metals	Au
K2O	0.424	In	0.281
S	0.380	Cd	0.163
Rb	0.342	Ag	0.102
Fe2O3(T)	0.288	Zn	0.061
In	0.286	Co	0.029
Cd	0.252	Ni	0.018
Zn	0.225	Fe2O3(T)	0.015
Ga	0.188	Ge	0.011
Sn	0.152	Bi	0.004
Hg	0.150	Cr	0.000
Cu	0.145	Sn	-0.003
Zr	0.118	Pb	-0.007
As	0.084	Ga	-0.014
Ag	0.081	Hg	-0.030
Lu	0.070	As	-0.057
Hf	0.064	Cu	-0.069
Ba	0.064	V	-0.073
B	0.061	Mo	-0.093
Nb	0.042	W	-0.097
Er	0.036	Sb	-0.158
Y	0.033	Tl	-0.226
Yb	0.027		
Ho	0.014		
U	0.009		
Tm	-0.012		
Ta	-0.017		
Dy	-0.017		
Th	-0.021		
Tl	-0.033		
SiO2	-0.037		
P2O5	-0.052		
Pr	-0.073		
La	-0.076		
W	-0.079		
Tb	-0.081		
Nd	-0.085		
Sm	-0.090		
Sb	-0.099		
Ce	-0.099		
Bi	-0.104		
Ni	-0.108		
Gd	-0.110		
Co	-0.115		
TiO2	-0.137		
Pb	-0.140		
Cs	-0.141		
Sc	-0.144		
Al2O3	-0.145		
Ge	-0.155		
V	-0.163		
Eu	-0.177		
MnO	-0.213		
Mo	-0.227		
Sr	-0.256		
Be	-0.258		
CO2	-0.289		
MgO	-0.301		
Cr	-0.321		
Li	-0.339		
CaO	-0.341		
Na2O	-0.359		

P=0.05 CriticalR=0.232 for a two tailed test

Table 4. Trace element ratios for Horne West lithofacies

	Rhy2*	XRhy	XRhy (Base)	AmygBr (top)	AmygBr (Base)	QRhyBr	LBr	WcBr	Rhy1 (Base)	CrBr	Mafic int
CCPI	42.36	68.01	66.99	55.92	71.48	79.26	73.61	83.02	73.06	84.21	93.87
σ	4.18	6.09	6.90	4.38	16.18	5.50	7.42	3.02	7.34	6.86	8.24
Al	17.18	67.44	52.16	25.20	49.45	51.85	72.88	90.94	85.77	87.17	41.84
σ	1.27	24.87	30.08	2.87	25.40	16.16	30.63	2.58	7.83	0.81	1.80
Na_2O/K_2O	5.17	0.63	0.53	3.62	0.77	0.83	0.34	0.09	0.17	0.11	9.77
σ	1.25	0.41	0.41	1.17	0.62	0.64	0.47	0.03	0.24	0.02	6.74
Zr/TiO_2	456.35	530.31	318.61	398.05	293.38	486.73	464.82	457.18	456.35	437.01	100.54
σ	53.16	64.75	49.12	16.65	107.58	36.08	84.13	43.18	53.16	21.41	43.94
Zr/Y	6.57	6.88	7.02	5.94	6.53	7.35	6.66	7.02	6.61	6.93	3.08
σ	0.66	0.80	0.59	0.14	0.90	0.19	0.26	0.73	0.73	2.75	0.07
Y/TiO_2	103.75	77.47	45.69	67.11	44.48	66.32	69.80	65.69	69.49	67.82	32.82
σ	11.58	8.75	8.33	4.36	14.14	6.49	12.09	8.70	9.20	23.85	15.00
Nb/Y	0.39	0.41	0.38	0.38	0.38	0.41	0.41	0.40	0.37	0.38	0.16
σ	0.03	0.06	0.05	0.02	0.04	0.02	0.04	0.04	0.04	0.15	0.03

CCPI = 100 $(Fe_2O_3(Total) + MgO)/(MgO + K_2O + FeO + Na_2O)$

Al = 100 $(K_2O + MgO)/(MgO + K_2O + CaO + Na_2O)$

Facies

Rhy2 =	Aphyric coherent rhyolite (top of succession)
XRhy =	Xenolith-bearing rhyolite
XRhy (Base) =	Xenolith-bearing rhyolite (base of succession)
AmygBr (top) =	Amygdular clast bearing breccia (top of succession)
AmygBr (Base) =	Amygdular clast bearing breccia (base of succession)
QRhyBr =	Quartz phyric rhyolite clast breccia
LBr =	Lithic clast dominated breccia and sandstone
WcBr =	Wispy clast-rich breccia
Rhy1 (Base) =	Aphyric coherent rhyolite (base of succession)
CrBr =	Clast-rotated monomictic breccia
Mafic int =	Mafic intrusive

References

Allen R.L., Lundsrtom I., Ripa, M., Simeonov, A., and Christofferson, H., 1996. Facies analysis of a 1.9 Ga, continental margin, back-arc, felsic caldera province with diverse Zn-Pb-Ag-(Cu-Au) sulfide and Fe-oxide deposits, Bergslagen region, Sweden: Economic Geology, v. 91, p. 979-1008.

Baragar, W.R.A., 1968. Major element geochemistry and the Noranda volcanic belt, Quebec-Ontario: Canadian Journal of Earth Sciences, v. 5, p. 773-790.

Barrett, T. J., Cattalani, S., and Maclean, W. H., 1991. Massive sulfide deposits of the Noranda area, Quebec. I: The Horne Mine.Canadian Journal of Earth Sciences, v. 28, p. 465-488.

Barrett, T.J., MacLean, W.H., and Tennant, S.C., 2001. Volcanic sequence and alteration at the Parys Mountain volcanic-hosted massive sulfide deposit, Wales, United Kingdom: Application of immobile element lithogeochemistry: Economic Geology, v. 96, p. 1279-1305.

Barrie, T.C., Ludden, J.N., and Green, T.H., 1993. Geochemistry of volcanic rocks associated with Cu-Zn and Ni-Cu deposits in the Abitibi Subprovince: Economic Geology, v. 88, p. 1341-1358.

Binney, W.P., 1987. A sedimentological investigation of MacLean channel transported sulphide ores, in Kirkham, R.V., ed., Buchans Geology, Newfoundland: Geological survey of Canada, Paper 86-24, p. 107-147, Report 8.

Cattalani, S., Barrett, T.J., MacLean, W.H., Hoy, L., Hubert, C., and Fox, J.F., 1993. Métallogènèse des gisements Horne et Quemont : Ministère de l'Énergie et des Resources du Québec : Report ET 90-07, p.1-121.

Cooke, H.C., 1928. Ore relations at the Horne and Aldermac mines, Quebec: Canadian Mining and Metallurgical Bulletin, v.198, no.31, p. 1184-1194.

de Rosen-Spence A.F., 1976. Stratigraphy, development, and petrogenesis of the central Noranda volcanic pile, Noranda, Quebec: Ph.D. thesis, University of Toronto, Toronto, Ontario, 166 p.

Dimroth, E., Imreh, L., Goulet, N., and Rocheleau, M., 1982. Evolution of the south-central segment of the Archean Abitibi Belt, Quebec. Part I: Stratigraphy and paleogeographic model: Canadian Journal of Earth Sciences, v. 19, p. 1729-1758.

Dimroth, E., Imreh, L., Goulet, N., and Rocheleau, M., 1983a. Evolution of the south-central segment of the Archean Abitibi Belt, Quebec. Part II: tectonic evolution and geomechanical model: Canadian Journal of Earth Sciences, v. 20, p. 1355-1373.

Dimroth, E., Imreh, L., Goulet, N., and Rocheleau, M., 1983b. Evolution of the south-central segment of the Archean Abitibi Belt, Quebec. Part III: Plutonic and metamorphic evolution and geotectonic model: Canadian Journal of Earth Sciences, v. 20, p. 1374-1388.

Doyle, G.M., and Allen R.L., 2003. Subsea-floor replacement in volcanic-hosted massive sulfide deposits: Ore Geology Reviews, v. 23, p. 183-222.

Dubé, B., Mercier-Langevin, P., Hannington, M.D., Lafrance, B., Gosselin, P., and Gosselin, G., 2007. The LaRonde Penna world-class Au-rich volcanogenic massive sulfide deposit, Abitibi, Québec: Mineralogy and geochemistry of alteration and implications for genesis and exploration: Economic Geology, v. 102, p. 633-666.

Fournier, R.O., 1998. Hydrothermal processes related to movement of fluid from plastic into brittle rock in the magmatic environment: Economic Geology, v. 94, p. 1193-1211.

Franklin K.M., Lydon, J.W., and Sangster, D.F., 1981. Volcanic-associated massive sulfide deposits: Economic Geology, 75th Anniversary Volume, p-485-627.

Gibson, H.L., Kerr, D.J., and Cattalani, S., 2000. The Horne Mine: geology, history, influence on genetic models, and a comparison to the Kidd Creek Mine: Exploration and Mining Geology, v.9, p. 91-111.

Gibson, H.L., and Galley, A.G., 2007. Volcanogenic massive sulfide deposits of the Archean, Noranda District, Quebec, in W.D. Goodfellow, ed., Mineral Deposits of Canada: a Synthesis of Major Deposit-types, District Metallogeny, The Evolution of Geological Provinces and Exploration Methods: Geological Association of Canada, Mineral Deposit division, Special Publication 5, p. 553-552.

Gibson, H.L. and Watkinson, D.H., 1990. Volcanogenic massive sulfide deposits of the Noranda Cauldron and Shield Volcano, Quebec, in The Northwestern Quebec Polymetallic Belt, (ed.) M. Rive, P. Verpaelst, Y. Gagnon, J.M., Lulin, G., Riverin, and A. Simard: The Canadian Institute of Mining and Metallurgy, Special Volume 43. p. 199-132.

Goodwin, A.M., 1982. Archean volcanoes in southwestern Abitibi Belt, Ontario and Quebec: form, composition, and development: Canadian Journal of Earth Sciences, v. 19, p. 1140-1155.

Gorton, M.P., and Schandl, E.S., 2000. From continents to island arcs; a geochemical index of tectonic setting for arc-related and within-plate felsic to intermediate volcanic rocks: The Canadian Mineralogist, v. 38, p. 1065-1073.

Hannington, M.D., 2004. Spectrum of gold-rich VMS deposits from the archaean to the present, in, Cooke, D.R., Deyell, C., Pongratz, J., eds., 24th Au Workshop, CODES special publication 5, University of Tasmania.

Hannington, M.D., Poulsen, K.H., Thompson, J.F.H., and Sillitoe, R.H., 1999. Volcanogenic gold in the massive sulfide environment: Reviews in Economic Geology, v. 8, p. 325-356.

Hart, T.R., Gibson, H.L., and Lesher, M.C., 2004. Trace element geochemistry and petrogenesis of felsic volcanic rocks associated with volcanogenic massive Cu-Zn-Pb sulfide deposits: Economic Geology, v. 99, p. 1003-1013.

Harrell, J., 1984, A visual comparator for the degree of sorting in thin and plane sections: Journal of Sedimentary Petrology, v.54, no.2, p.646-650.

Huston, D., and Large, R., 1989. A chemical model for the concentration of gold in volcanogenic massive sulphide deposits: Ore Geology Reviews, v. 4, p. 171-200.

Irvine, N.T., and Baragar, W.R.A., 1971. A guide to chemical classification of the common volcanic rocks: Canadian Journal of Earth Sciences, v. 8, p. 523-548.

Ishikawa, Y., Sawaguchi, T., Iwaya, S., and Horiuchi, M., 1976. Delineation of prospecting targets for Kuroko deposits based on modes of volcanism of underlying dacite and alteration halos: Mining Geology, v. 26, p. 105-117, (Japanese with English subtitles).

Kerr, D.J., and Gibson, H.L., 1993. A comparison of the Horne volcanogenic massive sulfide deposit and intracauldron deposits of the Mine Sequence, Noranda, Quebec: Economic Geology, v. 88, p. 1419-1442.

Kerr, D.L., and Mason, R., 1990. A re-appraisal of the geology and ore deposits of the Horne Mine complex at Rouyn-Noranda, Quebec, in M. Rive, P. Verpaelst, Y. Gagnon, J.M., Lulin, G., Riverin, and A. Simard, eds., The Northwestern Quebec Polymetallic Belt: The Canadian Institute of Mining and Metallurgy, Special Volume 43, p. 153-165.

Large, R.R., Gemmel, J. B., Holguer, P., and Huston, D.L., 2001. The alteration box plot: A simple approach to understanding the relationship between alteration mineralogy and lithogeochemistry associated with volcanic-hosted massive sulfide deposits: Economic Geology, v. 96, p. 957-971.

Larocque, A.C.L., Hodgson, C.J., and Lafleur, P., 1993. Gold distribution in the Mobrun volcanic-associated massive sulfide deposit, Noranda, Quebec: A preliminary evaluation of the role of metamorphic remobilization: Economic Geology, v. 88, p.1443-1459.

Lesher, C.M., Goodwin, A.M., Campbell, I.H., and Gorton, M.P., 1986. Trace-element geochemistry of ore-associated and barren, felsic metavolcanic rocks in the Superior province, Canada: Canadian Journal of Earth Sciences, v.23, p.222-237.

Lichtblau, A.P., and Dimroth, E., 1980. Stratigraphy and facies at the south margin of the Archean Noranda caldera, Noranda, Quebec: in Current Research, Part A; Geological Survey of Canada, Paper 80-1A, p. 69-76.

Lowe, D.R., 1982. Sedimentary Gravity flows: II. Depositional models with special reference to the deposits of high-density tubidity currents: Journal of Sedimentary Petrology, v. 52, p. 279-297.

Maclean, W.H., and Hoy, L.D., 1991. Geochemisty of hydrothermally altered rocks at the Horne Mine, Noranda, Quebec: Economic Geology, v. 86, p. 506-528.

McPhie, J., Doyle, M., and Allen, R., 1993. Volcanic textures: a guide to the interpretation of textures in volcanic rocks: Centre for Ore Deposit and Exploration Studies, University of Tasmania, Hobart, Tasmania, 198 p.

Mercier-Langevin, P., Dubé, B., Hannington, M.D., Davis D.W., Lafrance, B., and Gosselin, G., 2007. The LaRonde Penna Au-rich volcanogenic massive sulfide deposit, Abitibi Greenstone Belt, Québec: Part I. Geology and Geochronology: Economic Geology, v. 102, p. 585-609.

Mercier-Langevin, P., Dubé, B., Hannington, M.D., Richer-Laflèche, and M., Gosselin, G., 2007. The LaRonde Penna Au-rich volcanogenic massive sulfide deposit, Abitibi Greenstone Belt, Québec : Part II. Lithogeochemistry and paleotectonic setting: Economic Geology, v. 102, p. 585-609.

Monecke, T., Gibson, H., Dubé, B., Laurin, J., Hannington, M.D., and Martin L., 2008. Geology and volcanic setting of the Horne Deposit, Rouyn Noranda, Quebec: initial results of a new research project: Geological Survey of Canada, Current Research 2008-9, 16 p.

Mortensen, J.K., 1987. preliminary U-Pb zircon ages for volcanic and plutonic rock of the Noranda-Lac Abitibi area, Abitibi Subprovince, Quebec, in Paper - Geological Survey of Canada, v. 87-1a, p. 581-589.

Mulder, T., and Alexander, J., 2001. The physical character of subaqueous sedimentary density flows and their deposits: Sedimentology, v. 48, p. 269-299.

Pearson, V., 2005. The Blake River Group: an imbricated caldera complex; in Abstracts of Oral Presentations and Posters, Québec Exploration 2005, p. 45.

Powell, W.G., Carmichael, D.M., and Hodgson, C.J., 1995. Conditions and timing of metamorphism in the southern Abitibi greenstone belt, Quebec: Canadian Journal of Earth Sciences, v. 32, p 787-805.

Powers, M.C., 1953. A new roundness scale for sedimentary particles: Journal of Sedimentary Petrology, v. 23, p. 117-119.

Price, P., 1933. The Geology and ore deposits of the Horne mine, Noranda, Quebec: Ph.D. thesis, McGill University, Montreal, Canada, 288 p.

Price, P., 1934. The geology and ore deposits of the Horne Mine, Noranda, Quebec: The Transactions of the Canadian Institute of Mining and Metallurgy and of the Mining society of Nova Scotia, v. 37, p. 108-140.

Price, P., 1935. The geology and ore deposits of the Horne Mine, Noranda, Quebec: Transactions of the Canadian Institute of Mining and Metallurgy and of the Mining Society of Nova Scotia, v. 37, p. 108-140.

Price, P., 1948. Horne Mine, in Structural geology of Canadian ore deposits: Canadian institute of Mining and Metallurgy, Geological Division., Jubilee Volume, p. 763-772.

Price, P., 1949. Noranda Mines Limited, in Geology of Quebec: Quebec Department of Mines Report 20, v. 3, p. 338-361.

Richard M.G., 1998. Evolution of the Flavrian Pluton and its association with the VHMS deposits and granitoid-Hosted Gold deposits of the Noranda Cauldron, Rouyn Noranda, Quebec, Canada: Ph.D thesis, University of Montreal, Montreal, Quebec.

Roobol, M.J., and Hackett, D., 1987. Paleovolcanic facies and exhalite geochemistry: Guides for selecting exploration areas in volcano-sedimentary complexes: Economic Geology, v. 82, p. 691-705.

Ryznar, G., Campbell, F.A., and Krouse H.R., 1967. Sulfur isotopes and the origin of the Quemont orebody: Economic Geology, v. 62, p. 664-678.

Santaguida, F., and Hannington M.D., 1996. Characteristics of gold mineralization in volcanogenic massive sulphide deposits of the Notre Dame Bay area, central Newfoundland: Canadian Journal of Earth Sciences, v. 33, p. 316-334.

Santaguida, F., 1999. The paragenetic relationships of epidote-quartz hydrothermal alteration within the Noranda Volcanic Complex, Quebec: Ph.D. thesis, Carleton University, Ottawa, Ontario, 302 p.

Setterfield, T.N., Hodder, R.W., Gibson, H.L., and Watkins, J.J., 1995. The McDougall-Despina fault set, Noranda, Quebec: evidence for fault-controlled volcanism and hydrothermal fluid flow: Exploration and Mining Geology, v. 4, p. 381-193.

Sinclair, W.D., 1971, A volcanic Origin for the No. 5 Zone of the Horne Mine, Noranda Quebec: Economic Geology, v. 66, p. 1225-1231.

Skilling, I.P., White, J.D.L., and McPhie, J., 2002. Peperite; a review of magma-sediment mingling: Journal of Volcanology and Geothermal Research, v. 114, p. 1-17.

Spence, C.D., and de Rosen-Spence, A.F., 1975. The place of sulfide mineralization in the volcanic sequence at Noranda, Quebec: Economic Geology, v. 70, p. 90-101.

Sun, S., and McDonough, W.F., 1989. Chemical and isotopic systematics of oceanic basalts; implications for mantle composition and processes: Geological Society Special Publications, v. 42, p. 313-345.

Sundblad, K., 2003. Metallogeny of gold in the Precambrian of northern Europe: Economic Geology, v. 98. p. 1271-1290.

Winchester, J.A., and Floyd, P.A., 1977. Geochemical discrimination of different magma series and their different products using immobile elements: Chemical Geology, v. 20, p. 27-42.